CONTENTS

INTRODUCTION 5

Chapter 1 METEOROLOGICAL DATA FOR MODELLING BASED ON ECMWF 7

Chapter 2 INPUT DATA ON CONCENTRATIONS IN THE ATMOSPHERE OF AEROSOLS, SULPHURE DIOXIDE AND OH-RADICAL 19

2.1. CMAQ settings and input data 19

2.2. Results of modelling 20

Chapter 3 HEAVY METALS 31

3.1. Input data for the extended EMEP domain 31

3.2. Model sensitivity to refining of vertical structure 37

3.3. MSCE-HM model sensitivity to different sets of input meteorological data 42

3.4. Model results for 2006 over extended EMEP domain 47

Chapter 4 PERSISTENT ORGANIC POLLUTANTS 75

4.1. Modification of description of gas-particle partitioning of POPs in the atmosphere 75

4.2. Refinement of wet deposition of POPs 84

4.3. Parameterization of wind re-suspension of particle-bound POPs 93

4.4. Input data for the extended EMEP domain 95

4.4.1. Emission data 95

4.4.2. Geophysical information 100

4.5. Model results for 2006 over the extended EMEP domain 101

4.5.1. Polycyclic Aromatic Hydrocarbons (PAHs)

4.5.2. Polychlorinated dibenzo(p)dioxins and dibenzofurans (PCDD/Fs) 114

4.6. Hemispheric transport of POPs for 2006 127

4.6.1. Polychlorinated biphenyls (PCBs) 127

4.6.2. Lindane (γ-HCH) 129

4.6.3. Hexachlorobenzene (HCB) 132

CONCLUSIONS 135

REFERENCES 141

INTRODUCTION

The MSCE-HM and MSCE-POP regional-scale chemical transport models are used for the assessment of regional-scale pollution levels of heavy metals (e.g., Pb, Cd, Hg) and POPs, their long-term trends and source-receptor relationships between countries within the EMEP region. For the evaluation of the effects of global-scale atmospheric transport on pollution levels in Europe as well as the influence of European sources to the remote regions the hemispheric versions of these models were designed.

The performance and parameterizations of MSCE-HM and MSCE-POP models was reviewed by the EMEP Task Force on Measurements and Modelling (TFMM). The TFMM acknowledged the state-of-the-science status of the model approaches and approved the use of these models for operational modelling [ECE/EB.AIR/GE.1/2006/4]. Nevertheless, a number of recommendations aimed at further improvement of the models have been formulated. According to the TFMM recommendations, the development of wind re-suspension scheme for heavy metals and POPs was initiated, the transition to the use of ECMWF meteorological data as model input was began, improvements of process parameterizations relating to POPs were carried out [*Gusev at al*., 2006, *Ilyin et al.,* 2007].

In 2008 the transition from NCEP/DOE re-analysis to ECMWF data was completed and changes in the model results in response to the changes in meteorological input were analysed. The annual meteorological fields, processed by MM5 on the base of the two data sets - NCEP/DOE (2.5°x2.5° resolution) and ECMWF (1°x1° resolution) were compared with each other, and with observational data. This year the modelling of pollution levels of the HMs and POPs for 2006 is based on ECMWF analyses data.

Furthermore, the model activity on the inclusion of shallow lowest model layer in order to improve the model performance of air concentrations was initiated. The experimental model run was carried out with the refined vertical model structure. The study of sensitivity of modelling results to the refinement was initiated, and preliminary results are discussed in the report.

MSC–E continued the refinement of datasets of physical-chemical properties of selected POPs and model parameterizations of POP gas-particle partitioning in the atmosphere, removal of POPs from the atmosphere with precipitation, and POP re-suspension from underlying surface with aerosol particles. The effects of modifications of the MSCE-POP model parameterizations on the output modelling results were analyzed.

In addition to the work on implementation of the TFMM recommendations, a number of other activities relating to the model assessment of POPs and HMs took place. In 2008 the EMEP modelling domain was extended eastward in order to include the territories of Central Asian countries (Kazakhstan, Kyrgyzstan, Tajikistan, Turkmenistan, and Uzbekistan). The pilot model calculations of pollution levels of lead over the extended EMEP domain were carried for 2005 [*Ilyin et al.,* 2007]. This report is

focused on the results of the model assessment of HM and POP pollution levels over the extended domain for 2006.

MSCE-HM and MSCE-POP models include a number of atmospheric transformations of the targeted pollutants. For example, MSCE-POP model considers partitioning between gas and aerosol, reactions of POPs with OH radical etc. In order to provide the models with 3-dimensional input data with sufficient temporal resolution the input fields of the atmospheric constituents need to be previously calculated. At present the CMAQ model is used for this purpose. The results of simulations of O_3, OH, SO_2 and particulate matter are analyzed.

Essential part of the report is devoted to the comparison of the modelled and observed concentrations of HMs and POPs in air, in precipitation and wet depositions fluxes. Special attention was paid to the analysis of discrepancies between the modelled and observed quantities. In particular, the significant underestimation of the observed wet deposition fluxes of heavy metals at a number of stations may be connected with the uncertainties of emission data in neighbouring countries influencing the pollution levels at these stations through transboundary transport. The numerical experiments with variation of the emission values combined with the analysis of back trajectories made possible to improve the agreement between measurements and the model and to specify areas where officially reported emissions might be essentially underestimated.

Verification of calculated air concentrations and deposition fluxes of POPs in 2006 was carried out using the data of EMEP monitoring sites. On the whole, reasonable agreement between the model results and measurements was obtained. In particular, the model satisfactory reproduced observed air concentrations and deposition fluxes of B[a]P for most of the monitoring sites both on annual and seasonal levels. Reasonable agreement was found with data of most of the sites for PCB-153 and γ-HCH concentrations. In case of HCB the model tended to underestimate observed levels of concentrations in air and precipitation which is most likely connected with the underestimation of available HCB emission.

Chapter **1**

METEOROLOGICAL DATA FOR MODELLING BASED ON ECMWF

Meteorological information is one of the key input data for modelling atmospheric transport of pollutants. MSCE-HM and MSCE-POP models use meteorological data processed by MM5 on the base of NCEP/DOE reanalysis data. In order to improve quality of input data to the models the Task Force on Measurements and Modelling (TFMM) recommended to use input meteorological data provided by ECMWF. The transition from NCEP/DOE reanalysis data [*Kanamitsu et al.*, 2002] to ECMWF analyses started in 2007 [*Ilyin et al*., 2007], and in calculations of pollution levels for 2006 meteorological input to the models is based on ECMWF operational analyses. The aim of this chapter is to compare meteorological data sets generated by MM5 on the base of the two input data sets with each other and with observations, and to analyze the differences in modelled pollution levels based on these two input meteorological data.

1.1. Comparison of processed meteorological data with observations

This section presents the comparison of meteorological parameters, most relevant for modelling of atmospheric transport, processed by MM5 on the base of two different input data sets: ECWMF analyses and NCEP/DOE re-analyses, with each other and with observations. Detailed description of MM5 modelling system is presented in [*Grell et al*., 1995; http://www.mmm.ucar.edu/mm5/overview.html]. The selection of physical parameterization options and other adjustments are described in MSC-E technical report [*Travnikov and Ilyi*n, 2005].

Sources of meteorological observational data and statistical parameters

Surface observational data were derived from the Computational and Information Systems Laboratory (CISL) Research Data Archive, supported by National Centre for Atmospheric Research (NCAR), data set identification is ds464. This data set includes the land and marine reports received through Global Telecommunications System (GTS). For the comparison purposes 6-hour time series of air temperatures and wind speed were extracted from these data sets for each observational station. There are around 10000 of these time series available for 2006 over the globe, and 4000 of them are located within the extended EMEP grid (Fig. 1.1). As seen from the figure, the highest density of the stations takes place over the western, central and northern parts of Europe.

For verification of upper-air parameters, namely air temperature and wind speed, radiosonde observations, collected within RAOB database, were used. The RAOB dataset is developed jointly by National Climatic Data Centre (NCDC) and Forecast Systems Laboratory (FSL) and is freely available at site [http://raob.fsl.noaa.gov/]. It is based on reports available through GTS. The information for 2006 is presented from around 1900 sites over the globe. About 200 of them are located within the extended EMEP domain (Fig. 1.2). As seen, most of radisonde observations come from territories of central and western European countries and Russia. Over the Central Asian region the network is scarce.

Precipitation amounts, predicted by MM5 were compared with precipitation data obtained in the framework of GPCP project [http://cics.umd.edu/~yin/GPCP/, *Rudolf et al.,* 1994]. These data are so called “combined product”, prepared by means of blending of rain gauge observations and satellite data. Thus, over land territories with dense network of precipitation measurements the GPCP data are

mainly based on field observations. Over the areas with scarce network the data are mostly based on information obtained from satellites. Spatial resolution of these data is 1°x 1°, and temporal resolution is one day [*Huffman et al*., 2001]. Therefore, GPCP data seem to be especially relevant for purpose of evaluation of modelled precipitation, especially for regions with dense network of meteorological stations.

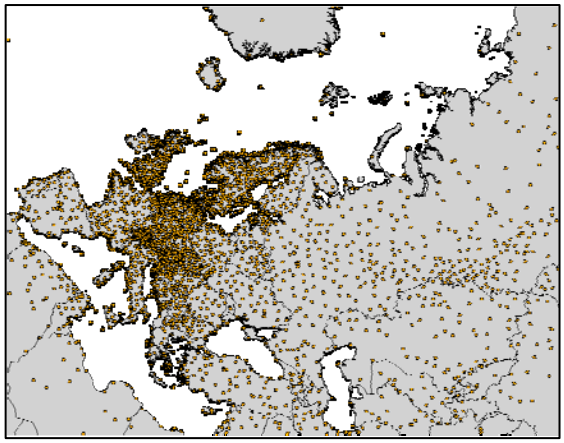

Fig. 1.1. *Location of surface observational stations within extended EMEP domain in 2006*

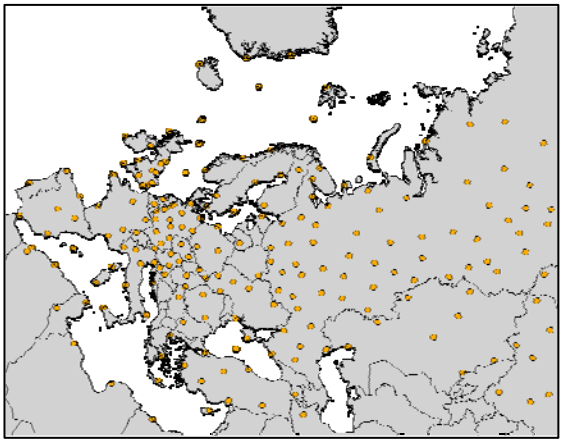

Fig. 1.2. *Location of radiosonde observational stations within extended EMEP domain in 2006*

Similarity of fields or time series of the observed and generated by MM5 meteorological parameters is characterized by the correlation coefficient:

$$R_{corr} = \frac{\sum_{i=1}^{N}(M_i - \overline{M})(O_i - \overline{O})}{\sqrt{\sum_{i=1}^{N}(M_i - \overline{M})^2 \sum_{i=1}^{N}(O_i - \overline{O})^2}}, \qquad \overline{M} = \frac{1}{N}\sum_{i=1}^{N} M_i, \qquad \overline{O} = \frac{1}{N}\sum_{i=1}^{N} O_i \tag{1.1}$$

where M stands for MM5 result, O – for the observations, N – number of values, $\overline{Q}$ and $\overline{M}$ are averaged observed and MM5-generated values.

In order to describe relative difference between MM5 and the observation data relative bias was calculated:

$$B_R = \frac{\overline{M} - \overline{O}}{\overline{O}} \cdot 100\% \tag{1.2}$$

The absolute difference was characterized by absolute bias:

$$B_A = \frac{1}{N} \cdot \sum_{i=1}^{N}(M_i - O_i) = \overline{M} - \overline{O} \tag{1.3}$$

However, in case of precipitation, $\overline{O}$ and $\overline{M}$ were replaced by more familiar accumulated values (e.g. annual or monthly sums).

In order to describe absolute difference between MM5 outputs, calculated on the base of two different input meteorological data, formulae (1.2) and (1.3) are modified:

$$B_R = \frac{\overline{M}(E) - \overline{M}(N)}{\overline{M}(E) + \overline{M}(N)} \times 2 \times 100\% \tag{1.4}$$

$$B_A = \frac{1}{N} \cdot \sum_{i=1}^{N}(M(E)_i - M(N)_i) = \overline{M}(N) - \overline{M}(N) \tag{1.5}$$

In formulae (1.4) and (1.5) *M(E)* and *M(N)* stands for parameter modelled by MM5 with the use of ECMWF and NCEP/DOE input data, respectively. Formulae (1.4) and (1.5) were also applied for description of differences between pollution levels, calculated on the base of the two MM5 outputs.

Near-surface air temperature

Spatial distribution of annual mean air temperatures, computed by MM5 on the base of different sources of meteorological data is very similar (Fig. 1.3 a,b). The differences between these two fields are within ±1 °C over most of the EMEP region (Fig. 1.4). Over most of land area the use of ECMWF data results to slightly higher (within 1°C) air temperature, compared to NCEP/DOE re-analysis. Over the Arctic the difference makes up around 1 – 2 °C. Over water areas the use of ECMWF data results to colder air compared to NCEP/DOE. When using ECMWF data, the air is 2-3 °C (and in some cases more than 3 °C) colder over coastal regions. This difference can possibly be explained by different spatial resolution of ECMWF and NCEP/DOE data. Spatial resolution of ECMWF analyses is 1°×1°, while that of NCEP/DOE – 2.5°×2.5°. This peculiarity requires more detailed investigation.

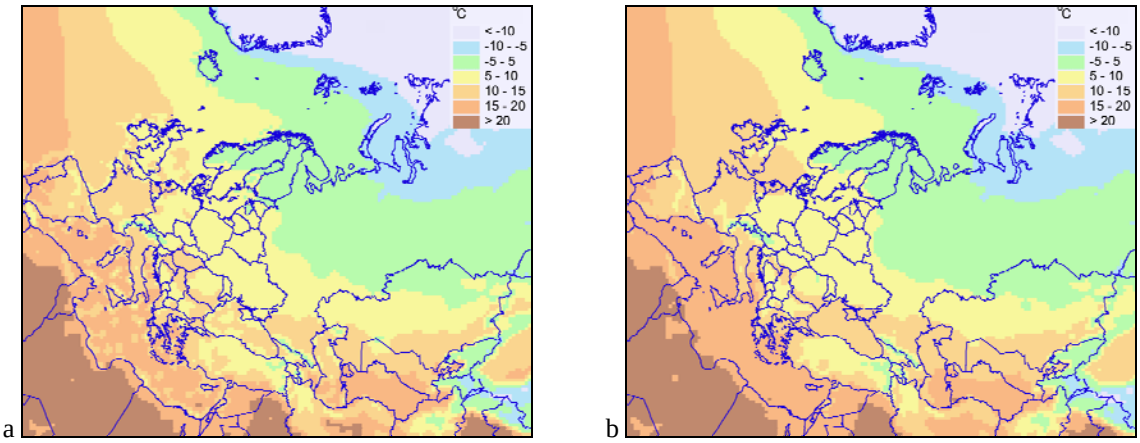

Fig. 1.3. *Annual mean air temperature at 2m height computed by MM5 on the base of ECMWF analyses (a) and NCEP/DOE re-analyses (b), ^{o}C*

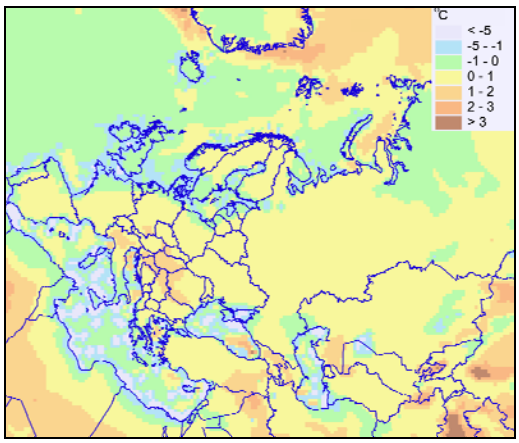

Fig. 1.4. *Absolute bias in annual mean 2 m air temperature, computed by MM5 on the base of ECMWF and NCEP/DOE data, ^{o}C*

Over most of measurement stations the difference between predicted and observed temperatures is within ±1°C (Fig. 1.5). Relatively high (more than 3°C) underprediction of the observed air temperatures is noted for mountainous regions of the southern part of Europe, Scandinavia and Central Asia. Besides, over coastal regions the use of ECMWF data results in negative absolute biases of air temperatures more often than the use of NCEP/DOE re-analyses.

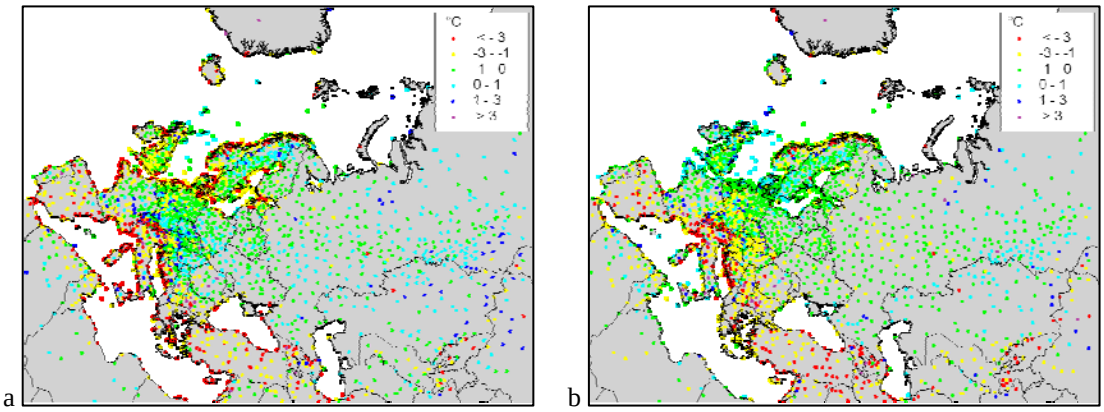

Fig. 1.5. *Absolute bias between observed and modelled by MM5 on the base of ECMWF analyses (a) and NCEP/DOE re-analyses (b) annual mean surface air temperatures in 2006, °C*

Annual variability of surface air temperatures averaged over points with observational stations was reproduced reasonably well by MM5. Both modelled and observed air temperatures demonstrate very similar annual variability. The temperatures, computed on the base of ECMWF are 0.8 – 1.8 °C lower, and on the base of NCEP/DOE - 0.6 – 1.4 °C lower compared to the observations (Fig. 1.6).

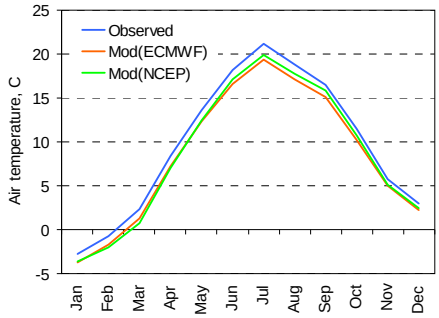

Fig. 1.6. *Monthly variations of spatial mean 2m air temperature over extended EMEP domain, °C*

Near-surface wind speed

Spatial distributions of annual mean wind speed over extended EMEP region, calculated by MM5 on the base of ECMWF analyses and NCEP/DOE re-analyses are shown in Fig. 1.7(a,b). The patterns of wind speed are quite similar. Higher wind speeds (8 – 10 m/s) were calculated over northern Atlantic. Over land area magnitude of annual mean wind speeds ranges from 1.5 to 5 m/s.

Over most of land areas and over the Atlantic waters the difference between wind speeds calculated on the base of ECMWF and NCEP/DOE data ranges within ±5% (Fig. 1.8a), or ±0.5 m/s (Fig. 1.8 b). The exception is southernmost regions of EMEP and high Arctic latitudes, where the use of ECMWF data results to higher wind speeds compared to NCEP/DOE. Over most of water areas along the coasts wind speeds based on ECMWF are up to 1.5 m/s lower compared to those based on NCEP/DOE. Most probably, the reason for this higher difference along coastline is the same as that for air temperatures and it requires further investigation.

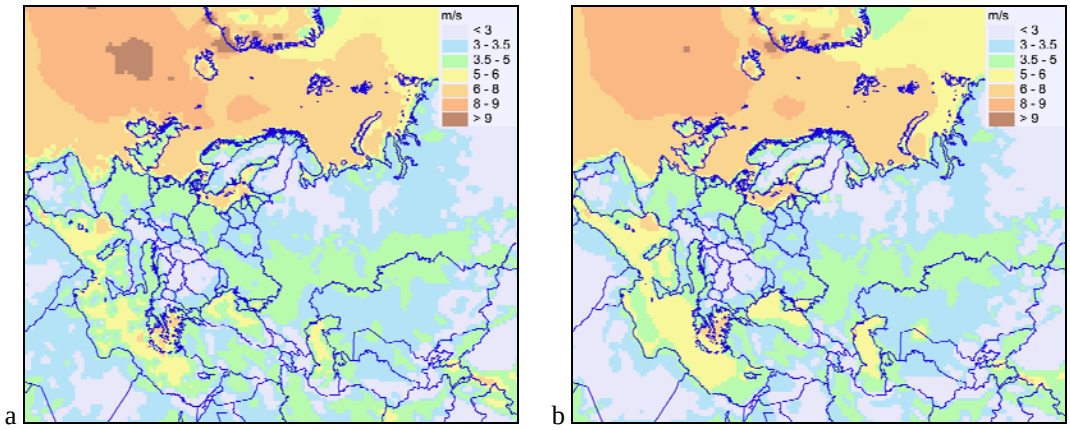

Fig. 1.7. *Annual mean wind speed at 10 m height computed by MM5 on the base of ECMWF analyses (a) and NCEP/DOE re-analyses (b), m/s*

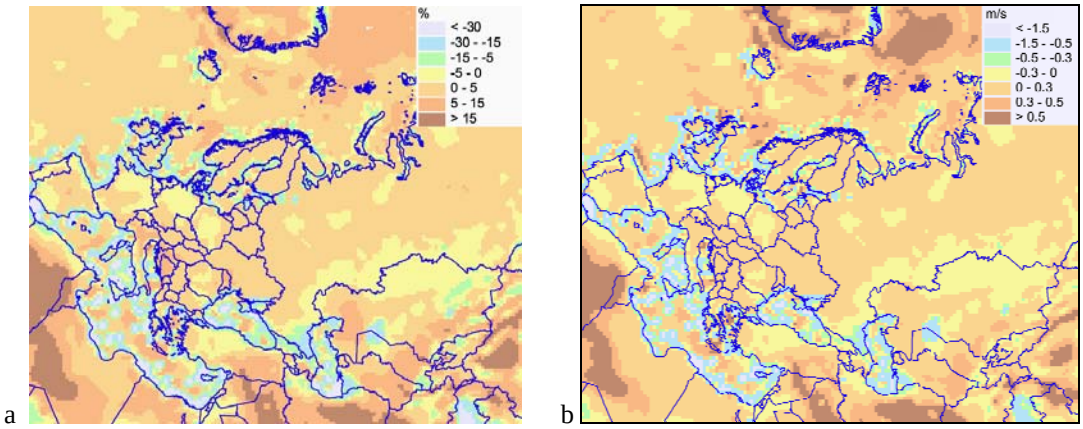

Fig. 1.8. *Relative (a) and absolute (b) difference in annual mean 10 m wind speed, computed by MM5 on the base of ECMWF (a) and NCEP (b) data*

For most of stations MM5 tends to overpredict annual mean wind speed by 15 – 30% regardless whether ECMWF or NCEP/DOE data were utilized (Fig. 1.9 a,b). The lowest difference between observed and calculated wind speed is noted for the central part of Europe. The overestimation is more pronounced in winter time (1 – 1.5 m/s), whereas in summer time the average values of modelled and observed wind speed are almost the same (Fig. 1.10). On average, the predicted wind speed exceeds the observed one by 9% or 11% if ECMWF or NCEP/DOE data are used.

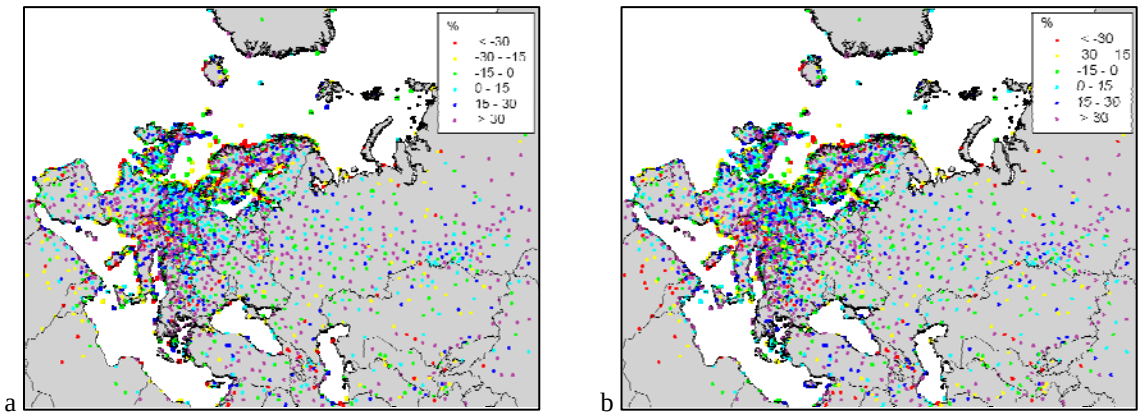

Fig. 1.9. *Relative bias between observed and modelled by MM5 on the base of ECMWF analyses (a) and NCEP/DOE re-analyses (b) annual mean 10-m wind speed magnitudes in 2006, %*

Short-term temporal variability of wind magnitude was reproduced satisfactorily over most of stations. Correlation coefficient (*Rc*) between 6-hour time series of modelled and observed wind speed is 0.6 – 0.8 over most of Central Europe, the Unite Kingdom, east of Russia and north of Kazakhstan (Fig. 1.11). Over most of stations of the Scandinavian Peninsula the *Rc* is 0.5 – 0.8 if ECMWF data are used, and 0.4 – 0.6 in case of NCEP/DOE. Over mountainous regions (e.g, the Alps, Caucasus, Pamir etc.) temporal variability of near-surface wind speed was poorly reproduced by MM5, using both ECMWF and NCEP/DOE data. This can possibly be explained by relatively rough (50 km) spatial resolution which leads to smoothing of complex terrain when modelling.

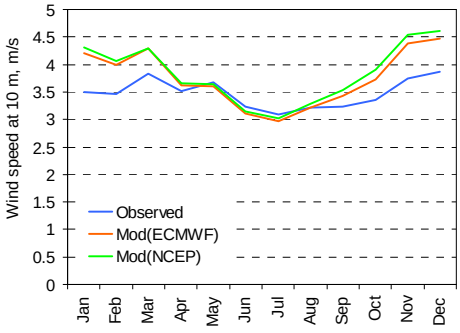

Fig. 1.10. *Monthly variations of spatial mean 10 m wind speed over the extended EMEP domain, m/s*

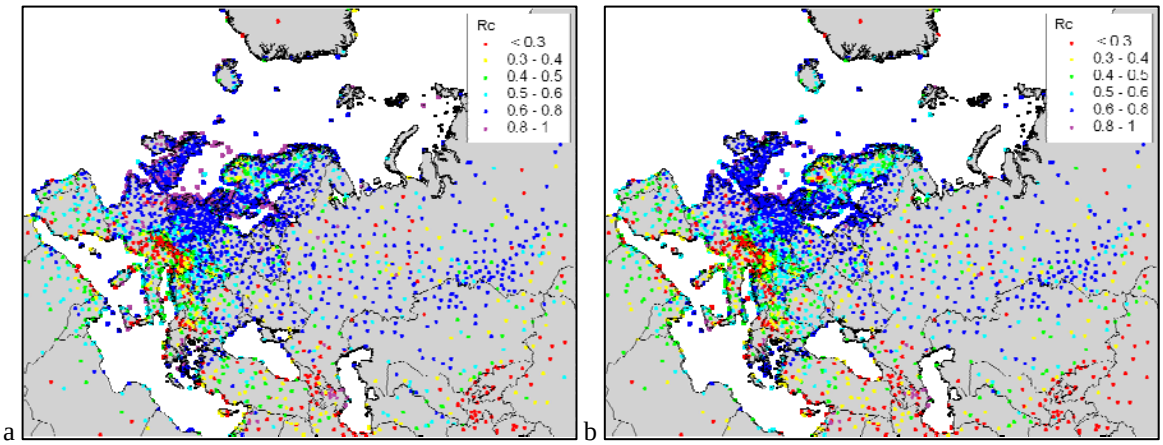

Fig. 1.11. *Temporal correlation coefficients between observed and modelled by MM5 6-hour time series of 10-m wind speed magnitude in 2006. Input data to MM5 are ECMWF analyses (a) and NCEP/DOE re-analyses (b)*

Precipitation

Annual sums of precipitation amounts simulated by MM5 with the use of ECMWF and NCEP data are demonstrated in Fig. 1.12 (a) and (b), respectively. As seen, the character of spatial distribution of the calculated precipitation amounts is similar. Relatively high (more than 1000 mm) precipitation amounts were obtained for northern Atlantic, and along mountain ridges. Over most of continental part of Europe the precipitation ranges from 500 to 1000 mm, over the Arctic, the Mediterranean Sea and central Asia annual precipitation sums are mostly around 150 – 300 mm.

Over most of EMEP domain relative bias between the two fields of precipitation lies within ±25% limits. The highest relative bias between precipitation amounts are noted either for areas where precipitation sums are not high, or over areas with complex terrain (Fig. 1.13, a). If precipitation sums are low (e.g, Sahara region, the Mediterranean Sea) even small change in absolute value results to essential relative difference. Over complex terrain regions, e.g., over the Central Asian mountain systems, the differences in input data for MM5 data can lead to changes in output precipitation.

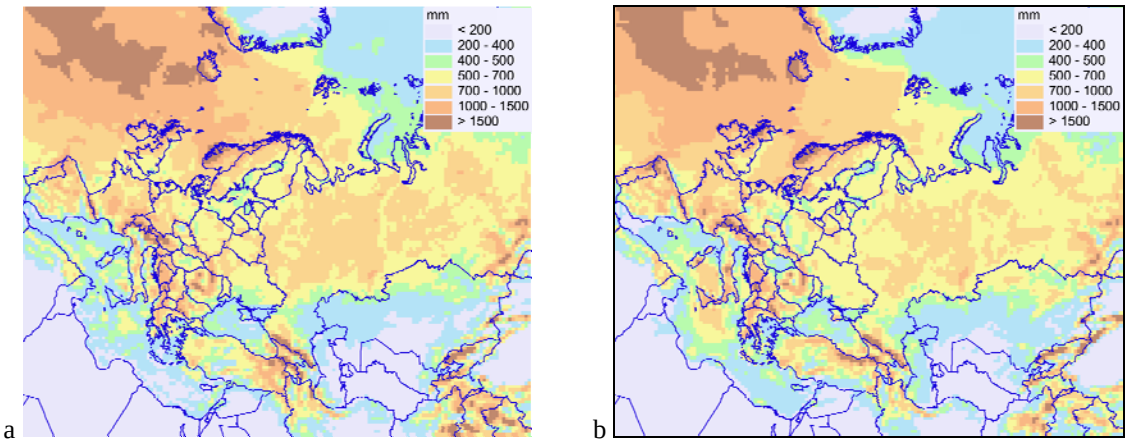

Fig. 1.12. *Surface precipitation amounts computed by MM5 on the base of ECMWF analyses (a) and NCEP/DOE re-analyses (b), mm*

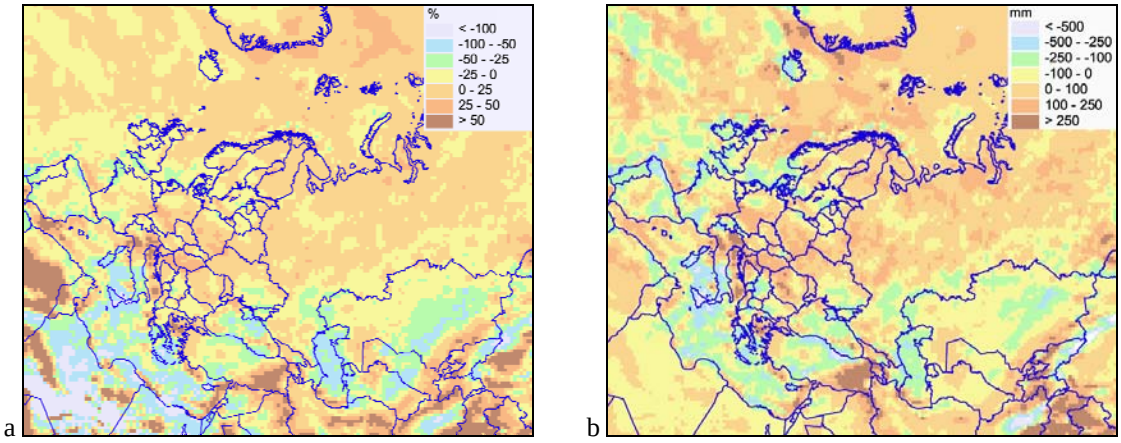

Fig. 1.13. *Relative (a) and absolute (b) bias in precipitation amounts, computed by MM5 on the base of ECMWF and NCEP data*

The highest absolute difference in precipitation amounts, computed on the base of the two input meteorological data sets is associated with the regions where predicted precipitation are significant (Fig. 1.13b). It is not surprising, because even small relative changes in modelled precipitation, caused by differences in input data, can result to significant changes in terms of absolute values. Therefore, over the Alps, Caucasus, and the Central Asian mountains the difference makes up 250 – 500 mm, over the central part of Europe and the north of the Atlantic - 100 – 250 mm.

Spatial pattern of the relative bias between GPCP data and precipitation sums computed on the base of ECMWF and NCEP/DOE data is similar (Fig. 1.14a, b). Relatively small bias (within ±25%) was obtained for eastern part of Europe, Scandinavia, north of Kazakhstan and the Mediterranean Sea. Over central part of Europe and northern Atlantic the bias reaches ±50%. Over southern arid regions of the EMEP domain MM5 tends to underestimate precipitation amounts, and over the Arctic – to overestimate. However, the precipitation over these regions are typically low and even small deviation in absolute terms results to considerable relative differences. Besides, measurement network over these regions is scarce. Hence, the uncertainty of GPCP data over these regions is likely higher compared to regions with dense network.

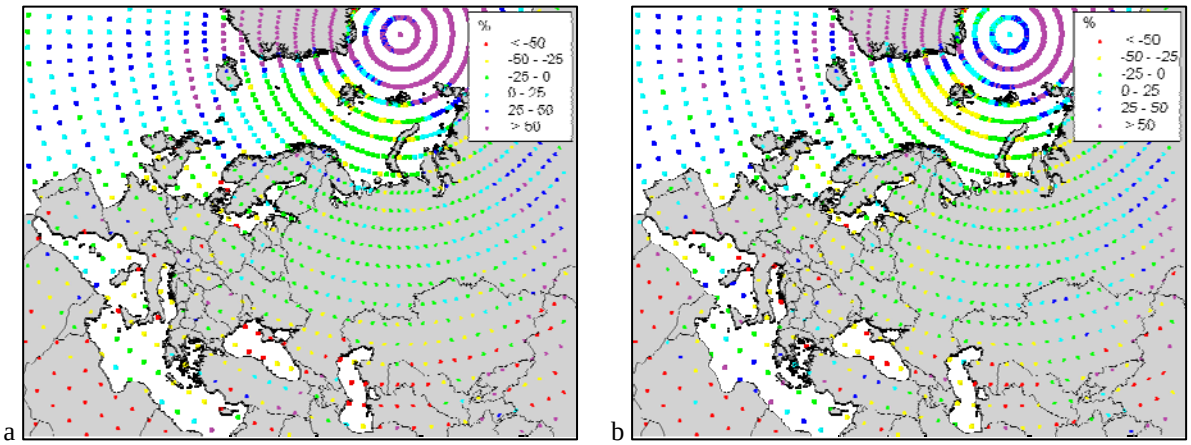

Fig. 1.14. *Relative bias between GPCP data and modelled by MM5 10-day time series of surface precipitation in 2006. Input data to MM5 are ECMWF analyses (a) and NCEP/DOE re-analyses (b), %*

Absolute bias between annual precipitation sums, predicted by MM5 and prepared within GPCP project, is demonstrated in Fig. 1.15 a,b. Relatively small (±150 mm) differences are noted for northern and eastern part of Europe and Central Asia. Over central part of Europe and the northern Atlantic the bias reaches 300 mm. As seen from Fig. 1.15 a, b, the use of ECMWF analyses data resulted to somewhat better agreement with GPCP data over northern and eastern Europe.

Both GPCP and MM5 spatially mean monthly sums of precipitation demonstrate similar annual variations. Minimum precipitation take place in the end of spring – beginning of summer, while the maximum – in winter (Fig. 1.16a). However, the observed precipitation in spring – beginning of summer are significantly lower compared to the predicted ones. Similar comparison presented for the EMEP area located southward from 60° latitude exhibits much better agreement between the observed and modelled precipitation (Fig. 1.16b). Therefore, this discrepancy can be caused by the overestimation of precipitation over the Arctic region by MM5. For this region the predicted and observed precipitation agree within ±10% limits. The agreement between spatial averaged precipitation amounts, generated by MM5 on the base of two sets of input data, also ranges within ±10%.

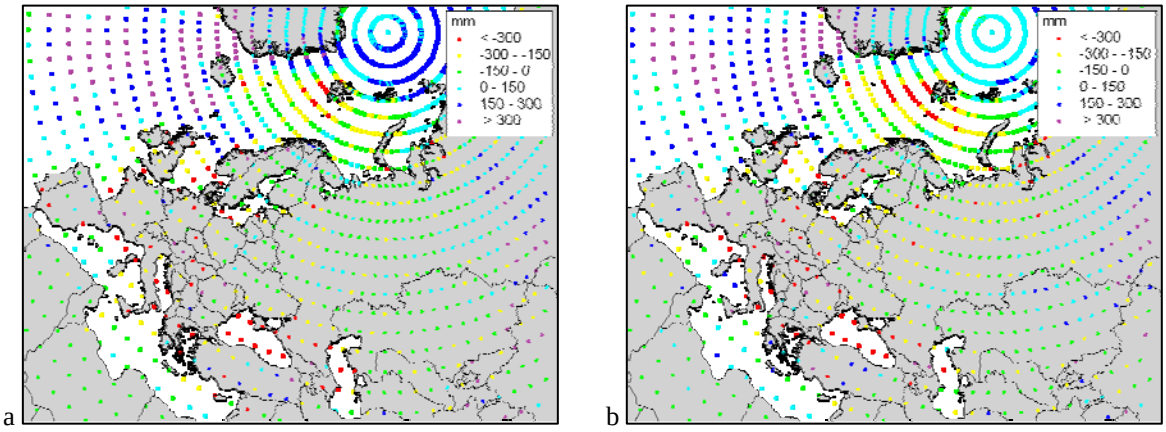

Fig. 1.15. *Absolute bias between GPCP data and modelled by MM5 10-day time series of surface precipitation in 2006. Input data to MM5 are ECMWF analyses (a) and NCEP/DOE re-analyses (b), mm*

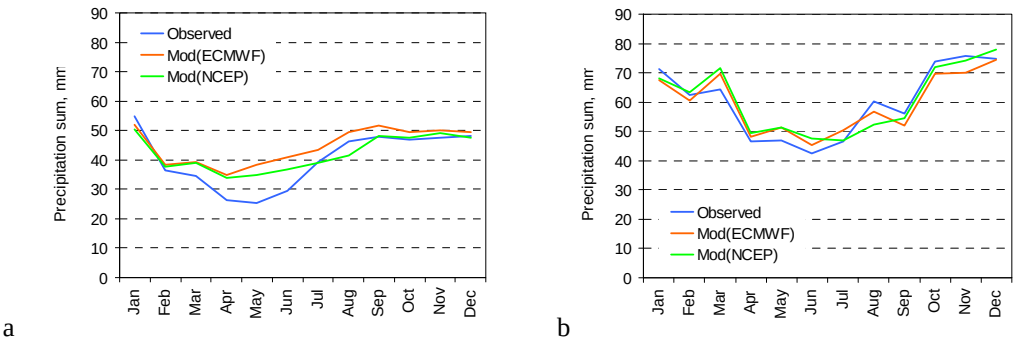

Fig. 1.16. *Monthly variations of spatial mean surface precipitation sums over entire extended EMEP domain (a) and over region to the south of 60° latitude, mm*

The performance of MM5 to predict temporal variability of precipitation amounts varies in different parts of the EMEP domain. Correlation coefficients between annual time series of 10-day precipitation sums, predicted by MM5 and produced within GPCP project is presented in Fig. 1.17 Significant correlation (> 0.6) was obtained for most of Europe and the northern Atlantic. Over the eastern part of Europe and the Arctic the correlation is 0.5 – 0.6. Over central Asian regions and Africa temporal variability was poorly reproduced. Spatial distribution of the correlation coefficients and their magnitudes derived on the base of the use of two different input datasets (ECMWF and NCEP/DOE) is very similar.

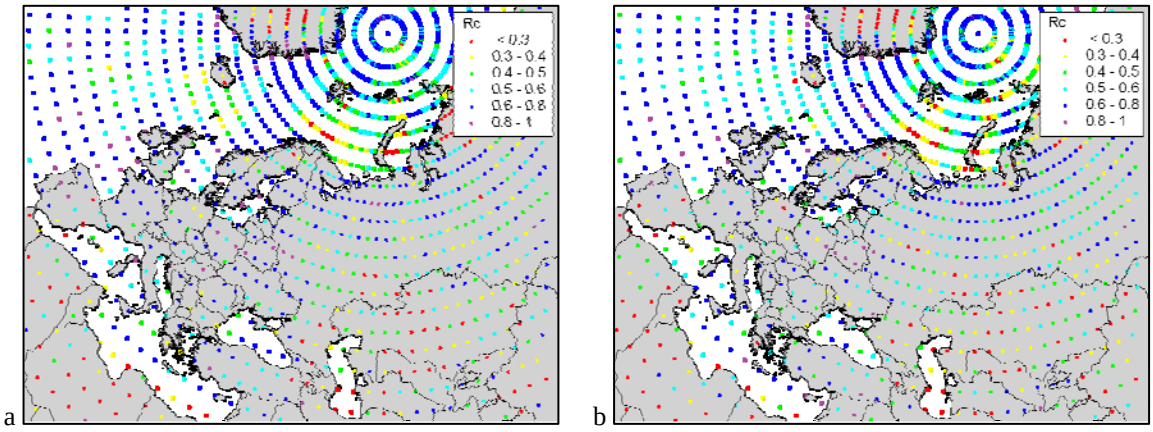

Fig. 1.17. *Temporal correlation coefficients between GPCP data and modelled by MM5 10-day time series of surface precipitation in 2006. Input data to MM5 are ECMWF analyses (a) and NCEP/DOE re-analyses (b)*

Upper-air parameters

Vertical distribution of averaged wind speeds, computed by MM5 with different input data almost coincide (Fig. 1.18). Modelled wind speeds on average reproduce the shape of the observed wind profile. As seen from the figure, MM5 tends to somewhat underpredict wind speed in the free atmosphere. On average, the underpediction reaches 3.3 ms/s at 300 hPa level.

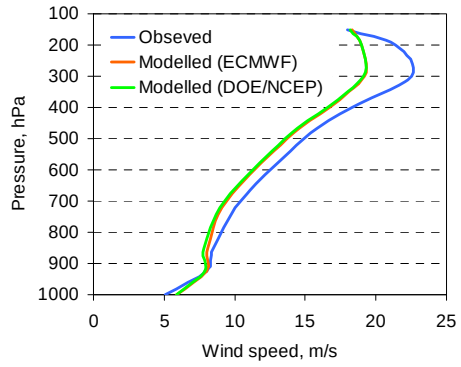

Fig. 1.18. *Vertical profiles of mean wind speed computed by MM5 and derived from observations, hPa*

Spatial distribution of relative and absolute bias between MM5 results and observational data over EMEP domain is similar for the two sets of predicted wind speeds. The example is provided for 925 hPa pressure level (Fig. 1.19, 1.20). At other levels the character of the distribution is similar. As seen from the figures, over most of the EMEP domain the difference between predicted and observed wind speeds is around ±15% (or ±1 m/s).

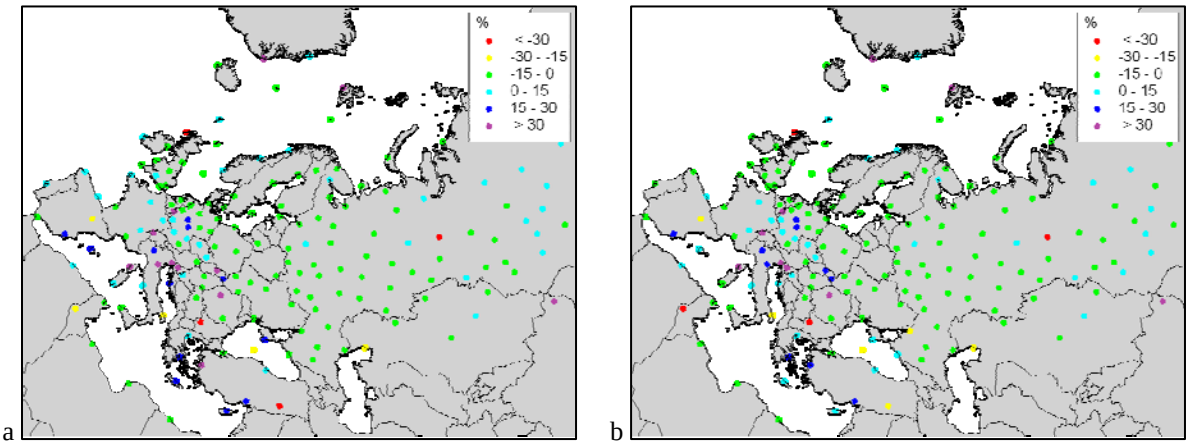

Fig. 1.19. *Relative bias between observed and modelled by MM5 annual mean wind speed magnitude at 925 hPa in 2006. Input data to MM5 are ECMWF analyses (a) and NCEP/DOE re-analyses (b), %*

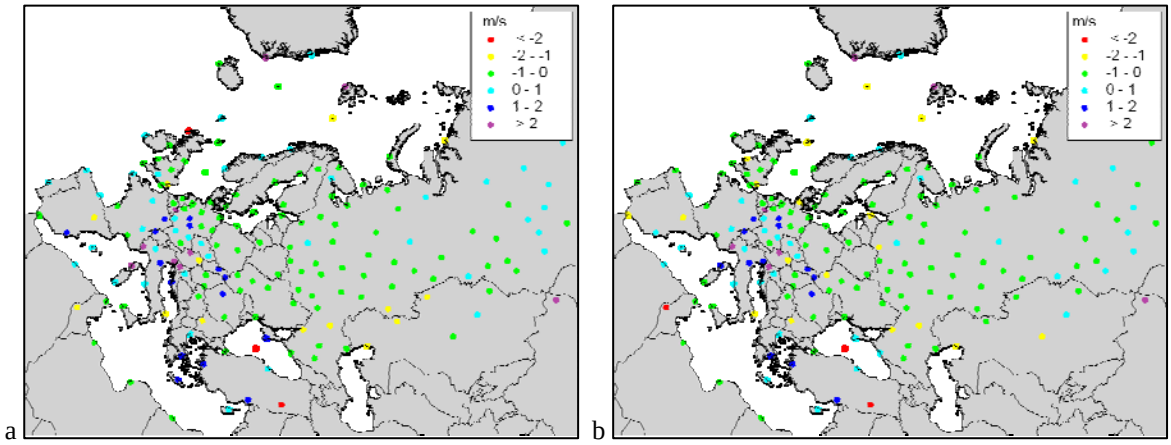

Fig. 1.20. *Absolute bias between observed and modelled by MM5 annual mean wind speed magnitude at 925 hPa in 2006. Input data to MM5 are ECMWF analyses (a) and NCEP/DOE re-analyses (b), m/s*

Short-term variability of wind speed over EMEP domain was reproduced by MM5 reasonably well. Over most of EMEP domain correlation coefficient between annual 12-hour time series of the predicted and observed wind speeds at 925 hPa level is above 0.6 (Fig. 1.21). As seen from the figures, the correlation coefficient for eastern European part is somewhat higher in case of use ECMWF data compared to the case whet NCEP/DOE re-analysis data are used. When higher levels are considered, the correlation coefficient tends to increase.

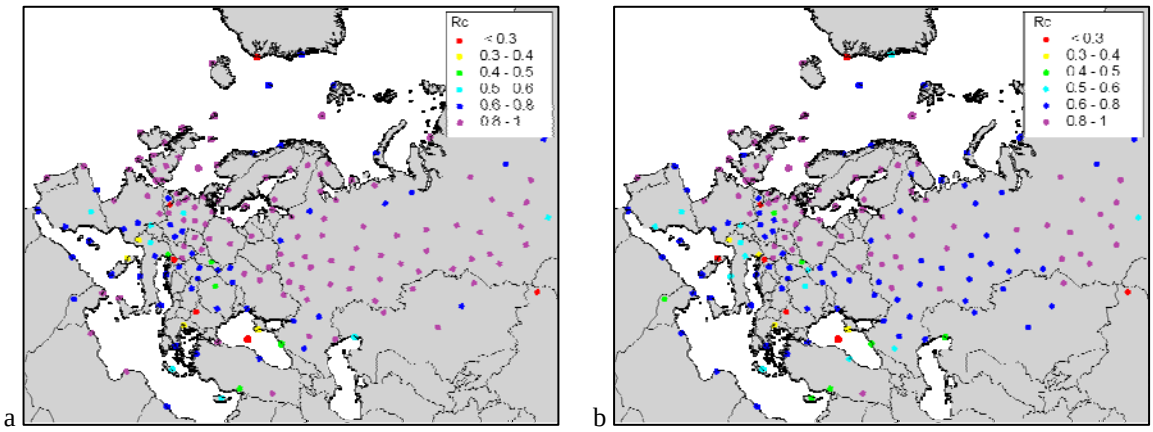

Fig. 1.21. *Temporal correlation coefficients between observed and modelled by MM5 12-hour time series of wind speed magnitude at 925 hPa in 2006. Input data to MM5 are ECMWF analyses (a) and NCEP/DOE re-analyses (b).*

Vertical distributions of averaged air temperature, derived from observations and simulated by MM5 are very similar (Fig. 1.22). The difference between the modelled and observed profiles is around ±0.5 °C in layer 925 – 700 hPa, and up to 4.5 °C at 300 hPa. Compared to annual mean air temperature of -55 °C at this level, the difference in 4.5 °C does not seem crucial.

Spatial distribution of absolute difference between annual mean air temperatures, derived from observations and predicted by MM5 at 925 hPa level is shown in Fig. 1.23. Over western part of Europe the difference is around -1°C, over the eastern part – about -1 - 2°C. As seen, the use of ECMWF analyses data allowed MM5 do demonstrate better performance in predicting air temperatures over Balkan region compared to the case when NCEP/DOE data are used. At other pressure levels the spatial distribution of the absolute difference is similar. Temporal variability was captured by MM5 favorably well. Correlation coefficient between modelled and observed 12-hour time series is more than 0.8 at majority of stations.

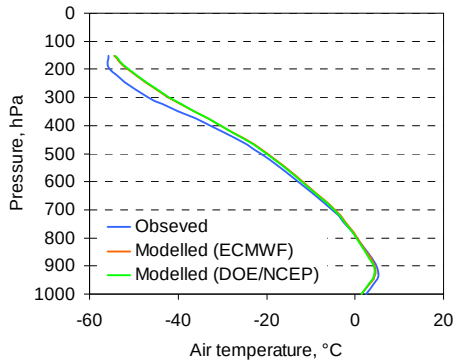

Fig. 1.22. *Vertical profiles of mean air temperature computed by MM5 and derived from observations*

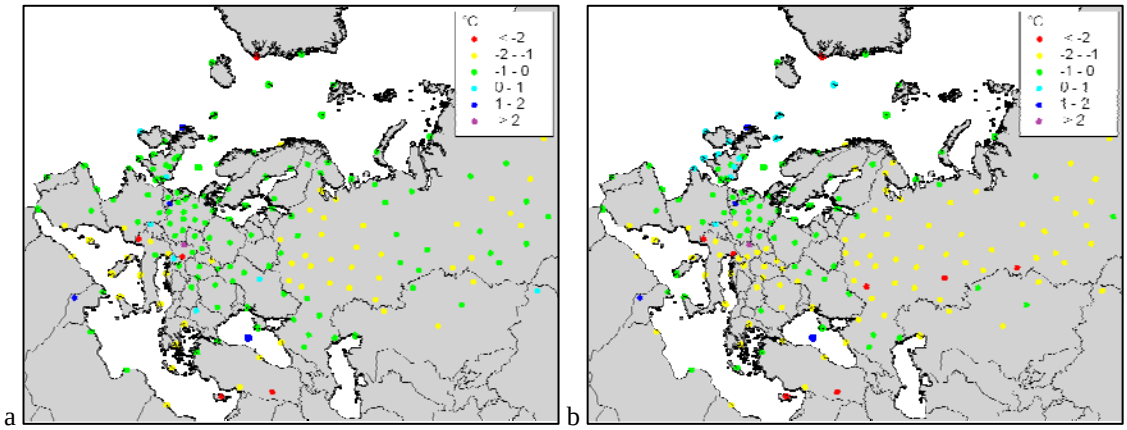

Fig. 1.23. *Absolute difference between observed and modelled by MM5 annual mean air temperatures at 925 hPa in 2006. Input data to MM5 are ECMWF analyses (a) and NCEP/DOE re-analyses (b) ,°C*

On the base of the carried out analysis the following conclusions can be outlined:

1. Over most of the extended EMEP domain air temperatures, wind speeds and precipitation amounts calculated by MM5 on the base of ECMWF analyses are similar to those based on NCEP/DOE re-analyses. This refers to both their annual mean values and temporal variability. Noticeable differences are indicated for specific areas (e.g., coastal zones, mountainous regions etc).

2. Fields of annual mean surface air temperatures simulated by MM5 on the base of ECMWF analyses and NCEP/DOE re-analyses for 2006 are similar. Absolute bias for air temperatures is around ±1 °C. MM5 tends to slightly underestimate surface air temperatures (around 1°C) compared to the observations.

3. Relative bias for annual mean wind speeds, simulated by MM5 on the base of ECMWF and NCEP/DOE is ±5%, and absolute bias - ±0.5 m/s over most of the extended EMEP domain. The use of ECMWF data as input information for MM5 results to overprediction of the observed wind speed on average by 9%, and NCEP/DOE – by 11%. Temporal variability of surface wind speed was reproduced reasonably well by MM5: *Rc* between 6-hour predicted and observed time series is higher than 0.6 over most of stations.

4. Over most of EMEP domain the relative bias between annual precipitation sums simulated by MM5 on the base of ECMWF and NCEP/DOE input data ranges within ±25%. Over dry or arid areas (Sahara, the Mediterranean Sea) as well as over mountainous regions the bias can be higher. Comparison of precipitation sums simulated by MM5 with GPCP data demonstrated relatively good (within ±25%) agreement over the eastern part of Europe, north of Kazakhstan and Scandinavia. Over central part of Europe and northern Atlantic the bias reaches ±50%.Temporal variability was satisfactorily captured by MM5: *Rc* is more than 0.6 over most of Europe.

5. Over mountainous regions the performance of MM5 lower compared to other regions, regardless whether ECMWF or NCEP/DOE input data were used. Both averaged values and temporal variability of air temperatures, wind speeds and precipitation sums were reproduced with lower accuracy.

6. MM5 tends to overpredict wind speed in the free troposphere, both using ECMWF analyses and NCEP/DOE re-analyses as input data. On average, the overprediction is minor at 925 hPa level and reaches 3.3 m/s at 300 hPa level. Nevertheless, temporal variability is reproduced well by MM5. *Rc* between observed and modelled 12-hour time series of wind speeds is higher than 0.8 at most of stations.

7. MM5 tends to overestimate air temperate in the free atmosphere compared to the observed values. On average, the overprediction reaches 4.5 °C at 300 hPa level. This however, does not seem high compared to mean value of -55°C at this level. Temporal variability of modelled air temperatures was reproduced with significant accuracy: *Rc* between modelled and measured 12-hour time series is higher than 0.8 over most of stations.

Chapter **2**

INPUT DATA ON CONCENTRATIONS IN THE ATMOSPHERE OF AEROSOLS, SULPHURE DIOXIDE AND OH-RADICAL

Calculations of transboundary atmospheric transport of POPs and HMs require input data on concentrations of some other compounds in the atmosphere. In particular, to define gas-particle equilibrium, data on concentrations of particle-bound organic carbon or on specific aerosol surface are used in the MSCE-POP model. Degradation rates of POPs in the atmosphere depend on OH-radical concentrations. In the mercury chemical mechanism of the MSCE-HM model there are reactions involving sulphur dioxide, OH-radical and ozone.

To perform experimental calculations of spatial-temporal distributions of the above compounds' concentrations the CMAQ model was used. 3-D 6-hour time resolution data sets covering the extended domain of EMEP have been obtained for 2006. Below a short description of work performed and results obtained is given.

2.1. CMAQ settings and input data

The Community Multiscale Air Quality modelling system (CMAQ) is a powerful third generation air quality modelling and assessment tool [*Byun and Ching*, 1999]. CMAQ is an active open-source development project of the US Environmental Protection Agency (US EPA) Atmospheric Science Modelling Division that consists of a suite of programs for conducting air quality model simulations (www.cmaq-model.org). CMAQ is supported and distributed by the CMAS Center (www.cmascenter.org).

To calculate concentrations in the air of aerosols, sulphure dioxide and OH-radical CMAQ v.4.5 with the following settings was used:

- **advection scheme**: **yamo** (Yamartino scheme for mass-conserving advection [*Yamartino,* 1992]);
- **chemical mechanism**: **cb4** (Carbon Bond-IV mechanism [*Gery et al.,* 1989; *Dodge,* 1989; *Carter,* 1996]);
- **aerosol module**: **aero4** (the 3rd generation modal CMAQ aerosol model with extensions for sea salt emissions and thermodynamics);
- **cloud parameterization**: **acm** (RADM-based cloud processor that uses the asymmetric convective model to compute convective mixing [*Dennis et al.,* 1993; *Walcek and Taylor,* 1986; *Chang et al,* 1987; *Chang et al.,* 1990]).

Input meteorological data were calculated by MM5 model on the basis of ECMWF analysis (for details see Chapter 1 of this report).

Emission data were compiled on the basis of the following sources:

- **EMEP** – *webdab.emep.int*;
- **EDGAR** (Emission Database for Global Atmospheric Research) - *www.mnp.nl/edgar*

- **GEIA** (Global Emission Inventory Activity) – *www.geiacenter.org*;
- **AEROCOM** (Global Aerosol Model Intercomparison) – *nansen.ipsl.jussieu.fr/AEROCOM;*
- **University of Illinois** – *cee.uiuc.edu.*

Table 2.1 shows data sources for particular pollutants.

Table 2.1. *Sources of emission data*

Pollutant	Data source
SO_2 (anthropogenic)	EMEP[1], EDGAR[2]
SO_2 (volcanoes)	GEIA
dimethyl sulfide	AEROCOM
NO_x (anthropogenic)	EMEP[1], EDGAR[2]
NO_x (lightnings)	GEIA
NO_x (soil)	GEIA
NH_3 (anthropogenic)	EMEP[1], EDGAR[2]
NH_3 (natural)	GEIA
NMVOC (anthropogenic)	EMEP[1], EDGAR[2]
NMVOC (natural)	GEIA
CO	EMEP[1], EDGAR[2]
Elemental carbon	University of Illinois
Organic carbon	University of Illinois
Dust	AEROCOM

Emission of sea salt was calculated inside CMAQ model on the basis of input data on spatial distribution of seawater and ice from ISLSCP (International Satellite Land Surface Climatology Project – *islscp2.sesda.com/ISLSCP2_1/html_pages/islscp2_home.html*) and meteorological data from MM5.

2.2. Results of modelling

Particulate matter

Spatial distributions of PM10 and PM2.5 mean annual concentrations in the surface air layer are shown in Fig. 2.1. Maximum levels of particulate matter concentrations in the air are take place over Sahara, Kara Kum and Gobi Deserts. Annual averages of PM10 concentrations in Europe normally do not exceed 20-25 $\mu g/m^3$ with the exception of some areas in Spain and Italy. A PM10 field differs from that of PM2.5 qualitatively by high concentration of sea salt appearing in the atmosphere mainly in the form of coarse particles (PM10-PM2.5).

Calculated annual averages of PM10 concentrations in the air are shown in Fig. 2.2. in comparison with data of measurements at EMEP sites currently available in the AIRBASE database (http://dataservice.eea.europa.eu). The model underestimates PM10 concentrations by 30% on the average. PM10 concentrations are underestimated for Scandinavian countries, the United Kingdom, Belgium, the Netherlands and northern part of Germany. In other parts of Europe the situation is not

[1] Expert emissions
[2] For grid cells, where EMEP data are not available

so simple: at some sites calculated concentrations either exceed measured concentrations or are very similar to them. This, in particular, refers to Spain and Switzerland. The coefficient of correlation between modelled and observed concentrations is 0.64. A considerable part of the territory of Europe is not covered with EMEP observations.

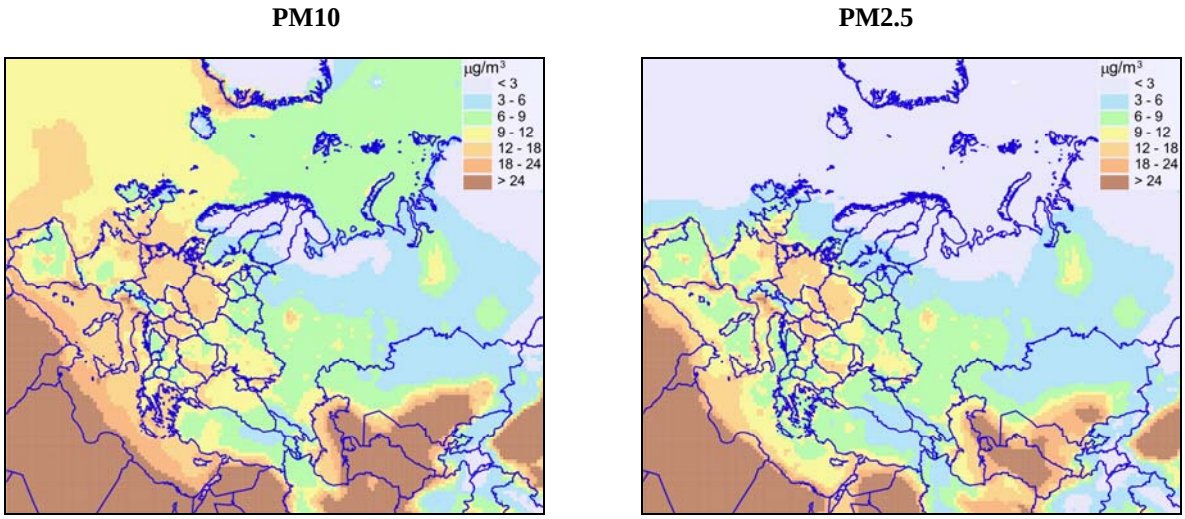

Fig. 2.1. *Spatial distributions of aerosol particles in the surface air layer in 2006 (annual averages), µg/m³*

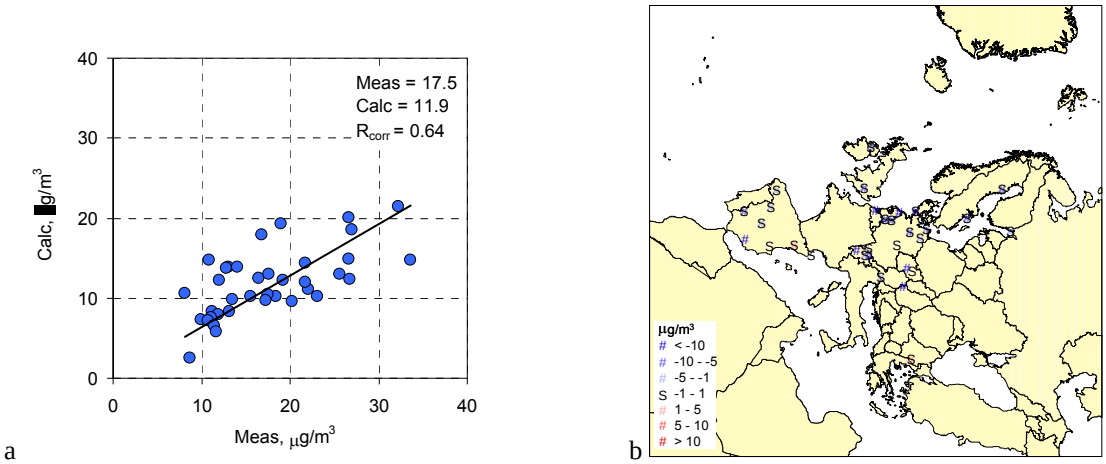

Fig. 2.2. *Comparison of calculated annual averages of PM10 concentrations in the air with data of measurements (EMEP sites) available in AIRBASE: a – scatter plot; b – difference between calculations and measurements, µg/m³*

The average level of PM2.5 concentrations reproduced by the model is fairly reasonable (Fig. 2.3). However, for some regions variations in mean annual concentrations are essential and due to this spatial correlation is not high (R_{corr} = 0.43). The model underestimates PM2.5 concentrations in the air by more than 3 µg/m³ (~30% on the average) for stations located in Sweden (2 stations), in the north of Germany and in Switzerland. But for stations in Spain (3 stations), in the south of Germany and in Bulgaria an overestimation of the same size is seen. It should be noted that for most of Spanish stations calculations and measurements are in good agreement.

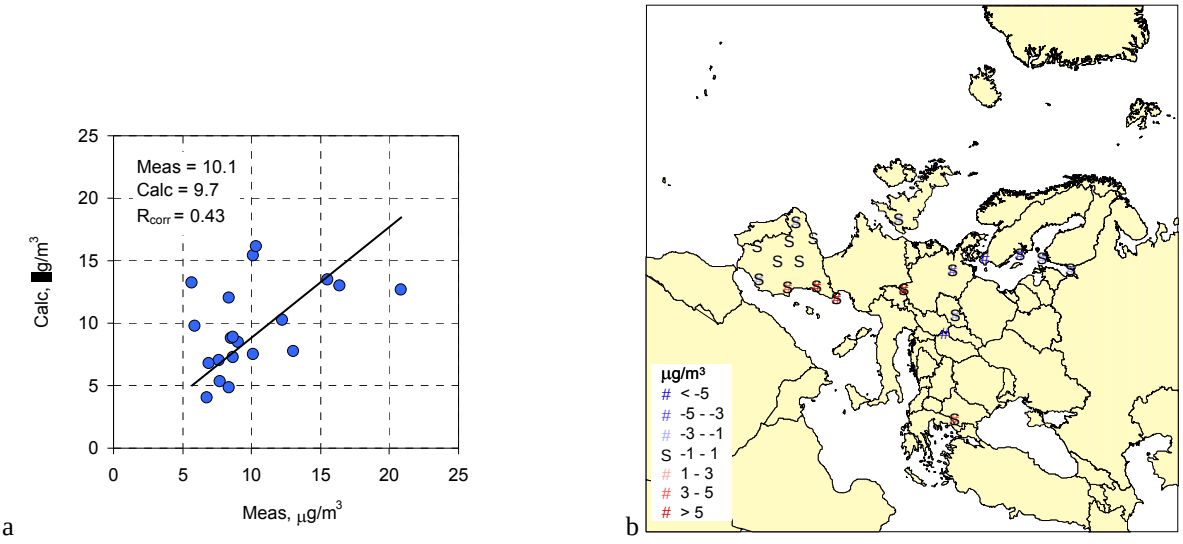

a b

Fig. 2.3. *Comparison of calculated annual averages of PM2.5 concentrations in the air with data of measurements (EMEP sites) available in AIRBASE: a – scatter plot; b – difference between calculations and measurements, μg/m^3*

Calculated concentrations of PM10 main components are shown in Fig.2.4. The largest contribution to the PM10 mass over Europe is made by organic matter. In some regions of Europe mean annual concentrations of organic aerosols exceed 10 μg/m^3. A significant share of the total mass of PM10 is accounted for by secondary inorganic aerosols: SO_4^{--}, NO_3^-, NH_4^+. Over Europe maximum concentrations in the surface air are as follows: ~ 5 μg/m^3 for sulphate, ~ 4 μg/m^3 for nitrate and ~ 3 μg/m^3 for ammonium. The highest mean annual concentrations of Na^+ and Cl^- emitted from the sea surface as part of sea salt reach 10 μg/m^3 and higher near the coast of Greenland. However over the most of continental Europe the contribution of Na^+ и Cl^- to the total mass of PM10 is relatively small. The exception is provided by the coastal areas where the total annual averages of Na^+ + Cl^- concentration amount to 1-3 μg/m^3. Within the boundaries of the domain under consideration most of dust emissions occurs in deserts. Maximum concentrations of dust in the air (up to several hundreds μg/m^3) also take place there.

Ranking of aerosol main components by their calculated contribution to the total mass of PM10 for most of European countries produces the following series (in decreasing order):

- organic matter (~ 45% average in Europe);
- SO_4^{--}(~ 20%);
- NO_3^-(~ 15 %);
- NH_4^+(~ 10%);
- dust / sea salt (less than 10%).

In Asia the proportions of various components in the total mass of PM10 are different. Particularly in Kazakhstan, Turkmenistan and Uzbekistan the greatest contribution is made by dust.

SO_4 (with sea salt sulphate)

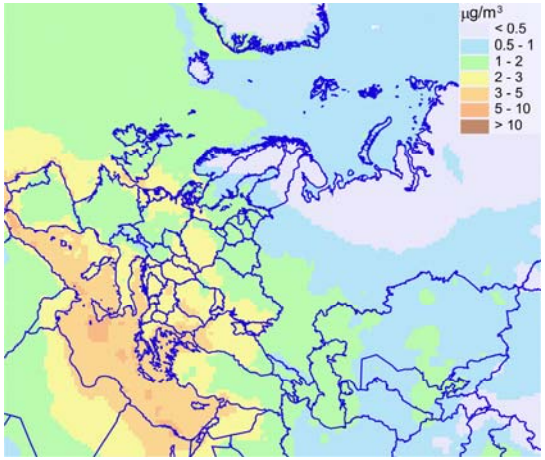

NO_3

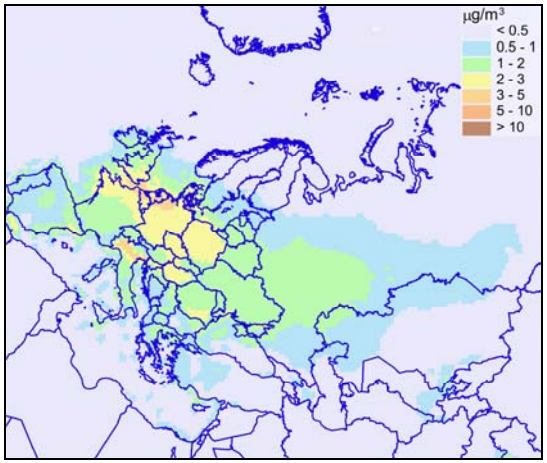

NH_4

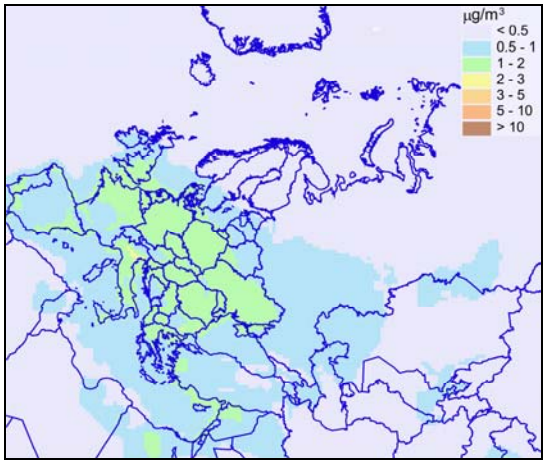

Na+Cl

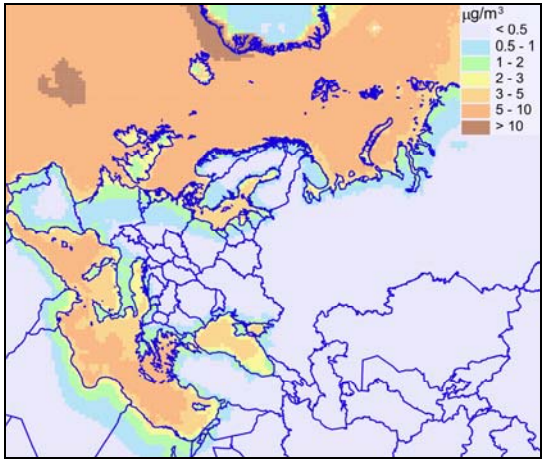

Organic matter

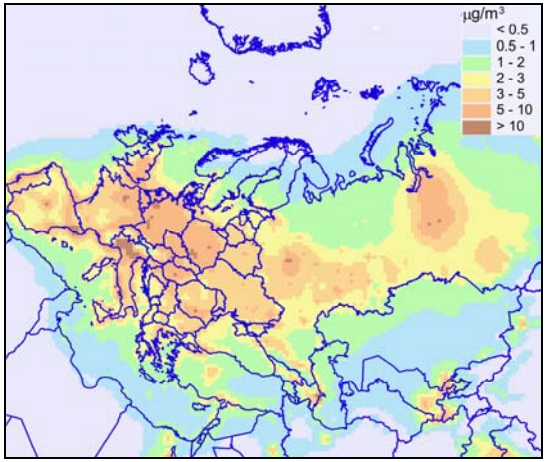

Dust

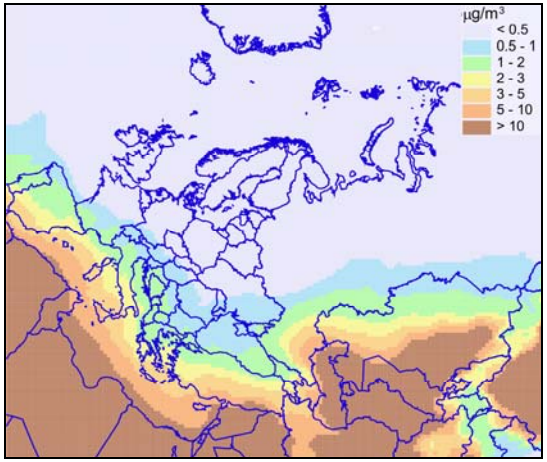

Fig. 2.4. *Spatial distributions of concentrations in the surface air of various PM10 components: SO_4, NO_3, NH_4, Na+Cl, organic matter, dust for 2006, $\mu g/m^3$*

Chemical composition of aerosol particles is measured only at several EMEP stations. Currently in the CREATE Aerosol Database [www.nilu.no/projects/ccc/create] data of measurements made in 2006 at stations DE44 (PM10 and PM2.5) and NO01 (PM2.5) are available. In Fig.2.5 and Fig.2.6 these data are compared with calculations*.

As is seen from the Figs the model underestimates annual averages of aerosol concentrations in the air for both stations. It should be noted that MSCW calculations made for July 2008 resulted in similar overestimation for these two stations [*Yttri et.al.*, 2007].

The difference between observed and modelled content of PM in the air for stations DE44 and NO01 is caused by the fact that CMAQ underestimates concentrations of secondary inorganic aerosols and elemental carbon (DE44). Concentrations of organic matter (OM) are overestimated by the model for DE44 and underestimated for NO01. Lack of a well pronounced regular overestimation or underestimation of organic matter concentration in the air is positive from the perspective of further use of information on OM concentration in the MSCE-POP model. Levels of Na^+ и Cl^- concentrations in the air are reproduced by CMAQ with adequately high accuracy. Chemical composition of a certain fraction of PM mass has not been determined by the measurements (in Figs it is marked as "unspecified") and due to this it is difficult to define exactly the main causes of model underestimation. MSCW experts suppose that a considerable part of unspecified PM mass determined by gravimetrical method is accounted for by particle bond water ([*Yttri et. al.,* 2007] and earlier EMEP/CCC&MSCW reports). Another factor responsible for CMAQ underestimation of coarse particles concentrations may be associated with the fact that in AEROCOM data used for comparison dust emission in Europe was underestimated.

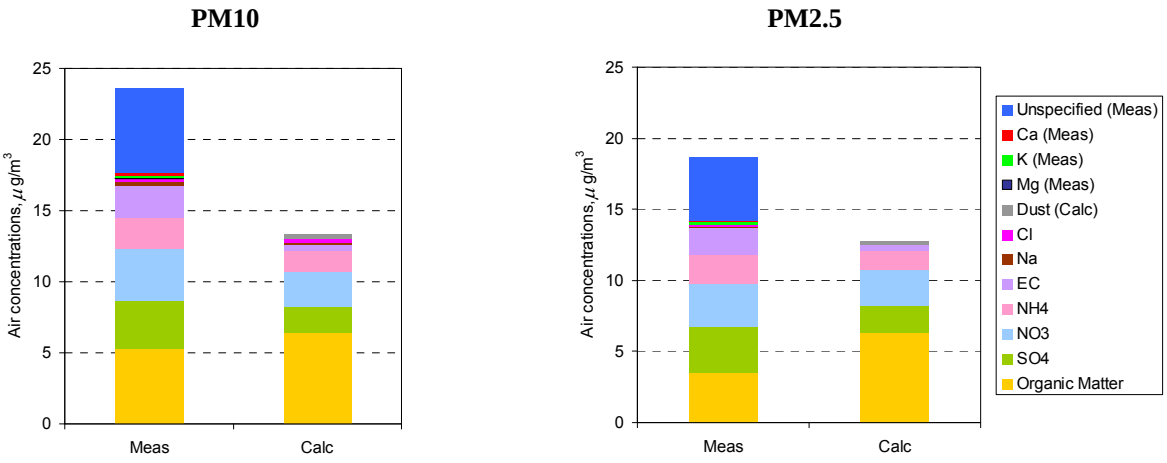

Fig. 2.5. *Composition of aerosol calculated by CMAQ and measured at station DE44. Annual averages of concentration in the air are given, μg/m³*

* Concentrations of organic matter were not measured directly. They were calculated by multiplying of organic carbon measured concentrations by factor 1.7 in accordance with [*Yttri et. al.*, 2007].

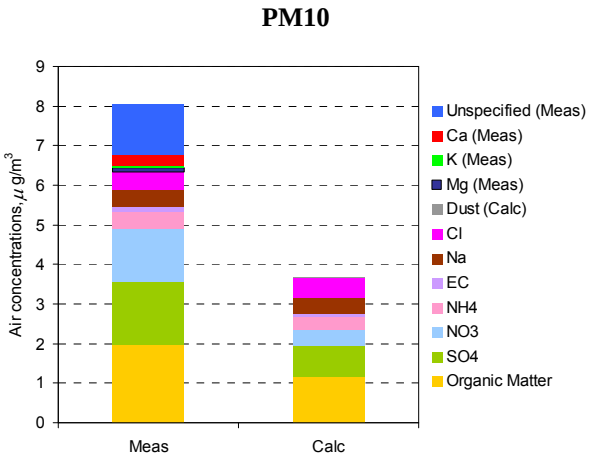

Fig. 2.6. *Composition of aerosol calculated by CMAQ and measured at station NO01. Annual averages of concentration in the air are given, μg/m^3*

As was mentioned above spatial distributions of aerosol organic matter and specific aerosol surface are used as input data in the MSCE-POP model. Calculated spatial distributions of their mean annual concentrations in the surface air are shown in Fig. 2.7 and Fig. 2.8 respectively. It should be mentioned that spatial distribution of aerosol surface is similar to that of PM (Fig.2.1), but slightly differs due to the difference in fine particle size distributions in various parts of the domain under calculation.

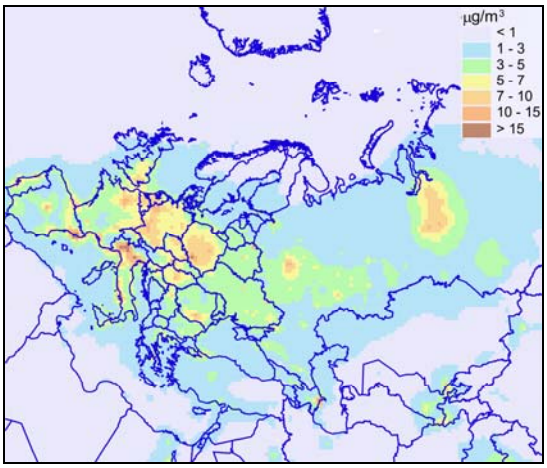

Fig. 2.7. *Spatial distribution of organic aerosol concentrations in surface air layer (annual averages), μg/m^3*

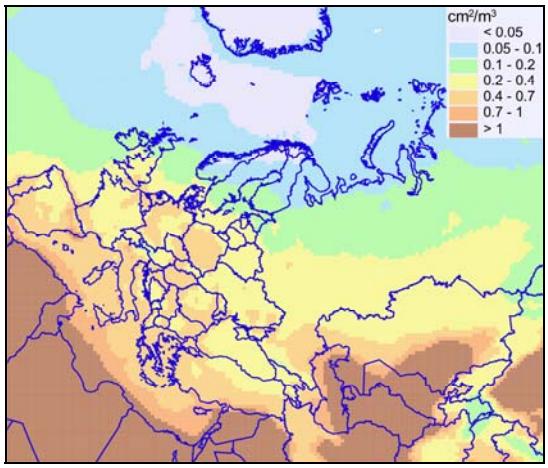

Fig. 2.8. *Spatial distribution of specific aerosol surface in surface air layer (annual averages), cm^2/m^3*

Sulphur dioxide

For most of Europe and Central Asia within the extended EMEP domain calculated annual averages of SO_2 concentration in the surface air amount to several micrograms per cubic meter (Fig.2.9). Maximum levels (over 5 μg/m^3) are reached in some regions of Eastern Europe (Poland, Ukraine, Romania, Bulgaria), Balkan countries, Russia and countries of Central Asia (Kazakhstan, Uzbekistan, Tajikistan). Minimum mean annual concentrations of SO_2 (less than 1 μg/m^3) take place in Norway, Sweden and Finland.

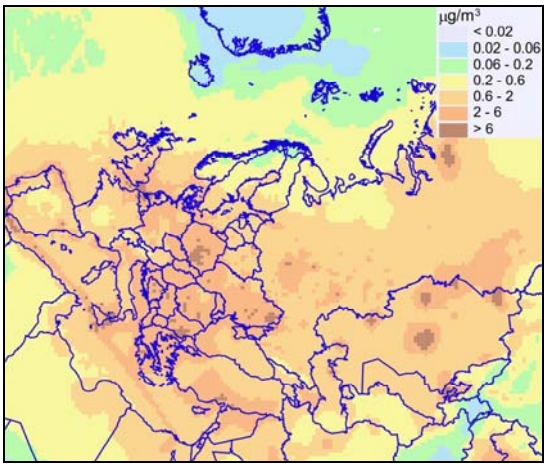

Fig. 2.9. *Spatial distribution of SO_2 concentrations in surface air layer (annual averages) for 2006, µg/m³*

Agreement between calculations of SO_2 concentrations in the air and data of measurements at EMEP stations currently available in the AIRBASE database is satisfactory (Fig.2.10). The average level of SO_2 concentrations is reproduced by CMAQ reasonably well. The coefficient of correlation between modelled and observed mean annual concentrations is 0.66. For one third of stations calculated concentrations differ from measured concentrations by less than 0.3 µg/m³ (~20% on the average). For 75% of stations this difference is within 1 µg/m³.

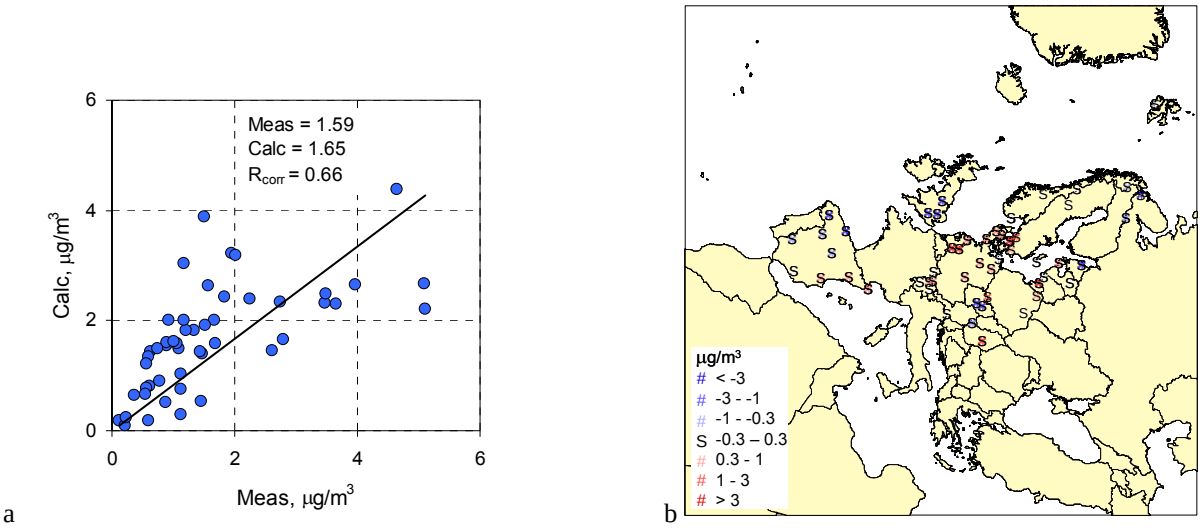

Fig. 2.10. *Comparison of calculated annual averages of SO_2 concentrations in the air with data of measurements (EMEP sites) available in AIRBASE: a – scatter plot; b – difference between calculations and measurements, µg/m³*

Ozone

Calculated spatial distribution of O_3 mean annual concentrations in the surface air is given in Fig.2.11. Basically it is similar to corresponding distributions given in EMEP/MSCW reports (e.g. see [*Tarrason et. al.,* 2007] with the results for 2005). Maximum levels of ozone concentration in the air take place over sea surfaces, in particular, over the Mediterranean Sea. Minimum concentrations was obtained for inland territories of Russia.

For most of the stations CMAQ slightly underestimates ozone concentrations in the air (Fig.2.12). On the average this underestimation is about 15%. Only at some stations in the central and southern parts of Europe calculated mean annual concentrations exceed measured concentrations.

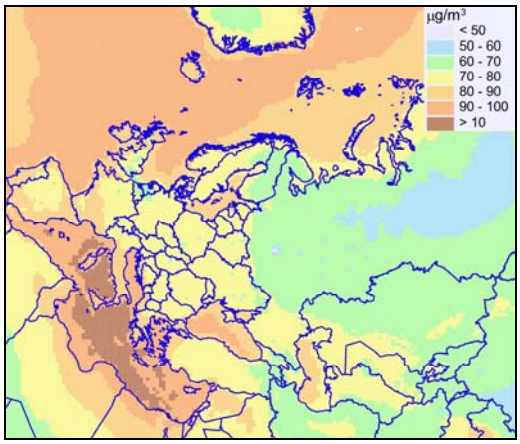

Fig. 2.11. *Spatial distribution of O_3 concentrations in the surface air(annual averages), $\mu g/m^3$*

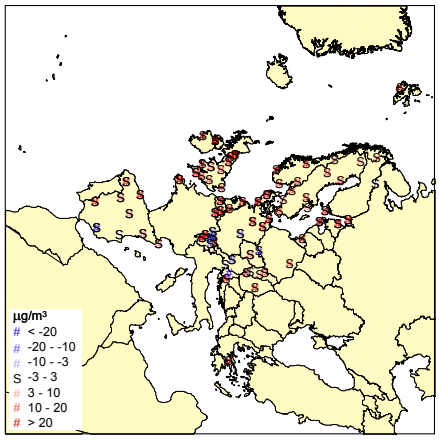

Fig. 2.12. *Difference between calculated annual averages of O_3 concentrations in the air and those measured at EMEP stations (measured concentrations are taken from the AIRBASE database) , $\mu g/m^3$*

Normally concentrations of ozone in the air are subject to well pronounced seasonal and diurnal variations ([*Fjæraa A. M. and Hjellbrekke A.-G.,* 2007] and earlier EMEP/CCC reports). Within a year maximum falls on summer and within a day it is observed in day time. In general CMAQ reproduces time variations of O_3 concentrations in the air, but in a slightly smoothed manner. As an example in Fig. 2.13 results of calculations and data of measurements for the AIRBASE station located in Italy are given. It is to be recalled that time resolution of data resulted from calculations is 6 hours (Fig. 2.13b).

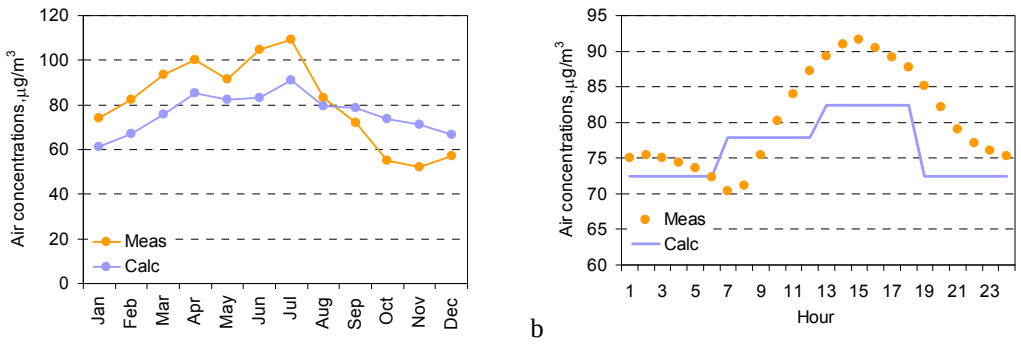

Fig. 2.13. *Time variation of ozone concentration in the air based on calculations and measurements at station IT0979A in 2006: a – annual variation (mean monthly concentrations); b – diurnal variation (hourly concentrations averaged over the whole of 2006), $\mu g/m^3$*

OH-radical

OH-radical is one of the important species in CMAQ chemical mechanisms. It is formed by photolysis and participates in oxidation of a number of pollutants. Calculated spatial distribution of annual averages of OH-radical concentrations in the atmosphere for 2006 is displayed in Fig. 2.14. It can be seen that concentrations of OH-radical in the air strongly depend on geographical latitude

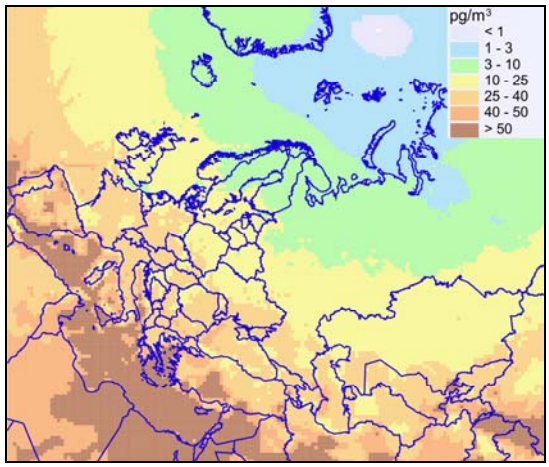

Fig. 2.14. *Spatial distribution of OH-radical concentrations in the surface air layer (averages for 2006), pg/m^3*

Time variation of OH-radical concentration in the air is illustrated in Fig. 2.15, where results of calculations are given the EMEP grid cell (69,35). As is seen maximum concentrations of OH take place in a summer period in day time.

In general results of modelling are in line with the common view on OH-radical behavior in the atmosphere. They are in reasonably good agreement with the available results of global calculations. It is evidenced, in particular, by mean annual zonally averaged OH concentrations given in Table 2.2, which were calculated by CMAQ and Global Change Research Program Atmospheric Chemistry Model (ACM) [*Bahm and Khalil,* 2004]. It is not possible to make more reliable assessment of the obtained data, since in 2006 regular measurements of OH-radical concentrations in the air were not performed in the EMEP region.

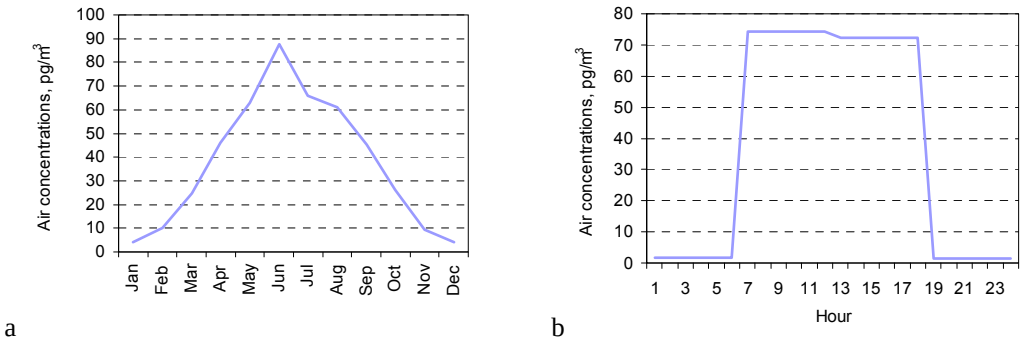

Fig. 2.15. *Calculated time variation of OH-radical concentration in the surface air in 2006 for the EMEP grid cell (69,35): a – annual variation (mean monthly concentrations); b – diurnal variation (hourly concentrations averaged over the whole of 2006), pg/m^3*

Table 2.2. *Zonally averaged mean annual OH-concentrations*

Latitude	Column mean concentrations (up to 14 km altitude), 10^5 mol/cm^3	
	ACM (global)	CMAQ (EMEP region)
65^0N	3.0	2.5
55^0N	3.8	4.3
45^0N	6.2	7.7
35^0N	9.6	12.6

Concluding remarks

So, to provide input data for regional modelling of HMs and POPs experimental calculations of particulate matter, sulphur dioxide, ozone and OH-radical atmospheric transport have been performed for 2006 at the extended EMEP grid using the CMAQ model. 6-hour time resolution data on concentrations of the above mentioned pollutants have been prepared. A brief analysis of these data allows the following conclusions to be made:

- The model underestimates PM10 concentrations in the air by 30% on the average. Air concentrations of PM2.5 are reproduced by the model with a reasonable accuracy. One of the possible reasons for CMAQ underestimation of coarse particles concentrations may be associated with the underestimation of dust emission in Europe.

- Calculations of SO_2 atmospheric transport are in fairly good agreement of measurements. CMAQ reproduces successfully both average levels of SO_2 concentrations in the air and their spatial distribution.

- The model overestimates ozone concentrations in the surface air by 15% on the average. To find the reasons of this overestimation a detailed analysis of the ozone chemical cycle is needed. Such analysis is planned to conduct next year.

- In general results of modelling of OH-radical atmospheric transport are in line with the common view on OH-radical behavior in the atmosphere and with the available results of global calculations. Currently it is not possible to assess the reliability of the obtained data since regular observations are not performed.

Chapter **3**

HEAVY METALS

This chapter is focused on the activities concerning heavy metals undertaken by MSC-E, including development of MSCE-HM model, preparation of input data and the analysis of calculated concentrations and depositions. EMEP domain was extended in order to completely cover the territories of the Central Asian countries (Kazakhstan, Kyrgyzstan, Turkmenistan, Tajikistan and Uzbekistan). The first model calculations of pollution levels of lead over the extended EMEP domain were carried for 2005 [*Ilyin et al.,* 2007]. Besides, pollution levels of lead for the Central Asian countries were evaluated in the framework of the CAPACT project [*Gusev et al,* 2007a]. This year the pollution levels over the extended grid for 2006 were evaluated for all three metals (Pb, Cd and Hg). In chapter significant attention was paid to the analysis of modelled concentrations and depositions with the observed parameters. Special attention was paid to preparation of input data for modelling. Sensitivity of model results to changes in input meteorological data was discussed. The study of the effect of the inclusion of shallow model layer was initiated and preliminary results were presented.

3.1. Input data for the extended EMEP domain

In order to include territories of the Central Asian countries, the EMEP domain was extended eastward (Fig. 3.1). Besides, significant area of Asian part of Russia was also covered by the extended domain. Significant work aimed at adaptation of the MSC-E models to the extended grid, including source code adjustments and modifications of input data was undertaken. This section describes the input data over the extended EMEP grid involved in modelling of atmospheric transport and depositions heavy metals.

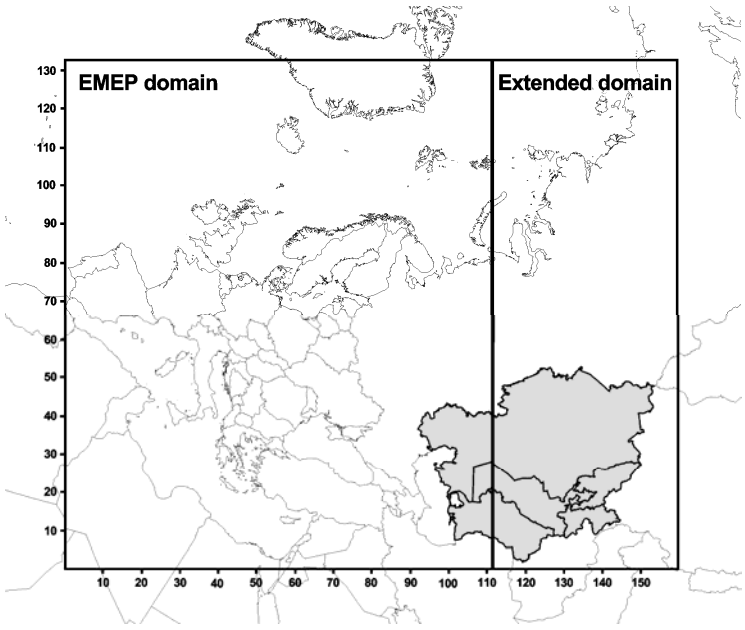

Fig. 3.1. *Extension of the model domain*

Emission

Emission data used in calculations of lead, cadmium and mercury are based on information, officially reported by EMEP Parties to the UN ECE Secretariat. If official emissions are not available, emission expert estimates were used. For countries which territories are covered entirely by so-called "old" EMEP domain, as well as for Kyrgyzstan, emissions of lead for 2006 were obtained by interpolation of emissions for 2000 and emission projections for 2010 available in TNO emission data set [*Denier van der Gon et al.*, 2005]. For Kazakhstan lead emissions were derived from the information, unofficially provided by national experts. For Turkmenistan, Tajikistan and Uzbekistan lead emissions were obtained from the GEIA global inventory [http://www.geiacenter.org/] for 1990 expecting the same emission reduction in these countries between 1990 and 2005 as in the Russian Federation according to the EMEP official data.

Emissions from the Asian part of Russia were assessed using official emission data for the European part of the country and keeping ratio between the European and Asian parts derived from the inventory [*Pacyna et al.,* 1995*;* http://www.ortech.ca/cgeic/index.html]. Besides, this inventory was used for other Asian and African countries, falling partly or fully into the modelling domain, assuming the same emission reduction between 1990 and 2005 as for Turkey. Turkey was selected for this purpose because it is the only country in Asia, for which TNO data on lead emission changes are available. Spatial distribution of lead emissions from all these countries was obtained by interpolation of GEIA gridded emissions with 1°×1° spatial resolution into the model grid.

Relatively high emission flux (more than 5 kg/km^2/y) is noted for some regions in central and south-eastern part of Europe, e.g., southern part of Poland, north of Italy, the Balkan region, eastern part of Ukraine (Fig. 3.2a). In the Central Asian region the highest lead emissions were estimated for the southern part of Kazakhstan and eastern part of Uzbekistan. High emission fluxes were obtained for populated regions of Africa and Asia, e.g., Algeria, Tunisia, Israel etc. However, these data are very uncertain and should be looked with caution.

Mercury emissions for Turkmenistan, Tajikistan, Uzbekistan, Kazakhstan, Kyrgyzstan, east of Russia, and Asian and African countries were derived from global mercury emission field for 2000 [*Pacyna et al*., 2006 http://amap.no/Resources/HgEmissions/]. It was assumed that the emissions were constant between 2000 and 2006. Cadmium emission in these regions were assumed to be proportional to emissions of mercury: $E_{Cd} = \alpha \cdot E_{Hg}$. For eastern part of Russia the proportionality coefficient (α) was 1.14, as that for European part. The factor for the three Central Asian countries was assumed to be the same as that for Kyrgyzstan and equaled to 0.56. For other Asian countries and Africa the factor as assumed to be the same as that for Turkey [*Denier van der Gon et al.*, 2005] and it was equal to 0.91. Keeping in mind high uncertainty of this approach the derived emissions data can be considered as a pilot dataset for research purposes. To improve quality of emissions data in the Central Asian region close co-operation with national experts is required.

Spatial distribution of cadmium emissions is highly inhomogeneous (Fig. 3.2b). Poland is characterized by the highest emission fluxes (30 – 300 g/km^2/y). Other regions with relatively high emissions are southern part of Russia, north of Italy, Spain, the Balkan counters, the Benelux region. In the Central Asia the region with elevated emissions are noted for the north and south of Kazakhstan. Some spots of elevated emissions of cadmium are noted for the eastern part of Russia.

Relatively high emission fluxes of mercury are indicated for Poland, north of Italy, southern part of the United Kingdom, the Balkans region (Fig. 3.2c). Since the proportionality between cadmium and mercury

emissions were assumed for Central Asia region and for the eastern part of Russia, comparatively high mercury emissions are noted for the northern and southern parts of Kazakhstan and the eastern part of Russia.

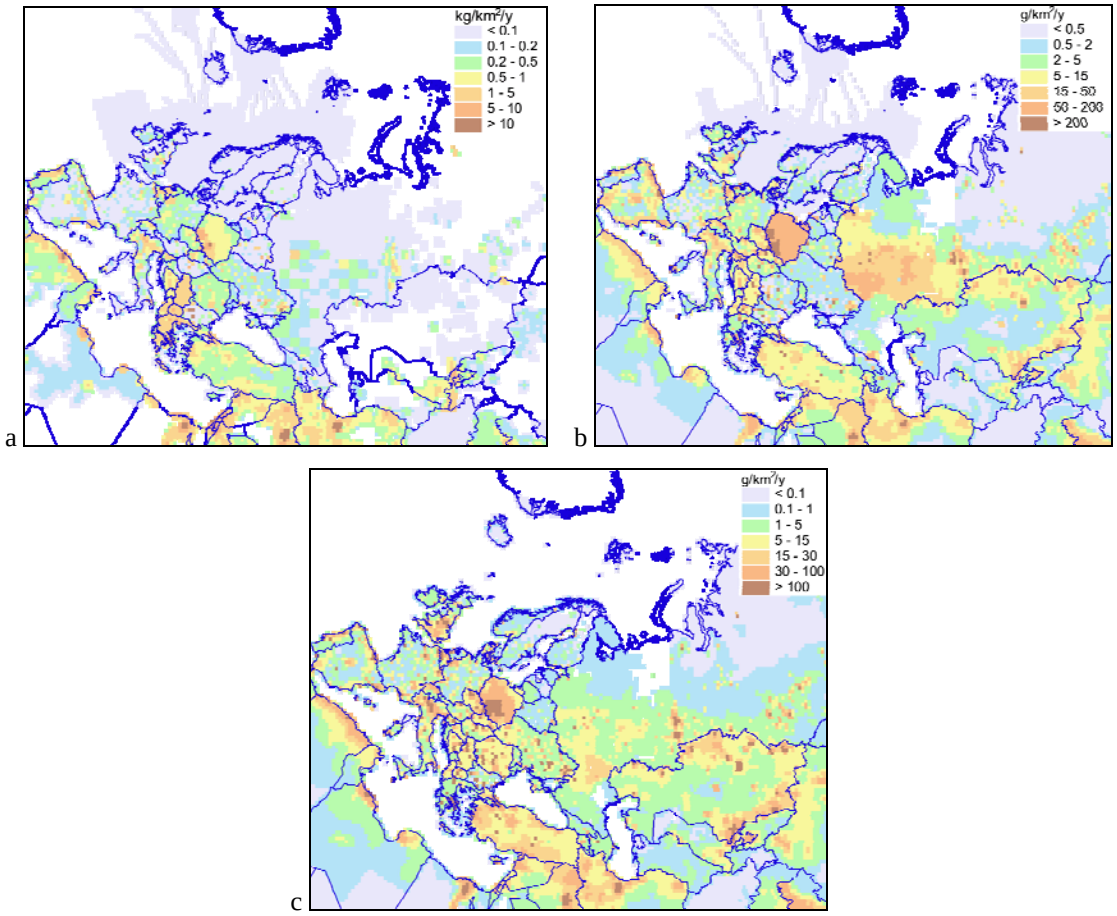

Fig. 3.2. *Spatial distribution of lead, kg/km^2/y (a), cadmium, g/km^2/y (b) and mercury g/km^2/y (c) emissions over the extended EMEP domain in 2006*

Land cover

Land cover data is required for evaluation of the dry deposition velocities and assessment of ecosystem-specific depositions. Currently a preliminary land cover dataset developed within the Working Group of Effects (WGE) for the Convention is used in the model. The dataset consider 17 land-use/land-cover categories listed in Table 3.1.

The WGE land-cover distribution dataset was developed for the standard EMEP domain (135x111 grid cells). The extension of the modelling domain caused a necessity to provide land-cover distribution for the extended area. For this purpose a global land-cover dataset prepared by Geological Survey of the United States (USGS) was utilized [*Guo and Chen,* 1994, http://edcsns17.cr.usgs.gov/glcc/]. This data contain spatial distribution of 24 land cover types with 10'x10' spatial resolution. It is worth noting that

nomenclature of the USGS land-cover data differs from that provided by WGE. In order to adjust the USGS data to the nomenclature of WGE some assumptions were used (Table 3.1).

Table 3.1. *Combination of WGE and USGS land-cover types (for the extension of the modelling domain)*

WGE types	USGS types
1. Temperate coniferous forest	Deciduous needleleaf forest Evergreen needleleaf forest Mixed forest
2. Temperate deciduous forest	Deciduous broadleaf Evergreen broadleaf Shrubland (if latitude >55°N)
3. Mediterranean needleleaf forest	n/a*
4. Mediterranean broadleaf forest	n/a
5. Temperate crops	Dryland crops and pastures Irrigated crops and pastures Mixed Dry/Irrigated crops and pastures Cropland / Grassland mosaic Cropland / Wood mosaic
6. Mediterranean crops	n/a
7. Root crops	n/a
8. Grasslands	Grassland Mixed shrubland/grassland Savanna
9. Wheat	n/a
10. Semi-natural	n/a
11. Mediterranean scrub	Shrubland (if latitude <55°N)
12. Wetlands	Herbaceous wetlands Wooded wetlands
13. Tundra	Herbaceous tundra Wooden tundra Mixed tundra Bare ground tundra
14. Desert/Barren	Bare or sparse vegetation
15. Water	Water bodies
16. Ice	Snow or Ice
17. Urban	Urban

* - not available in USGS data base

Wind re-suspension

Wind erosion and heavy metal re-suspension from soil strongly depends on soil properties such as size distribution of soil grains and heavy metal content in the upper soil layer. To derive spatially resolved data of soil size distribution we utilized global soil characteristics dataset from the International Satellite Land-Surface Climatology Project (ISLSCP), Initiative II [http://islscp2.sesda.com]. Different soil types were classified according to the classic sand/silt/clay triangle of texture composition [*Hillel*, 1982]. Resulting spatial distribution of different soil types in Europe and Central Asia is presented in Fig. 3.3. As seen, according to this data, loam soils prevail over Central and Eastern Europe, whereas Southern Europe is dominated by clay loam. Sandy soils are characteristics of Africa and Central Asia.

For estimation of heavy metal emission with dust suspension from soils detailed measurement data on heavy metals concentration in topsoil from the Geochemical Atlas of Europe developed under the auspices of the Forum of European Geological Surveys (FOREGS) [*Salminen et al.,* 2005; www.gtk.fi/publ/foregsatlas/] were used. The kriging interpolation was applied to obtain spatial distribution of heavy metal concentration in soil. For the eastern part of Europe, Central Asia and for the rest of the model domain we used default concentration values of lead (15 mg/kg) and cadmium (0.2 mg/kg) and based on the literature data [e.g., *Riemann and Caritat,* 1998].

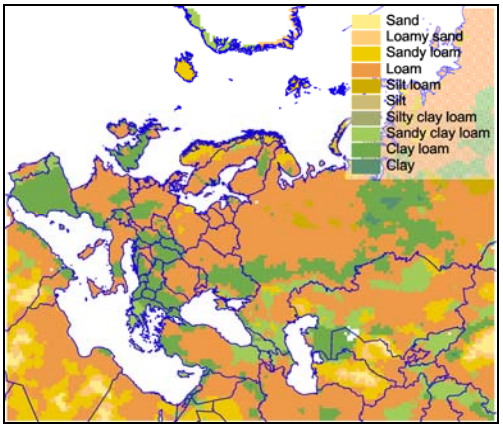

Fig. 3.3. *Spatial distribution of soil texture types in Europe and Central Asia*

The soil properties data were used for evaluation of lead re-suspension because of wind erosion. Spatial distribution of wind re-suspension fluxes of lead and cadmium from European and Central Asian soils and from seawater in 2006 are presented in Fig. 3.4. Lead and cadmium re-suspension from soil is presented for dust particles size below 10 μm (PM10). As seen the most significant re-suspension fluxes of lead and cadmium were obtained for central, western and southern parts of Europe and some areas in Africa and Central Asia (Fig. 3.4 a,b). In Europe the elevated fluxes of lead and cadmium are resulted from combination of relatively high concentration in soil and significant dust suspension from agricultural and urban areas. Whereas high natural fluxes of lead and cadmium in African and Central Asian desert areas are conditioned by significant mineral dust suspension. In the Central Asian countries elevated lead and cadmium natural emission or re-suspension fluxes are characteristics of Karakum and Kyzylkum deserts and some urban areas.

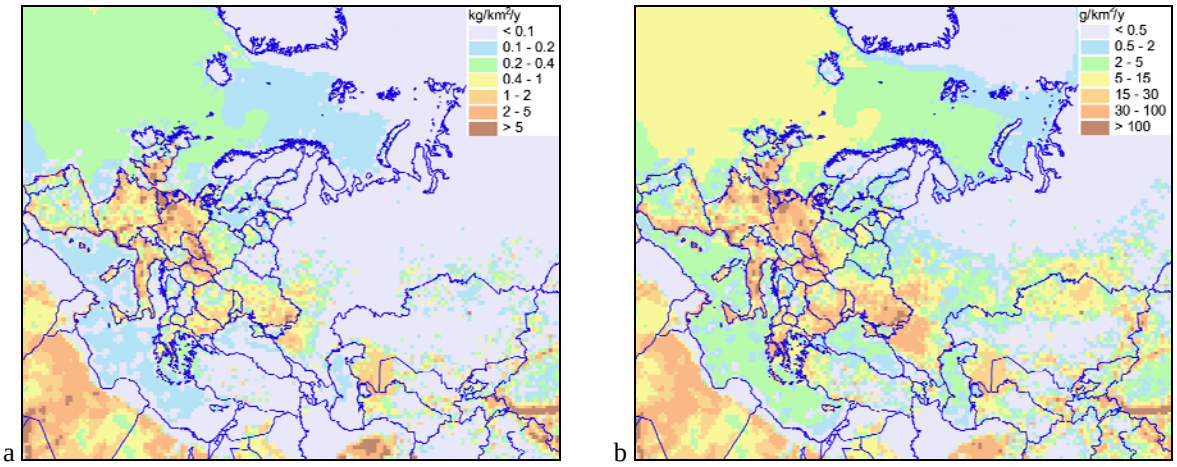

Fig. 3.4. *Spatial distribution of lead, kg/km^2/y (a) and cadmium, g/km^2/y (b) re-suspension flux from soil and seawater in 2006 in the extended modelling domain*

Chemical reactants

For calculations of chemical transformations of mercury in the atmosphere MSCE-HM model involves input data on a number of reactants. These are air concentrations of SO_2, OH radical and ozone. Monthly mean three-dimensional concentrations SO_2 and O_3 were originally calculated by global-scale model MOZART. For hydroxyl radical in the atmosphere modelled monthly mean concentrations based on [*Spivakovsky et al.*, 2000] were used. Global-scale three-dimensional concentrations of SO_2, ozone and hydroxyl-radical were interpolated to the extended EMEP domain. Similar information was prepared by CMAQ model, as described in chapter 2 of this report. However, in the model calculations for 2006 these data have not been used yet.

Annual mean concentrations of sulphur dioxide in surface air vary from 0.2 to 10 ppbv (Fig. 3.5a). The highest levels (>10 ppbv) take place over central part of Europe. Over Central Asian countries the concentrations are low (0.2 – 2 ppbv) compared to those in Europe. In the eastern part of Russia and mountainous regions of Central Asia (Kyrgyzstan, Tajikistan) the levels can lie below 0.2 ppbv. The concentrations of SO_2 tend to decrease rapidly with altitude (Fig. 3.5b). In the first two km the concentrations over clean oceanic environment (averaged along line i = 20) decrease twice, and over polluted area (along line i = 75) – around 10 times relative to the near-surface values.

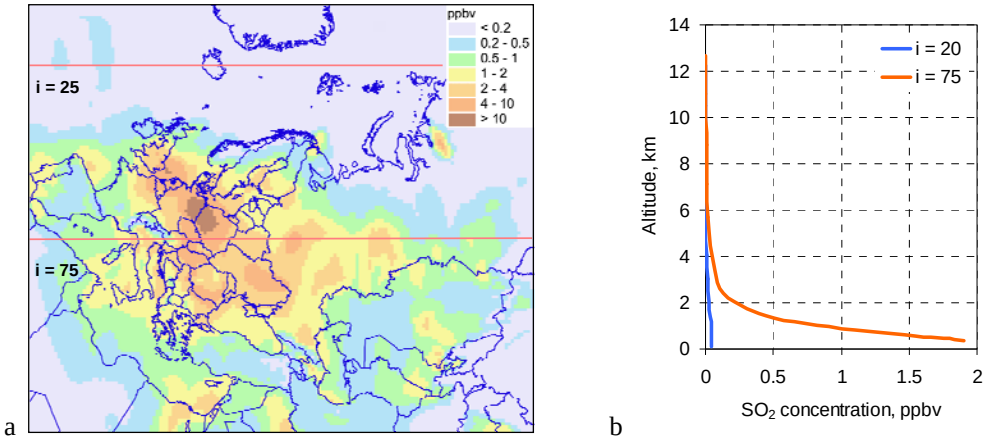

Fig. 3.5. *Annual mean concentration of SO_2 in the surface air (a) and vertical profiles along i = 20 and i = 75 (b)*

Annual mean concentrations of ozone in the surface air distributed highly unevenly over the EMEP domain. Over northern and central part of Europe the concentrations range from values below 30 ppbv to 40 ppbv (Fig. 3.6a). Over southern part of Europe and the Mediterranean the concentrations are much higher and can reach 60 ppbv, which is caused by higher solar radiation over these regions. In central Asia the concentrations are relatively low over lowlands, e.g., 30 – 40 ppbv over most pf Kazakhstan and 35 – 45 ppbv over Turkmenistan and Uzbekistan. In mountainous regions (Kazakhstan, Tajikistan) the concentrations can exceed 60 ppbv. Along vertical the ozone concentrations tend to moderately increase up to 8 – 10 km height and rapidly grow above 10 km height (Fig. 3.6b).

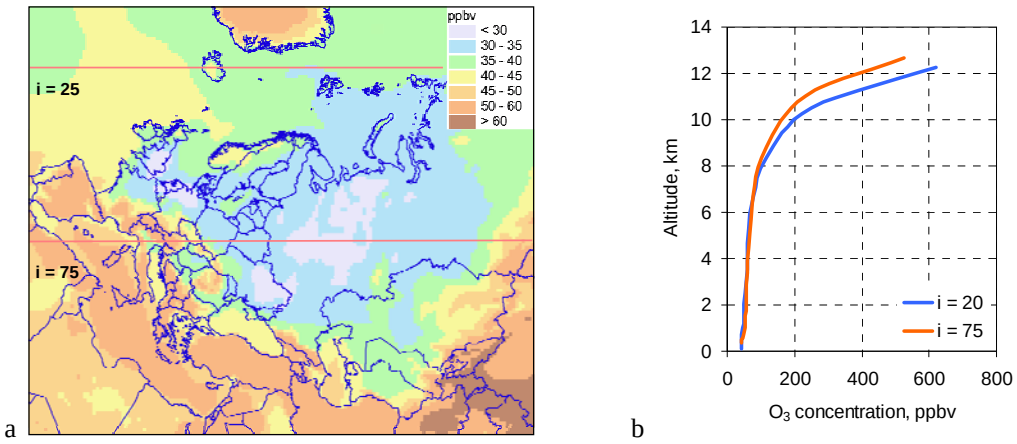

Fig. 3.6. *Annual mean concentration of ozone in the surface air (a) and vertical profiles along i = 20 and i = 75 (b)*

Annual mean concentrations of OH-radical in surface air decrease from 0.06 – 0.08 pptv to values below 0.01 pptv in the northward direction (Fig. 3.7a). Along latitudes the concentrations do not vary much. Elevated concentrations exceeding 0.08 pptv are indicated over mountain regions such as the Alps, Caucasus, highland regions of the Central Asia. Concentrations of hydroxyl- radical decreases with height (Fig. 3.7b). Local increase in concentrations averaged over line i = 75 are explained by the fact that the line crosses the Alps, where the concentrations are elevated.

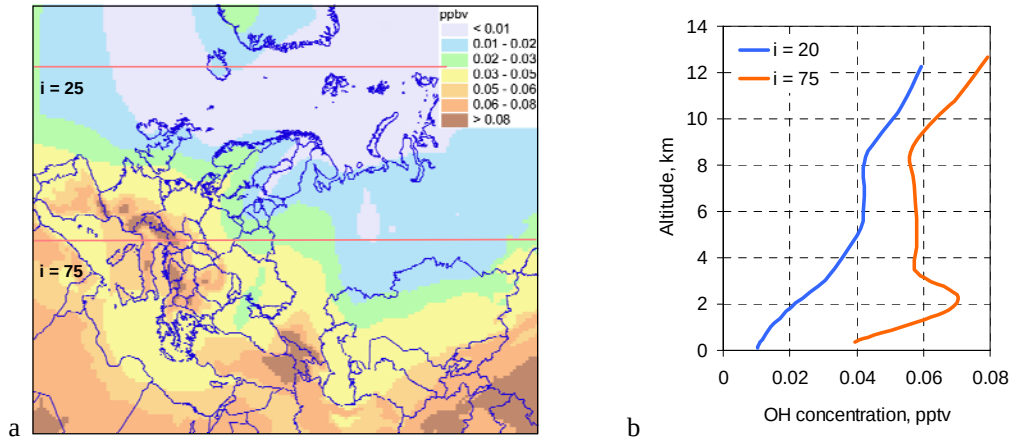

Fig. 3.7. *Annual mean concentration of OH–radical in the surface air (a) and vertical profiles along i = 20 and i = 75 (b)*

3.2. Model sensitivity to refining of vertical structure

In order to improve MSCE-HM model performance in modelling of concentrations in air TFMM recommended inclusion of shallower lowest model layer. The experimental activity on this refinement of vertical model structure was initiated. Two experimental calculations of concentrations and depositions of lead were carried out. In the first experiment (run #1) standard vertical discretization of MSCE-HM model was used. In the second one (run #2) the lowest layer (around 70 m depth) of the model was split in two almost equal sub-layers. The same changes in the vertical structure were carried out in MM5 modelling

system in order to prepare meteorological input data for run #2. In the standard version of MSCE-HM model pollutants are emitted into three lowest model layers. It was assumed that the emission values entering the first (lowest) layer in the run #1 are split in two equal parts for the run #2. Obviously, total amount of lead, emitted into the atmosphere by anthropogenic sources is the same in both experiments. Other input model data (e.g. land-cover) and process parameterizations (e.g., dry deposition) were the same in the two experimental runs. Calculations were carried out for January, 2006. In order to investigate the effect of anthropogenic sources on the near-surface concentrations, the re-suspension of lead was switched off.

Figure 3.8(a,b) demonstrates maps of spatial distribution of monthly mean lead air concentrations simulated by the experiments #1 and #2. Magnitudes and spatial pattern of the concentrations calculated in run #2 are very similar to those obtained by run #1. Relative bias between the two concentration fields, evaluated as $(C_{run2} - C_{run1})/C_{run1}$ x 100%, vary in different parts of the EMEP domain. Over central and north-eastern part of Europe (Scandinavian Peninsula, Poland, Germany, Russia, Belarus) the bias is negative and can fall below -50%, indicating the decrease of the concentrations if shallow lowest layer is introduced (Fig. 3.9a). In the southern part of Europe, Atlantic and most of part of Central Asia the bias is -25 - 0%. It is worth mentioning that the areas with large negative bias are very similar to the areas covered by forests (Fig. 3.9b). The increase of concentrations is noted for regions with significant emission sources (e.g, east of Ukraine, Benelux region, north of Italy). On average, the concentrations due to the refinement of vertical structure decrease by 15% over Europe and Central Asia.

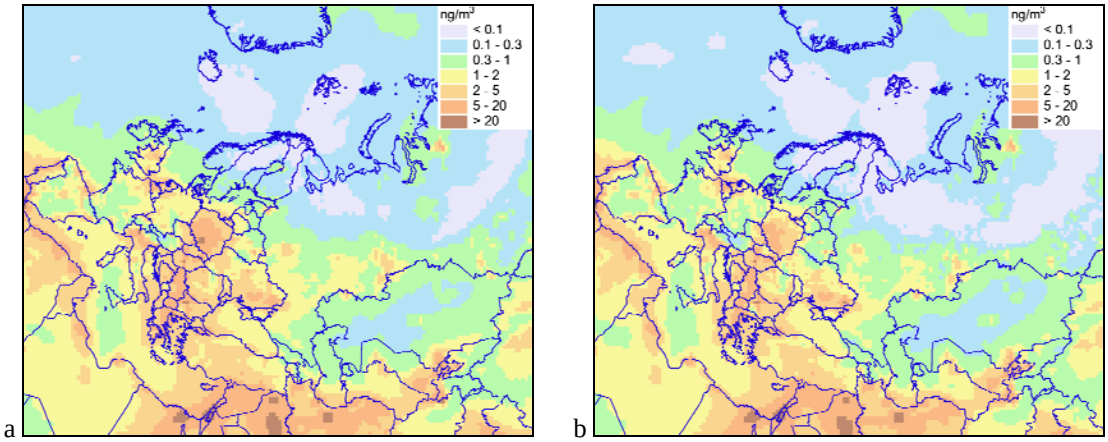

Fig. 3.8. *Monthly mean concentrations of lead in near-surface air calculated on the base of standard vertical discretization (run #1) (a) and shallow lowest model layer (run #2) (b) in January, 2006, ng/m^3*

Similar to air concentrations, spatial distributions of total depositions of lead calculated in run #1 and run #2 look quite similar (Fig. 3.10a,b). Both runs produce high deposition fluxes over the central and southern parts of Europe, and low depositions over eastern part of the EMEP region. Deposition magnitudes computed in run #2 (shallow first layer) are lower over most of the extended EMEP domain (Fig. 3.10c). The increase of depositions due to the refinement of the vertical structure takes place in regions known for significant emission sources, such as southern part of Poland, north of Italy, Benelux, the east of Ukraine, Moscow and Urals regions of Russia etc. On average, total depositions in Europe and Central Asia decrease by 1.5% because of the refinement of the vertical structure of the model.

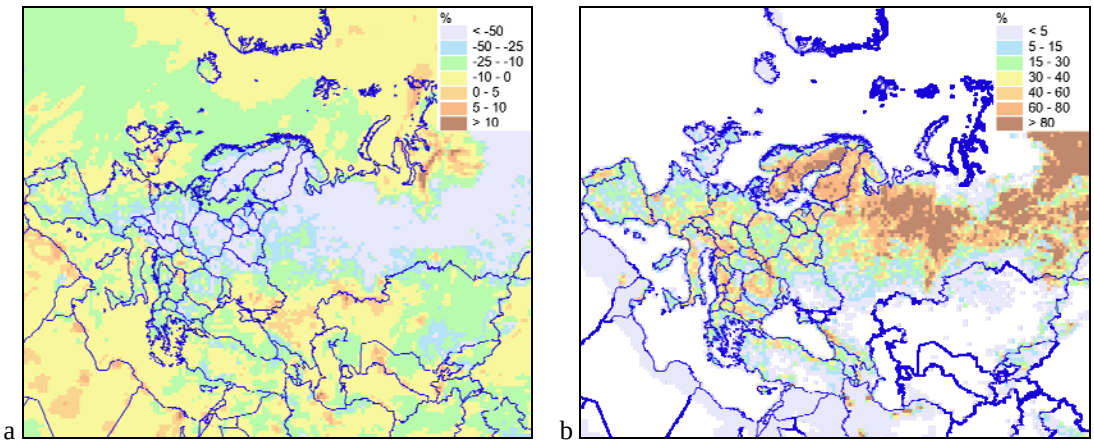

Fig. 3.9. *Relative bias between the concentrations obtained in the two model runs (Crun2 – Crun1)/Crun1 x 100%, % (a) in January, 2006 and map of gridcell fraction covered by forests (b), %*

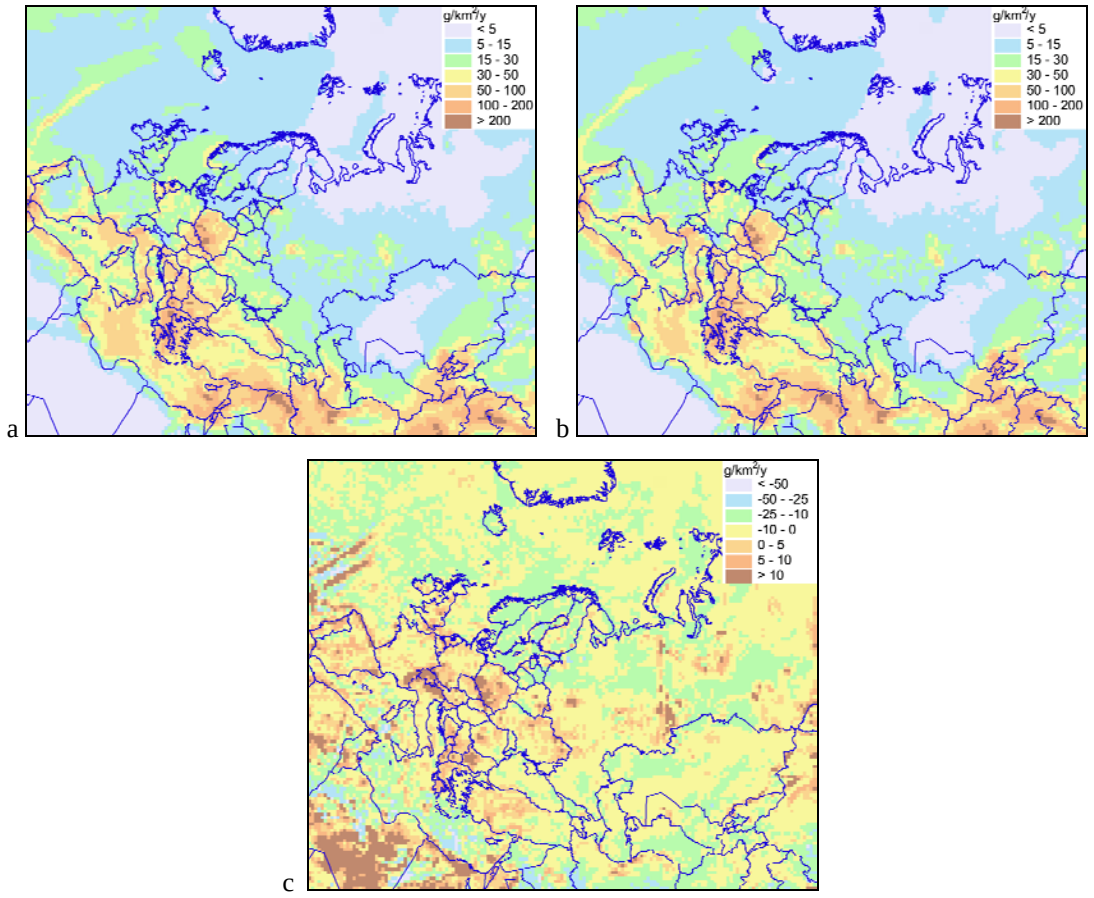

Fig. 3.10. *Monthly total depositions of lead calculated on the base of standard vertical discretization (run #1) (a), shallow lowest model layer (run #2) (b), g/km^2/y, and relative bias between the depositions obtained in the two model runs (Drun2 – Drun1)/Drun1 x 100%, % (c) in January, 2006*

From the comparison of concentration and deposition fields obtained in two experiments it is seen that the refinement of vertical structure led to the decrease of pollution levels over most of EMEP domain. Only in some regions where large emission sources are located, the concentrations and depositions increased. The effect of refinement of the lowest model layer was studied in more detail using vertical profiles of the concentrations at different locations.

Concentrations at point (91, 72) in the eastern Ukraine increased by 5% due to the refinement of vertical structure (Fig. 3.11a). Significant emission sources are located in this point. Another example of the profile in polluted location is grid point (74, 57) in south-western Poland (Fig. 3.11b). Although this point is also characterized by significant emission, the expected increase of concentrations did not occur. It is believed that the reason for this is considerable (around 30% of grid cell area) fraction of forests in this gridcell. According to the model parameterization, dry deposition velocity over forested areas is much higher than that over low vegetation areas. The two-fold decrease of the lowest vertical layer leads to the fact that much finer layer of air was involved in dry deposition removal. Besides, the finer layer means the smaller distance between the middle of the layer and the top of forest canopy. This, in turn can favors the reduction of aerodynamic resistance and hence, the increase of dry deposition velocity. Indeed, the total deposition flux at this point increased by about 20%. For comparison, the mentioned above grid point in the eastern Ukraine has no forests at all, according to land cover map applied in modelling, and depositions increased only by 5%. It is also possible that in case of high vegetation the dry deposition scheme used in MSCE-HM model may be not applicable to so shallow lowest model layer. However, this question requires additional consideration.

In the remote regions where anthropogenic emissions are minor or absent, the refinement of vertical structure leads to the decrease of air concentrations along the whole profile (Fig. 3.11 c,d). The refinement of the lowest model layer results in the increase of removal of pollutant mass from the atmosphere over emission regions due to deposition. Therefore, the mass of pollutants carried by long-range transport to remote regions decreases. Over regions without high vegetation the decrease of surface air concentrations because of the refinement is relatively small (Fig. 3.11c). Over the forested gridcells (e.g., in Finland, Fig. 3.11d) the decrease is rather high.

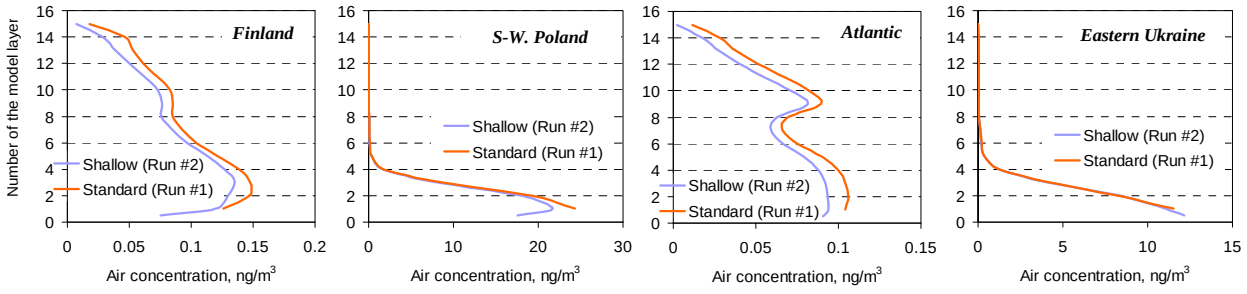

Fig. 3.11*. Vertical profiles of air concentrations of lead derived in the two experiments from individual points in Eastern Ukraine (a), South-western Poland (b), Atlantic Ocean (c), and Finland (d)*

The refinement of the lowest model layer was intended to overcome the underestimation of measured air concentrations due to the expected increase of calculated concentrations. The performed experiments demonstrated that the increase of the concentrations takes place only over polluted regions. In addition to

this, even over pollution regions the increase does not occur if the region is covered by forests. Over the remote regions the concentrations in air decrease. One possible reason for this is substantial increase of dry deposition caused by the refinement. It is possible, that the description of the atmospheric processes in surface layer, in particular, dry deposition to forests, are not applicable for so fine vertical resolution. Besides, the experimental vertical distribution of emissions probably needs revision. Emission value entering the first model layer at standard vertical structure was split in two equal parts. Probably, if the higher fraction of emissions is assumed to enter the lowest shallow layer, the results of the experiment could be different.

The changes in the model performance can be evaluated via comparison of modelled quantities with the observed values. In order to study the effect of the refinement of lower model layer the experimental runs were repeated including wind re-suspension. Similar to previous experiments run #1 refers to the case of standard vertical structure, and run #2 – to the case with shallow lowest model layer. The comparison between monthly mean concentrations in air modelled in the experiments and the observed ones at EMEP stations is demonstrated in Fig. 3.12. As seen, the model results, computed in case of shallow first model layer (Run #2) are lower compared to the results based on the standard discretization (Run #1). The bias between the two results is within ±30% for the 70% of run#1 – run#2 pairs of values. On average, the bias is almost -10%. It is shown in the section of 3.4 of this report that MSCE-HM model tends to underestimate measured air concentrations of lead. As seen from the Figure, only at eight stations (among 33) the concentrations calculated in run #2 are higher than those of run #1, whereas for the rest stations they are lower. Therefore, no distinct improvements in modelled air concentrations after reducing the depth of the lowest model layer are identified.

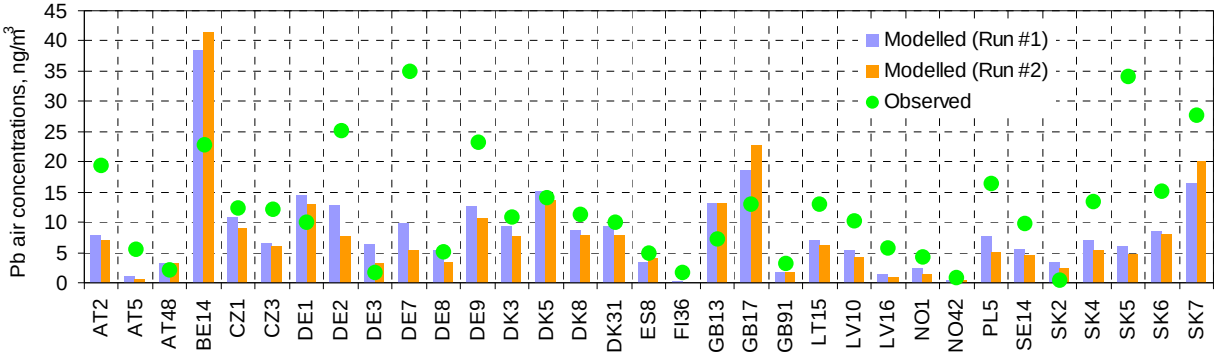

Fig 3.12. *Monthly mean air concentrations of lead calculated by the two experimental runs and observed at EMEP monitoring stations in January, 2006. Run #1 – standard vertical discretization, Run #2 – discretization with shallow lowest model layer, ng/m^3*

The bias between concentrations in precipitation calculated in run #1 and run #2 is within ±20% (Fig.3.13). On average, the concentrations obtained in run #2 (shallow lowest layer) are about 4% lower than those from run #1. The differences in concentrations in precipitation are significantly lower than those found for concentrations in air. It is not surprising because air concentrations for the analysis are extracted from the lowest model layer, because measurements are also carried out directly in the surface layer. Wet depositions and concentrations in precipitation are formed because of wet scavenging through the entire atmospheric column from precipitation level to the surface. Therefore, the response on the changes in vertical discretization is more pronounced for surface air concentrations rather then concentrations in precipitation.

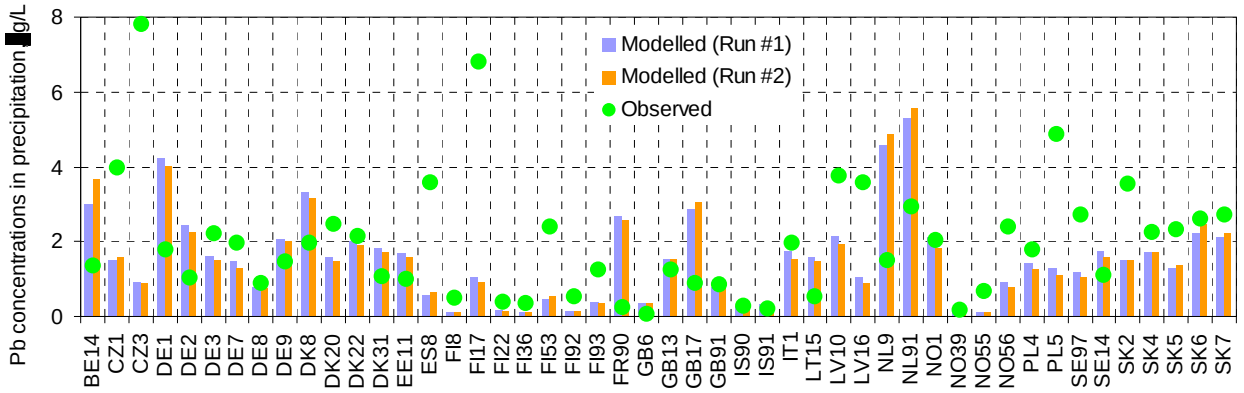

Fig. 3.13. *Monthly mean concentrations of lead in precipitation calculated by the two experimental runs and observed at EMEP monitoring stations in January, 2006. Run #1 – standard vertical discretization, Run #2 – discretization with shallow lowest model layer, µg/L*

The experiment with reducing thickness of the lowest model layer demonstrated that the reduction leads to some decrease (15%) of air concentrations and the decrease of depositions about 1.5% over the European and the Central Asian countries on average. However, over smaller-scale regions the changes can be higher. The comparison of the results based on the two experiments at monitoring stations demonstrated that the reduction of lowest model layer does not lead to evident improvement of the model performance. However, these are preliminary results, and further investigations are needed.

3.3. MSCE-HM model sensitivity to different sets of input meteorological data

Changes in input meteorological data lead to differences in output sets of meteorological parameters simulated by MM5. This, in turn, should cause differences in pollution levels (e.g., air concentrations, depositions, etc.) computed on the base of these different sets of meteorological information. Concentrations and depositions of lead and mercury were computed by MSCE-HM model on the base of two data sets of meteorological data. The first one is based on ECMWF analyses and the second one – on the base of NCEP/DOE re-analysis for 2006. All other input parameters such as anthropogenic emissions, wind re-suspension etc. were the same. This section is focused on the analyses of differences in model results obtained by these two experimental model runs.

The use of ECMWF data resulted in higher concentrations over most of Europe and adjacent water bodies (the Mediterranean Sea, the Black Sea, north-east of the Atlantic etc). Relative bias between mean annual air concentrations of lead over the European and Central Asian countries (Kazakhstan, Kyrgyzstan, Uzbekistan, Tajikistan and Turkmenistan) is 2.6%, over the Atlantic – around 10%, over the Mediterranean – almost 15% (Fig. 3.14a). Over some areas the bias can make up ±25%. Over the Arctic and some regions of Central Asia the concentrations based on ECMWF are lower, compared to those based on NCEP/DOE.

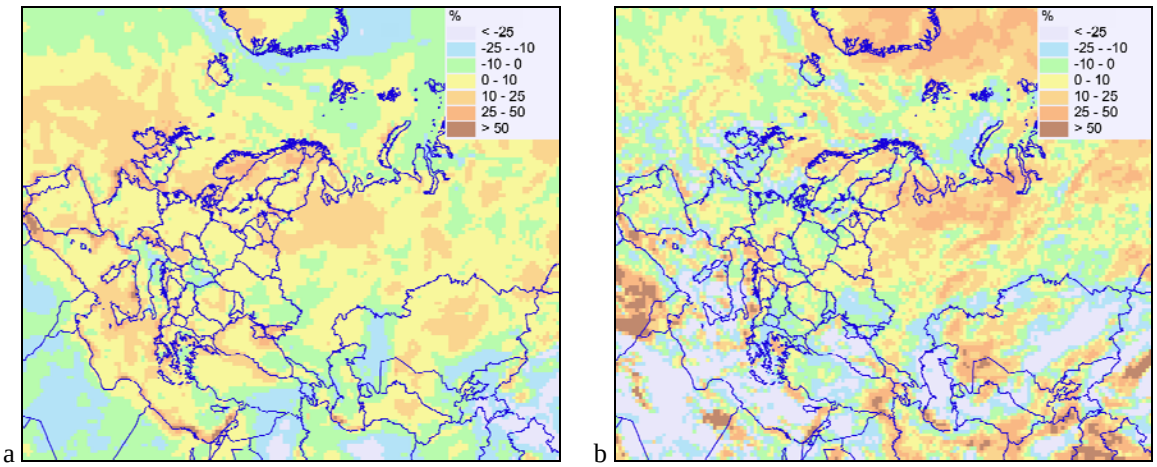

Fig. 3.14. *Relative differences for annual mean air concentrations (a) and total depositions (b) of lead, computed on the base of ECMWF analyses and NCEP/DOE re-analyses, %*

Atmospheric depositions over central and western Europe, modelled on the base of ECMWF analyses are generally similar to those based on re-analysis: The relative bias is within ±10% (Fig. 3.14b). The depositions based on ECMWF data are on average 0.7% lower over European and Central Asian countries, and about 1% higher over the Atlantic than those based on NCEP/DOE. In some regions, e.g., over the eastern part of Europe, the Arctic, north of Atlantic and the western part of Kazakhstan ECMWF-based depositions exceed, and over the Mediterranean, Caspian and Black Seas, the British Isles, and east of Kazakhstan lie 25 – 50% below those based on NCEP/DOE re-analysis.

The change of meteorological data resulted in positive change in concentrations and simultaneous negative change in depositions (or vice versa) over some regions. The most evident examples are the Arctic, the British Isles, the Black and Mediterranean Sea, north of the Atlantic, eastern part of Kazakhstan. The bias in calculated depositions over these areas are most probably caused by differences in precipitation amounts predicted by MM5 (Fig. 1.12a). Higher precipitation lead to higher depositions and lower air concentrations, and vice versa. However, over some other regions, e.g., north of European part of Russia or Scandinavian Peninsula, both air concentrations and total depositions, calculated on the base of ECMWF data, are higher than those on the base of NCEP/DOE data. In this case the changes of the pollution levels can be explained by differences in atmospheric transport patterns, atmospheric stability, and other parameters.

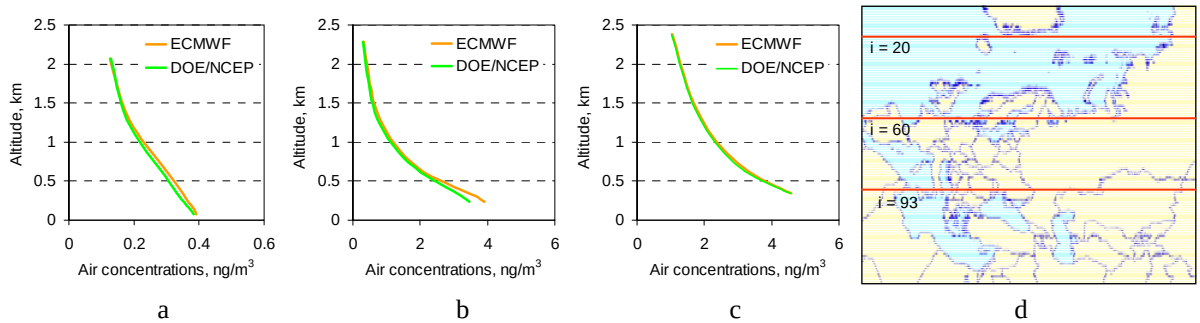

Fig. 3.15. *Vertical profiles of annual mean concentrations of lead, averaged along lines with EMEP coordinate i = 20 (a), i = 60(b) and i = 93(c), and map with location of the lines (d)*

Analysis of vertical distribution of air concentrations was performed for three profiles cutting EMEP area along EMEP i-coordinate equal to 20, 60, and 93. The first profile characterizes background conditions mostly over the oceans, the second and third ones – continental part of Europe. The most remarkable differences between air concentrations based on ECMWF and NCEP/DOE data were found nearby surface, while above the height of around 2.5 km or higher the differences are negligible (Fig. 3.15). As seen, the use of ECMWF data causes somewhat higher near-surface concentrations of lead, compared to NCEP/DOE.

Performance of a numerical model is evaluated via comparison of modelled quantities with measurement data. That is why comparison of concentrations in air and in precipitation modelled on the base of the two different input meteorological data sets at monitoring stations, was performed.

The relative difference between annual mean calculated air concentrations of lead is not very high (Fig. 3.16). For almost 90% of stations relative bias does not exceed 20%, and for 70% of stations – 10%. On average, the concentrations based on ECMWF are 7% higher than those based on NCEP/DOE. The differences between monthly mean values are somewhat higher compared to annual means. However, for 90% of stations the bias is less then 25%. The comparison of monthly mean values based on the two meteorological data revealed, that for more than 90% of pairs of values the bias is within ±30%.

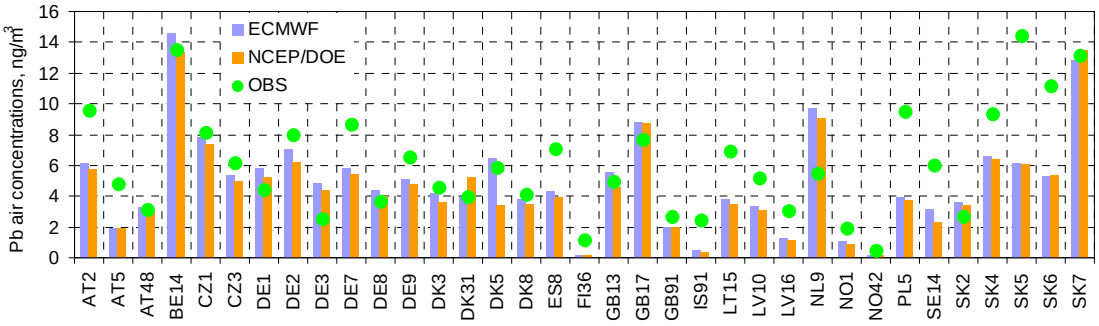

Fig. 3.16. *Annual mean air concentrations of lead modelled on the base of ECWMF analysis and NCEP/DOE re-analysis and observed at EMEP stations in 2006, ng/m^3*

Similar results were obtained for concentrations in precipitation (Fig. 3.17). For about than 90% of stations the relative bias between concentrations in precipitation based on ECMWF and NCEP/DOE is below 20%. When ECMWF input data are used, the model tends to simulate somewhat higher concentrations in precipitation and wet deposition fluxes compared to the case when NCEP/DOE data are involved. The average difference between the concentrations at the stations is around 10%, and for wet deposition fluxes – 2.5%. The bias for monthly mean concentrations in precipitation is about 35% for 90% of stations. The difference between the monthly-mean concentrations in precipitation is within ±30% for about 70% of pairs of the values.

As seen from Figures 3.16 and 3.17, MSCE-HM modelled concentrations are lower than measured ones. Therefore, higher concentrations calculated with the use of ECMWF data compared to those based on NCEP/DOE re-analyses, favours better agreement between measurement and modelling results. However, more detailed analysis of the model verification is presented in chapter 3 of this report.

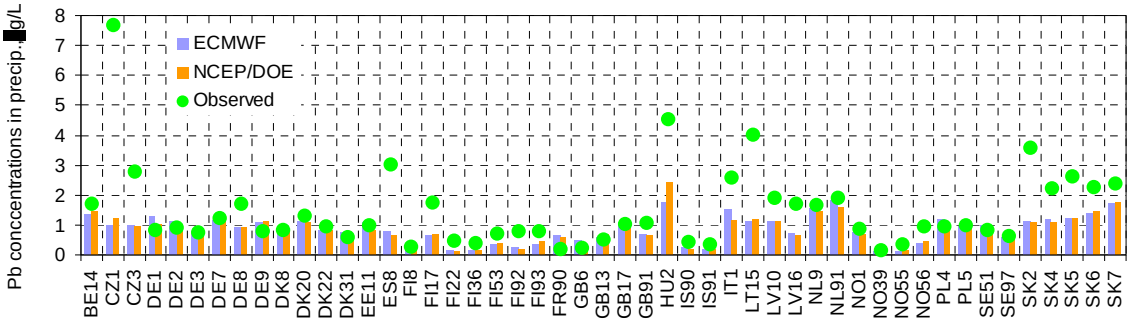

Fig. 3.17. *Annual mean concentrations of lead in precipitation modelled on the base of ECWMF analysis and NCEP/DOE re-analysis, µg/L*

The results of analysis of differences in computed depositions and concentrations of lead are in general applicable to other airborne aerosol metals, e.g., cadmium. However, mercury is a special case. Unlike lead or cadmium, it is characterized by much longer atmospheric life time, and by occurrence in the atmosphere in different physical-chemical forms. Therefore, similar comparison was carried out for concentrations of Total Gaseous Mercury (TGM) concentrations and total depositions of mercury.

Relative bias between TGM concentrations is relatively small over most of EMEP domain and ranges within ±1.5% (Fig. 3.18a). It is not surprising because modelled TGM concentrations are mainly controlled by transport through the domain borders. Boundary concentrations of mercury were the same for the both model runs, and differences in wind patterns in free troposphere were not very high.

Depositions of mercury are mainly formed by gaseous oxidized and particulate forms of mercury. The spatial distribution of relative bias in mercury depositions is similar to that of lead (Fig. 3.18b, 3.14b). Total depositions, computed for European and Central Asian countries on the base of ECMWF data are on average about 3% higher than those based on NCEP/DOE re-analyses. Over the Atlantic the relative bias is about 1%, and over Mediterranean – about 20%. Over some regions over the Arctic, Mediterranean and Central Asia the bias can exceed 50%. The reasons explaining the spatial distribution of the relative bias are most likely similar to these for lead.

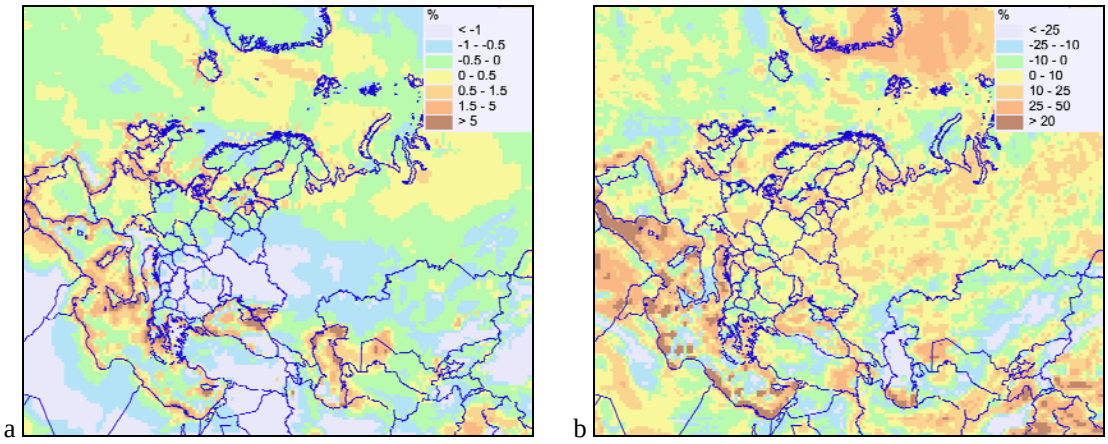

Fig. 3.18. *Relative bias for annual mean total gaseous mercury concentrations (a) and total depositions of mercury (b), computed on the base of ECMWF analyses and NCEP/DOE re-analyses, %*

Annual mean concentrations of TGM at monitoring stations, calculated on the base of ECMWF and NCEP/DOE meteorological data differ by less then 3%. Relative bias for monthly mean values is less then 5%. The bias for annual mean mercury concentrations in precipitation is within 20%, except for two stations, and reaches 30% if all stations are considered (Fig. 3.19). Similar to lead, the use of ECMWF input data leads to 13% higher concentrations in precipitation compared to NCEP/DOE re-analysis, and to 1% lower wet deposition flux, averaged over the available stations. This is explained by lower precipitation amounts simulated by MM5 for the stations if ECMWF analyses are used as input data compared to the NCEP/DOE re-analysis: Mean predicted precipitation sums for these stations are 780 mm (ECMWF) versus 900 mm (NCEP/DOE). Similar to lead, the use of ECMWF meteorological data leads to somewhat better agreement between modelled and measured mercury concentrations in precipitation compared to NCEP/DOE re-analyses.

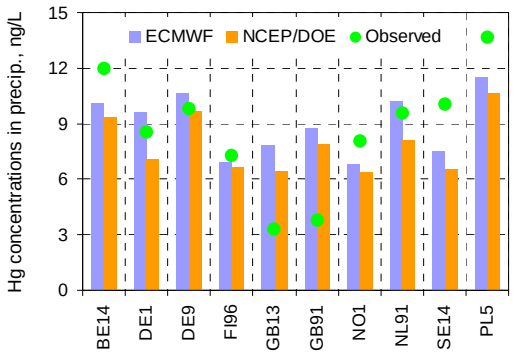

Fig. 3.19. *Annual mean concentrations of mercury in precipitation modelled on the base of ECWMF analysis and NCEP/DOE re-analysis, ng/L*

On the base of the performed analysis the following conclusions can be formulated:

1. Annual mean concentrations of lead, calculated by MSCE-HM on the base of ECMWF are 2.6% higher than those based on NCEP/DOE input data over the European and Central Asian countries (Kazakhstan, Kyrgyzstan, Uzbekistan, Tajikistan and Turkmenistan). The depositions of lead based on ECMWF data are 0.7% lower, and of mercury 3% higher compared to those based on NCEP/DOE over the same countries. However, over some areas the difference between concentrations computed with the use of the two different meteorological datasets makes up ±25%, and between depositions - up to ±50%.

2. At individual monitoring stations the pollution levels computed on the base of ECMWF data on average exceed those based n NCEP/DOE re-analysis by 7% for annual mean air concentrations, by 10% for concentrations in precipitation and by 2.5% for wet deposition flux.

3. Over most of the extended EMEP domain the difference between TGM annual mean concentrations, calculated on the base of ECMWF and NCEP/DOE input data, is around ±1.5%. The difference in annual total depositions of mercury is within ±25% over most of the EMEP domain, and within ±50% over the Arctic, the Mediterranean Sea and the Central Asian Region.

4. Annual mean concentrations in precipitation averaged over the monitoring stations computed on the base of ECMWF meteorological data are 13% higher and wet deposition fluxes – by 1% lower than those based on NCEP/DOE data. The difference between TGM concentrations is within ±3%.

3.4. Model results for 2006 over the extended EMEP domain

This section is devoted to the analysis of the model results over the extended EMEP grid. Concentration and deposition fields of lead, cadmium and mercury were overviewed. The main focus of this section is made on the verification of the modelling results. The comparison of calculated and measured concentrations in air and in precipitation was performed on annual basis as well as short-term variability of these parameters was analyzed.

Lead

Over most part of Europe concentrations of lead varies from 1 to 10 ng/m^3 (Fig 3.20a). Relatively high concentrations (over 20 ng/m^3) were obtained for the Benelux region, Poland, north of Italy, southern part of the United Kingdom, south of Pyrenean Peninsula, over Balkan Peninsula, and southern part of Kazakhstan. These elevated concentrations were caused by joint influence of anthropogenic emissions and wind re-suspension (Fig. 3.2a, 3.4a). Over north of Russia and Scandinavian Peninsula the concentrations are the lowest and as a rule lie below 0.3 ng/m^3.

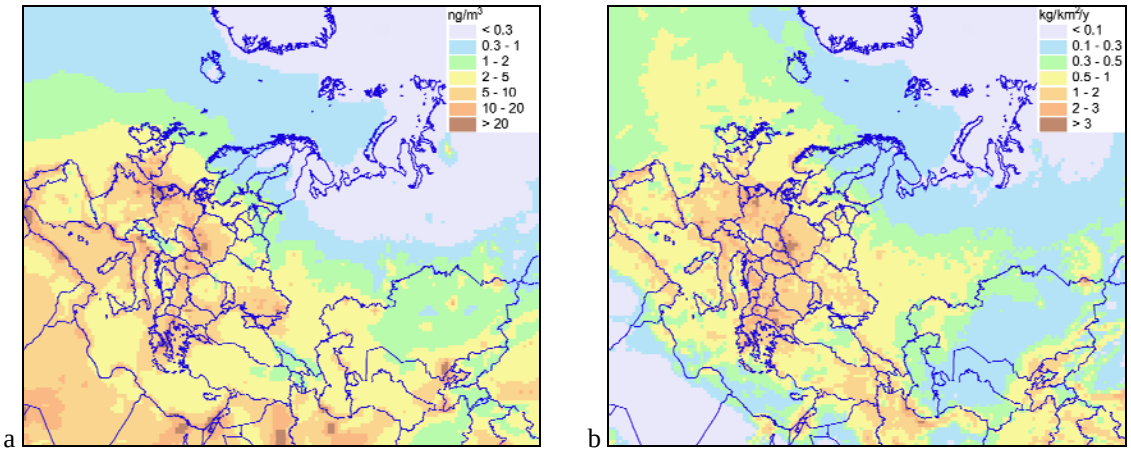

Fig. 3.20. *Annual mean concentrations, ng/m^3 (a) and annual total depositions, kg/km^2/y (b) of lead in 2006*

Total depositions of lead ranges from 0.4 to 2 kg/km^2/y over most part of EMEP countries (Fig, 3.20b). The highest depositions are associated with regions with significant emissions (anthropogenic and wind re-suspension) combined with high or moderate annual precipitation. These are Benelux countries, Poland, northern part of Italy, Balkan region. Unlike air concentrations, depositions in the southern part of Kazakhstan are moderate. In spite of significant anthropogenic emissions and essential contribution of wind re-suspension, the depositions do not reach high levels because of low precipitation. The lowest depositions of lead took place over northern part of Russia and Scandinavian Peninsula.

Concentrations of lead in the Central Asian region range from 1 – 5 ng/m^3 in the steppe and deserted areas to 20 ng/m^3 or even more nearby large emission sources. These concentrations are comparable with those obtained for Europe. The highest concentrations are noted for the southern part of Kazakhstan and eastern part of Uzbekistan, which are characterized by relatively high emission sources. Depositions of lead over most of Central Asia are low compared to Europe. Over most of Kazakhstan, Uzbekistan and

Turkmenistan the depositions ranges from 0.1 to 0.4 kg/km^2/y. The reason for this is relatively low precipitation amounts typical for dry or arid central Asian region (Fig. 1.12a). Higher precipitation amounts take place in mountainous regions of Kyrgyzstan and Tajikistan. This leads to relatively high depositions in these countries ranging from 0.6 to 2 kg/km^2/y.

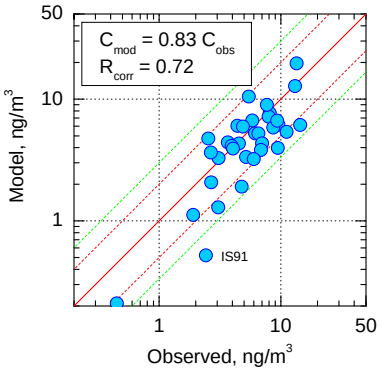

a

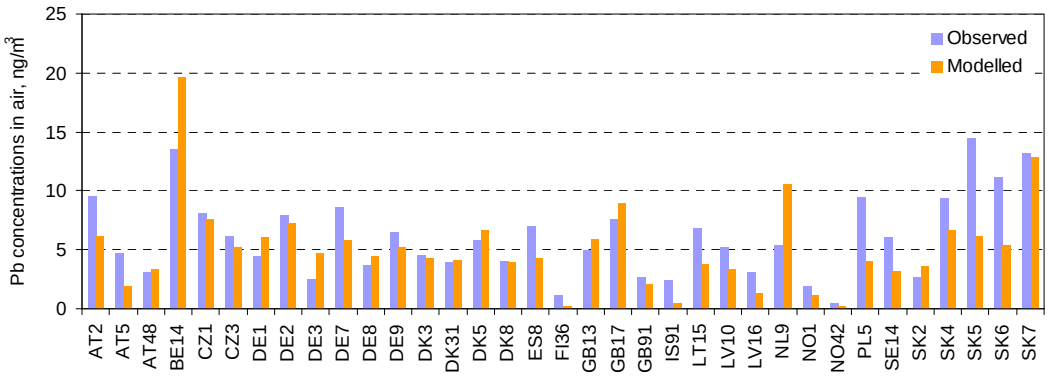

b

Fig. 3.21. *Comparison of modelled and measured annual mean concentrations of lead in air. (a) - Scatter plot, (b) – individual stations. Red solid line delineates 1:1 ratio, red and green dashed lines show deviation by a factor of two and three, respectively, ng/m^3*

Air concentrations of lead were reported from 37 EMEP stations. Information from Slovenian site SI8 was not involved into the verification process because all measured values are below detection limit. Data on air concentrations from Spanish site ES17 were ignored because of short measurement period. Comparison of modelled and measured concentrations in air was performed for 35 selected EMEP stations. The model slightly (around 20%) underestimates measured concentrations of lead in air (Fig. 3.21a). Correlation coefficient between annual mean measured and modelled air concentrations is 0.7. Around 40% of measurement-modelling pairs of values agree within ±30%, and 70% - within ±50%.

Comparison of annual mean values differs for individual sites (Fig. 3.21b). Relatively good agreement is indicated for stations in Austria, Germany, Denmark, and the United Kingdom. Concentrations at Belgium station BE14 were overestimated by the model by about 50%, and at the Dutch station NL9 – almost twice. Some underestimation of measured concentrations was obtained for Polish, Swedish and Slovak sites and essential (up to an order of magnitude) – for Finnish site FI36 and Icelandic site IS91.

Concentrations of lead in precipitation in 2006 were available from 55 stations. Data from Portuguese stations PT1, PT3, PT4 and PT10, Irish site IE1 were ignored because most of raw data are below

detection limit. Information of station NO47 was not considered because the station is located close to large emission source and thus is not representative [*Ilyin and Travnikov*, 2005].

Comparison of measured and modelled concentrations of lead in precipitation and wet deposition fluxes for all stations selected for the verification is demonstrated in Fig. 3.22. Both concentrations and deposition fluxes are underestimated about 2.5 times. However, the model performance at individual stations is highly different. Concentrations and wet deposition fluxes were reasonably well reproduced for stations in Belgium, Germany, United Kingdom, Poland, Sweden and the Netherlands (Fig. 3.23, 3.24). At most of stations in these countries modelled and measured wet depositions and concentrations in precipitation agree within ±40%.

The significant overall underestimation of the observed concentrations of lead in precipitation and wet deposition fluxes is mostly conditioned by large underestimation at a few stations, such as CZ1, ES8, HU2, LT15 and SK2. These stations are considered below. Without these stations the statistical parameters are improved: correlation coefficient rises from 0.5 to 0.7 and regression coefficient increases to 0.7 both for concentrations in precipitation and wet deposition fluxes (Fig. 3.22a, b).

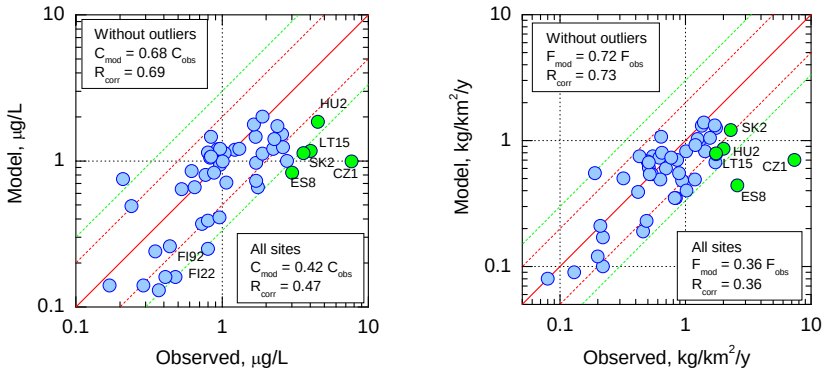

a b

Fig. 3.22. *Calculated and observed annual mean concentrations in precipitation, µg/L (a) and wet deposition fluxes, kg/km²/y (b) of lead in 2006. Red solid line delineates 1:1 ratio, red and green dashed lines show deviation by a factor of two and three, respectively*

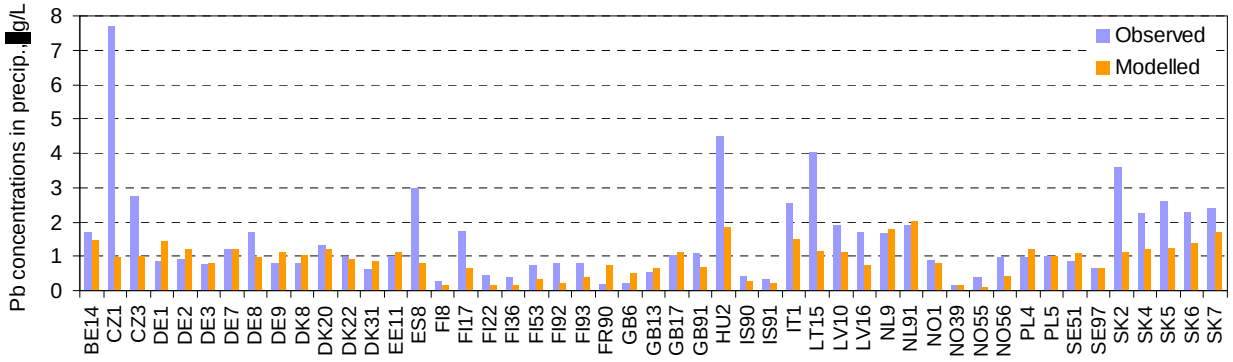

Fig. 3.23. *Modelled and measured annual mean concentrations of lead in precipitation at individual stations for 2006, µg/L*

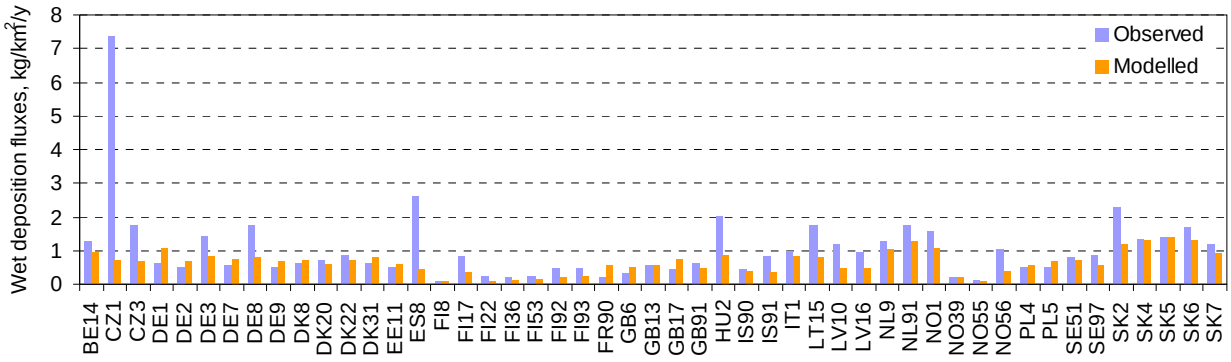

Fig. 3.24. *Modelled and measured annual wet deposition flux of lead at individual stations for 2006, kg/km²/y*

Concentrations of Pb in precipitation at site CZ1 looks doubtful. According to available measurements for the period from 1996 to 2006 Pb concentrations tended to decrease (Fig. 3.25). The annual mean value for 2006 is the highest among all available annual mean values. The reason of so high concentrations standing out of long-term tendency at this station could be linked with either quality of the measurement data or establishment of new emission source located close to the station.

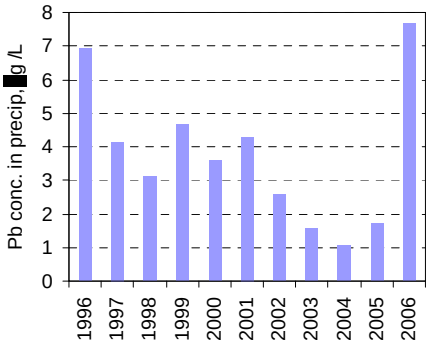

Fig. 3.25. *Concentrations of Pb in precipitation at CZ1 for 1996 – 2006 period, µg/L*

Elevated observed concentrations at LT15 are explained by peak concentrations taking place in the end of April and middle of May (Fig. 3.26). Similar peaks were identified for some other metals (e.g., Ni, Cu and Cr), but not for cadmium. It is not clear whether these peaks are real values or they reflect the influence of local pollution sources or measurement errors. If these peak values are removed, the annual mean concentrations changes from about 4 µg/L to 1.9 µg/L, which would result in better agreement between the modelled and observed concentrations.

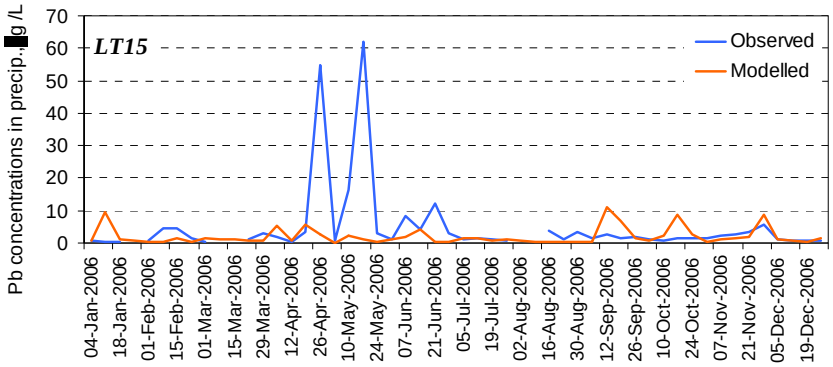

Fig. 3.26. *Weekly mean measured and modelled concentrations of lead in precipitation at station LT15 (Preila, Lithuania) in 2006, µg/L*

Similar to LT15, high concentrations of lead at station HU2 are most probably conditioned by peak values in January and May (Fig. 3.27a). Measured precipitation sums (around 17 mm in January and 40 mm in May) are not so low to be a reason of such significant peaks. The analysis of back trajectories for May and January did not reveal any specific peculiarities compared to other months where the agreement between measurements and modelling is more successful, e.g, September. Without these two peaks the observed concentration changes from 4.5 to 2 μg/L, and this is very similar to the modelled value (1.85 μg/L).

Station SK2 is located at the altitude about 2000 m above sea level. Nevertheless, measured concentrations of lead at this station are very high compared to other regions. Annual variability of concentrations does not demonstrate any peaks which can be considered as doubtful (Fig. 3.27b). The nature of these high concentrations is not clear.

Short-term variability of the observed lead concentrations was well captured by the model, especially for stations located in Germany, Denmark, the Netherlands, Belgium, the Czech Republic and others. Station DE9 (Zingst, Germany) is selected as an example demonstrating good agreement between modelled and measured concentrations of lead in air (Fig 3.28). Most of weekly-mean measured values were caught by the model.

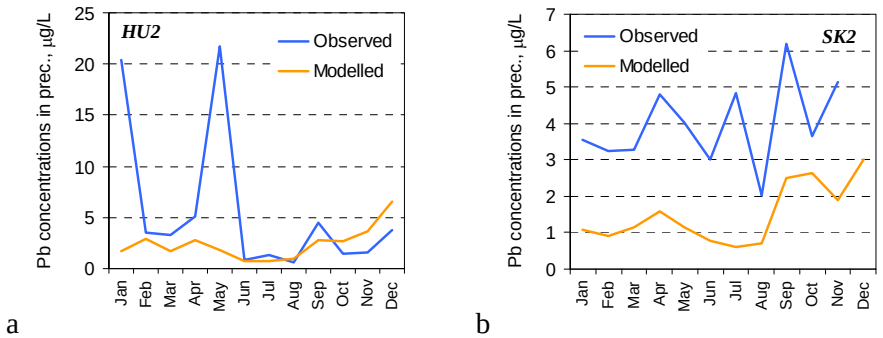

a b

Fig. 3.27. *Monthly mean measured and modelled concentrations of lead in precipitation at station HU2 (K-Puszta, Hungary)(a) and SK2 (Chopok, Slovakia) (b) in 2006, μg/L*

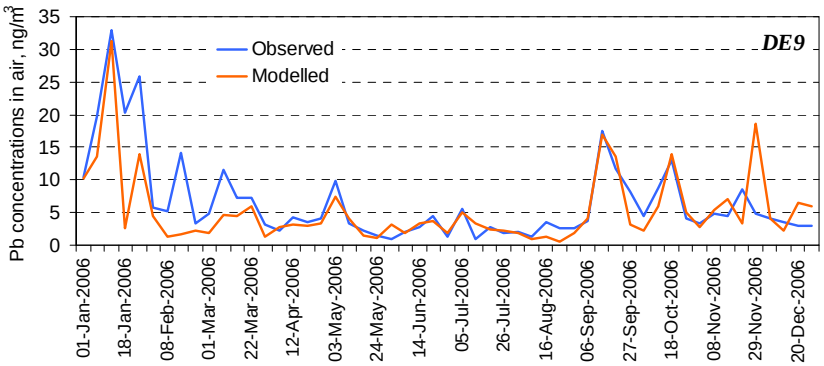

Fig 3.28. *Weekly mean measured and observed concentrations of lead in air at station DE9 (Zingst, Germany), ng/m^3*

The performance of the modes varies at different stations. For example, at station GB13 (Yarner Wood, the United Kingdom) both concentrations in precipitation and wet deposition flux were reasonably well simulated by the model, compared to measured fluxes (Fig. 3.29). With few exceptions, the agreement between modelled and observed concentrations and wet deposition fluxes is within ±50%. Correlation coefficients for monthly mean time series are 0.8 (concentrations in precipitation) and 0.6 (wet deposition).

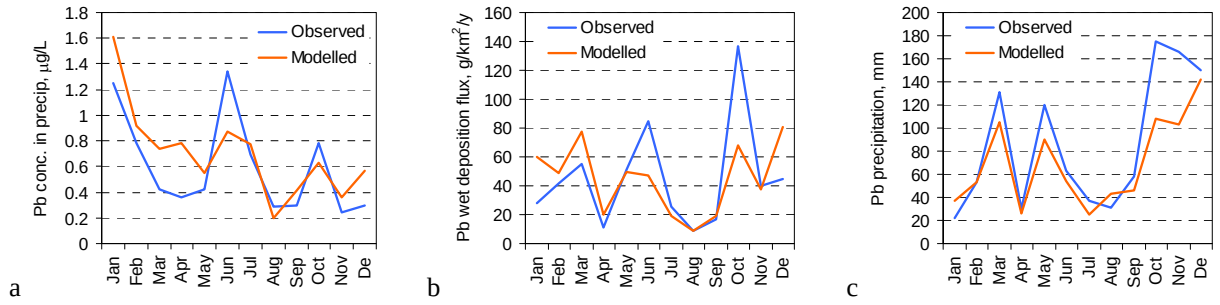

Fig. 3.29. *Monthly mean modelled and observed concentrations of lead in precipitation, µg/L (a), monthly sums of wet depositions, g/km^2/y (b) and precipitation amounts, mm (c) at station GB13*

Good agreement between modelled and measured quantities can be noted for a number of other stations. However, there are some stations where the model considerably underpredicts the observed concentrations in air, in precipitation and wet deposition fluxes. Significant underestimation of measured concentrations of lead in precipitation was indicated for most of Finnish sites. Comparison of measured and modelled monthly mean values reveals that for most of Finnish in some months the agreement is reasonable, whereas in other month the discrepancy is significant. For example, at stations FI22 and FI93 measured and modelled concentrations and fluxes in June agree within ±30%, while in August the difference reaches an order of magnitude (Fig. 3.30, 3.31). Similar situation was also obtained for other Finnish stations.

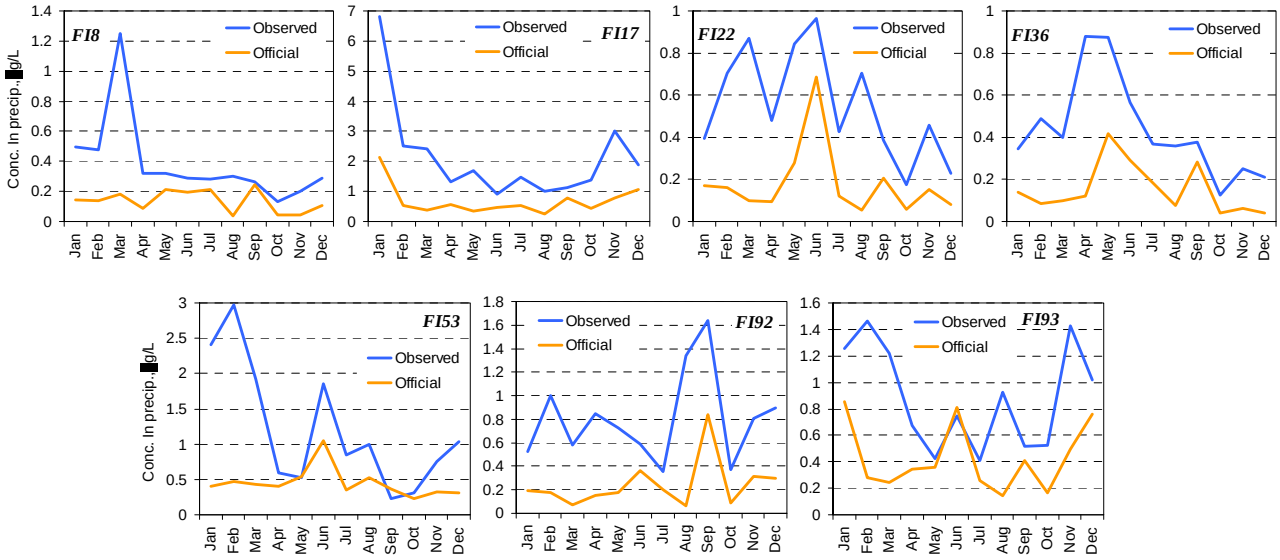

Fig. 3.30. *Measured and calculated (on the base of official emissions) concentrations of lead in precipitation at Finnish stations in 2006, µg/L*

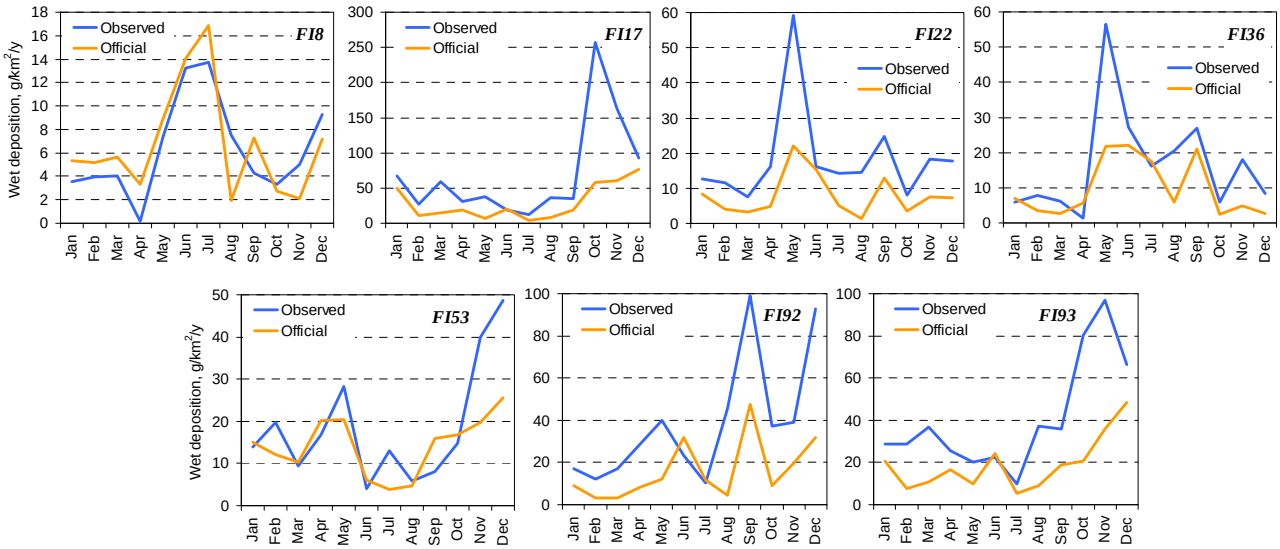

Fig. 3.31. *Measured and calculated (on the base of official emissions) wet deposition flux of lead at Finnish stations in 2006, g/km^2/y*

Analysis of back trajectories arriving to these stations in June and August was performed. Every six hours a 4-day back trajectory was calculated during June and August, and probability of the trajectory crossing each grid cell was evaluated (Fig. 3.32). As seen from Fig. 3.32 a,c high probability of atmospheric transport in August from Russia took place, in particular, from regions of St. Petersburg and Kola Peninsula. In June the air masses were arriving to the stations with the highest probability from Scandinavian Peninsula (Fig. 3.32 b,d).

Essential underestimation of the observed concentrations in precipitation in months when air masses are transported from Russian territory may indicate that emissions over north-west of Russia are likely underestimated. In order to test this hypothesis, two numerical experiments were performed. In the first one the officially submitted emission of lead from Russia (Fig. 3.33a) was replaced by that prepared within ESPREME project [http://espreme.ier.uni-stuttgart.de] (Fig.3.33b). In the second experiment ESPREME emission from Russia were increased 5 times over region surrounding St. Petersburg and 20 times – over Kola Peninsula (Fig. 3.33c). The approach to increase emissions in some regions may seem rough, but the purpose of the experiments is not a correction of the existing spatial distribution of the emissions, but investigation of the sensitivity of the model output at Finnish stations to changes of the emissions over the neighboring region, revealing areas with potentially high emission uncertainty.

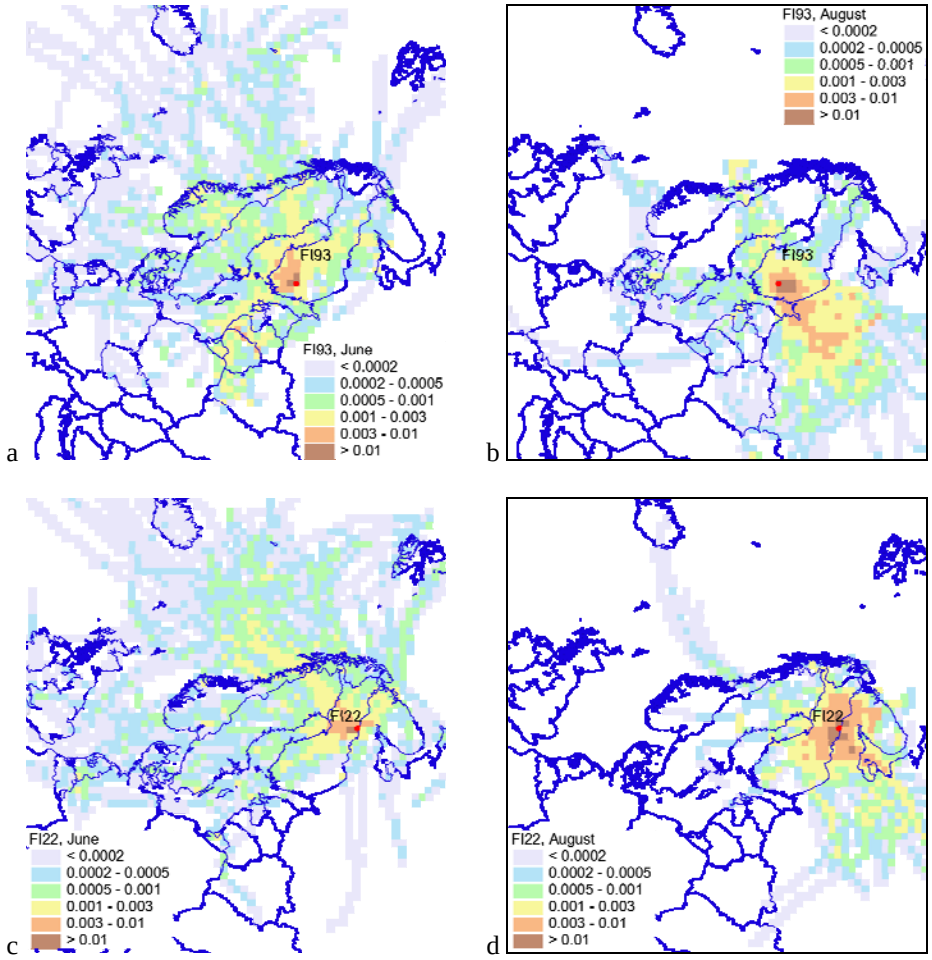

Fig 3.32. *Spatial distribution of probability of back trajectory crossing a grid cells for Finnish stations FI93 (a,b) and FI22 (c,d) in June and August*

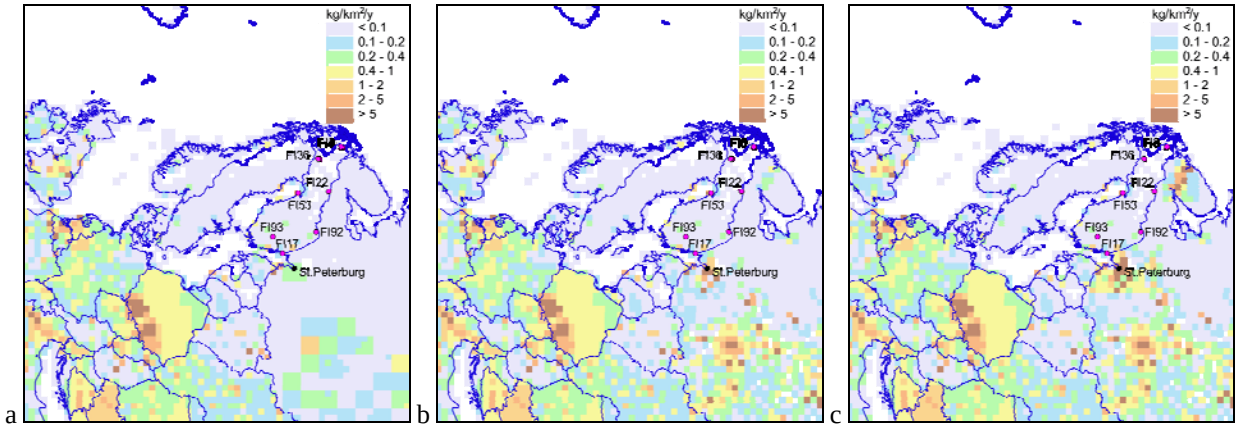

Fig. 3.33. *Emission data used in numerical experiments. a) – official emission data; b) – ESPREME emission over Russia, c) - ESPREME emission for Russia is increased 5 times over region surrounding St. Petersburg, and over Kola region – 20 times, kg/km^2/y*

The use of ESPREME emissions resulted to better agreement between measured and modelled wet deposition fluxes in some months. For example, fluxes at stations FI17 and FI93 in August the agreement between measurements and modelling significantly improved (Fig. 3.34). Besides, distinct improvement is noted for air concentrations in April and May at station FI36. The second experiment resulted to marked improvements of agreement between modelled and observed wet deposition fluxes in some months at a number of stations. For example, the agreement improved for October at stations FI17 and FI93, for May at FI22 and FI92, for March at FI17, FI22 and FI93 (Fig 3.34). However, the observed wet deposition fluxes in August at FI93 and FI17 were overpredicted by the model by almost 3 times, which can be explained by roughness of the approach.

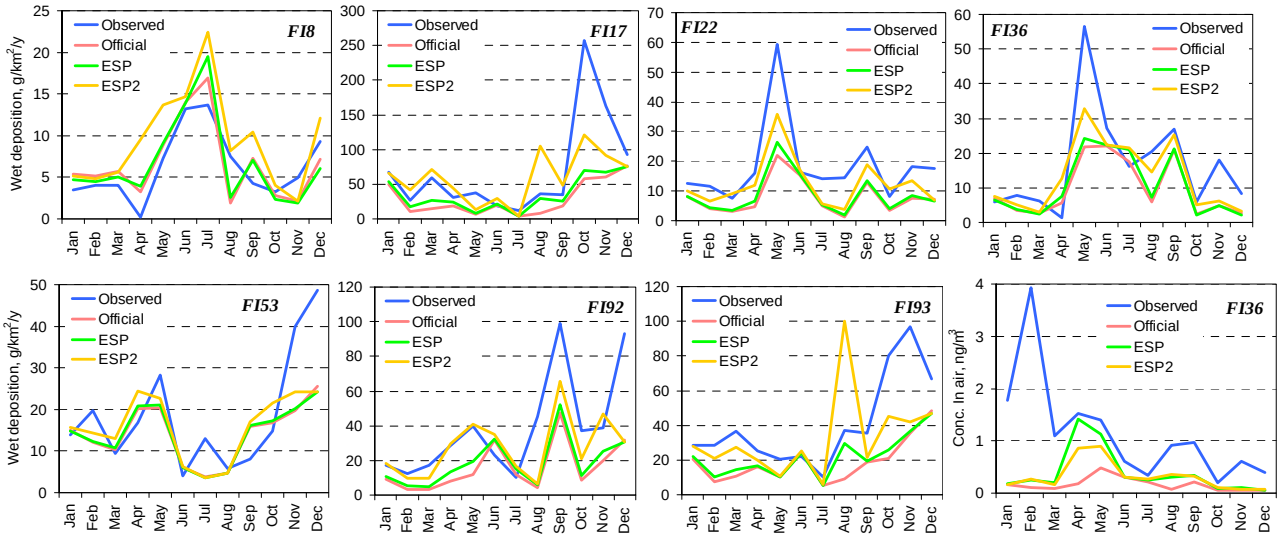

Fig. 3.34 *Measured and calculated wet deposition fluxes and air concentrations of lead at Finnish stations in 2006. "ESP" refers to the first experiment, and "ESP2" – for the second experiment, described in the text.*

In some months the modelled fluxes remained almost the same or changed slightly despite the changes in emission data. The examples are November (at FI17, FI36, FI93) or December (FI92, FI22, FI93). The lack of response in modelled values after the experimental increase of the emissions is not surprising. According to analysis of back trajectories, the air mass transport in these months takes place not from territory of Russia, but from other regions (Fig. 3.35).

The numerical experiments carried out to investigate the sensitivity of concentrations and wet depositions of lead at Finnish stations to changes of the emission data demonstrated that the model results are very sensitive to both total emission of lead and its spatial distribution. The revision of the reported magnitudes and spatial distribution of emissions can significantly improve the agreement between the modelled and measured wet depositions.

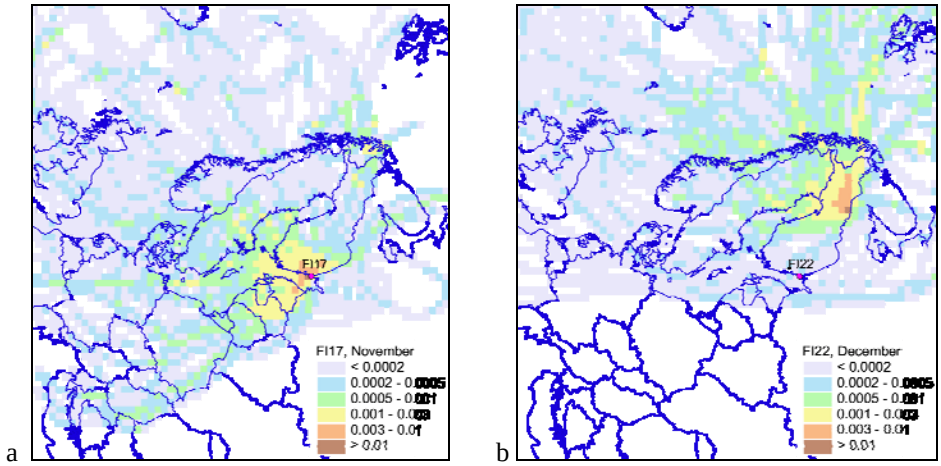

Fig. 3.35. *Spatial distribution of probability of back trajectory crossing a grid cells for Finnish stations FI17 in November and FI22 in December*

Concentrations in air and in precipitation at Slovak stations are underestimated by the model. Monthly mean modelled air concentrations demonstrate similar annual variability as the observed ones (except for SK5), but significantly (up to 3 times) lower than the observed ones (Fig. 3.36). Similar situation is noted if weekly mean values are compared. Besides, some observed peaks, e.g., in the middle of January at SK5 and SK6, were underestimated by a factor of 5 (Fig. 3.37).

Concentrations in precipitation can be underestimated because of precipitation amounts overestimated by MM5 at these stations. Annual measured and modelled wet deposition fluxes agree within 25%. However, some peak monthly depositions, e.g., in August at SK4, SK6 and SK7 or in April and May at SK6 were missed by the model (Fig. 3.38).

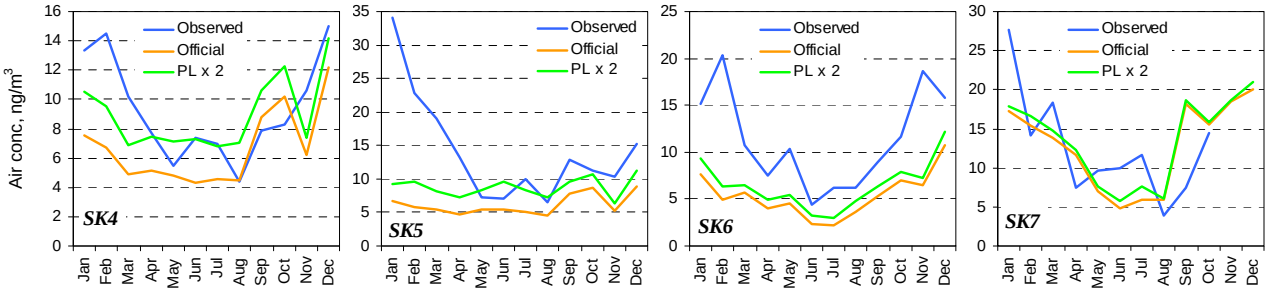

Fig. 3.36. *Modelled and measured concentrations of lead in air at stations in Slovakia in 2006. PL×2 refers to the experimental increase of official emissions in Poland., ng/m^3*

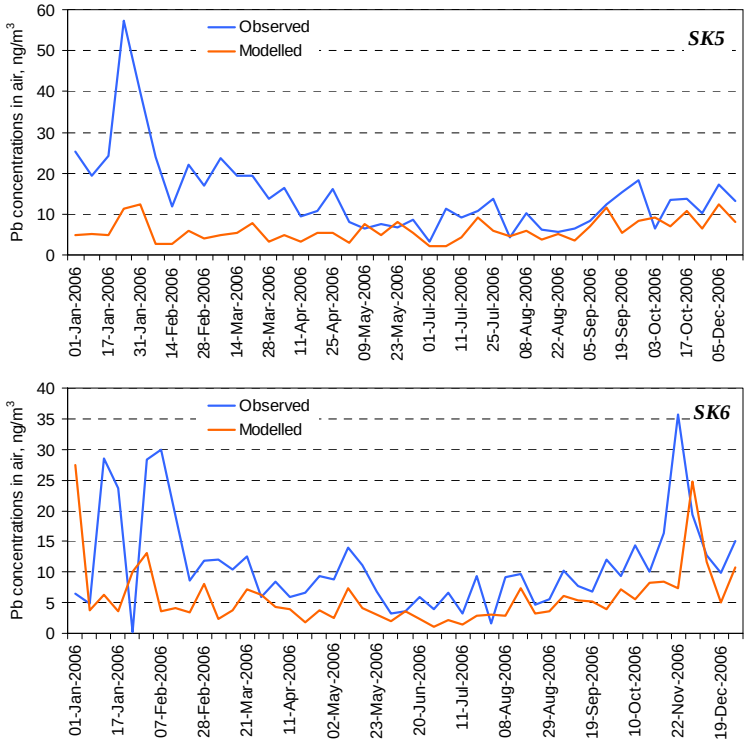

Fig. 3.37. *Comparison of weekly mean measured and modelled concentrations of lead at stations SK5 and SK6 in 2006, ng/m^3*

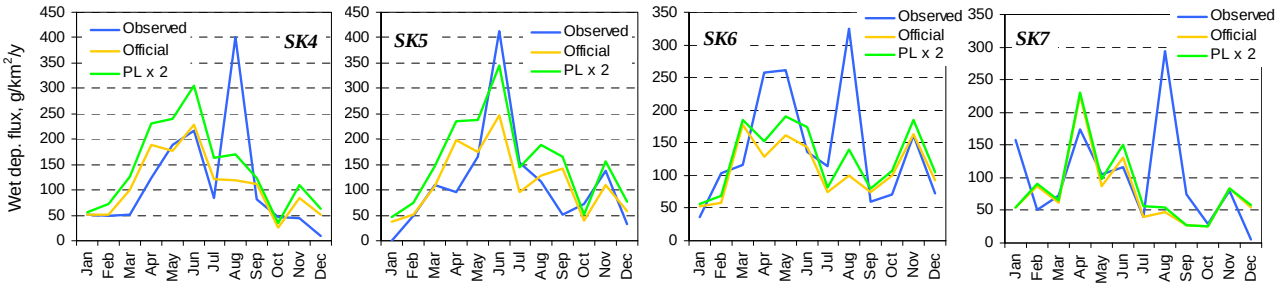

Fig. 3.38. *Modelled and measured wet deposition fluxes of lead at stations in Slovakia in 2006. PL×2 refers to the experimental increase of official emissions in Poland, g/km^2/y*

Analysis of back trajectories was applied to determine regions potentially influencing the pollution levels at these stations. According to this analysis, peak concentrations of lead at stations SK5 and SK6, observed in January and February could be associated with atmospheric transport from Poland or the west of the Ukraine (Fig. 3.39). In August the atmospheric transport to SK5 took place from the western or south-western direction (the Czech Republic, south of Germany, Hungary) (Fig. 3.40a). Similar pattern was obtained for SK6 and SK7 in April (Fig 3.40b).

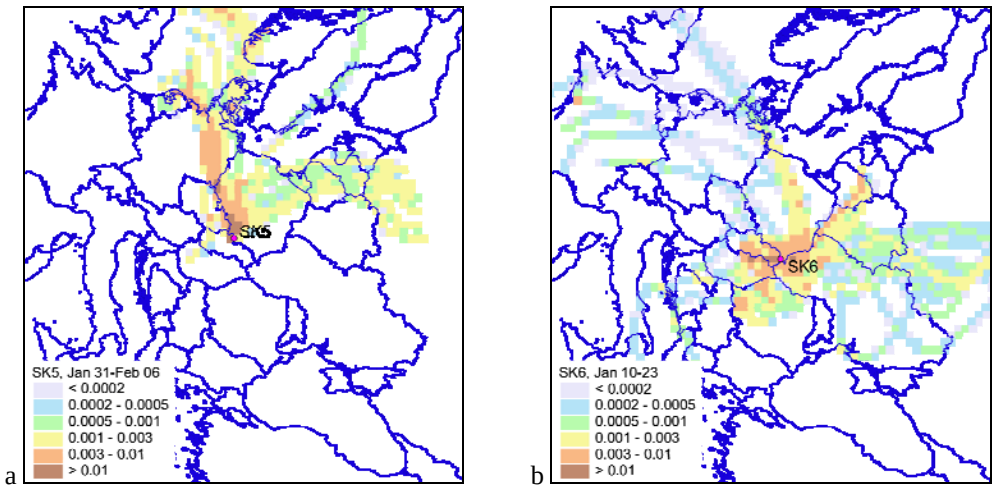

Fig. 3.39. *Spatial distribution of probability of back trajectory crossing a grid cells for Slovak stations SK5 in the beginning of February (a) and SK6 in the middle of January (b), 2006*

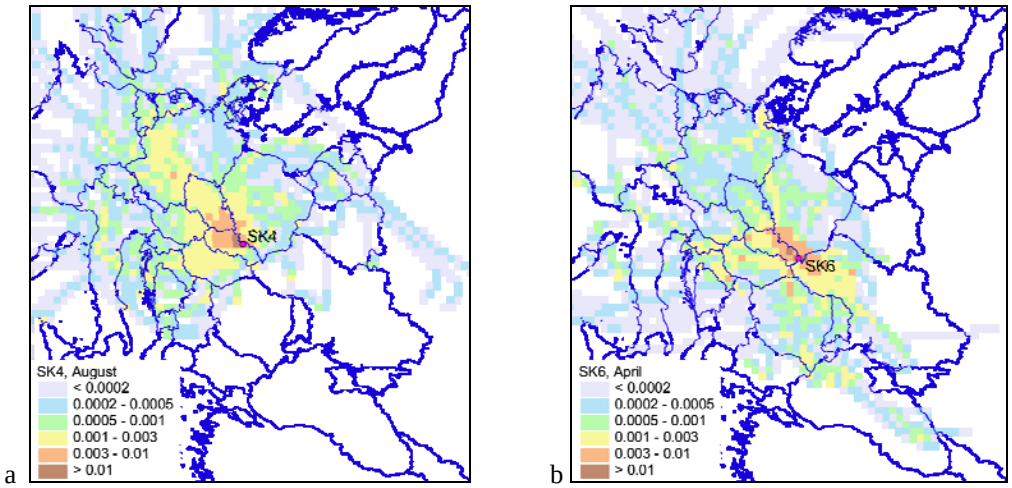

Fig. 3.40. *Spatial distribution of probability of back trajectory crossing a grid cells for Slovak stations SK4 in August (a) and SK6 in April (b), 2006*

Several experimental model runs with modified emission data was performed. The replacement of official emissions of Hungary and Ukraine by much larger values (2.5 times for Hungary and 4 times for Ukraine) from the ESPREME database did not result in noticeable positive changes in modelled air concentrations and wet depositions. The experimental 2-fold increase of official emission data in Slovakia also resulted in minor rise of concentrations and depositions of lead at the stations. In the final experiment the official emissions of Poland were increased by a factor of two. It is worth stating that this increased Polish emission is most likely unrealistically high. Officially reported emission of lead in Poland is already the highest among EMEP countries. Besides, officially reported annual Polish emission of lead in 2006 (524 tonnes) is even greater than the expert estimates of ESPREME project relating to 2000 (446 tonnes). Nevertheless, even this experimental increase of the Polish emissions did not assist in resolving the problem of the underprediction. Although monthly air concentrations and wet deposition fluxes increased up to 80 % in some month the indicated observed peak values were not captured (Fig. 3.36, 3.38).

The experiment with modifications of emissions in order to produce better agreement between modelled and measured concentrations at Slovak stations demonstrated that even significant changes of emissions in Slovakia or surrounding countries do not allow the model to reproduce available peak concentrations and depositions and thus do not allow to solve the problem of underestimation of the observed values. Therefore, the underestimation may possibly be caused by the influence of local emission sources not taken into account when modelling or by local meteorological conditions. To confirm or disprove this hypothesis, additional researches are needed.

Cadmium

Over major part of Europe concentrations of cadmium range from 0.02-0.3 ng/m^3 (Fig. 3.41a). Poland, Balkan region, Benelux countries, eastern part of Ukraine and south-east of Russia are characterized by relatively high concentrations of cadmium (>0.3 ng/m^3). High concentrations in these regions are associated with considerable emissions (Fig. 3.2b). Lowest concentrations were obtained for Arctic and sub-Arctic regions (Northern Scandinavian Peninsula, north of Russia). However, spots of elevated concentrations in the Arctic are clearly seen over Norilsk region.

Annual cadmium depositions over most part of EMEP area varies from 10 to 50 g/km^2/y (Fig. 3.41 b). Pattern of cadmium total depositions is similar to that of air concentrations. The highest depositions (50 – 200 g/km^2/y) are indicated for regions win high anthropogenic emissions (e.g. Poland, Balkans, Benelux etc.). However, over central Asian region the depositions are relatively low (3-10 g/km^2/y), mainly due to low precipitation amounts. Relatively low depositions are also seen over northern part of EMEP region.

Annual mean cadmium concentrations over the Central Asian region are within 0.02 – 0.1 ng/m^3. Higher concentrations (up to 0.5 ng/m^3) are noted in the north and south of Kazakhstan and east of Uzbekistan. Elevated concentrations are found in regions with relatively high emissions. Calculated depositions of cadmium in the Central Asian region are significantly lower than those obtained for Europe. Over most of the region they range from 3 to 30 g/km^2/y. Similar to lead, this is connected with low precipitation amounts.

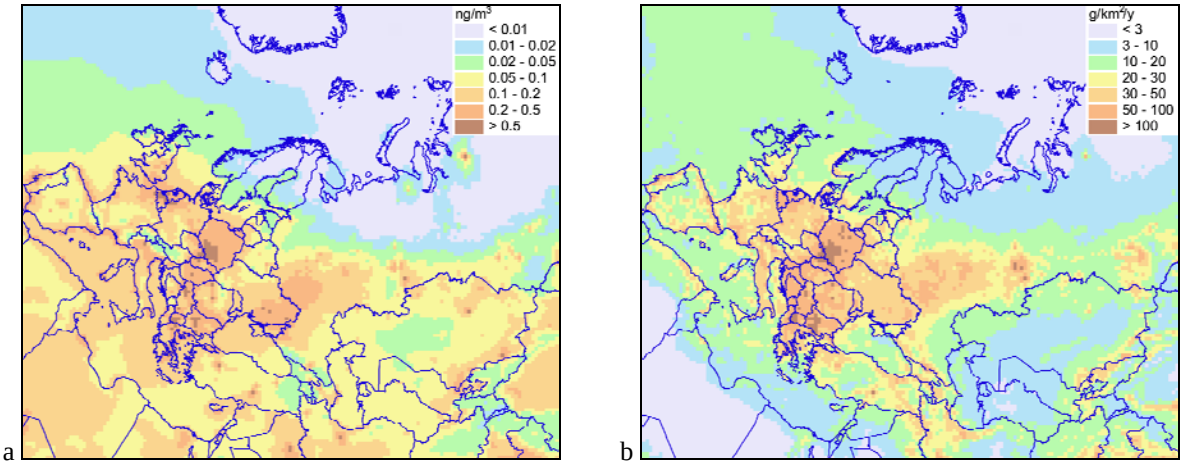

Fig. 3.41. *Annual mean concentrations, ng/m^3 (a) and annual total depositions, g/km^2/y (b) of cadmium in 2006*

Information on cadmium concentrations in air was submitted by 34 EMEP stations. Among them the data from 32 stations were involved into the comparison. The data from ES17 were not used because of short period of measurements, and SI8 – because all raw data values were below detection limit. Annual mean air concentrations of cadmium, measured at EMEP stations, were relatively well reproduced by the model. The concentrations were underestimated by 20% (Fig. 3.42a). For almost 60% of stations the difference between observed and modelled values lies within ±50%. Correlation coefficient is 0.6.

The agreement between observed and calculated values varies among different stations. Observed concentrations at Czech, British, Lithuanian and most of German stations were simulated by the model reasonably well: the difference between modelled and measured quantities is less then ±35% (Fig. 3.42b). Similar to lead, concentrations at Dutch station NL9 and Belgium station BE14 were 1.6-1.8 times overpredicted by the model. Underestimation of the observed concentrations takes place for Austrian, Scandinavian, Latvian and Hungarian stations. At some Slovak stations the agreement between model and observations is satisfactory, and for some stations an underestimation was obtained.

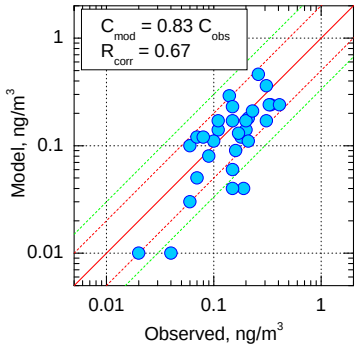

a

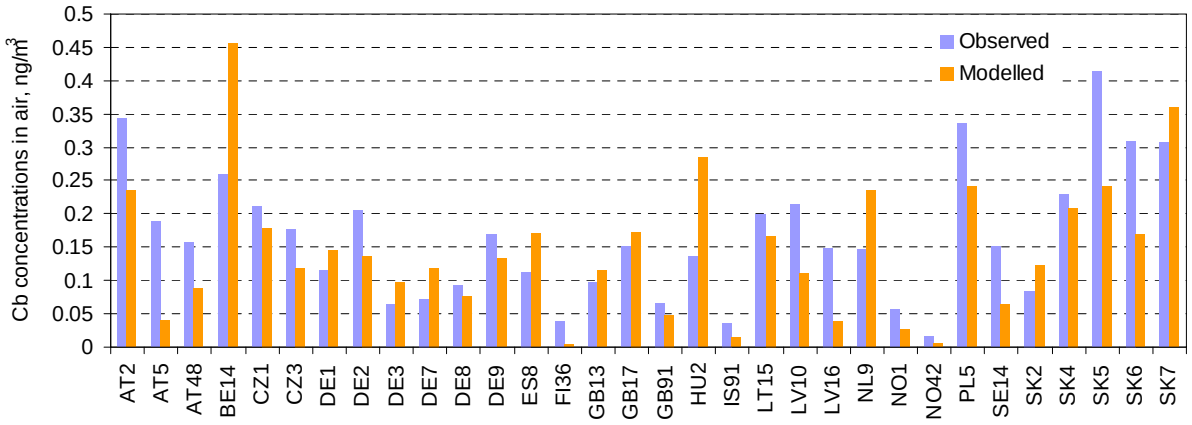

b

Fig. 3.42. *Comparison of modelled and measured annual mean concentrations of cadmium in air. (a) - Scatter plot, (b) – individual stations. Red solid line delineates 1:1 ratio, red and green dashed lines show deviation by a factor of two and three, respectively, ng/m^3*

Data on measured cadmium concentrations in precipitation were reported from 50 EMEP stations, and 40 annual-mean values were used in the comparison. The data from Portuguese stations PT1, PT4 and PT10, Irish site IE1 and Norwegian stations NO1, NO39, NO55 and NO56 were ignored because most of raw values lie below detection limits. Station NO47 is not representative. Concentrations of Cd at Italian

station were too high and not recommended for use in the verification procedure [*W. Aas*, private communication].

When all stations selected for the verification are involved, the model demonstrates overall underestimation of concentrations and wet deposition fluxes by 2.5 – 3 times (Fig. 3.43). Nevertheless, significant correlation coefficients (0.69 and 0.72, respectively) mean that spatial variability was caught by the model. Overall underestimation of wet deposition fluxes and concentrations in precipitation of cadmium is to great extent caused by underestimation of the observed parameters at stations SK2, SK4 CZ3 and HU2. These stations are analyzed below. Without these stations the underestimation of the observed concentrations and wet deposition fluxes is reduced to 2 times, and correlation coefficient increases to 0.8 (Fig. 3.43a, b).

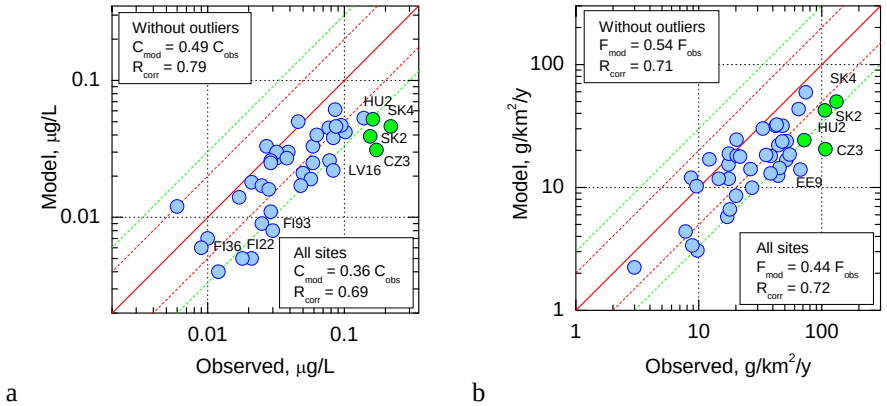

Fig. 3.43. *Calculated and observed annual mean concentrations in precipitation, μg/L (a) and wet deposition fluxes, g/km²/y (b) of cadmium in 2006. Red solid line delineates 1:1 ratio, red and green dashed lines show deviation by a factor of two and three, respectively*

Model performance for cadmium concentrations in precipitation varies between different stations. Measured concentrations at German, Dutch and British stations were simulated relatively well by the model: the agreement between measured and modelled concentrations is mostly kept within ±30% (Fig. 3.44), and for fluxes – within ±40% (Fig. 3.45). Some underestimation of concentrations in precipitation and the fluxes is noted for Swedish and Belgium, Lithuanian stations. Significant underestimation at some Slovak stations can partly be caused by substantial (up to twice) overprediction of precipitation amounts by MM5. At least, modelled wet deposition fluxes for stations SK5, SK6 and SK7 agree with the observed ones within ±35%. The modelled concentrations at Latvian, Polish, Spanish and Finnish stations were around 2 - 2.5 times lower than the observed ones.

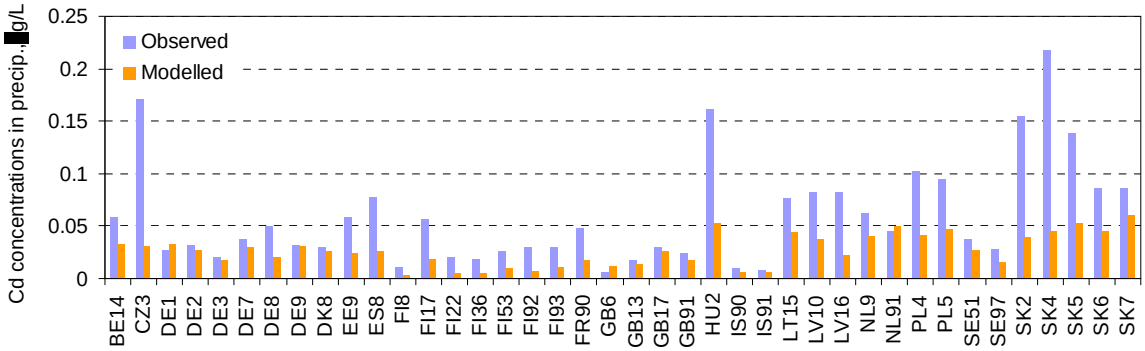

Fig. 3.44. *Modelled and measured annual mean concentrations of cadmium in precipitation at individual stations for 2006, µg/L*

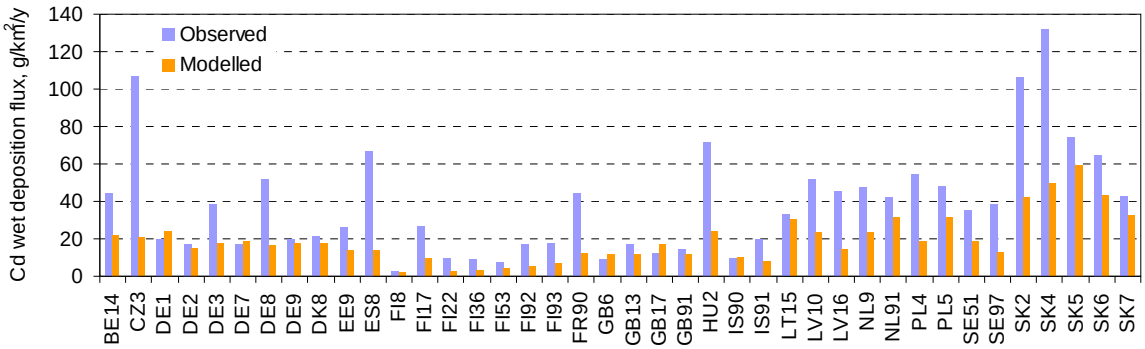

Fig. 3.45. *Modelled and measured annual wet deposition flux of cadmium at individual stations for 2006, g/km^2/y*

At a number of stations (e.g., at German, Belgium, Dutch, Lithuanian stations) the model reproduced short-term variability of concentrations of cadmium in air. Example demonstrating modelled and measured weekly mean concentrations at station LT15 (Preila, Lithuania) is shown in Fig. 3.46. Most of peaks were captured, and magnitudes of most of peaks were reproduced by the model. As seen from the Figure, the modelled concentrations are mainly originated from anthropogenic sources. However, the introduction of wind re-suspension significantly improves the model performance. For example, peaks of measured concentrations in the end of January, end of April and middle of October are much better reproduced due to the use of wind re-suspension.

At station HU2 the model overestimated annual mean observed concentrations of cadmium in air. Comparison of short-term time series of modelled and measured concentrations demonstrates that in some periods, e.g., end of February or end of October the overestimation can partly be explained by the overestimated influence of re-suspension (Fig. 3.47). It is possible to assume that re-suspension of cadmium was overestimated in this region. Indeed, in February, March and April the use of anthropogenic emission alone provides satisfactory fit between measured and modelled values. However, over a number of periods (e.g., December) even the switching off the re-suspension still resulted to the overestimation. In addition to this, in some periods, e.g., June, or end of October the measured raw concentration values represent detection limit. Therefore, measurement information for these periods may be unreliable.

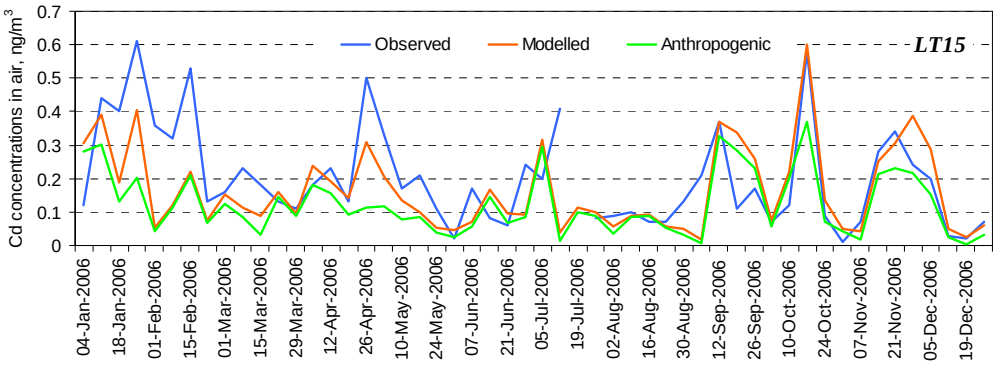

Fig 3.46. *Weekly mean measured and observed concentrations of cadmium at station LT15 (Preila, Lithuania), ng/m^3*

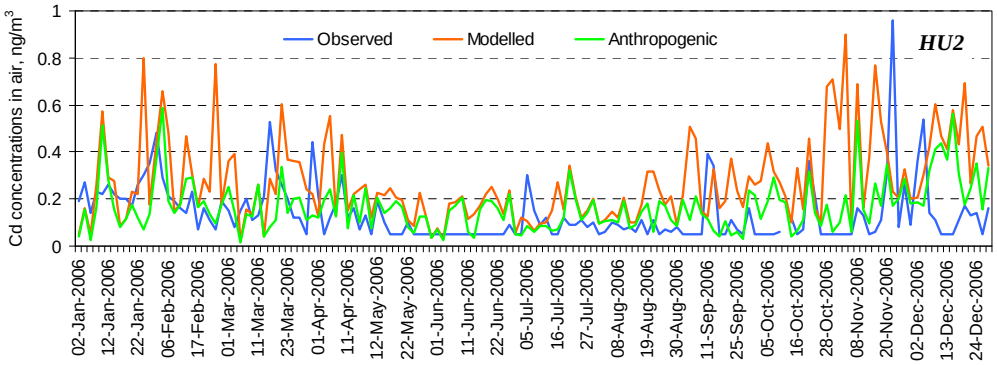

Fig. 3.47. *Daily mean measured and observed concentrations of cadmium in air at station HU2 (K-Puzsta, Hungary), ng/m^3*

Essential underestimation is indicated for stations CZ3, HU2, SK2 and SK4. Calculated concentrations and wet deposition fluxes of cadmium at stations CZ3, SK4 and HU2 exceed the measured ones by 3 – 6 times. These high concentrations and depositions are significantly higher than those measured at most of other European stations, e.g. in Germany, the United Kingdom, Latvia, Lithuania. Anthropogenic emission flux in the Czech Republic and Hungary and nearby countries typically ranges from 2 to 15 g/km^2 in central and western European countries (the Czech Republic, Germany, southern part of the United Kingdom, Hungary) (Fig. 3.2b). In Lithuania and Latvia the emission flux is even lower (0.5 – 2 g/km^2/y). Moreover, even in Poland where emission flux ranges from 30 to 300 g/km^2/y measured concentrations and depositions are 1.5 - 2 times lower than those measured at CZ3, SK4 and HU2. Therefore, these high concentrations and wet depositions at CZ3, SK4 and HU2 can hardly be explained by long-range transport from national sources or by transboundary transport from sources located in neighbouring countries. Measurements at these stations may be affected by the influence of local emission sources. Another possible reason could be connected with quality of measurement data, but there is no available evidence for this.

It was already mentioned that mountain station SK2 is situated at 2000 m above sea level. This altitude is higher than typical height of planetary boundary layer, and the expected levels of heavy metals should be low compared to lowland stations. Nevertheless, cadmium concentrations in precipitation measured at this station are among the highest for 2006. The observed monthly mean concentrations are at least twice

higher than the calculated ones (Fig. 3.48). The reasons of the discrepancy can possibly be explained by the influence of local sources, or by peculiarities of local meteorological conditions not reproduced adequately by meteorological driver, or by uncertainties of measurements. Additional attempts should be maid to find, explain and if possible, to remove the causes leading to the discrepancies.

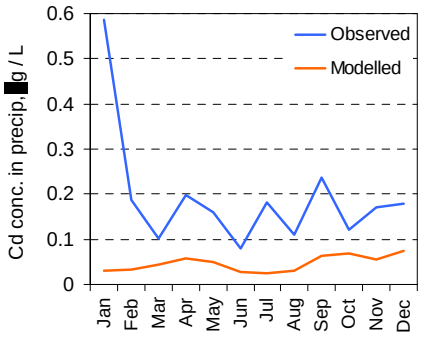

Fig. 3.48. *Monthly mean modelled and measured concentrations of cadmium in precipitation at station SK2 (Chopok, Slovakia), μg/L*

Poland is characterized by significant atmospheric emissions of cadmium, which is reflected in relatively high concentrations measured at Polish stations. Nevertheless, the observed concentrations and wet deposition fluxes are underestimated by the model by a factor of 1.5 – 3. Annual mean air concentrations were underestimated by 40%. However, the model performance for this station varies during the year. For example, the model well captured concentrations in air in late spring, summer, and early autumn, and did not reproduce the magnitude of high peaks in winter and late autumn (Fig. 3.49).

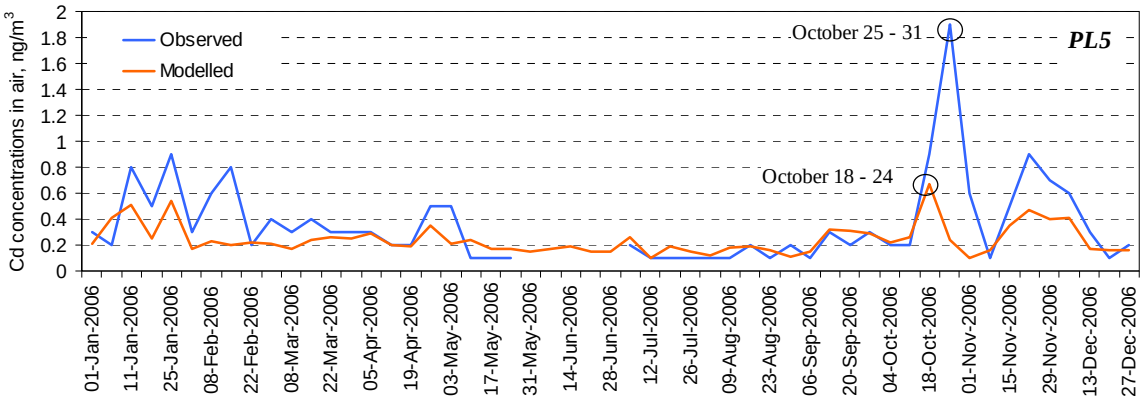

Fig. 3.49. *Weekly mean modelled and measured concentrations of cadmium in air in 2006 at station PL5 (Diabla Gora, Poland), ng/m^3*

Periods with high peak concentrations were considered in more detail using back trajectories approach. For the period from 18th – 24th of October the model captured relatively high concentrations of cadmium (Fig 3.49). Analysis of atmospheric boundary layer back trajectories arriving to PL5 station demonstrates that most of the trajectories are crossing regions of southern Poland characterized by significant emissions (Fig. 3.50). However, the underestimated peak concentrations measured in the period from 25th to 31st of October are contributed by sources located not only in Poland, but also in Baltic countries (Lithuania, Latvia, Estonia), Kaliningrad region of Russia, and southern Scandinavia, where no significant emission sources are located according to the reported information.

Observed time series of weekly-mean wet deposition fluxes at this station were reproduced by the models with different accuracy for different periods (Fig. 3.51). Some weekly mean values were captured by the model well (e.g., beginning of August, middle of May). However, some high measured peak fluxes were

not adequately simulated by the model (e.g, in the middle of February, in December, in the end of November).

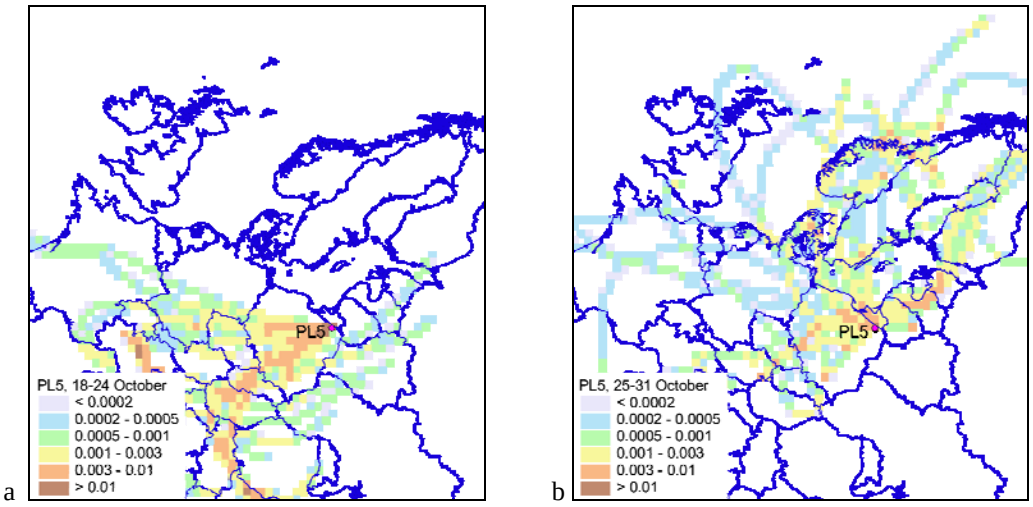

Fig. 3.50. *Spatial distribution of probability of back trajectory crossing a grid cells for Polish station PL5 for 18 - 24 October (a) 25-31 October (b) periods*

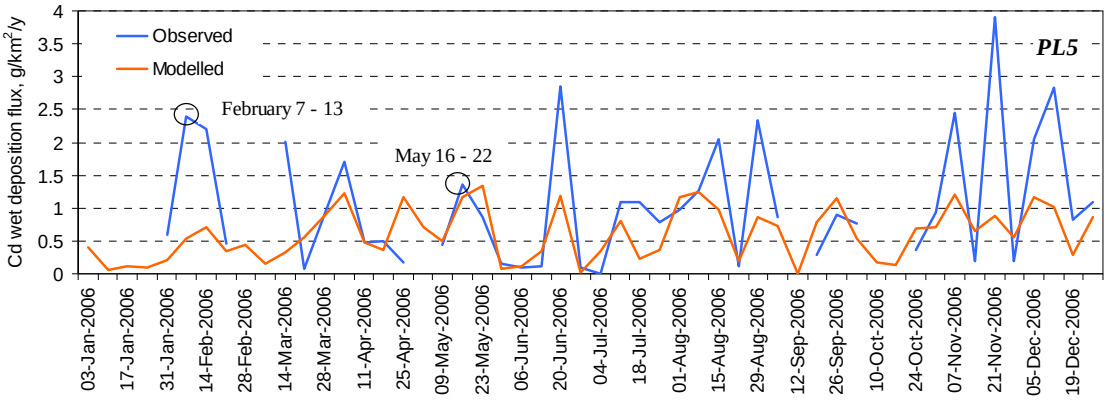

Fig. 3.51. *Weekly mean modelled and measured wet deposition fluxes of cadmium in 2006 at station PL5 (Diabla Gora, Poland), g/km^2/y*

For most of the measurement periods back trajectory statistic was calculated. Because the duration of measurement periods makes up about a week, it is difficult to single out periods when air masses are arriving from one direction. In a number of cases when the atmospheric transport took place mostly from territory of Poland, modelled wet deposition fluxes agree well with the observed ones. For example, in the period of 16th – 22nd of May atmospheric transport took place through southern Poland, Denmark and north-eastern Germany (Fig. 3.52a). Modelled and measured wet deposition fluxes for this period agree within 15%. In the period from 7th to 13th of February the model substantially (more than 4 times) underestimated the measured wet deposition flux (Fig. 3.51). The most probable area from which air masses are arriving to the station is Kaliningrad Region of Russia, Lithuania and Latvia (Fig. 3.52b). However, other regions such as Poland, south of Scandinavia, or western part of Ukraine also contribute to cadmium pollution levels indicated at this station. Some high concentration and deposition peaks not

resolved by the model may be explained by the influence of local emission sources. More extensive investigations including modelling tests, analysis of emission data and quality of measurements are needed to establish reasons of mentioned discrepancies between measurements and the model results.

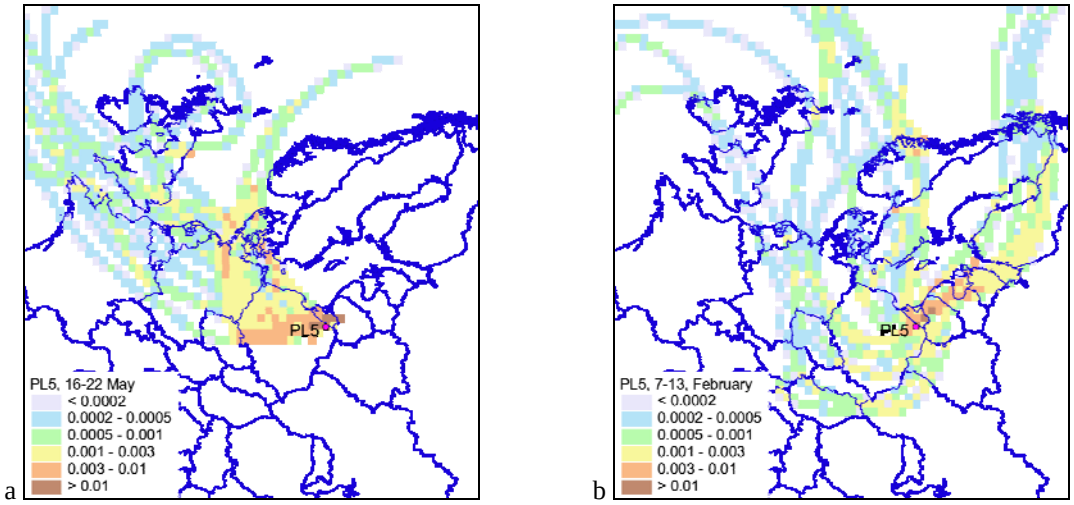

Fig. 3.52. *Spatial distribution of probability of back trajectory crossing a grid cells for Polish station PL5 for 16 - 22 May (a) 7-13 February (b) periods*

Significant underestimation of concentrations in precipitation and wet deposition fluxes is noted for Finnish and some Slovak stations. Annual dynamics of concentrations and wet depositions of lead and cadmium are very similar. In Fig. 3.53 the example is given for three Finnish stations (FI22, FI93 and FI17). Therefore, the main outcomes of experiments aimed at analyses of lead concentrations and depositions at Finnish and Slovak stations are in general valid for cadmium.

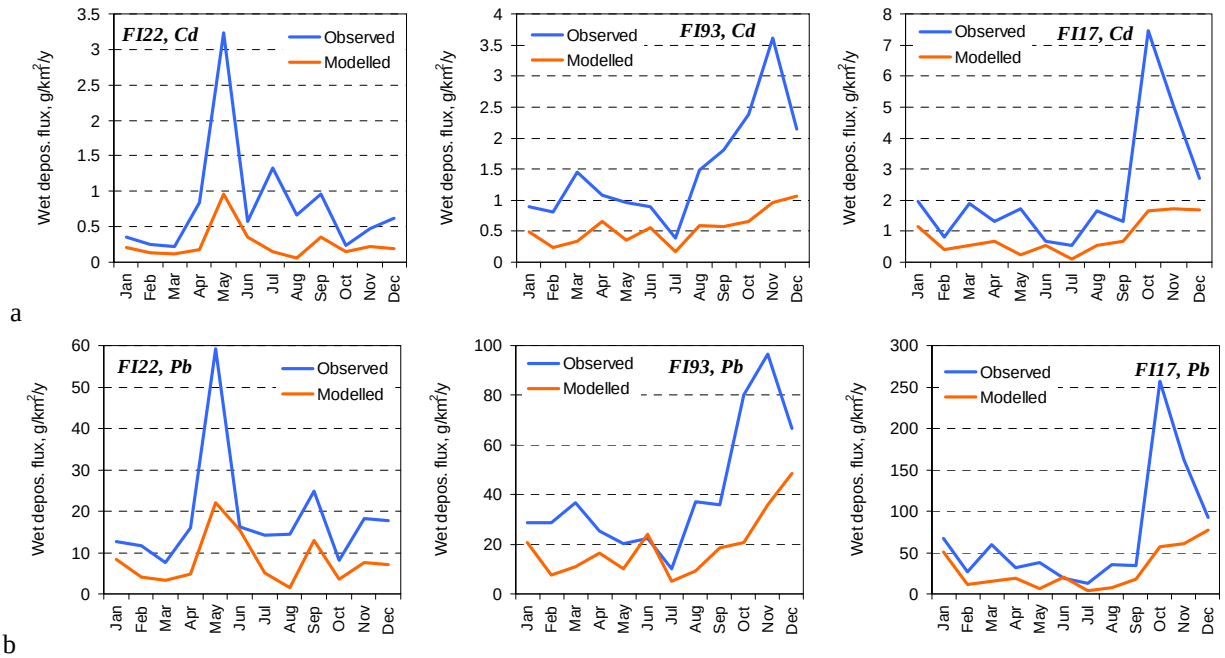

Fig. 3.53. *Monthly modelled and measured wet deposition fluxes of cadmium (a) and lead (b) at Finnish stations FI22 (Oulanka), FI93 (Kotinen) and FI17 (Virolahti II) for 2006, g/km^2/y*

Mercury

Spatial variability of annual mean concentrations of total gaseous mercury (TGM) concentrations is low. This is explained by long (around a year) atmospheric lifetime of main component of atmospheric mercury - its elemental form. Over most of EMEP domain the TGM concentrations ranges from 1.4 to 1.7 ng/m^3 (Fig. 3.54a). Comparatively high concentrations in Poland, south of Kazakhstan and over Balkan region are caused by significant emissions. Low concertinos over Greenland, southern Scandinavia, Caucasus and over Central Asian mountain systems are explained by decrease of air density, and hence, mass concentration of mercury as altitude increases.

Depositions of mercury are formed mostly by particulate and reactive forms of mercury. Over major part of EMEP domain annual deposition flux ranges from 7 to 30 g/km^2/y (Fig. 3.54b). Mercury deposition pattern in general is similar to that of depositions of other metals like lead and cadmium. Relatively high depositions are associated with anthropogenic emissions and take place over Poland, Balkan region, south-east of Russia, and south-east of Kazakhstan. The Arctic and central-Asian dessert areas are characterized by the lowest depositions.

Concentrations of TGM over the Central Asian region are smoothly range from 1.4 to 1.6 ng/m^3. In mountainous regions they lie below 1.3 ng/m^3 due to high altitude above the sea level. Spots of elevated (1.7 – 1.8 ng/m^3) concentrations of TGM are associated with significant emission sources. Regions with significant emissions are characterized by elevated depositions (12 – 30 g/km^2/y). In the eastern part of Turkmenistan and Uzbekistan and south-eastern part of Kazakhstan the depositions are low (3 – 5 g/km^2/y or even lower) because of low precipitation amount and lack of significant emission sources.

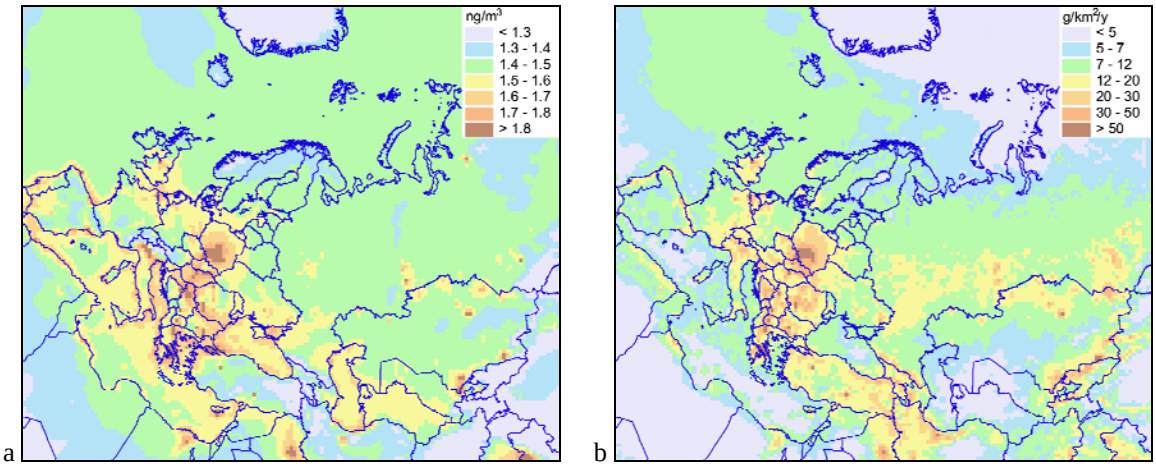

Fig. 3.54. *Annual mean concentrations, ng/m^3 (a) and annual total depositions, g/km^2/y (b) of mercury in 2006*

Mercury concentrations in air (as gaseous elemental mercury or TGM) were reported by 9 stations. However, the information from ES8 was not used because of short period of observations. The data from Polish station PL5 was removed from the comparison because of unrealistic temporal variability (Fig.

3.55). Measured concentrations of mercury vary from 0.5 to 3.5 – 4.5 ng/m^3 throughout the whole year, which is not consistent with current knowledge on mercury levels and behavior in the atmosphere.

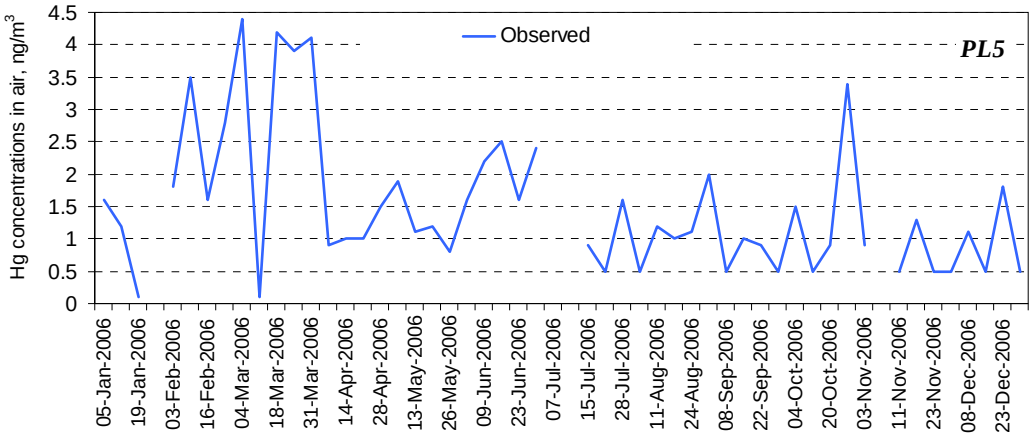

Fig. 3.55. *Concentrations of mercury at Polish station PL5 in 2006, ng/m^3*

Concentrations of the elemental or total gaseous mercury, observed at six EMEP stations, were compared with calculated ones. For stations DE2 and NO1 the difference between the observed and calculated values is around 20% (Fig. 3.56). For the rest of stations the difference is less then 15%, which is comparable with the uncertainty of modelled TGM concentrations relative to uncertainties of the input data for MSCE-HM model [*Travnikov and Ilyin*, 2005].

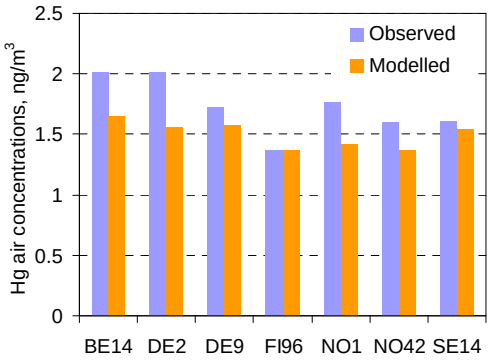

Fig. 3.56. *Comparison of annual mean modelled and measured concentrations of mercury in air, ng/m^3*

Short-term variability of mercury concentrations in air was satisfactorily reproduced by the model over most of stations. For example, at station DE9 most of peaks were caught by the model (Fig. 3.57). Magnitude of some peaks, for example, in January, October and December, was underestimated by the model.

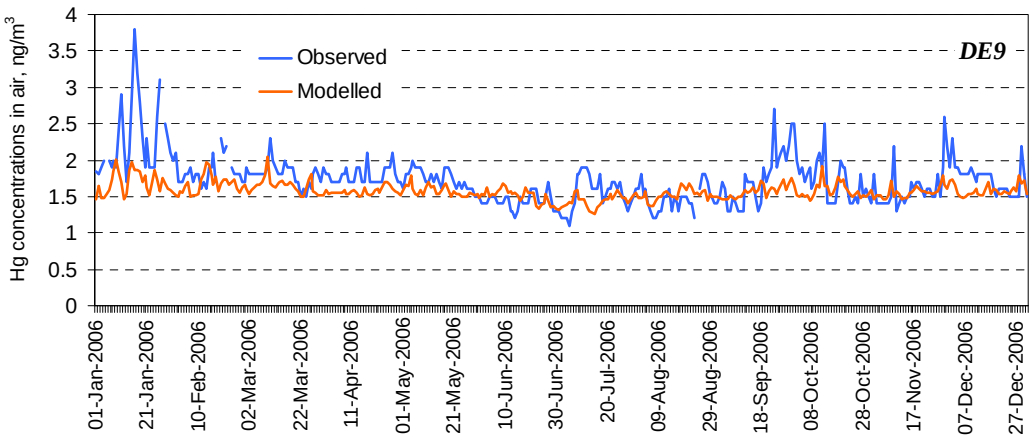

Fig. 3.57. *Daily mean modelled and measured concentrations of mercury in air in 2006 at station DE9 (Zings, Germany), ng/m^3*

Back trajectories were evaluated for days with high peaks of the observed mercury concentrations, not corresponding with calculated ones. For example, high observed concentrations were measured in the middle of January and the beginning of October. In these days the back trajectories were passing over German territory where emissions used in the model are relatively low (Fig. 3.58a, b). Therefore, the modelled concentrations do not exhibit peaks in these days.

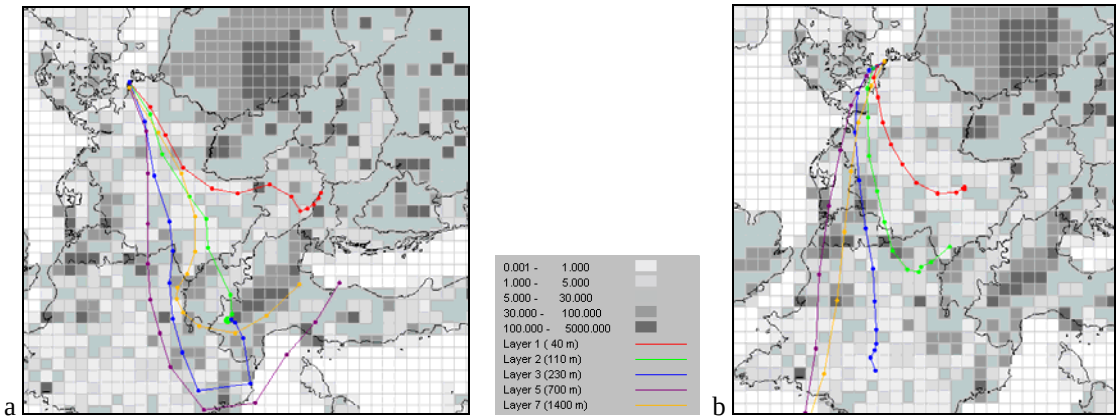

Fig. 3.58. *Back trajectories arriving to station DE9 on January, 16 (a) and October, 1 (b) in 2006 at different model layers. Map background demonstrates spatial distribution of mercury anthropogenic emissions*

At some stations, e.g., NO1 or DE2, the annual mean modelled concentrations of mercury underpredicts the observed ones by around 20% (Fig. 3.56). Comparison of daily mean calculated and observed concentrations, performed for NO1, shows that the observed concentrations exhibit a number of high (up to 2.5 ng/m^3) peaks of concentrations (Fig. 3.59). The duration of these periods with elevated concentrations is about few days.

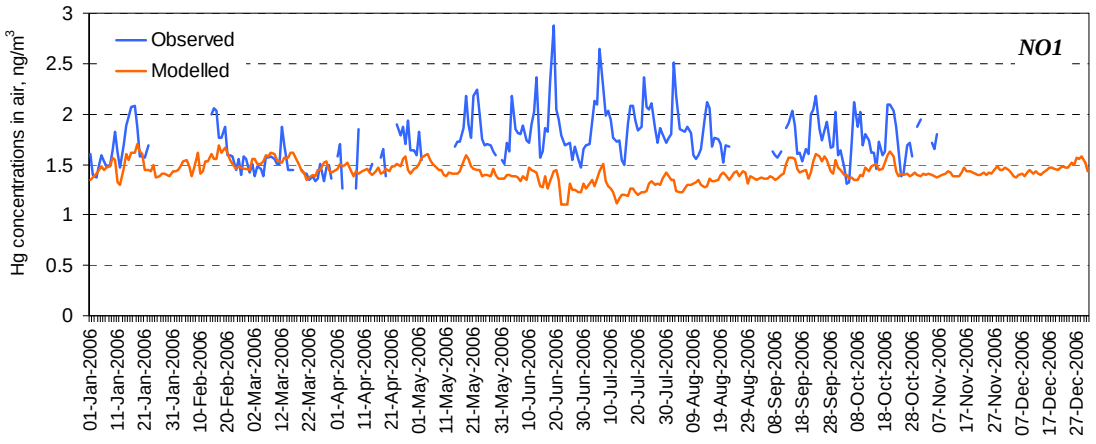

Fig. 3.59. *Daily mean modelled and measured concentrations of mercury in air in 2006 at station NO1 (Birkenes, Norway), ng/m^3*

Back trajectories evaluated for station NO1 for the periods with high peak concentrations of mercury are mostly crossing territories of Denmark, northern part of Germany, and Benelux region (Fig. 3.60 a,b). On the one hand, it is possible that these peaks can be caused by long-range transport from some emission sources located in the countries and missed in the inventories used in the modelling. On the other hand, these peaks may be explained by the influence of local emission sources of anthropogenic or natural origin.

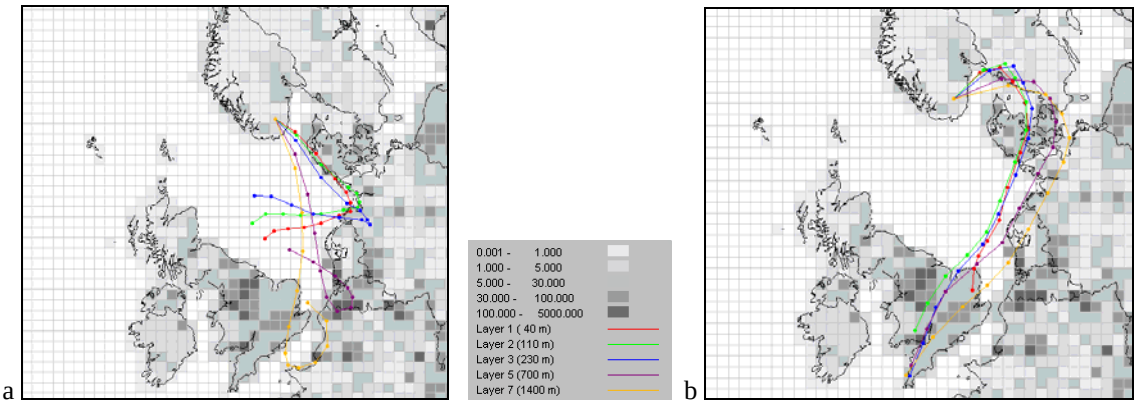

Fig. 3.60. *Back trajectories arriving to station NO1 on June, 19 (a) and August, 02 (b) in 2006 at different model layers. Map background demonstrates spatial distribution of mercury anthropogenic emissions*

Mercury data on concentrations in precipitation are available from 11 stations. The data from 10 of them were used in the verification, while the data from Irish site IE1 were not used. The reason for this is too high detection limit.

The agreement between annual mean calculated and measured concentrations of mercury in precipitation lies within ±25%, and correlation coefficient between modelled and measured values is 0.6 (Fig. 3.61a). The exception is two British stations: GB13 and GB91, where modelled concentrations exceed the observed ones by a factor of 2.3 (Fig. 3.61b). Annual wet deposition fluxes of mercury were on average underestimated by the model by about 20% (Fig. 3.62a). However, at some stations the modelled value either exceeds or lies below the observed one. At stations BE14 and NO1 the concentrations in precipitation agree within ±15%, whereas wet deposition fluxes are underestimated by 40 – 50% (Fig. 3.62b). The reason for this is differences in precipitation amounts measured at the stations and simulated by MM5. Observed precipitation at BE14 were about 1050 mm, and at NO1 – 1840 mm, while modelled values were around 660 and 1300 mm. The opposite situation is noted for station FI96. Calculated and observed concentrations in precipitation agree within 6%, but two-fold difference in precipitation sums resulted to the same difference in deposition fluxes. Nevertheless, spatial variability of the observed wet deposition fluxes was relatively well restored by the model: correlation coefficient is 0.72.

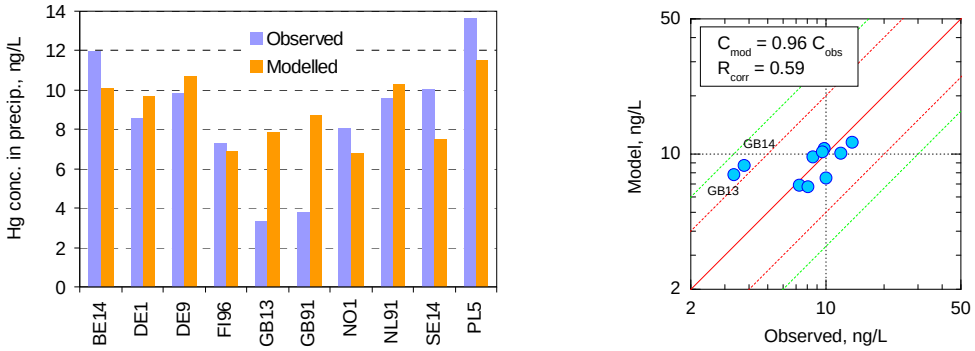

Fig. 3.61. *Comparison of annual mean modelled and measured concentrations of mercury in precipitation Red solid line delineates 1:1 ratio, red and green dashed lines show deviation by a factor of two and three, respectively, ng/L*

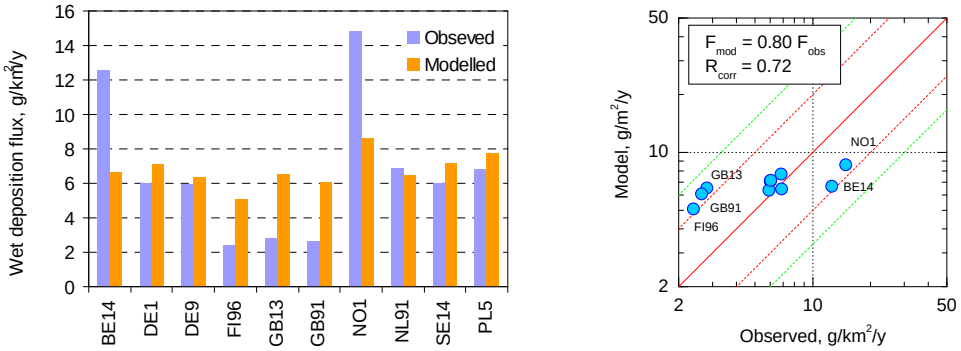

Fig. 3.62. *Modelled and measured annual wet deposition flux of mercury at individual stations for 2006 Red solid line delineates 1:1 ratio, red and green dashed lines show deviation by a factor of two and three, respectively, g/km²/y*

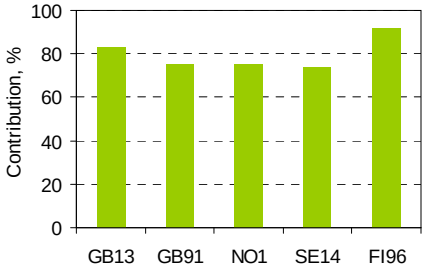

Fig. 3.63. *Contribution of sources located outside EMEP domain to annual mean mercury concentrations in precipitation at remote stations, %*

At two stations - GB13 and GB91 both concentrations in precipitation and wet deposition fluxes are underestimated by the model by about 2.3 times. Both stations are situated in the remote regions far from significant anthropogenic sources. However, at a number of other remote background stations, e.g., FI96, NO1 or SE14 wet depositions and concentrations are significantly higher. Unlike lead or cadmium, mercury is actively involved in the atmospheric chemistry, which includes various reactions of oxidation and reduction. Oxidized forms of mercury are dissolved in cloud drops much better, and particulate mercury is washed out much easier than the elemental form. According to the model calculations, the main contribution (at least 75%) to concentrations in precipitation at GB13 and GB91, as well as at other remote stations (NO1, FI96, SE14) is made by sources (both anthropogenic and natural) located outside EMEP domain (Fig. 3.63). These sources are responsible for a formation of a relatively uniform field of concentrations of elemental mercury around 1.3 – 1.4 ng/m^3. This is in turn favours the establishment of relatively smooth field of

concentrations in precipitation (4 – 10 ng/L) over northern regions of the EMEP domain (Fig. 3.64), where anthropogenic emissions are relatively low (Fig. 3.2c). Therefore, under the current understanding of atmospheric chemistry of mercury, incorporated in the model schemes and the existing input data on chemical reactants (O3, OH-radical etc.) the modelled concentrations in precipitation can hardly vary considerably at the remote stations. On one hand, these low measured concentrations could possibly be controlled by either very specific conditions favouring low wet removal of mercury or by uncertainties of measurements. On the other hand, atmospheric chemistry of mercury remains one of the main sources of uncertainties of modelling results [e.g., *Calvert and Lindberg*, 2005, *Lin et al*., 2006, *Seigneur et al*., 2006]. New findings in this field and the following improvements of model parameterizations could contribute to the solution of this discrepancy.

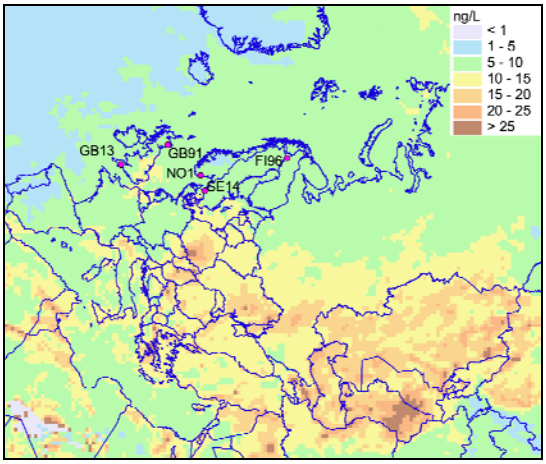

Fig. 3.64. *Annual mean calculated concentrations of mercury in precipitation in 2006, ng/L*

Short-term variability of mercury concentrations in precipitation over most of stations was also satisfactorily well reproduced by the model. For example, location and magnitude of most of weekly mean peaks or low concentrations at stations DE1 (Westerland, Germany) and NL91 (De Zilk, the Netherlands) were captured by the model (Figs. 3.65, 3.66).

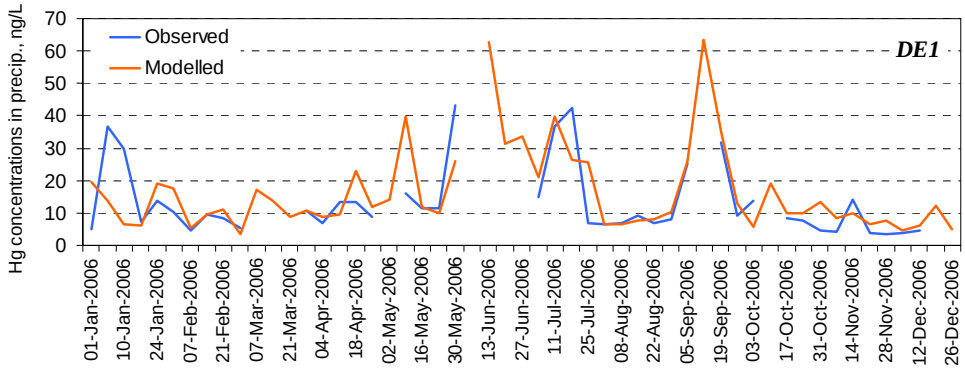

Fig. 3.65*. Weekly mean modelled and measured concentrations of mercury in precipitation in 2006 at station DE1 (Westerland, Germany), ng/L*

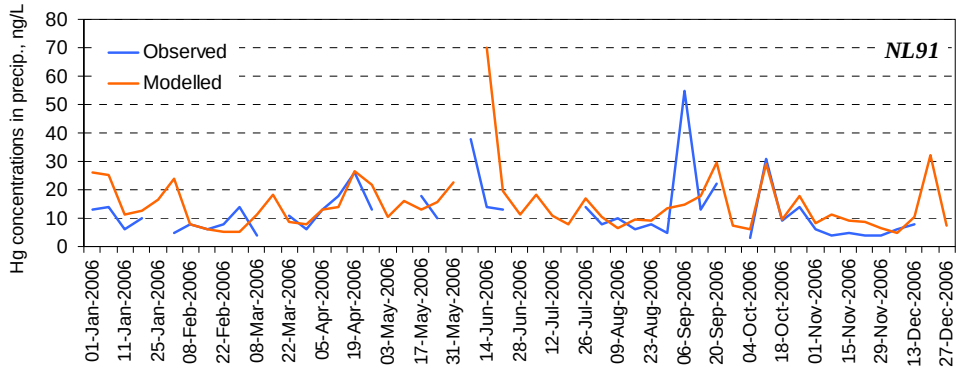

Fig. 3.66. *Weekly mean modelled and measured concentrations of mercury in precipitation in 2006 at station NL91 (De Zilk, the Netherlands), ng/L*

On the base of presented analysis the following concluding remarks can be formulated:

1. Annual mea air concentrations of lead and cadmium were simulated with significant accuracy. The underestimation of the observed values is around 20%, and spatial correlation coefficient is about 0.7.

2. Calculated concentrations of lead and cadmium in precipitation and their wet deposition fluxes are characterized by higher deviation from the observed quantities. For lead the underestimation of the concentrations and the fluxes is around 30%, and for cadmium – about 50%. Nevertheless, temporal variability of measured concentrations and fluxes was reproduced favourably well: the correlation coefficients are around 0.7.

3. Numerical experiments with different emission data were carried out in order to evaluate sensitivity of modelled concentrations and depositions at measurement stations to selection of emission data. It was demonstrated that in some cases (e.g., at Finnish stations) the incorrect emission total value and/or its spatial distribution can possible be a reason explaining the underestimation, at least, in some periods of the year. Nevertheless, in some cases (e.g. at Slovak stations) the possible uncertainties of the emission data alone do not allow to explain the discrepancies between measurements and modelling. In this case possible reason of the discrepancies can be linked with the influence of local emission sources, measurement uncertainties etc.

4. Concentrations of annual mean modelled total gaseous mercury (TGM) agree with the observed ones within ±20%. Modelled concentrations of mercury in precipitation well match the measured ones on average, but wet deposition flux is about 20% lower than the observed one.

5. In addition to annual mean concentrations and depositions of lead, cadmium and mercury, the model is capable of reproducing their short-term variability. Most of the observed peak values were captured by the model both in term of location and magnitude. By means of back trajectory analysis it was shown that the peaks not caught by the model are often associated with air mass transport from regions where emission data used in modelling is low.

Chapter **4**

PERSISTENT ORGANIC POLLUTANTS

This chapter is devoted to the description of the progress in further development of the EMEP multicompartment POP transport model (MSCE-POP). In accordance with the EMEP work plan for 2008 MSC–E continued the refinement of datasets of physical-chemical properties of selected POPs and model parameterizations of POP gas-particle partitioning in the atmosphere, removal of POPs from the atmosphere with precipitation, and POP re-suspension from underlying surface with aerosol particles. Several model experiments were carried out to study the effect of modifications of currently used parameterizations. Model simulations were performed for 2005 since at the moment of these investigations the information on emissions and meteorology for 2006 was not available. The results of model experiments were compared with available measurement data of EMEP network.

Along with the refinement of model parameterizations, appropriate modifications of the regional and hemispheric MSCE-POP models were performed as a result of the extension of EMEP modelling domain. Necessary input data for the MSCE-POP model were prepared. The modifications of the model code and the description of environmental compartments within the extended modelling domain were performed. In particular, the adaptation of the soil, vegetation, and seawater modules describing POP distribution, degradation, and exchange with atmosphere to the extended EMEP grid was started. Preliminary versions of these modules were prepared and used in model simulations for 2006. Further work is required to fully adapt these modules to the extended modelling area and to make them compatible with the hemispheric MSCE-POP model. Some minor modifications were also carried out for the hemispheric MSCE-POP model in order to support the preparation of initial and boundary concentrations for model simulations over the extended EMEP grid.

The extension made it possible to include the Central Asia countries and the Asian part of Russia in the routine EMEP calculations of POP transboundary transport. In this Chapter modelling results obtained for the four indicator PAHs (B[a]P, B[b]F, B[k]F, and I_P), PCDD/Fs, PCB-153, γ-HCH, and HCB are presented. Levels of pollution and transboundary fluxes within the extended EMEP grid for 2006 are described. Extensive verification of modelling results against the measurements of EMEP monitoring network was performed on the example of B[a]P. For other pollutants preliminary comparison with measurements on the level of annual mean concentrations was performed.

4.1. Modification of description of gas-particle partitioning of POPs in the atmosphere

In this section the investigations of model description of POP gas-particle partitioning performed during the current year are described. The gas-particle partitioning process is one of the most important processes influencing long-range transport of POPs both on regional and global scales. First, the gaseous phase of a POP is mostly subject to degradation in the atmosphere. So, the larger the relative fraction of a pollutant in the gaseous phase is, the faster the degradation process goes and, as a consequence, the pollutant is transported through less distance. Second, deposition velocities of gaseous and particle-bound POPs are quite different, so that the process of gas-particle partitioning strongly influences POP deposition process. Thus, the considered process plays a very important role in modelling of long-range transport of POPs.

Description of gas-particle partitioning: approaches

Different approaches to model description of gas-particle partitioning are intensively discussed in the scientific literature (see [*Xiao and Wania*, 2003; *Lohman et al*., 2007; *Meng et al*., 2007; *Li et al*., 2008; *Arp et al*., 2008; *Wei et al*., 2007; *Lohman and Lammel*, 2004; *Götz et al*., 2007] and others). There are two main mechanisms of POP sorption on the atmospheric aerosol: adsorption at the surface of different aerosol particles (mineral dust, soot, etc.) and absorption by the aerosol organic matter. However, at present it is recognized that for proper description of POP gas-particle partitioning several sorption mechanisms should be taken into consideration [*Lohman et al*., 2007; *Götz et al*., 2007].

To describe gas-particle partitioning of POPs the dimensionless distribution coefficient K_p^* between particulate and gaseous air concentrations can be chosen (see [*Götz et al*., 2007]):

$$K_p^* = C_p \Big/ C_g \,, \tag{4.1}$$

where C_p is the concentration of particle-bound POP in the atmosphere (mol/m^3 air), and C_g is the concentration of the POP in the gaseous form (mol/m^3 air). This parameter can be derived through more frequently used partitioning coefficient K_p (mol/μg aerosol) by multiplication of the latter by total suspended particle concentration (TSP, μg aerosol/m^3 air). The aim of the description of gas-particle partitioning is to express the coefficient (4.1) via physical-chemical characteristics of aerosol and a POP in question. Where K_p^* is determined, the fraction φ of aerosol-bound POP can be expressed as:

$$\varphi = K_p^* \Big/ \left(K_p^* + 1\right). \tag{4.2}$$

Two sorption mechanisms – adsorption on the aerosol surface and absorption into the aerosol organic matter – are traditionally used for modelling. The former is described via the subcooled liquid vapour pressure P_{oL} by Yunge-Pankow model [*Junge*, 1977; *Pankow*, 1987].

$$K_p^* = c\theta \Big/ P_{oL} \,, \tag{4.3}$$

where c is the constant dependant on the thermodynamic parameters of the adsorption process and on the properties of aerosol particle surface (it is assumed c = 0.17 Pa·m [*Junge*, 1977] for background aerosol) and θ is the specific surface of aerosol particles, m^2/m^3.

The coefficient K_p^* for absorption into organic matter of the atmospheric aerosol can be evaluated via octanol-air partitioning coefficient K_{oa} [*Harner and Bidleman*, 1998]. Here we use the following relation [*Finizio et al*., 1997; *Pankow*, 1998]:

$$K_p^* = 10^{-9} K_{oa} \cdot C_{OC} / \rho_{oct} \,, \tag{4.4}$$

where C_{OC} is the concentration of organic carbon in the atmosphere (μg/m^3 air) and ρ_{oct} is the density of octanol (kg/m^3).

Besides, there are other mechanisms of gas-particle partitioning such as adsorption on soot surface, etc [*Götz et al.,* 2007]. However, here we consider relative importance of the two above sorption mechanisms for model description of gas-particle partitioning process postponing the consideration of other mechanisms to future research.

Input data

From formulas (4.3) and (4.4) it is seen that for usage the two considered sorption processes in spatially resolved gridded models it is necessary to have spatial distributions of specific aerosol surface θ and the concentration C_{OC} of organic carbon in the atmosphere. Prior to evaluation of relative importance of the above processes for the description of gas-particle partitioning we consider typical values of the parameters θ and C_{OC} in the atmosphere and possible sources of spatial distributions of these parameters.

Typical values for θ and C_{OC} for various regions in Europe (urban, suburban, background and remote) may be found, for example, in [*Lohman and Lammel*, 2004], see Table 4.1.

Table 4.1. *Typical values of aerosol parameters needed for the description of gas-particle partitioning in various European regions according to [Lohman and Lammel, 2004]*

	urban	suburban	background	remote
θ [a], m^2/m^3	$1.1 \cdot 10^{-3}$	$3.5 \cdot 10^{-4}$	$1 \cdot 10^{-4}$	$1 \cdot 10^{-5}$
TSP [a], $\mu g/m^3$	55	22	14	7.7
f_{OM} [a]	0.4	0.25	0.19	0.13
C_{OC} [b], $\mu g/m^3$	22	5.5	2.7	1

[a] Taken from [*Lohman and Lammel*, 2004]

[b] Calculated on the basis of TSP and f_{OM}

Further, *Cohen et al*. [2002] reports the average value of specific aerosol surface of $3.5 \cdot 10^{-4}$ m^2/m^3, and [*Falconer*, 2004] – values of $1.1 \cdot 10^{-3}$ m^2/m^3 for urban aerosols, $1.5 \cdot 10^{-4}$ m^2/m^3 for average continental background, and $4.2 \cdot 10^{-5}$ for clean continental background (cited from [*Meng et al*., 2007]). In [*Meng et al*., 2007] the following values for TSP are reported: 84 $\mu g/m^3$ for urban regions, 66 $\mu g/m^3$ for over-water regions, 57 $\mu g/m^3$ for coastal regions, and 40 $\mu g/m^3$ for rural regions. In the same paper values of C_{OC} of 1 $\mu g/m^3$ for rural and coastal regions and 6.6 $\mu g/m^3$ for urban regions are given. All these figures are in a reasonable agreement with the data of Table 4.1.

For generating spatial distributions of specific aerosol surface and of concentration of organic carbon in the atmospheric aerosol MSC-E attempted to use CMAQ model. With the use of this model spatial distribution of the two above parameters were generated with 6 hours temporal resolution for 2006. The values of specific aerosol surface and OC concentrations for the generated data (annual means averaged over European region together with minimum and maximum values) are presented in Table 4.2.

Table 4.2. *The values of specific aerosol surface and OC concentrations generated by CMAQ (annual means averaged over European region)*

	Average	Minimum	Maximum
θ, m^2/m^3	$6.13 \cdot 10^{-5}$	$1.37 \cdot 10^{-7}$	$2.06 \cdot 10^{-3}$
C_{OC}, $\mu g/m^3$	2.42	0	15.1

The comparison of data presented in Tables 4.1 and 4.2 leads to the conclusion that the results of CMAQ modelling underestimate values of specific aerosol surface obtained by the above measurements. Indeed, average value of specific aerosol surface over Europe obtained by CMAQ ($6.13 \cdot 10^{-5}$ m^2/m^3) is lower than values measured for background European region ($1 \cdot 10^{-4}$ – $1.5 \cdot 10^{-4}$ m^2/m^3). The reason of such underestimation is that CMAQ estimates the aerosol surface area basing on the assumption of spherical form of aerosol particles. As it is noted in the description of CMAQ

algorithms [*Byun and Ching,* 1999] “It is also important to note that the surface area predicted by CMAQ is the surface area for *spherical* particles and may not represent the true surface area available in nonspherical particles or in porous particles such as carbon soot. Empirical correction fractions may be needed for use of CMAQ surface area predictions in certain applications”.

Similarly, the concentration of organic carbon in the aerosol particulate matter seems to be underestimated by CMAQ. This underestimation was earlier mentioned by [*Meng et al*., 2007]: “CMAQ may underestimate the organic fraction of the aerosol, either from the primary organic PM emissions or the secondary organic aerosol formation [*Zhang et al.,* 2004]”.

So, the input data for modelling of gas-particle partitioning both by adsorption and absorption models needs further refinement.

Comparison of particulate fractions predicted by adsorption and absorption models

Here we compare the relative importance of the two considered partitioning mechanisms, that is, the values of partitioning coefficients $K_{p,ad}^*$ and $K_{p,ab}^*$ calculated by formulas (4.3) (adsorption) and (4.4) (absorption), respectively, for various values of environmental parameters (specific aerosol surface θ and organic carbon concentration C_{OC}) and of pollutant-specific parameters (subcooled liquid vapour pressure P_{oL} and octanol-air partitioning coefficient K_{oa}). The values of pollutant-specific parameters are taken at 10 ºC.

The comparison of relative importance of ad- and absorption mechanisms is presented by four plots (Fig. 4.1) corresponding to four pairs of values of (θ, C_{OC}) characteristic of urban (a), suburban (b), background (c) and remote (d) European regions (see Table 4.1). Each plot is drawn in the plane (Log P_{oL}, Log K_{oa}) and contains:

- The thin solid black line at which $K_{p,ad}^* = K_{p,ab}^*$:

$$\log(c\theta) - \log P_{oL} = \log K_{oa} + \log C_{OC} - \log \rho_{oct} - 9\,, \tag{4.5}$$

  according to formulas (4.3) and (4.4). Below this line $K_{p,ab}^* < K_{p,ad}^*$, that is, absorption mechanism is less important than the adsorption one.

- Two dotted green lines, at which $K_{p,ad}^*$ and $K_{p,ab}^*$ differ by one order of magnitude.

- Two solid thick green lines, at which $K_{p,ad}^*$ and $K_{p,ab}^*$ differ by two orders of magnitude.

- Points, corresponding to values of P_{oL} and K_{oa} for three groups of pollutants: polyaromatic hydrocarbons (four indicator compounds – B[a]P, B[b]F, B[k]F and I_P), PCBs (8 congeners – PCB-28, PCB-52, PCB-101, PCB-105, PCB-118, PCB-138, PCB-153, PCB-180), and PCDD/Fs (4 congeners – 2,3,4,7,8-PeCDF, 1,2,3,6,7,8-HxCDD, 1,2,3,7,8,9-HxCDD, and 1,2,3,4,6,7,8-HpCDF).

The choice of the above four PCDD/F congeners is conditioned by the fact that the mixture of these congeners can represent the transport of PCDD/F mixture with accuracy of 20% compared with the transport of the mixture of all 17 toxic PCDD/F congeners (see [*Dutchak et al.,* 2004]).

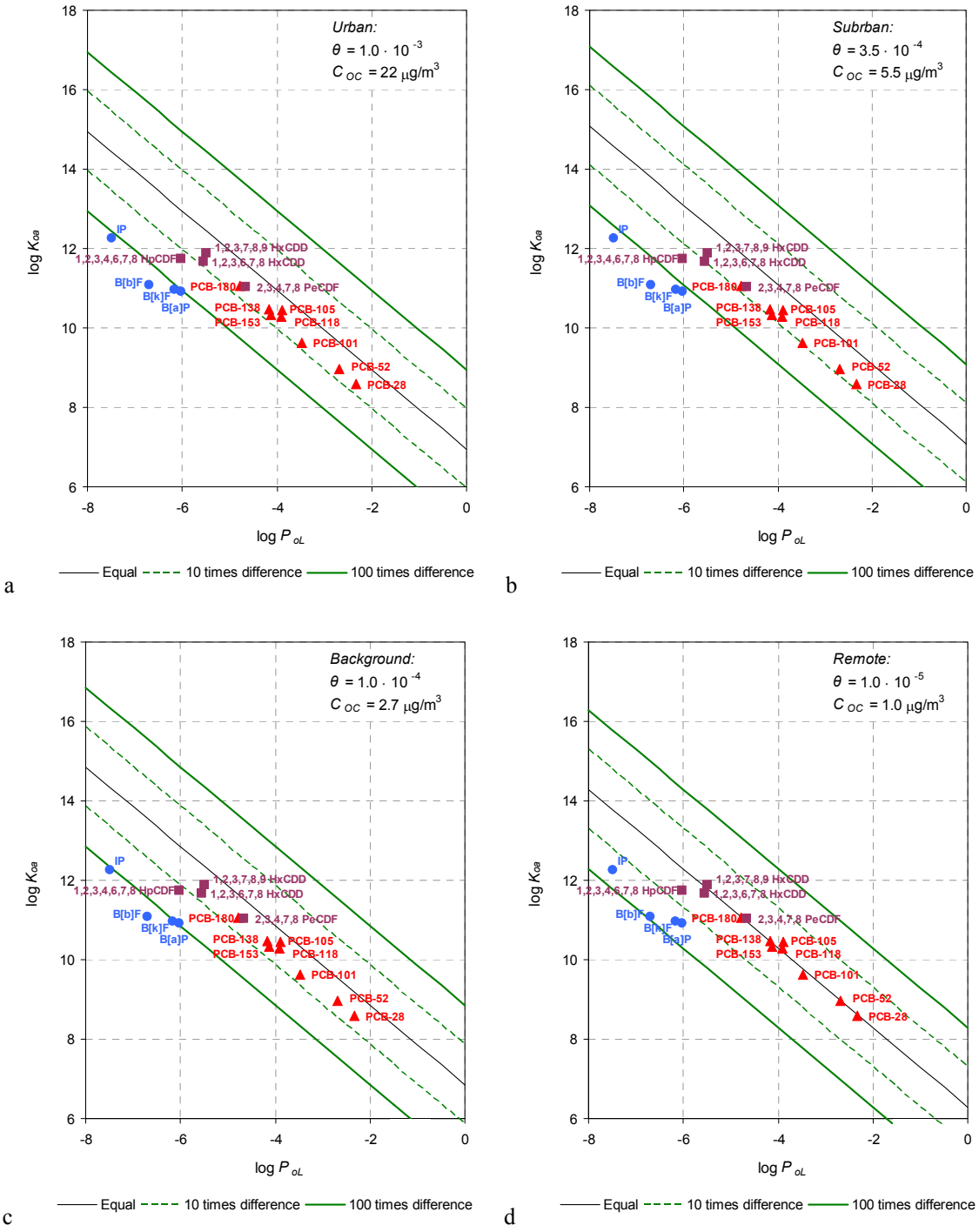

Fig. 4.1. *Comparison of partitioning coefficients $K_{p,ad}^{*}$ and $K_{p,ab}^{*}$ for four typical values of environmental parameters: a – urban, b – suburban, c – background, d – remote. Thin solid line represents the value of the parameters for which $K_{p,ad}^{*} = K_{p,ab}^{*}$, dotted lines correspond to points where $K_{p,ad}^{*}$ and $K_{p,ab}^{*}$ differ by an order of magnitude, and thick solid lines correspond to points where $K_{p,ad}^{*}$ and $K_{p,ab}^{*}$ differ by two orders of magnitude*

The comparison of these four plots leads to the following conclusions:

1. For all considered pollutants except for PAHs the contribution of ad- and absorption mechanisms to the gas-particle partitioning differ not more than by an order of magnitude in urban, suburban and background regions. In remote regions the importance of ad- and ab-

sorption mechanisms for these pollutants is close to each other (at plot Fig 4.1d all five lines lie lower than these lines at plots Fig. 4.1 a–c).

2. The importance of absorption mechanisms for the considered pollutants is lower than the importance of adsorption mechanism for urban, suburban and background regions.

3. For all region types absorption mechanism is of low importance for considered PAHs. For PCBs and PCDD/Fs absorption can contribute considerably to gas/particle partitioning (in urban, suburban and background regions coefficients $K_{p,ab}^{*}$ is only 5 – 10 times less than $K_{p,ad}^{*}$).

While analyzing the importance of ad- and absorption mechanisms one should also take into account temperature dependences of the parameters P_{oL} and K_{oa}. These dependencies are exemplified by PCB-153 at Fig.4.2a and b, respectively. It is seen that the values of P_{oL} and K_{oa} may change about two orders of magnitude in temperature range from – 10 ºC to 25 ºC characteristic of European region.

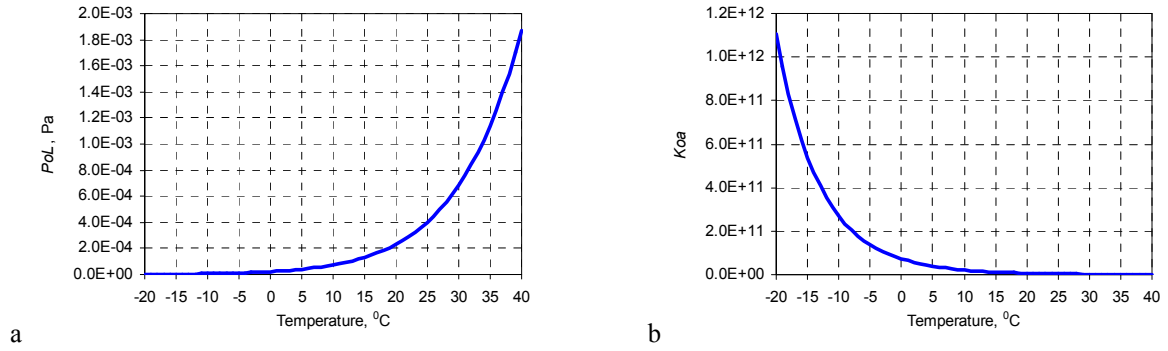

Fig. 4.2. *Temperature dependencies of P_{oL} (a) and K_{oa} (b) for PCB-153*

However, temperature dependencies of P_{oL} and K_{oa} act in opposite directions (P_{oL} is growing with temperature and K_{oa} is decreasing). Further, coefficients of temperature dependence for these two parameters differ by that for octanol-water partitioning coefficient K_{ow}. The latter for the considered pollutants is essentially lower than the coefficient for P_{oL} and K_{oa}. So, temperature dependencies for P_{oL} and K_{oa} are very close to each other.

These two facts lead to the conclusion that, in spite of strong temperature dependence of P_{oL} and K_{oa}, the relative importance of ad- and absorption mechanisms depends weakly on temperature. To illustrate this, the line representing values of P_{oL} and K_{oa} in the considered temperature range is plotted in Fig. 4.3.

It is seen that this line is almost parallel to the lines determining the relations between $K_{p,ad}^{*}$ and $K_{p,ab}^{*}$. Hence, the ratio $K_{p,ad}^{*}$ / $K_{p,ab}^{*}$ is almost constant along the line, and ad- and absorption mechanisms have one and the same importance for different values of temperature.

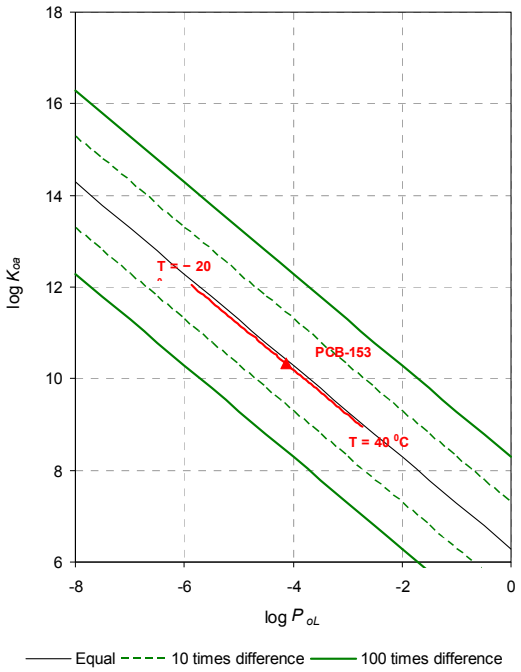

Fig. 4.3. *Comparison of partitioning coefficients $K_{p,ad}^{*}$ and $K_{p,ab}^{*}$ for PCB-153 for temperature values in the range from -20 ºC to 40 ºC*

Calculation experiments

To confirm the above conclusions by model calculations and to reveal the influence of the description of gas/particle partitioning on the main model output four model runs were performed:

- Two model runs for B[a]P in 2005 using the description of gas-particle partitioning by single adsorption and by combined ad- and absorption mechanisms.
- Two model runs for PCB-153 in 2005 using the description of gas-particle partitioning by single adsorption and by combined ad- and absorption mechanisms.

For both pairs of runs emission data and meteorological data are one and the same, so that the only difference between two runs within each pair is gas-particle partitioning mechanism used. The data on specific aerosol surface was taken the same as used in previous MSCE-POP simulations (see [*Gusev et al.,* 2005]). The data on concentrations of organic matter in the atmospheric aerosol were simulated by CMAQ model. As it was already noticed, CMAQ can underestimate specific aerosol surface and OC concentrations in the atmospheric aerosol. It should be noted that usage of elevated organic matter concentrations can lead to the enhanced role of absorption mechanism in calculation results.

Below the difference between model results using adsorption mechanism and combined mechanism are analyzed for these two pollutants.

First of all, calculations of B[a]P transport with two different mechanisms of gas particle partitioning have led to calculated air concentrations, which differ not more than 0.2% over all cells of the EMEP grid. This is in a good agreement with the above analysis of relative importance of ad- and absorption mechanisms for PAHs.

More essential difference between the results using different gas-particle partitioning description is obtained for PCB-153. To analyze this difference we note first that the change in particulate fraction of the pollutant influences mostly deposition processes. The changes in depositions then lead to changes of the calculated air concentrations of the pollutant in question. It was found that for PCB-153 major changes take place for wet deposition process. Thus, we begin the analysis of changes from wet depositions, and then turn to changes of air concentrations resulting from usage of alternative gas-particle partitioning scheme.

The maps of air concentrations and wet depositions obtained in the model run using adsorption only are presented in Fig. 4.4.

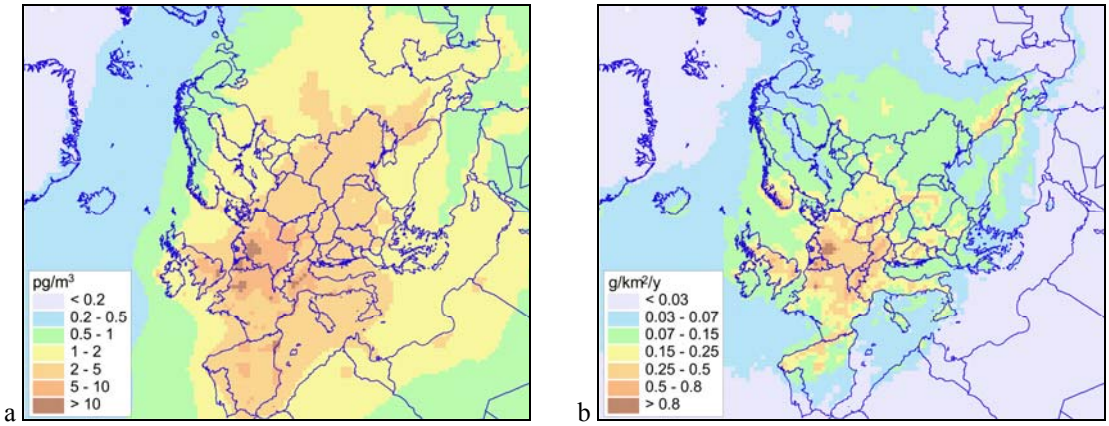

Fig. 4.4. *Calculation results for PCB-153 obtained by usage adsorption gas-particle partitioning scheme: air concentrations, pg/m^3 (a), wet depositions, g/km^2/y (b)*

Fig. 4.4a and b represent typical pattern of contamination in the European region taking into account that European emission sources only were taken into account in calculations.

Now let us turn our attention to the changes due to the use of the combined ad- and absorption scheme. The difference in wet deposition spatial distribution between model runs with two different partitioning schemes (adsorption only and combined ad- and absorption) is presented in Fig. 4.5.

Typical value of the difference between the results of the two model runs in Europe is 2% – 4%. However, in some regions this difference can be higher – from 4% to 6%. The highest values of the difference is obtained at the southern border of Spain – 10% – 20% and higher. This can be explained by the relation between specific aerosol surface and concentrations of organic matter in the region. The comparison of the values of these two parameters in this subregion of Spain and in the entire Europe is presented in Table 4.3.

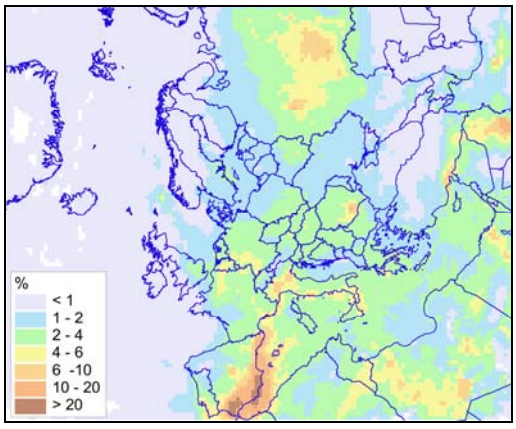

Fig. 4.5. *Difference in PCB-153 wet depositions between calculations using adsorption only and combined ad- and absorption gas/particle partitioning schemes, %*

Table 4.3. *The comparison of data on specific aerosol surface θ and organic matter concentrations C_{OC} in the atmospheric aerosol for entire Europe and southern border of Spain*

	θ, m^2/m^3	C_{OC}, $\mu g/m^3$
Europe	$1.1 \cdot 10^{-3}$	2.42
Southern Spain border	$6.6 \cdot 10^{-4}$	5.38

Thus, in the considered region the average value of specific aerosol surface is almost twice less than in the Europe as a whole whereas the average concentration of organic matter in the atmospheric aerosol is more than two times higher. This leads to the enhanced role of the absorption mechanism in the description of gas-particle partitioning and, as a consequence, to the enhanced difference between the results of the two runs.

Concerning the difference between air concentrations calculated with the use of adsorption only and combined ad- and absorption mechanism, calculations show that the decrease of gaseous PCB-153 fraction due to inclusion of the absorption mechanism can be up to 12%, and the increase of particulate fraction is up to 20%. We recall that the concentrations of organic matter in the atmospheric aerosol used in modelling are obtained from CMAQ model and can be underestimated. The usage of data with higher values of organic matter concentrations can lead to the additional increasing of the influence of absorption mechanism on air concentrations and depositions in the European region.

Conclusions

From the above analysis it can be concluded that:

- There exist several mechanisms of gas-particle partitioning, which can act in the atmosphere simultaneously. The adsorption on particle surface and absorption on organic matter in the atmospheric aerosol are presently included into the model. In future relative influence of the process of adsorption on black carbon (soot particles) should be investigated.
- The data on specific aerosol surface and on concentrations of organic carbon in the atmospheric aerosol generated by CMAQ can be underestimated. At the same time, these data play an important role in the model description of gas-partitioning process. Thus, further work on improvement of the data on the above two environmental parameters is needed.
- The influence of absorption mechanism in gas-particle partitioning for four indicator PAH congeners (B[a]P, B[b]F, B[k]F and I_P) seems to be negligible. However, for other pollutants (PCBs, PCDD/Fs) absorption mechanism can noticeably change gas/particle partitioning.
- Temperature dependence of the subcooled liquid vapour pressure P_{oL} and octanol-air partitioning coefficient K_{oa} do not affect relative influence of ad- and ab-sorption mechanisms, at least for pollutants with weak temperature dependence of octanol-water partitioning coefficient K_{ow}.
- For PCB-153, the output parameter mostly influenced by the change of gas-particle partitioning scheme is wet deposition. The change of wet deposition due to the change of partitioning scheme strongly depend on the data on specific aerosol surface and on concentrations of organic carbon in the atmospheric aerosol.

4.2. Refinement of wet deposition of POPs

This section is aimed at the comparison of different approaches to model description of wet deposition of POP gaseous form. The process of wet removal of POPs from the atmosphere is one of main processes affecting their long-range transport.

The section considers two possible approaches to model description of POP wet deposition and presents the analysis of the influence of the choice of wet deposition scheme on model results (atmospheric concentrations and depositions). Two pollutants (PCB-28 and PCB-153) with different fractions of particulate form in the atmosphere are chosen for the analysis. For each of them two model runs using two different descriptions of wet deposition are carried out and calculation results are compared with each other. Further we perform the comparison of calculation results with measurements at the EMEP monitoring network from the viewpoint of the relation between atmospheric concentrations and wet deposition rates.

Model approaches

Most of the models use the following assumptions for the description of wet deposition process for gaseous form of persistent organic pollutants:

- POP rain water concentrations are in an instantaneous equilibrium with atmospheric concentrations.
- Partitioning between air and rain water is determined by Henry's law constant of the considered POP.

Under these assumptions POP concentrations in the atmosphere and in the rain water are related to each other by

$$C_w = (1 / K_{aw}) \cdot C_a^g \,, \tag{4.6}$$

where C_a^g is the atmospheric concentration of the pollutant in the gaseous form, ng/(m^3 air), C_w is the pollutant concentration in the rain water, ng/(m^3 water), and K_{aw} is the (dimensionless) air-water partitioning coefficient, which is expressed via the Henry's law constant H, Pa · m^3 / mol, by:

$$K_{aw} = H / (R \cdot T), \tag{4.7}$$

where T is the ambient temperature, ºK, and R is the universal gas constant, R = 8.314 Pa·m^3/mol/ºK. The coefficient 1 / K_{aw} in (4.6) is usually named *washout ratio for gaseous form* and is denoted by W_g^0, so that relation (4.6) can be rewritten in the form:

$$C_w = W_g^0 \cdot C_a^g \,, \tag{4.6'}$$

The value of wet deposition flux F_{wd}^g of gaseous form of the pollutant in question, ng/m^2/sec, can be now expressed as:

$$F_{wd}^g = P \cdot C_w \cdot 10^{-3} = P \cdot W_g^0 \cdot C_a^g \cdot 10^{-3}, \tag{4.8}$$

where P, mm/sec, is the precipitation intensity.

While using relations (4.6) – (4.8) for calculations of wet deposition flux, one should take into account temperature dependence of Henry's law constant H:

$$H = \frac{H_0}{RT} \exp\left(- a_H \left(\frac{1}{T} - \frac{1}{T_0} \right) \right), \tag{4.9}$$

where H_0 is the value of Henry's law constant H at the reference temperature T_0 = 283.15 ºK = 10 ºC, and a_H is the coefficient of Henry's law temperature dependence, ºK. The values of H_0 and a_H used in calculations in MSCE-POP model for various pollutants can be found in [*Gusev et al.,* 2005], Annex A.

The above described approach to calculation of wet deposition flux we shall refer as *base*. This is exactly the approach used up to now in MSCE-POP model to calculate wet deposition of POP gaseous form.

However, in the atmosphere rain drops contain not only pure water but also some impurities. These impurities can essentially change the partitioning between atmosphere and rain drops. Here we consider the influence of organic matter (being a part of atmospheric aerosol) on wet deposition. To take this influence into account we consider two different concentrations of a pollutant in a rain drop: the concentration of the dissolved pollutant in the rain water and the concentration of the pollutant sorbed on organic matter contained in the rain water. These two concentrations are related to each other with the help of octanol-water partitioning coefficient K_{ow}:

$$C_w^s = K_{ow} \cdot C_w^d , \tag{4.10}$$

where C_w^d, ng/(m^3 water) is the concentration of a pollutant in the rain drop in the dissolved form, C_w^s, ng/(m^3 OC) is the pollutant concentration in the organic carbon contained in the rain drop, and K_{ow} is the (dimensionless) octanol/water partitioning coefficient. Then total concentration of a pollutant in rain drops C_w, ng/(m^3 rain drops) is given by:

$$C_w = (1 - V_{OC}) \cdot C_w^d + V_{OC} \cdot C_w^s, \tag{4.11}$$

where V_{OC}, (m^3 OC) / (m^3 rain drops) is specific volume of organic carbon in the rain drop. This specific volume can be calculated as:

$$V_{OC} = C_{OC} / \rho_{OC} \cdot 10^{-9}, \tag{4.12}$$

where C_{OC}, (μg OC) / (m^3 rain drops), is organic carbon concentration in rain drops, and ρ_{OC}, kg/(m^3 OC), is the density of organic carbon, The latter is assumed to be equal to the density of octanol, ρ_{OC}=820 kg/(m^3 OC). Since V_{OC} << 1, formula (4.11) can be rewritten in the form:

$$C_w = C_w^d + V_{OC} \cdot C_w^s, \tag{4.11'}$$

Substituting relation (4.12) to (4.11') and taking into account relations (4.6') and (4.10) we obtain:

$$C_w = C_w^d + C_w^d \cdot K_{ow} \cdot C_{OC} / \rho_{OC} \cdot 10^{-9} = W_g^0 \cdot C_a \cdot (1 + K_{ow} \cdot C_{OC} / \rho_{OC} \cdot 10^{-9}), \tag{4.13}$$

The latter formula has the form (4.6') with W_g^0 replaced by the corrected washout ratio for gaseous form W_g^{corr} given by:

$$W_g^{corr} = W_g^0 \cdot (1 + K_{ow} \cdot C_{OC} / \rho_{OC} \cdot 10^{-9}). \tag{4.14}$$

So, total washout ratio W_T (for both particulate and gaseous forms of a pollutant) is expressed as (see [*Gusev et al.,* 2005], Chapter 1):

$$W_T = W_g^{\text{corr}} \cdot (1 - \varphi_{part}) + W_p \cdot \varphi_{\text{part}}, \quad (4.15)$$

where W_p is the washout ratio for particulate form of a pollutant, and φ_{part} is the fraction of the particulate form of a pollutant in the atmosphere.

The approach to the model description of wet deposition process that takes into account sorption on organic matter accumulated by rain drops we shall refer as *modified*.

To implement this approach one needs to calculate the concentrations of organic carbon in rain drops within the model. This is done with the help of wet deposition scheme for particulate form of pollutants using the data on atmospheric organic carbon concentrations obtained by CMAQ model. The value of washout ratio for organic carbon was evaluated with the help of wet deposition scheme realized in MSCE-HM model. To compensate underestimation of OC concentrations in the atmosphere by CMAQ model (see Section 4.1 above), washout ratio was enlarged and assumed to be $1.5 \cdot 10^6$.

Influence of the choice of wet deposition scheme

Let us turn our mind to the evaluation of differences between model calculations using the two above approaches to the description of wet deposition of POP in gaseous form. The expressions for total washout ratios for the two above described approaches are:

base approach: $$W_T = W_g^0 \cdot (1 - \varphi_{part}) + W_p \cdot \varphi_{part}, \quad (4.16)$$

modified approach: $$W_T = W_g^0 \cdot (1 + K_{ow} \cdot C_{OC} / \rho_{OC} \cdot 10^{-9}) \cdot (1 - \varphi_{part}) + W_p \cdot \varphi_{part}. \quad (4.17)$$

The difference between these approaches depends on:

- correction coefficient $1 + K_{ow} \cdot C_{OC} / \rho_{OC} \cdot 10^{-9}$;
- washout ratio for gaseous form $W_g^0 = R \cdot T / H$;
- washout ratio for particulate form W_p.

These parameters depend in turn on environmental parameters such as the concentrations of organic carbon in rain drops, ambient temperature, and on intrinsic pollutant properties such as octanol-water partitioning coefficient, Henry's law constant, fraction of particulate form of the pollutant in the atmosphere. The latter in turn depends on environmental parameters and pollutant's physical-chemical properties. To reveal possible differences due to application of this or that approach, two pollutants were chosen: PCB-28 and PCB-153. These two PCB congeners represent POPs with small particulate fraction (PCB-28) and with large particulate fraction (PCB-153). Calculations show that the value of correction coefficient for PCB-153 is much higher than for PCB-28 due to larger value of octanol-water partitioning coefficient ($1.28 \cdot 10^7$ for PCB-153 against $8.07 \cdot 10^5$ for PCB-28). However, as it will be shown below, the difference in other parameters (mainly in the values of particulate fraction) leads to the fact that usage of the modified scheme for PCB-28 leads to larger changes of wet deposition flux than for PCB-153. Further, atmospheric conditions (ambient temperature, atmospheric aerosol content, concentration of OC in the atmosphere) leads to huge spatial variation of the results (in particular, of differences between wet deposition calculated by the two schemes under

consideration). To analyze such multiple-factor effects, there is a need to perform model calculations using both approaches and to compare them with each other and with measurements.

For each of the two above pollutants model runs using base and modified wet deposition schemes were performed with meteorology for 2005. To take into account the influence of accumulation of PCBs in the environmental compartments and of emission sources located outside the EMEP domain, boundary and initial conditions were prepared on the basis of hemispheric simulations for the period from 1970 to 2005. In this subsection we present the description of the obtained results. Here and below the calculations using base wet deposition scheme will be referred as *base*, and calculations using modified deposition scheme – as *modified*.

Wet deposition. The maps of annual wet depositions for PCB-28 calculated on the basis of base and modified wet deposition schemes are presented in Fig. 4.6.

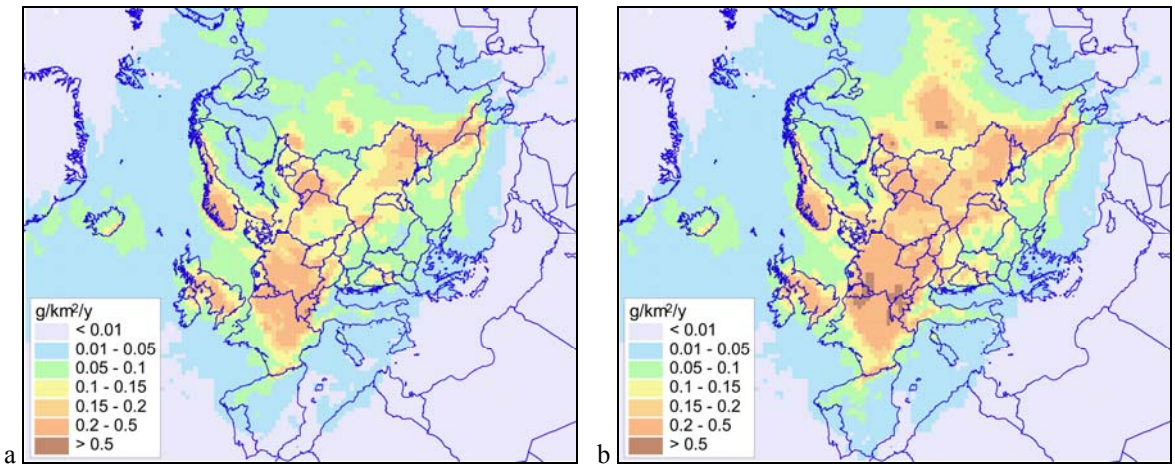

Fig. 4.6. *Annual wet depositions of PCB-28 in 2005: (a) calculations with base deposition scheme, (b) calculations with modified deposition scheme, g/km^2/y*

It is seen that the values of wet deposition flux calculated with the modified scheme are higher than that calculated with the base scheme. Main differences are obtained in the central part of Europe. The differences in wet deposition flux at the periphery of the EMEP region are less pronounced. This fact can be explained by enhanced atmospheric OC concentrations in central parts of European region.

Spatial distribution of wet deposition flux for PCB-153 in 2005 obtained with the two calculation schemes are presented at Fig. 4.7.

The difference in spatial distribution of wet deposition flux obtained for PCB-153 is considerably lower than that obtained for PCB-28. Again, main differences take place in the central part of Europe.

Let us present a numerical description of differences in wet deposition flux obtained with the two above deposition schemes. For PCB-28, the difference between annual wet depositions calculated with the help of base and modified schemes amounts to 22% on the average. For PCB-153 the average is 9%. Cumulative distribution functions for differences due to the change of wet deposition scheme for both pollutants are presented in Fig. 4.8.

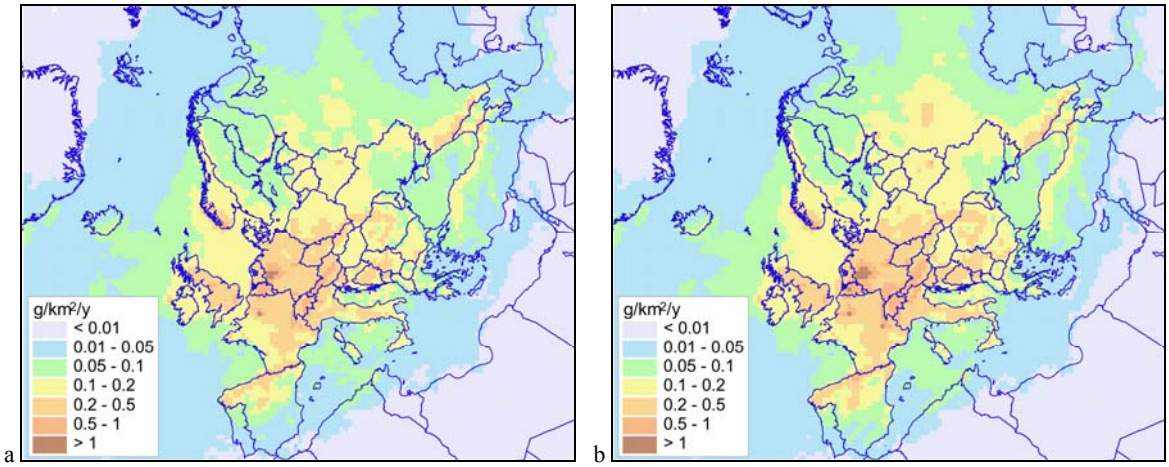

Fig. 4.7. *Annual wet depositions of PCB-153 in 2005: (a) calculations with base deposition scheme, (b) calculations with modified deposition scheme, g/km^2/y*

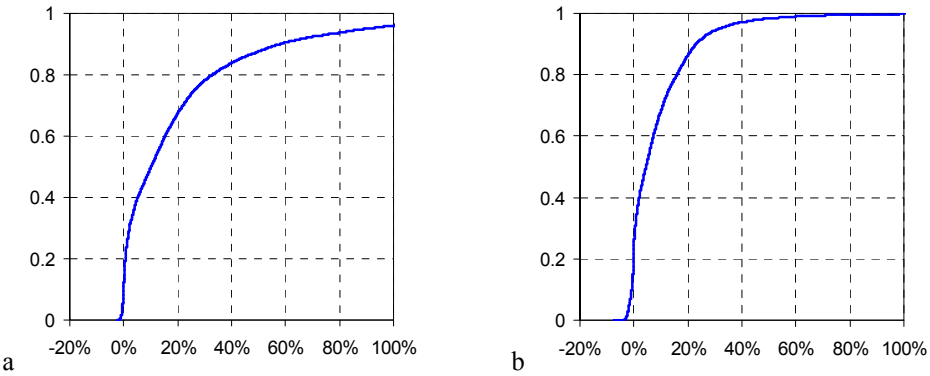

Fig. 4.8. *Cumulative distribution functions for differences in wet deposition flux due to the change of wet deposition scheme: (a) PCB-28, (b) PCB-153*

90% confidence intervals of differences in calculations are from − 0.4% to 90% and from − 1.7% to 31.5%, for PCB-28 and PCB-153 respectively. Negative values of differences are due to the fact that at the periphery of the EMEP region air concentrations are diminished for calculations with the modified scheme due to enlarged depositions in the vicinity of main emission sources. This leads also to the diminishing of the difference between calculations with two wet deposition schemes.

Atmospheric concentrations. First of all, it is worth noting that changes in atmospheric concentrations are not directly determined by changes in wet deposition flux. The reason is that wet deposition process plays different role in the removal of different pollutants from the atmosphere. Relative importance of various removal processes for PCB-28 and PCB-153 is demonstrated by pie charts in Fig. 4.9.

It is seen that the role of wet deposition process for PCB-28 is considerably lower than for PCB-153. This is explained by enhancing role of wet deposition and gaseous exchange with underlying surface characteristic of PCB-28 in contrast to PCB-153 due to larger fraction of the gaseous phase (92% for PCB-28 against 47% for PCB-153 on the average). Further, for both PCB-28 and PCB-153 wet deposition process does not play main role in the removal from the atmosphere. So, it can be expected that the influence of the change in wet deposition scheme will not have essential effect for the considered PCB congeners and that this effect can be larger for PCB-153. Calculations confirm

this expectation showing that the differences in air concentrations due to the change of wet deposition scheme range from − 2% to 1% for PCB-28 and from − 6% to 1% for PCB-153 among the EMEP grid cells. Negative values of the differences show that the change of wet deposition scheme leads to decreasing of air concentrations due to enhanced deposition flux.

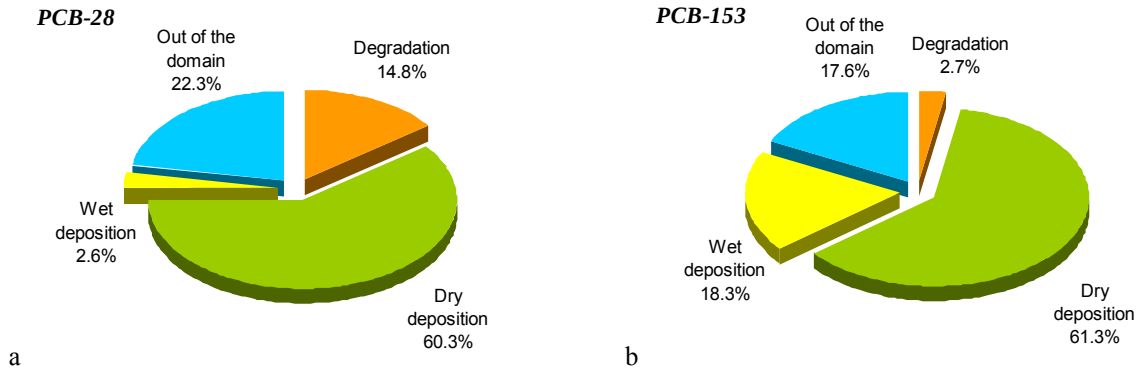

Fig. 4.9. *Relative importance of various removal processes: PCB-28 (a), PCB-153(b), %*

However, in spite of the fact that air concentrations are weakly affected by the change of deposition scheme, it can be expected that enlargement of wet deposition can lead to the enlarging long-term accumulation in media. This assumption should be tested in future in the process of long-term calculations.

Comparison with measurements

Here the comparison of calculation results with measurement data obtained at the EMEP monitoring network is presented. It should be stressed that the aim of the comparison is to validate approaches to model description of wet deposition. So, the focus of the comparison will be the relation between air concentrations and wet depositions rather than absolute values of these parameters. The comparison of calculated absolute values of air concentrations and depositions with measurements is presented in Section 4.6.1 below.

To validate different schemes of wet deposition description, depositions calculated at locations of those monitoring sites where both air concentrations and depositions are measured are normalized. Normalization coefficients are chosen in such a way that annual averages of measured and calculated air concentrations coincide. After that calculated and measured values of wet deposition flux are compared. More precisely, average values of wet deposition fluxes (measured and calculated) are proportional to air concentrations:

$$F_c = k_c \cdot C_c, \tag{4.18}$$

$$F_m = k_m \cdot C_m, \tag{4.19}$$

where F_c and F_m are annual averages of wet deposition fluxes (calculated and measured, respectively), C_c and C_m are annual averages of air concentrations of the pollutant, and k_c and k_m are coefficients depending on washout ratios and precipitation rates. The quality of wet deposition scheme is determined by closeness of the coefficients k_c and k_m. If calculated values of fluxes and

concentrations are normalized in such a way that $C_c = C_m$, then closeness of the coefficients k_c and k_m is equivalent to the closeness of F_c and F_m. For the sites where measurements of air concentrations are absent the average of normalization coefficients over sites with simultaneous measurements in air and precipitation is used.

Such normalization allows excluding to some extent the uncertainties of emission data from the comparison.

PCB-28. Measurements of air concentrations of PCB-28 are available at 7 EMEP sites: CZ3, FI96, NO1, SE12, SE14, IS91 and NO42. Since the comparison of wet deposition flux will be carried out at background sites, for calculation of the average normalization coefficient remote sites IS91 and NO42 were excluded and the comparison for air concentrations were performed over 5 background sites CZ3, FI96, NO1, SE12 and SE14. The comparison of annual averages of air concentrations at these sites is shown in Fig. 4.10.

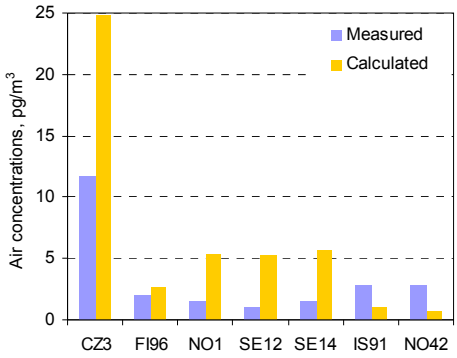

Fig. 4.10. *Calculated and measured annual mean air concentrations of PCB-28 in 2005 at selected EMEP monitoring sites, pg/m^3*

The comparison of calculated and measured air concentrations at the selected sites shows that the model overestimates the values of air concentrations. The reason is that maximum emission scenario by [*Breivik et al.,* 2002b] used in calculations possibly overestimates emission values of PCB-28. To exclude the uncertainties in the emission data, calculation/measurement ratios at all selected sites were obtained (Table 4.4).

Table 4.4. *Calculation/measurement ratios for PCB-28 at the selected EMEP sites*

Site	Air concentrations, pg/m^3		Calc/Meas ratio
	Measured	Calculated	
CZ3	11.6	24.8	2.13
FI96	1.94	2.60	1.34
NO1	1.55	5.33	3.45
SE12	1.01	5.24	5.21
SE14	1.56	5.67	3.65
Average			3.16

Measurements of wet deposition flux are available at 7 monitoring sites: DE1, DE9, NO1, SE12, FI96, SE14 and IS91. However, at three last sites measurements are flagged as being below detection limit (all data at FI96, SE14 and 18 of 23 measurements at IS91), and these sites are excluded from the comparison. The comparison of normalized calculated values of wet deposition flux with the results of base and modified model runs is presented in Fig. 4.11.

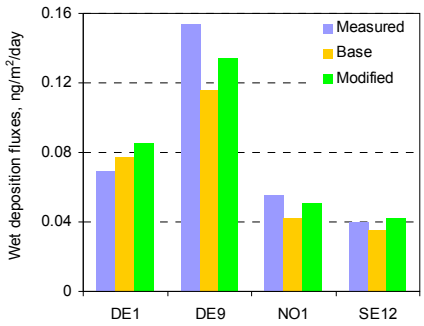

Fig. 4.11. *Comparison of calculated normalized annual wet deposition fluxes for PCB-28 in 2005 obtained by base and modified model runs with measurements at selected EMEP monitoring sites, ng/m^2/day*

It is seen that the agreement between measurements and calculations from the

viewpoint of the quality of wet deposition scheme is reasonable. In most cases modified scheme is closer to measurements than the base one. Certainly, more simultaneous measurements in air and precipitation are needed for better validation of wet deposition schemes used in the model.

The model representation of seasonal variations in wet depositions used presently needs further refinement. To exemplify this, we present the comparison of measured and calculated values of wet deposition flux at two EMEP monitoring sites (Fig. 4.12).

One of the reasons of such discrepancies could be the difference between measured precipitation rates and those used in the model (see Fig. 4.13).

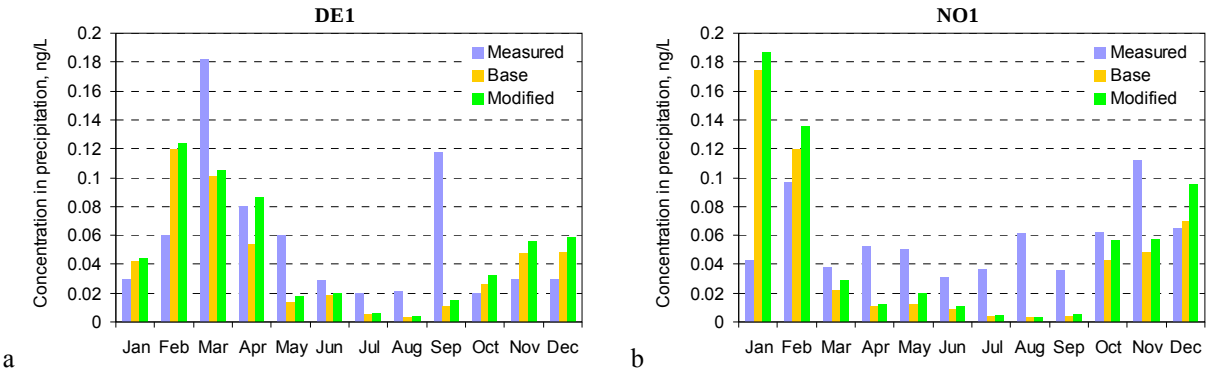

Fig. 4.12. *Comparison of seasonal variations of calculated normalized wet deposition fluxes of PCB-28 in 2005 obtained by base and modified model runs with measurements at two EMEP monitoring sites, ng/L*

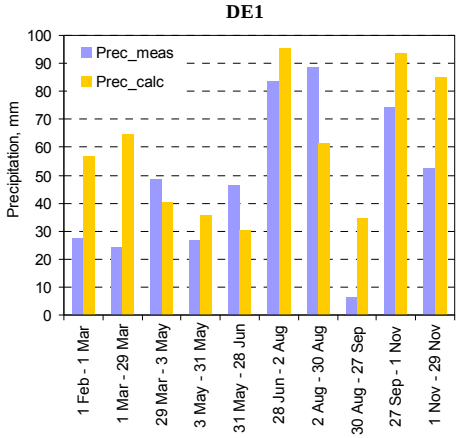

Fig. 4.13. *Comparison of precipitations used in the model in 2005 with measurements at DE1 within periods of observations, mm*

PCB-153. Measurements of air concentrations of PCB-153 are available at 7 EMEP sites: CZ3, FI96, NO1, SE12, SE14, IS91 and NO42. Similar to the case of PCB-28, for calculations of the average normalization coefficient remote sites IS91 and NO42 were excluded from consideration. The comparison of calculated and measured air concentrations at the rest 5 sites is presented in Fig. 4.14.

The comparison of calculated and measured air concentrations at the selected sites for PCB-153 shows that the calculations agree with observations

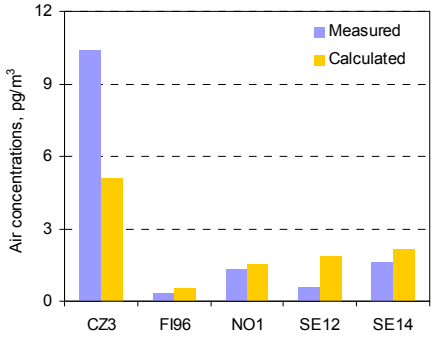

Fig. 4.14. *Calculated and measured annual means of air concentrations of PCB-153 in 2005 at selected EMEP monitoring sites, pg/m^3*

better than for PCB-28. The agreement is mostly within a factor of two with exception of the site SE12. The calculation/measurement ratios at all selected sites are presented in Table 4.5.

Table 4.5. *Calculation/measurement ratios for PCB-153 at the selected EMEP sites*

Site	Air concentrations, pg/m^3		Calc/Meas ratio
	Measured	Calculated	
CZ3	10.4	5.09	0.49
FI96	0.29	0.55	1.89
NO1	1.29	1.50	1.16
SE12	0.57	1.86	3.23
SE14	1.64	2.17	1.32
Average			1.62

Measurements of wet deposition flux of PCB-153 are available at 7 EMEP sites: DE1, DE9, NO1, FI96, SE14, SE12 and IS91. Measurements at two last sites contain values below detection limit and are excluded from consideration. The comparison of normalized calculated values of wet deposition flux for base and modified model runs is presented in Fig. 4.15.

Calculations show that the changes in the value of wet deposition flux due to the change of wet deposition scheme are lower than for PCB-28. Further, at all sites with exception of DE1 the agreement between calculated and measured values of wet deposition flux is reasonable. The reason of the discrepancy between calculations and measurements at DE1 can be due to the difference between measured precipitation rates and those used for modelling.

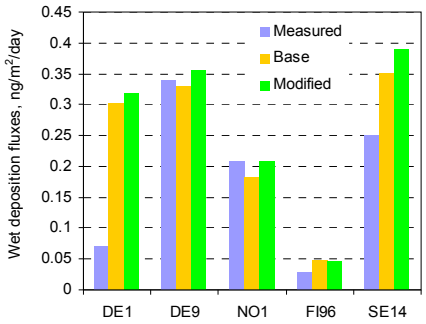

Fig.4.15. *Comparison of calculated normalized annual wet deposition fluxes for PCB-153 in 2005 obtained by base and modified model runs with measurements at selected EMEP monitoring sites, ng/m^2/day*

Conclusions

- A lot of parameters both environmental and pollutant-dependent can govern the wet deposition process. So, for evaluation of the effect of such modification model calculations are reasonable.
- Modification of model description of wet deposition in MSCE-POP model can lead to significant changes in values of wet deposition flux at some locations. In particular, calculations show changes in wet deposition flux up to 4 times for PCB-153 and up to 2 times and more for PCB-28 among the cells of the EMEP grid.
- Changes of wet deposition flux are more pronounced for PCB-28 than for PCB-153. On the average, annual wet deposition flux for PCB-28 have been increased by 22% and for PCB-153 − by 9% only.
- It is reasonable to expect that enhanced values of wet deposition flux can strongly affect POP accumulation in the environmental compartments. This assumption is to be tested in future by long-term calculations.

- For PCB-28 comparison of calculations with measurement data obtained at the EMEP monitoring network shows that the model reasonably describes wet deposition process and that modified scheme of wet deposition is in most cases closer to measurements than the base one. For better validation of wet deposition schemes used in modelling more data on simultaneous measurements in air and precipitation are needed.

- Model representation of seasonal variations of wet deposition fluxes needs further refinement of deposition rates and temperature used in calculations.

4.3. Parameterization of wind re-suspension of particle-bound POPs

The parameterization of wind re-suspension of particle-bound POPs was developed and included in the MSCE-POP model which was described in the MSC-E Technical Report 1/2007 [*Gusev et al.*, 2007]. The pilot simulations with the modified MSCE-POP model for B[a]P were carried out to evaluate the importance of POP re-suspension process with regard to air pollution. This year the analysis of the obtained results and the factors influencing the POP re-suspension from the soil was continued.

Preliminary modelling results for B[a]P presented in the Technical report [*Gusev et al.*, 2007] showed that on average the contribution of B[a]P re-suspension flux to air pollution levels was relatively small in comparison to anthropogenic emissions and re-volatilization fluxes. At the same time it was shown that the re-suspension essentially varied over the Europe and in some regions under the certain conditions its contribution could be quite significant. In particular, the re-suspension flux of B[a]P in several regions of the UK was obtained comparable with the re-volatilization flux from soils varying from 0.1 to 5 g/km^2/y (Fig. 4.16). On the average about 50% of B[a]P re-emitted to the atmosphere from these areas was contributed by the re-suspension. It can be also seen that the same levels of re-suspension takes place in Belgium, Germany, Poland, the Czech Republic, and in some other regions of Europe. However, due to significant anthropogenic emissions the influence of re-suspension flux there is relatively low.

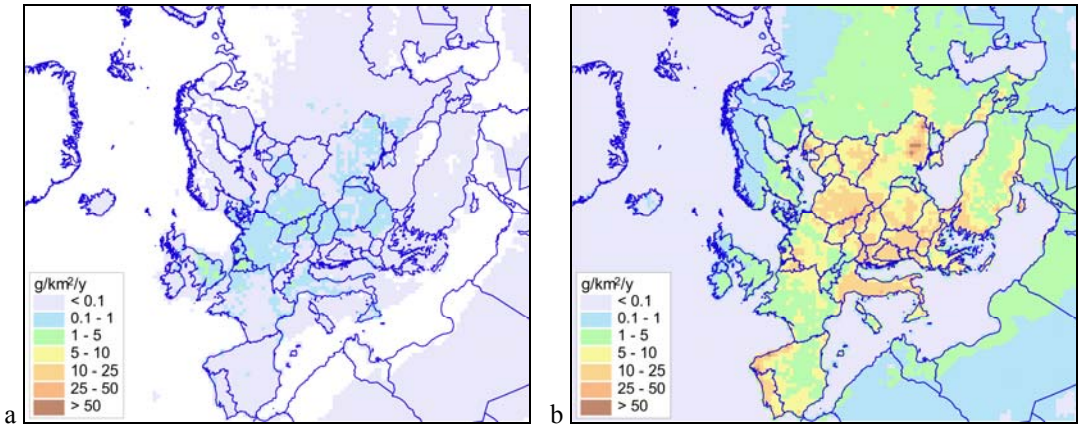

Fig. 4.16. *Spatial distribution of B[a]P re-suspension flux (a) and B[a]P re-volatilization flux (b) to the atmosphere from other compartments (soil, seawater, vegetation) for 2004, g/km^2/y*

Several factors can make the re-suspension process rather essential and almost comparable with anthropogenic emissions and re-volatilization. The role of B[a]P re-suspension from the underlying

surface to the atmosphere can be essential in urbanized and open soil areas which were previously contaminated by PAHs. Certain meteorological conditions like intensive winds and dry weather can also lead to the increasing of re-suspension flux. Its relative contribution can become essential in regions with previously high emission after its decreasing (like, in particular, in the UK).

Additional parameter which can influence the re-suspension flux of POPs from the soil is the POP soil concentrations. Computed levels of B[a]P concentrations were compared with available soil measurements. It should be noted that the number of studies which carried out measurements of PAH soil concentrations in Europe is quite limited. According to these data levels of B[a]P concentrations in soil essentially vary over the Europe. Measurements campaign [*Nam et al.*, 2008] performed in 1998 has obtained the levels of B[a]P concentrations in upper soil layer in the background locations ranging from 1.6 to 1600 μg/kg in the UK and from 0.5 to 86 μg/kg in Norway (Table 4.1).

Results of this study have shown that B[a]P concentrations in soils in the UK were much higher than in Norway and the variations of concentrations is very significant. Comparison of modelling results with these measurements revealed that the MSCE-POP model tended to underestimate the levels of B[a]P in soils and provide more smooth distribution of soil concentrations.

Measurement of PAH concentrations in soils are performed on regular basis at the Košetice (CZ3) monitoring site in the Czech Republic. Comparing the range of measured B[a]P soil concentrations at the CZ3 site with model estimate for 2004 it can be seen that the computed value is within the observed concentration range (Table 4.6). At the same time there is some tendency to underestimate measured B[a]P soil concentrations.

Table 4.6. *Comparison of measured B[a]P concentrations in soil in different parts of the Europe with modelling results of MSCE-POP model, ng/g soil (dry weight soil)*

Location	Year	Measurements	Model results	Reference
UK	1998	1.6 - 1600	0.02 – 1.25	*Nam et al.* [2008]
Norway	1998	0.5 - 86	0.02 – 0.7	*Nam et al.* [2008]
Košetice (Czech Republic)	2004	1.6 - 88	1.8	*Holoubek* [2008]

The underestimation may be caused by several reasons, including underestimation of B[a]P emission in previous years, uncertainties in parameterization of B[a]P degradation in soil, and spatial resolution of the model. It might be necessary also to use longer simulation period to achieve higher levels of concentrations in soil. Taking this into account further work is required to refine model parameterization of PAH degradation in soil, to study historical emission of PAH, and to improve the agreement between the observed and calculated values of B[a]P concentrations in soil.

4.4. Input data for the extended EMEP domain

Necessary input information for the extended EMEP modelling domain (namely emissions, meteorological data, land-cover, data on reactants content in the atmosphere, sea currents and soil properties) was prepared and analyzed in order to be consistent with the previously used data. The preparation of the meteorological input, land cover, and data on reactants for the extended EMEP grid is described in the Chapter 3, where the modification of MSCE-HM model is considered. In this section a brief discussion of the emissions for 2006 and preparation of the data on sea currents and soil properties for the extended grid is presented.

4.4.1. Emission data

Polycyclic Aromatic Hydrocarbons (PAHs)

Evaluation of pollution of European region and Central Asian countries by Polycyclic Aromatic Hydrocarbons (PAHs) for 2006 was carried out for the four indicator compounds of PAHs (benzo[a]pyrene (B[a]P), benzo[b]fluoranthene (B[b]F), benzo[k]fluoranthene (B[k]F) and indeno[1,2,3-cd]pyrene (I_P)). The official information on total emission of these four PAHs is available for 27 European countries for 1990-2006 (for at least one year) among which 20 countries submitted emissions of each indicator PAH for at least one year from the considered period. The information on spatial distribution of PAH emissions was provided by 24 European countries. Denmark, Norway and Sweden submitted additionally the spatial distribution of PAH emission from shipping.

For the evaluation of pollution levels within the EMEP region officially submitted PAH emissions were complemented by unofficial emission data. In particular, for European countries, which did not report their emissions, unofficial data of TNO emission inventory [*Denier van der Gon et al*., 2005] were used. The PAH emissions in the Asian part of Russia were estimated using official emission data for the European part of the country and the ratio between the population [*Li*, 1996] of European and Asian parts of the country. The PAH emission values for Tajikistan, Turkmenistan and Uzbekistan for 2004 were taken from the global atmospheric emission inventory of PAHs prepared by *Zhang* [2008] and used for modelling of pollution levels in 2006. For Kazakhstan and Kyrgyzstan unofficial emission data from TNO inventory [*Denier van der Gon et al*., 2005] were applied. The spatial distribution of PAH emissions in the Central Asian countries and the Asian part of Russia was determined on the basis of data on population density [*Li*, 1996] obtained from the web site of Canadian Global Emissions Interpretation Centre [http://www.ortech.ca/cgeic].

The spatial distribution of annual emissions of four indicator PAHs within the extended EMEP grid for 2006 is shown in Fig. 4.17. It can be seen that the emissions of all four indicator PAHs have similar spatial distribution.

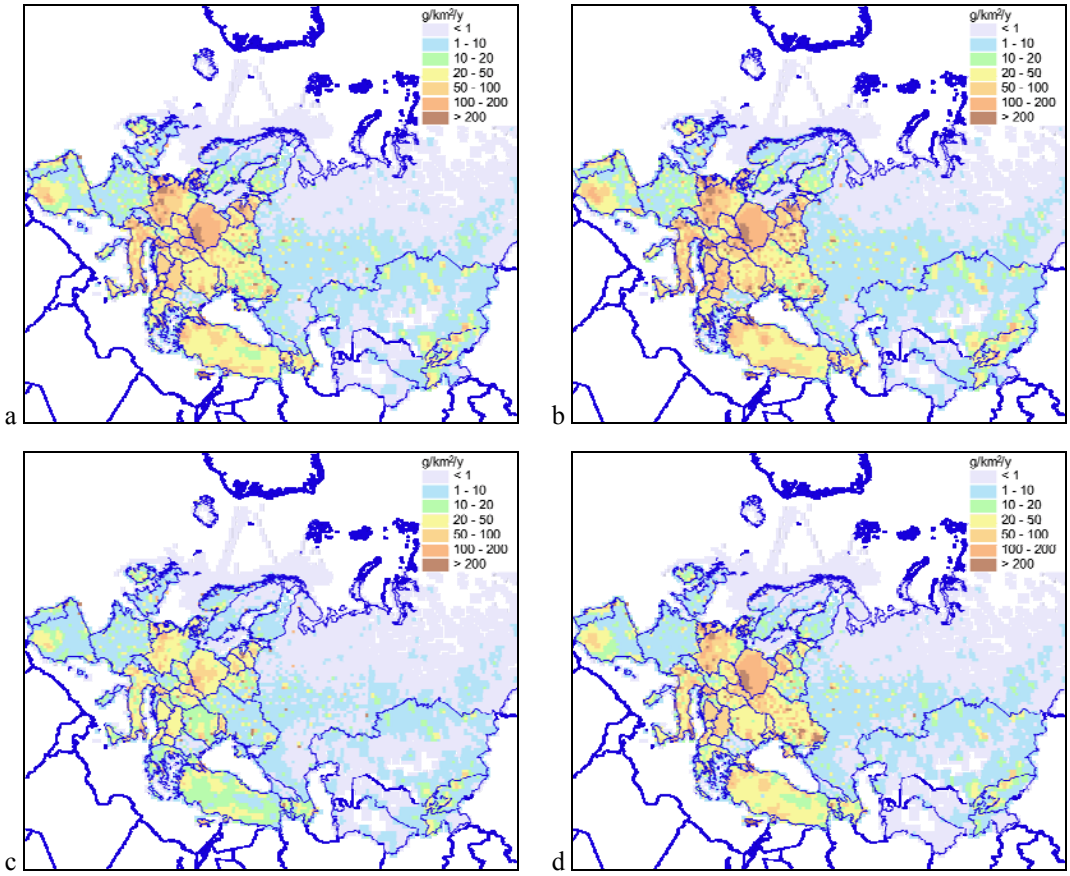

Fig. 4.17. *Spatial distribution of annual emission of B[a]P (a), B[b]F (b), B[k]F (c), I_P (d) for 2006 over the extended EMEP grid with resolution 50x50 km^2, g/km^2/y*

Polychlorinated dibenzo(p)dioxins and dibenzofurans (PCDD/Fs)

Modelling of polychlorinated dibenzo(p)dioxins and dibenzofurans (PCDD/Fs) long-range transport and depositions within the extended EMEP grid for 2006 was performed on the basis of officially submitted emission data and unofficial information on emissions. Official data on total emissions of PCDD/Fs (sum of toxicities of 17 toxic PCDD/F congeners) were reported by 35 European countries and Canada for the period from 1990 to 2006 (for at least one year).

In absence of officially reported information unofficial data of emission inventories [*Denier van der Gon et al*., 2005; *Pulles et al.,* 2006] were applied. The PCDD/F emission for the Asian part of Russia was estimated using official emission data for the European part of the country and data on population density similar to PAHs. The PCDD/F emission values in Tajikistan, Turkmenistan and Uzbekistan for 2006 were taken from the unofficial inventory of PCDD/F emissions in the Central Asian countries made in the framework of the global International POPs Elimination Project (IPEP) [*Hodjamberdiev,* 2006]. The latest available information on PCDD/F emission in the USA was taken from the dioxin and furan inventories prepared by [*UNEP*, 1999] for 1995. The spatial distribution of PCDD/F emissions in the Central Asian countries and the Asian part of Russia was determined on the basis of data on population density [*Li*, 1996] obtained from the web site of the Canadian Global Emissions Interpretation Centre [http://www.ortech.ca/cgeic].

Spatial distribution of PCDD/F emissions within the extended EMEP grid was prepared on the basis of officially submitted gridded data of 24 European countries. Data of Denmark, Norway and Sweden included information on spatial distribution of shipping emissions. For other European countries, unofficial emission data of TNO inventory [*Denier van der Gon et al*., 2005] was applied. For the evaluation of spatial distribution of PCDD/F emission in Asian part of Russia, Kazakhstan, Kyrgyzstan, Tajikistan, Turkmenistan and Uzbekistan data on the population density for 1990 were used.

The spatial distribution of annual emissions of PCDD/F within the extended EMEP grid for 2006 is shown in Fig. 4.18.

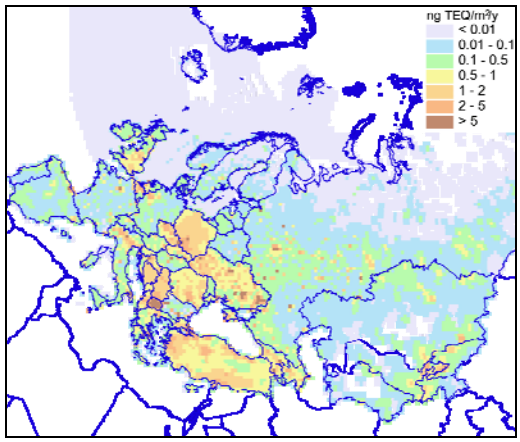

Fig. 4.18. *Spatial distribution of PCDD/F annual emission for 2006 over extended EMEP grid with resolution 50x50 km^2, ng TEQ/m^2/y*

Polychlorinated biphenyls (PCB-153)

Since the official information on PCB emissions within the European region is currently available for a limited number of countries and it does not provide the information on PCB congener composition, the evaluation of PCB long-range transport is currently based on unofficial global inventory of PCB usage and emission [*Breivik et al*., 2007]. The inventory provides consistent set of historical emissions of PCBs to the atmosphere obtained on the basis of available data on production and consumption of PCB mixtures and projection of future levels of emissions up to 2100. Along with temporal variations of PCB emissions of individual countries the spatial distribution of annual emissions of 22 individual PCB congeners on global scale with resolution 1°x1° was prepared. Three different scenarios of global PCB emissions, namely, minimum scenario, default scenario, and maximum scenario, describe the range of emission variations estimated to an order of magnitude [*Breivik et al*., 2002 a,b].

Preliminary computations with the hemispheric MSCE-POP model using these three emission scenarios allowed to evaluate what emission data could be used as input information for modelling to get reasonable description of pollution levels within the EMEP region. Using the results of these computations, the emission values between the maximum and default emission scenario were selected for the investigation of PCB long-range transport and depositions. The indicator congener PCB-153 was selected for the evaluation of pollution levels for 2006 on regional and hemispheric scales. On the basis of this information the spatial distribution of PCB-153 emission for the European region with resolution 50x50 km^2 (Fig. 4.19b) and within the Northern Hemisphere with resolution 2.5°x2.5° (Fig. 4.19a) was prepared for MSCE-POP model simulations. It can be seen that the most significant levels of PCB-153 emission fluxes are the characteristic of the European region. Other regions are characterised by comparatively lower annual emissions. Since there was no information on seasonal variation of PCB emissions to the atmosphere it was assumed that it was uniformly distributed over a year.

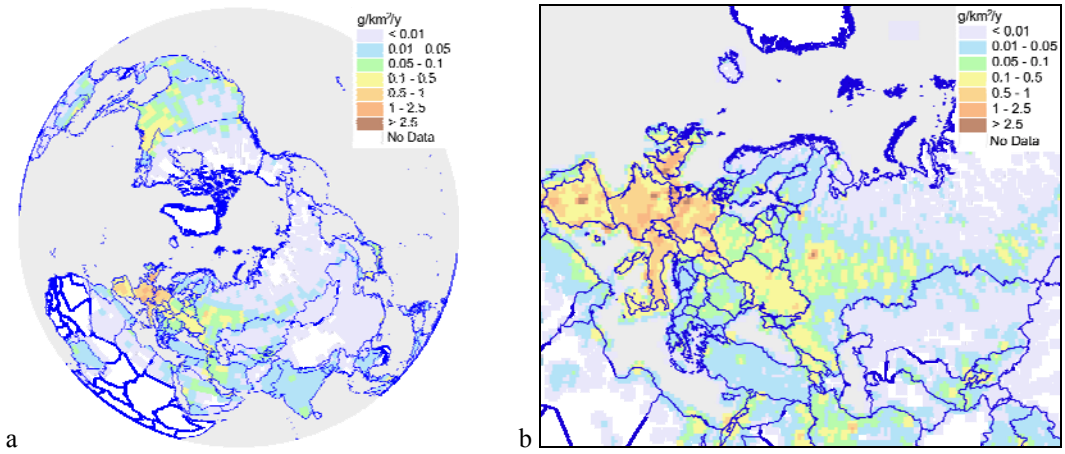

Fig. 4.19. *Spatial distribution of PCB-153 annual emission for 2006 over the hemispheric model grid with resolution 2.5°x2.5° (a) and the extended EMEP grid with resolution 50x50 km² (b), g/km²/y*

Hexachlorobenzene (HCB)

For modelling purposes officially submitted data were complemented by unofficial emission estimates of [*Pacyna et al.*, 1999] in cases when there were no officially reported emissions. Official data on the emission totals of HCB were submitted by 25 European countries and Canada for the period from 1990 to 2006 (for at least one year). The information on the spatial distribution of HCB emissions was submitted by 12 countries.

The HCB emission values for Kazakhstan, Kyrgyzstan, Tajikistan, Turkmenistan and Uzbekistan were estimated on the basis of the gross domestic product of these countries. Relationship between the gross domestic product and unofficial HCB emissions for these countries was obtained on the basis of the data for Azerbaijan taken from [*Pacyna et al.*, 1999].

To compile the distribution of HCB emission within the Northern Hemisphere unofficial information of *Bailey* [2001] was used. The HCB emission for Japan for 2002 was taken from the emission inventory of *Toda* [2005]. The HCB emission values in China, Pakistan, Republic of Korea and the Asian part of Russia were estimated on the basis of the relationship of the gross domestic product and official HCB emission data for 2006 taken for countries with similar economic indexes. The HCB emission value in India was taken from the previous studies of HCB pollution levels presented in EMEP Technical Report 7/2005 [*Shatalov et al.*, 2005].

The distribution of HCB emissions over the EMEP grid was prepared on the basis of officially submitted gridded emission data of 12 European countries. For other European countries, the spatial distribution of HCB emissions from TNO inventory [*Denier van der Gon et al.*, 2005] was used. For the evaluation of the HCB emission spatial distribution in the Asian part of Russia, Kazakhstan, Kyrgyzstan, Tajikistan, Turkmenistan and Uzbekistan within the EMEP grid as well as in the Northern Hemisphere the data on the population density for 1990 [*Li*, 1996] were implemented.

The spatial distributions of HCB emissions for 2006 within the EMEP domain and the Northern Hemisphere are shown in Figs. 4.20. It can be seen that there is a significant difference between the national emission levels of individual countries. In particular, the highest HCB emission fluxes can be noted for Spain (over 9 g/km^2/y). Moderate values of emission fluxes (3-9 g/km^2/y) are characteristic of the Russian Federation, the Ukraine, and the UK. Levels of emissions in other European countries are considerably lower.

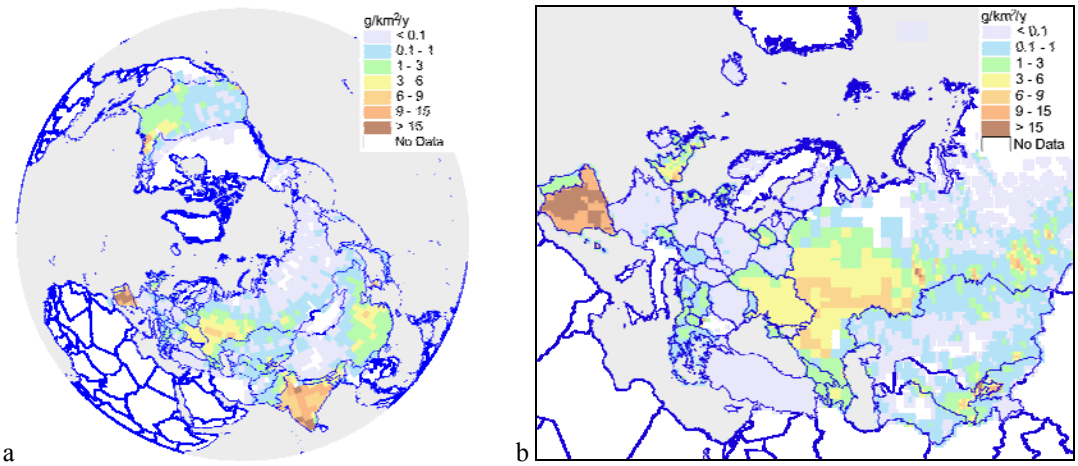

Fig. 4.20. *Spatial distribution of HCB annual emission for 2006 over the hemispheric model grid with resolution 2.5°x2.5° (a) and the extended EMEP grid with resolution 50x50 km² (b), g/km²/y*

Lindane (γ-HCH)

Model evaluation of pollution levels of lindane (γ-HCH) within the EMEP region was based on the official emission data and unofficial information on emission. Data on emissions or usage of γ-HCH for hemispheric modelling for the period 1990-2006 were compiled from several sources and covered only part of the Northern Hemisphere being thus subject of significant uncertainties. Three groups of emission sources were considered, namely, European, North American, and Chinese emission sources. For European region official information on emissions was complemented by unofficial estimates on γ-HCH usage in period 1990-1996 [*Pacyna et al.*, 1999] and expert estimates of γ-HCH emission for 2000 [*Denier van der Gon et al.*, 2005]. The γ-HCH emission values in North America and China were estimated on the basis of information from [*Shatalov et al.*, 2003 [*Li et al.*, 1996; *Macdonald et al.*, 2000], [*Gusev et al.*, 2005 [*Li et al.*, 2001]], and [*Li,* 2004].

The spatial distribution of γ-HCH emissions within the European region was obtained from the officially submitted data (Belgium, Germany, and Spain) and from expert estimates [*Pacyna et al.*, 1999; *Denier van der Gon et al.*, 2005]. The gridded γ-HCH emissions for North America was prepared by *Li* [2004]. For the evaluation of the γ-HCH emission spatial distribution in China over the 2.5°x2.5° calculation grid, data on using cropland area available in the Canadian Global Emissions Interpretation Centre [http://www.ortech.ca/cgeic] were used.

The spatial distribution of γ-HCH emissions within the Northern Hemisphere and over the EMEP grid for 2006 used for model simulations is presented in Fig. 4.21. Taking into account that the usage of lindane (γ-HCH) is severely restricted in Europe and that most of countries reported no application of lindane, no emission of γ-HCH in 2006 was assumed for these countries in model simulations.

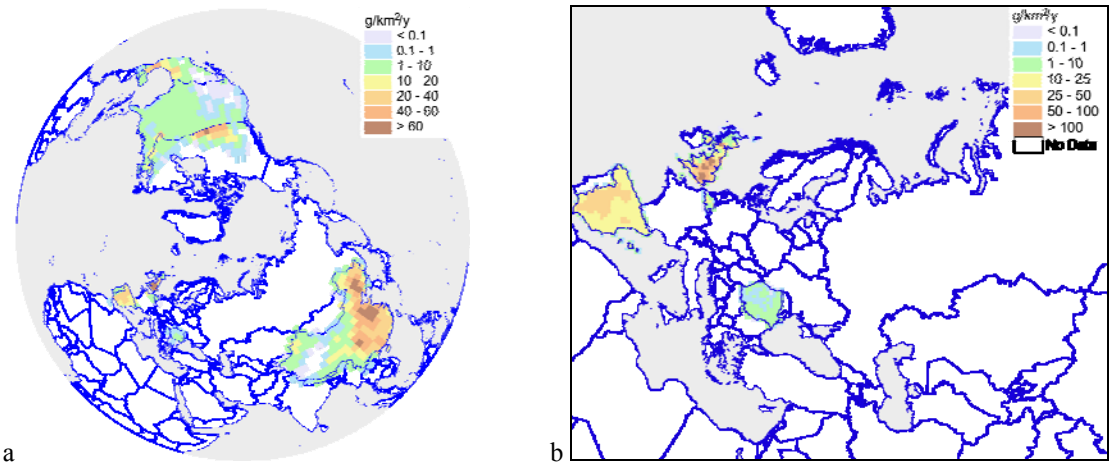

Fig. 4.21. *Spatial distribution of γ-HCH annual emission for 2006 over the hemispheric model grid with resolution 2.5°x2.5° (a) and the extended EMEP grid with resolution 50x50 km² (b), g/km²/y*

4.4.2. Geophysical information

The geophysical information required by the MSCE-POP model includes data on land-cover, data on reactants content in the atmosphere, specific aerosol surface in air, sea currents, and soil properties. MSCE-POP and MSCE-HM models use the same land cover information and data on reactants content in the atmosphere. These data sets are described in the Chapter 3 of this report, where the modification of MSCE-HM model is considered. In addition to them MSCE-POP utilizes the data on organic carbon content in soil, data on specific aerosol surface in air and data on sea currents.

Data on the organic carbon content in top soil layer for the extended EMEP grid were constructed on the basis of spatial distribution of soil types and their specific organic matter content. The spatial distribution of soil types was adopted from the GIS dataset "Global Distribution of FAO Soil Units at 1°×1° Resolution", which distinguishes 27 soil types [*Zobler*, 1986; http://www.giss.nasa.gov/data/landuse]. The specific soil organic matter content for individual soil types is obtained on the basis of the information from [*Fraters*, 1993]. Using these data the fraction of organic carbon content in soils for all grid cells of the regional MSCE-POP model was calculated.

The spatial distribution of specific aerosol surface at global scale and its temporal variations were provided by Dr. Sunling Gong (Canada). This information was interpolated to the extended EMEP modelling grid system.

The MSCE-POP model uses the data on sea currents obtained from the ocean general circulation model (OGCM) [*Resnyansky and Zelenko*, 1991; 1992; 1999]. These data describe three-dimensional structure of velocity fields in the oceanic depth and the surface mixed layer depths within the EMEP grid. The velocity fields and the upper mixed layer thickness are defined for every two days with linear interpolation of values obtained within this period of time. Description of this information can be found in MSC-E Technical Note 5/2000 [*Strukov et al.*, 2000]. The work on preparation of sea currents data for the new extended EMEP grid and adaptation of seawater module has been started. At this stage the data on sea currents are defined within the boundaries of previous EMEP grid. For the seawater areas beyond this grid no sea currents is currently assumed. Further work is required to fully adapt and test the seawater module to the extended area and to make it compatible with the hemispheric MSCE-POP model and being developed global EMEP model for POPs.

4.5. Model results for 2006 over the extended EMEP domain

In this section the information on spatial distribution of air concentrations and annual depositions of B[a]P and PCDD/Fs within the EMEP domain along with the evaluation of transboundary transport is presented.

4.5.1. Polycyclic Aromatic Hydrocarbons (PAHs)

Calculations of pollution levels of the four indicator PAH congeners (B[a]P, B[b]F, B[k]F and I_P) for 2006 were performed with the help of regional model with resolution 50x50 km^2 in the extended EMEP domain. This domain includes, in particular, Central Asian countries (Kazakhstan, Kyrgyzstan, Tajikistan, Turkmenistan and Uzbekistan). Special attention was paid to the evaluation of contamination in these countries.

The results of the calculations were compared with available measurement data obtained at the EMEP monitoring network. Further, on the example of B[a]P the transboundary transport of PAHs between the European and Central Asian countries within the extended EMEP region was evaluated. The results of model calculations are presented in the form of country-to-country matrices of total annual depositions.

For the evaluation of atmospheric pollution levels (air concentrations and depositions) model calculations were carried out for one-year period. The emission information used in the calculations is based on official data and includes unofficial data when official information is not available (section 4.4.1 of this chapter). The meteorological data for the calculations for 2006 were prepared on the basis of ECMWF meteorological analyses.

Benzo[a]pyrene (B[a]P)

Evaluation of contamination levels

The calculated maps of spatial distributions of B[a]P concentrations in surface atmospheric layer and depositions in 2006 in comparison with emissions are shown in Fig. 4.22.

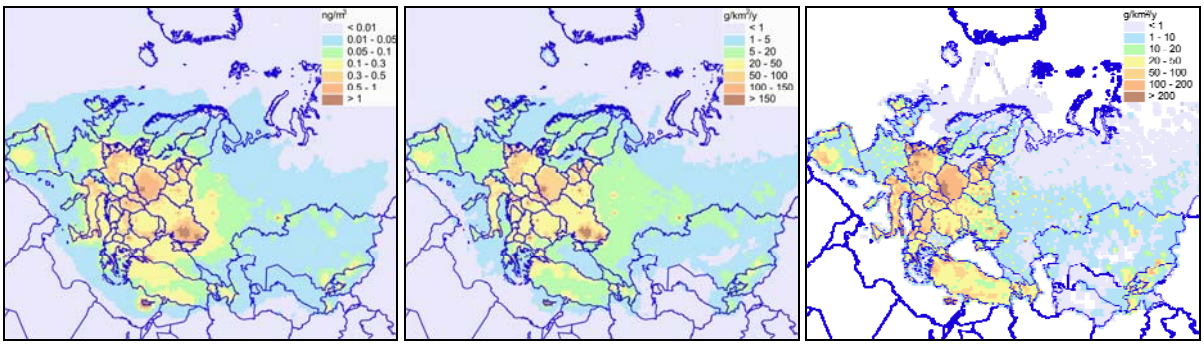

a b c

Fig. 4.22. *Spatial distribution of calculated air concentrations, ng/m^3 (a) and deposition fluxes, g/km^2/y (b) of B[a]P in comparison with emissions, g/km^2/y (c) for 2006*

On the basis of these calculations average values of air concentrations and total depositions in European and Central Asian countries were evaluated (Table 4.7).

Table 4.7. *Average air concentrations and total depositions in European and Central Asian countries*

Country	Air concentrations, ng/m^3	Total deposition, t
Cyprus	1.22	1.65
Ukraine	0.60	47.87
Poland	0.53	23.61
Latvia	0.44	5.56
Slovakia	0.42	2.96
Hungary	0.40	4.18
Slovenia	0.39	1.31
Netherlands	0.36	1.89
Germany	0.34	19.49
Belgium	0.34	1.87
Czech Republic	0.33	3.81
Lithuania	0.30	3.11
Romania	0.29	9.14
Serbia and Montenegro	0.29	4.13
Italy	0.28	12.18
Republic of Moldova	0.27	0.99
Belarus	0.27	8.72
Croatia	0.26	2.00
Bulgaria	0.26	3.95
Estonia	0.25	2.27
Luxembourg	0.24	0.11
Bosnia and Herzegovina	0.22	2.01
Macedonia	0.20	0.76
Albania	0.20	0.96
Denmark	0.19	1.28
Austria	0.17	2.31
Armenia	0.16	0.69
Greece	0.14	2.47
Turkey	0.14	15.91
Azerbaijan	0.12	1.42
Monaco	0.09	0.00
Spain	0.09	7.34
Portugal	0.08	1.33
France	0.07	5.82
Ireland	0.07	1.31
Switzerland	0.06	0.45
Russian Federation	0.06	31.26
Kyrgyzstan	0.06	1.65
Sweden	0.05	5.65
United Kingdom	0.05	2.43
Finland	0.05	3.90
Georgia	0.04	0.55
Tajikistan	0.04	0.71
Kazakhstan	0.04	9.73
Uzbekistan	0.03	0.94
Malta	0.02	0.00
Norway	0.02	2.75
Russian Federation (Asian part)	0.01	8.28
Turkmenistan	0.01	0.22
Iceland	0.002	0.12
Annual	0.09	273

Comparison of modelling results with measurements

Calculation results were compared with available B[a]P measurements of the EMEP monitoring network.

Measurements of B[a]P atmospheric concentrations in 2006 are available at EMEP stations SE12, SE14, FI96, CZ3, NO42, GB14 and ES8. The comparison of annual means of measured and calculated air concentrations is shown in the plot in Fig. 4.23.

All calculated values at monitoring station locations except for ES8 agree with measurements within a factor of 2. For three stations (SE12, FI96 and CZ3) calculations and measurements differ not more than by 25%. Seasonal variations of air concentrations at these three sited are displayed in Fig. 4.24.

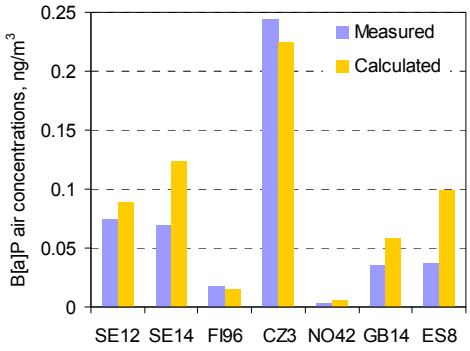

Fig. 4.23. *Calculated and measured annual means of air concentrations of B[a]P at EMEP monitoring stations in 2006, ng/m^3*

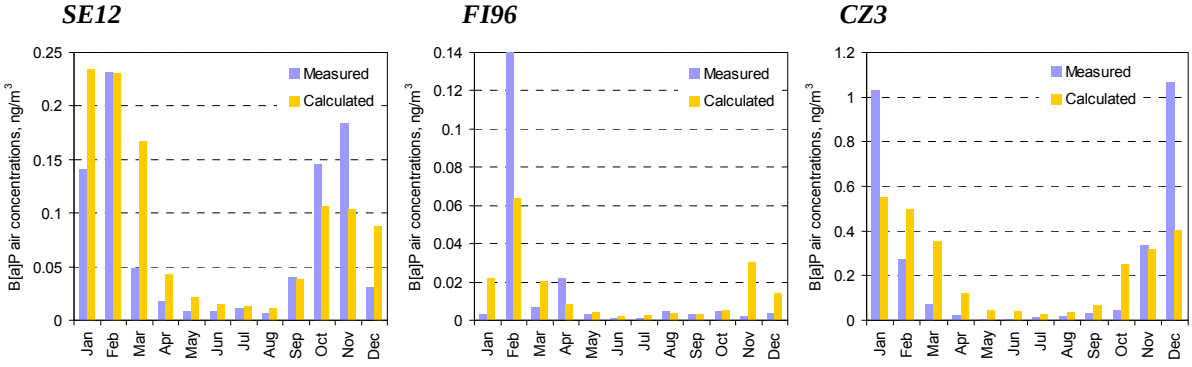

Fig. 4.24. *Calculated and measured monthly means of air concentrations of B[a]P, ng/m^3 at three EMEP monitoring stations in 2006, ng/m^3*

The agreement between calculations and measurements at these stations at the level of monthly means is worse than for annual means. However, the comparison of measured and calculated concentrations show that the model correctly reproduces seasonal variations of contamination. In particular, peak value of B[a]P air concentrations at FI96 in February 2006 is reproduced by the model. It can be seen that seasonal variations of measured air concentrations are more pronounced than that calculated by the model. This may be conditioned by underestimation of seasonal variations of B[a]P emissions, since no official information on this subject is available.

Let us consider the comparison of monthly mean air concentrations at monitoring sites with maximum differences in annual means. The comparison for SE14 (calculation to measurement ratio equal to 1.8) and for ES8 (calculation to measurement ratio equal to 2.7) is given in Fig. 4.25.

The reason of disagreement between calculations and measurements at SE14 is that the cell containing this measurement site contains also such powerful emission source as Gothenburg. Due to this fact, calculation results being averaged over the whole cell can differ from measurements, which are characteristic of a particular point in this cell. More detailed analysis of this phenomenon is given in [*Shatalov et al.*, 2005]. It can be noticed that seasonal variations of measurements at ES8 are not

typical for B[a]P. The differences between calculations and measurements at this station can be conditioned by the lack of information on emissions and their seasonal variations (at present no official information on Spain emissions are available and unofficial data are used for modelling).

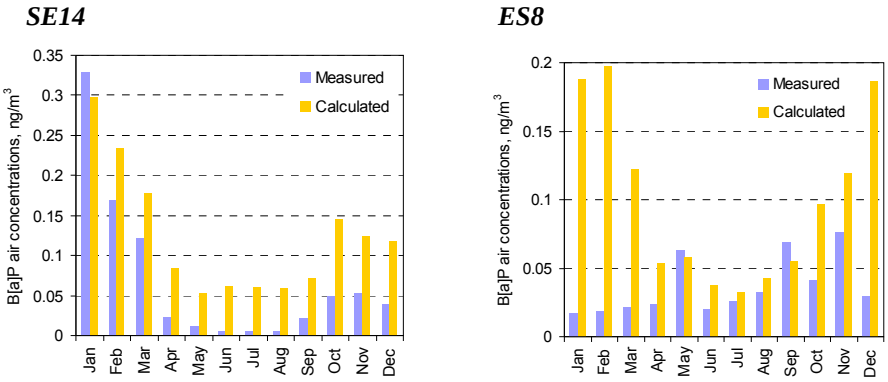

Fig. 4.25. *Calculated and measured monthly mean air concentrations of B[a]P at SE14 and ES8 in 2006, ng/m^3*

Let us proceed with the comparison of the data on concentrations in precipitation and deposition fluxes. The measurement information on these parameters is available at stations DE1, DE9 (concentrations in precipitation), FI96, SE12 and SE14 (deposition fluxes). In the interpretation of the comparison of measured and calculated concentrations in precipitation and deposition fluxes it should be taken into account that these parameters strongly depend on precipitation amount − the parameter, which is characterized by strong variability. Due to this fact the comparison for these two parameters is done directly for real periods of measurements using raw data from EMEP stations.

The comparison of concentrations in precipitation at DE1 and DE9 is given in the plots in Fig. 4.26.

The comparison shows that in general the model correctly reproduces seasonal variations of concentrations in precipitation at these two stations. Further, measured and calculated annual mean concentrations for these two stations are close enough to one another (calculated values are 2.7 ng/L at DE1 and 3.0 ng/L at DE9 whereas measured values are 2.9 at DE1 and 4.7 at DE9).

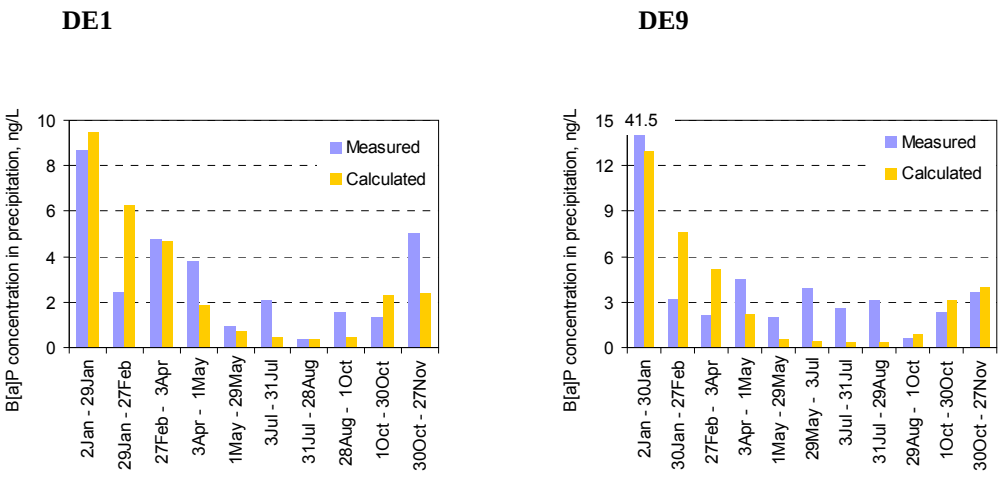

Fig. 4.26. *Calculated and measured B[a]P concentrations in precipitation at DE1 and DE9 in 2006, ng/L*

It should be noticed, however, that the comparison of measured and calculated wet deposition flux at these sites differ more essentially than concentrations in precipitations. This situation is exemplified in Fig. 4.27a where calculated and measured deposition fluxes are shown.

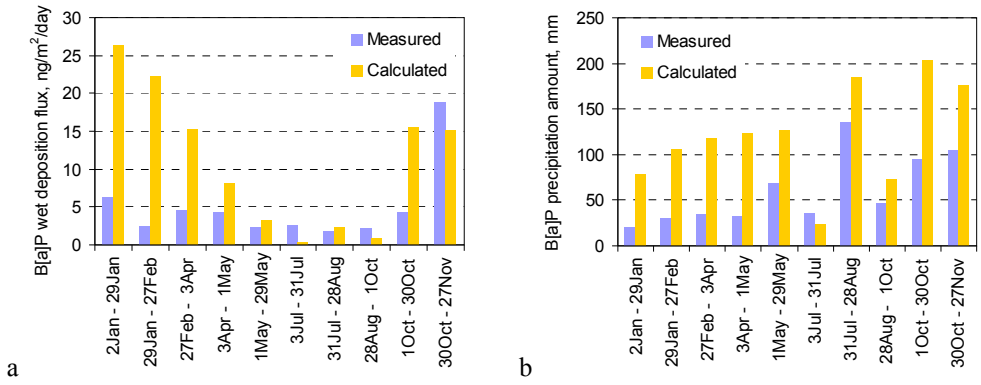

Fig. 4.27. *Calculated and measured B[a]P wet deposition fluxes, ng/m^2/day (a) and precipitation amounts, mm (b) at DE1*

It can be seen that the disagreement between calculated and measured wet deposition fluxes is more essential than that for concentrations in precipitation. The reason is that the values of precipitation amounts measured and used for calculations essentially differ from one another (Fig. 4.27b). To solve this problem, further analysis together with measurement community is needed.

The comparison of measured and calculated deposition fluxes at monitoring stations FI96, SE12 and SE14 is presented in Fig. 4.28.

From the comparison of measured and calculated deposition fluxes at FI96 and SE12 it can be seen that the model can reproduce the events with high deposition fluxes. Annual totals of depositions at these two sites agree within a factor of 2. The reasons for overestimation of deposition flux at SE14 are similar to that for air concentrations (see above).

From the above analysis, it can be concluded that the agreement between the measured and calculated concentrations in air and in precipitation is reasonable in view of current limitation of emission and monitoring data.

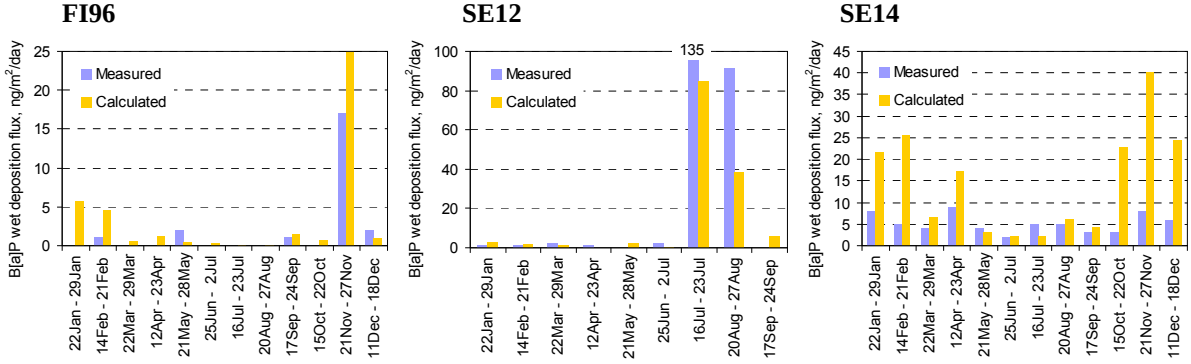

Fig. 4.28. *Calculated and measured B[a]P deposition fluxes at FI96, SE12 and SE14 in 2006, ng/m^2/day*

Transboundary transport of B[a]P

Here the calculated source-receptor relationships in the EMEP region for B[a]P in 2006 is presented. In calculations the above-described emission data were used. Source-receptor matrices for B[a]P in 2006 were calculated both for deposition and for air concentrations. Below we illustrate source-receptor relationships by the example of deposition matrix. In comparison with calculations of the previous year some sources and receptors were added. These are Central Asian countries and part of Asian Russia included into the extended EMEP domain.

To evaluate the transboundary transport of B[a]P, the contributions to air concentrations and depositions from emission sources of each EMEP country is calculated in the process of simulation of long-range transport. So, the most important model output in model simulations of source-receptor relationships is maps of air concentrations and depositions originated from national emission sources for each particular country. Fig. 4.29 shows spatial distributions of depositions due to emission sources of the Czech Republic and Italy.

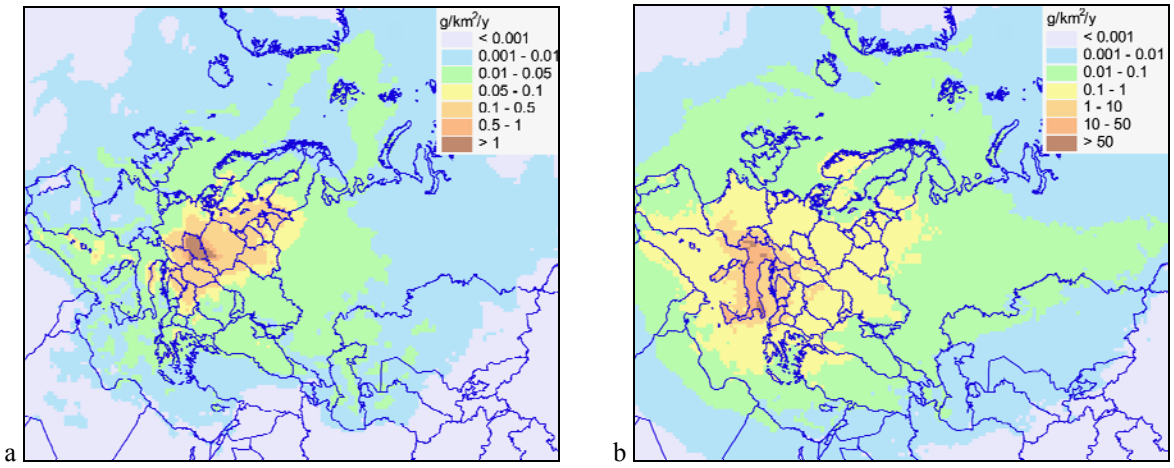

Fig. 4.29. *Annual total depositions of B[a]P originated from national emissions of the Czech Republic (a) and Italy (b), g/km²/y*

On the basis of spatial distribution of depositions caused by each source region source-receptor relationships (export and import) in the EMEP region was evaluated.

Export. The splitting of total depositions to EMEP region due to national anthropogenic sources of a country to deposition to the territory of the country itself and deposition to the rest EMEP territory (export) in 2006 is shown in Fig. 4.30.

The plot of the fraction of depositions to the entire (extended) EMEP domain due to emissions of the given country deposited to the territory of all the rest countries (export fraction) is displayed in Fig. 4.31. Typically, about 20 – 60% of depositions caused by national emission sources of a country are deposited outside this country (such countries are marked by the frame in Fig. 4.31).

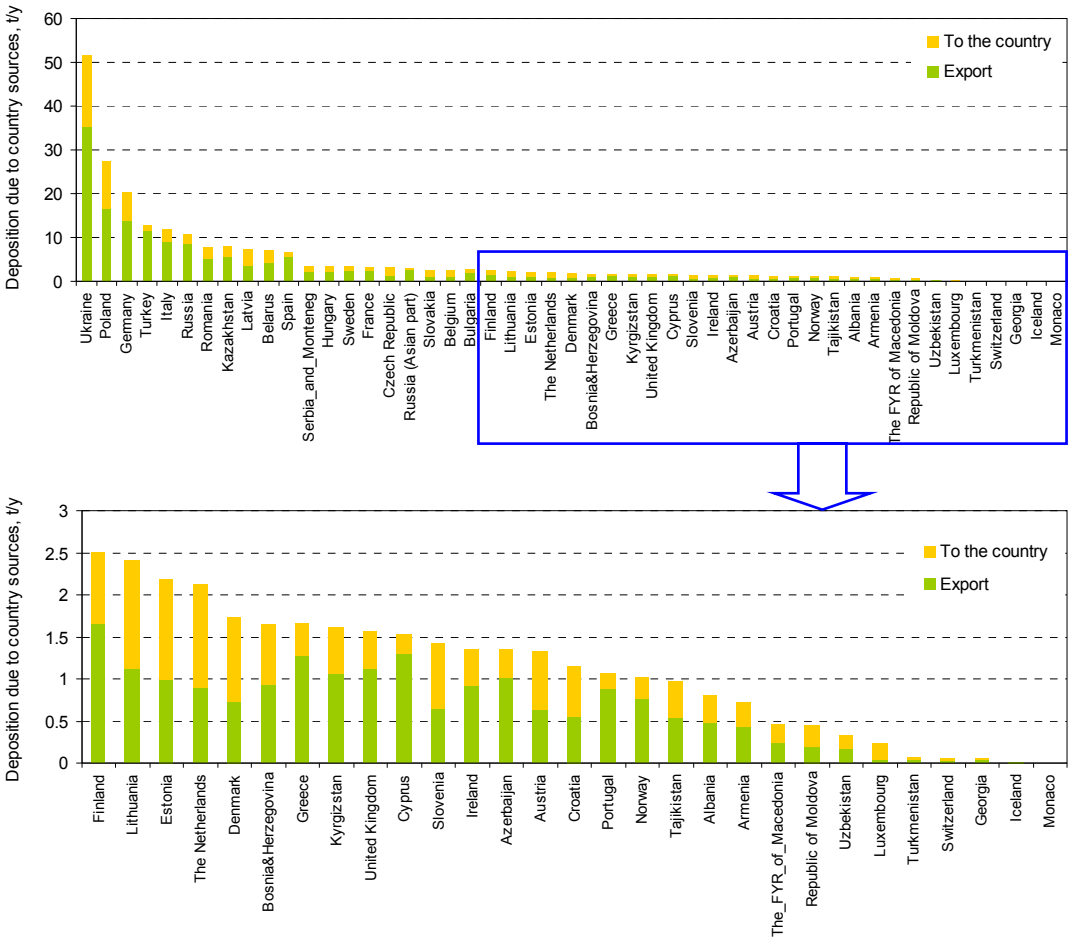

Fig. 4.30. *Depositions of B[a]P to the own territory and depositions to the rest EMEP territory (export) due to national emissions of particular countries, t/y*

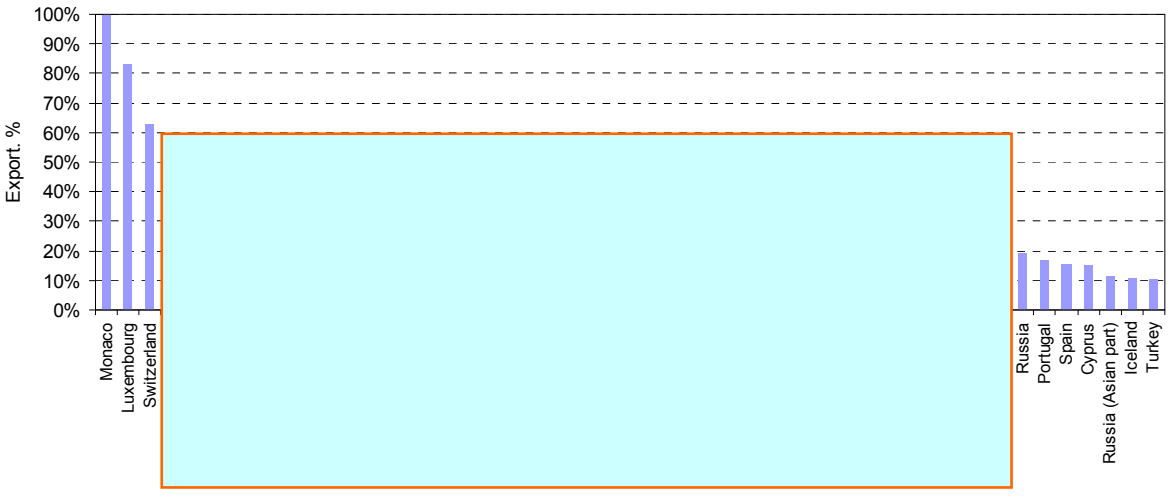

Fig. 4.31. *Export fractions of B[a]P for European countries, %*

The depositions from sources of a particular country can be further specified by calculation fractions of total deposition from sources of a given country to other particular countries. Pie charts showing such specification for the Netherlands (export = 58%), Finland (export = 34%) and Portugal (export = 18%) in Fig. 4.32.

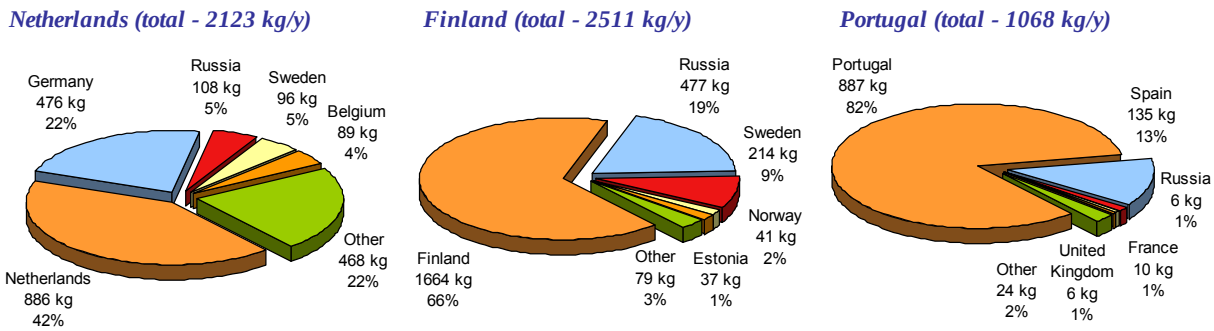

***Fig. 4.32**. Transboundary transport from several countries, % of depositions*

The value of export fraction for a particular country depends on its area, location, and meteorology of the current year. In particular, in Finland export fraction amounts to more than 50%. This means that for this country more than a half of depositions to the EMEP domain caused by their national emissions fall at the territory of other European countries. On the opposite, export fraction of Portugal amounts to 17% only. This means that the most part of depositions from Portugal sources falls onto the territory of this country, marine regions or is transported outside the EMEP domain.

Import. The calculated values of total depositions of B[a]P to the territories of European countries in 2006 together with their splitting to depositions due to own sources and due to sources of other countries (import) are displayed in Fig. 4.33.

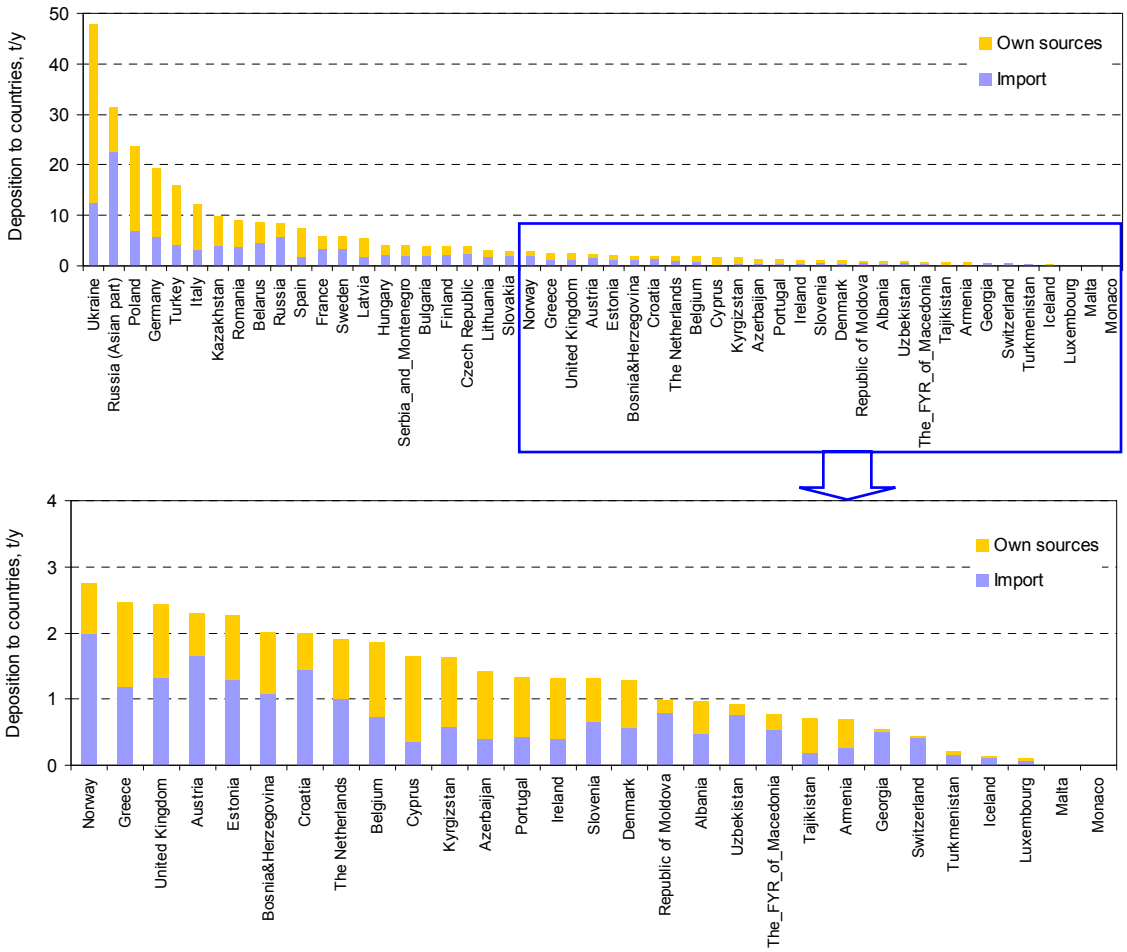

***Fig. 4.33.** Total depositions of B[a]P to the territories of European countries, t/y*

The contributions (in %) of direct atmospheric transboundary transport (without taking re-emission into account) to depositions to European countries, that is, the fractions of depositions originated by emission sources of other European countries (import) are shown in the plot in Fig. 4.34.

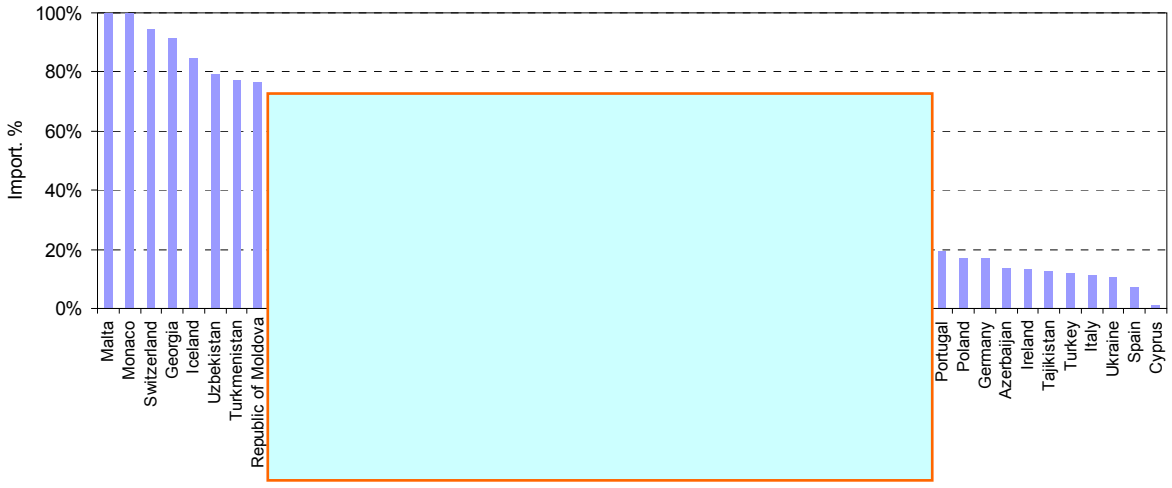

Fig. 4.34. *Contributions of transboundary transport to total annual depositions of B[a]P from European emission sources for each European country, %*

Typically contributions of other European countries to the deposition levels of a particular country vary from 20% to 70% (such countries are marked by the frame in Fig. 4.34).

Further specification of depositions to a particular country from European sources leads to calculation of fractions of total depositions to the country originated by emission sources of each other country. Pie charts showing such specification for Norway (import = 68%), Hungary (import = 43%) and Germany (import = 18%) in Fig. 4.35.

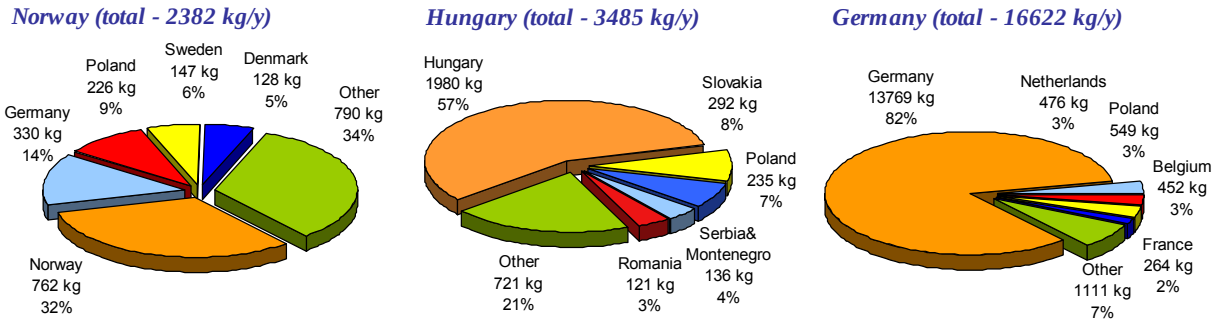

Fig. 4.35. *Fractions of B[a]P depositions to Norway, Hungary, and Germany originated from atmospheric transport of EMEP countries, %*

It is worth noticing that, in contrast to the case of export, import fraction depends not only on country's area and location, and meteorology of the current year, but also on the fraction of national sources in emission totals. For example, import fraction of Germany is low enough (18% only) due to high fraction of German emissions in EMEP total (about 8%).

Finally, it should be noticed that import pie charts present only average figures of the contribution of transboundary transport over the country. However, these contributions are subject to strong spatial variations. For example, the map of transboundary transport contributions for France is shown in Fig. 4.36.

The contributions of transboundary transport to depositions to the country are larger at the country's boundary. In addition, fractions of deposition due to transboundary transport are less in the regions with high national emissions.

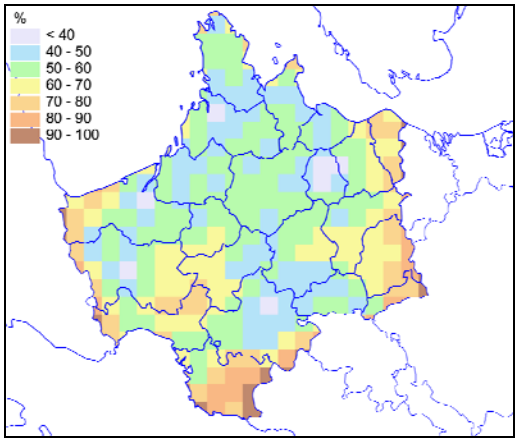

Fig. 4.36. *Spatial distribution of deposition fractions due to transboundary transport for France in 2006, %*

Contamination of Central Asia countries. Due to the extension of EMEP domain, it became possible to generate the full set of information on contamination levels and transboundary transport of B[a]P for Central Asian countries (Kazakhstan, Kyrgyzstan, Tajikistan, Turkmenistan and Uzbekistan).

The information includes:

a) Average concentrations of B[a]P in the atmosphere and precipitation and deposition fluxes. This information is contained in Table 4.7 above.

b) Spatial distribution of contamination by national sources, depositions (Fig. 4.37).

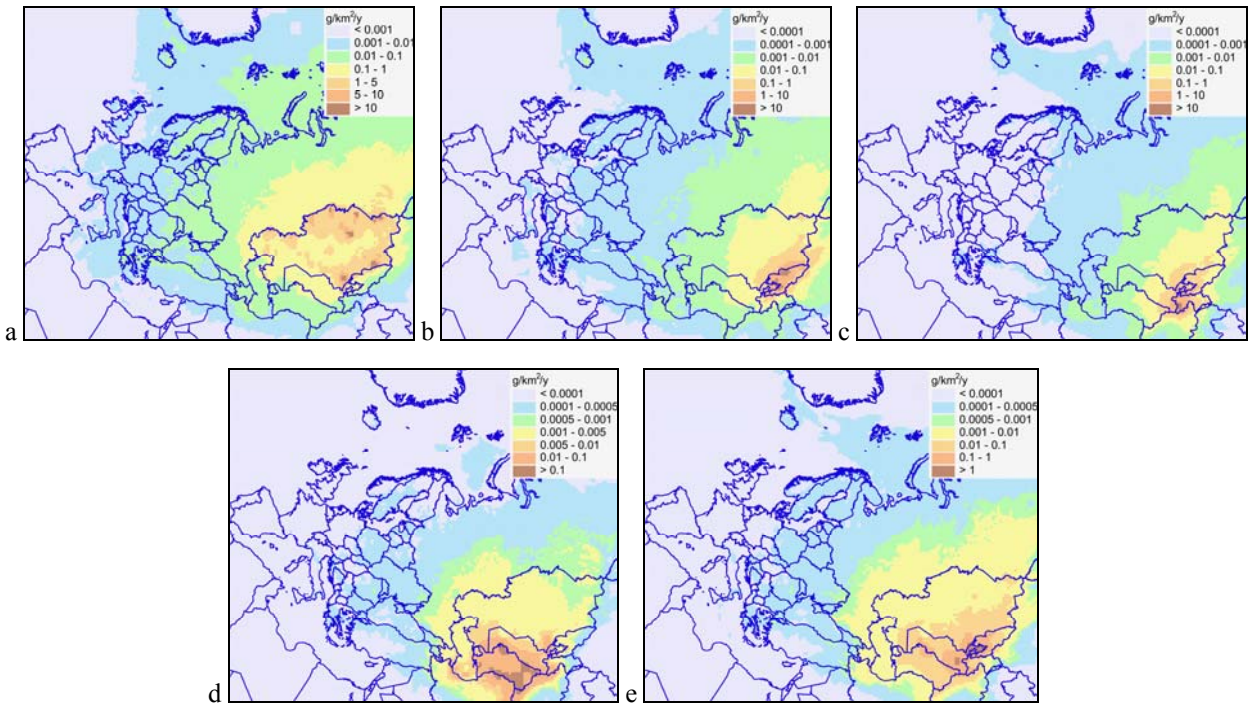

Fig. 4.37. *Spatial distribution of contamination originated by national sources of Kazakhstan (a), Kyrgyzstan (b), Tajikistan (c), Turkmenistan (d) and Uzbekistan (e), g/km^2/y*

c) Spatial distribution of depositions to the country (Fig.4.38).

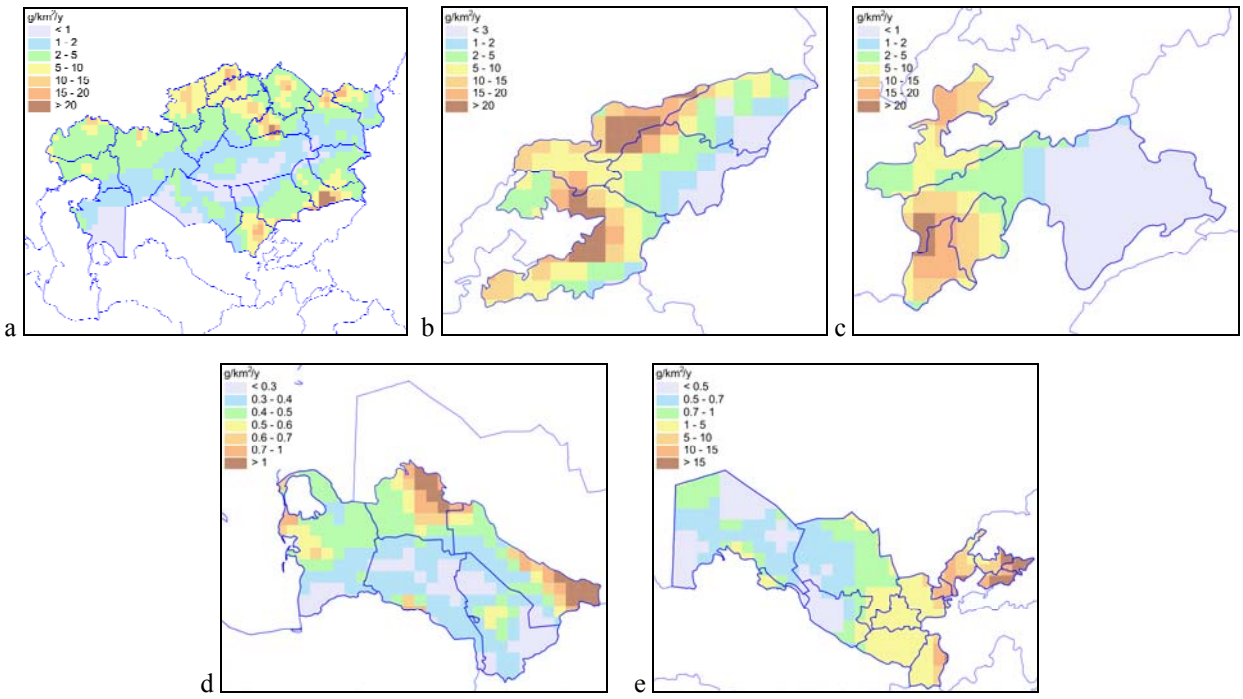

Fig. 4.38. *Spatial distribution of contamination originated in Kazakhstan (a), Kyrgyzstan (b), Tajikistan (c), Turkmenistan (d) and Uzbekistan (e), g/km²/y*

d) Export diagrams (Fig. 4.39).

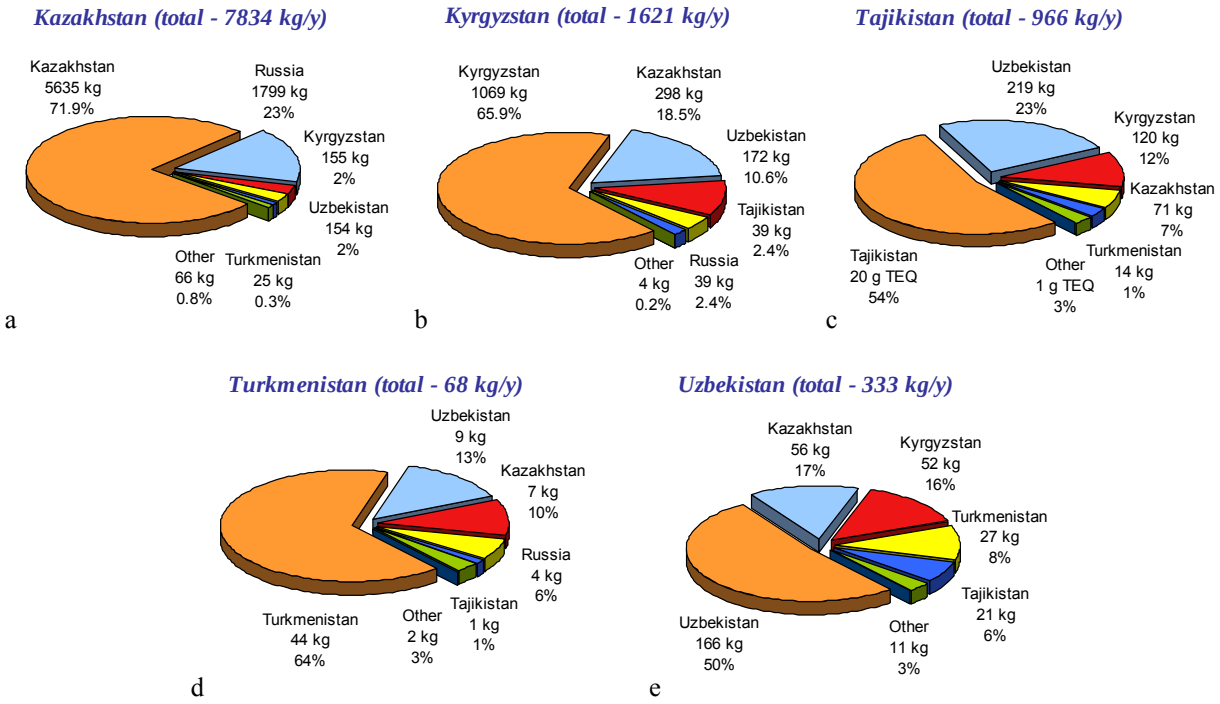

Fig. 4.39*. Transboundary transport from Kazakhstan (a), Kirgizstan (b), Tajikistan (c), Turkmenistan (d) and Uzbekistan (e), % of depositions*

e) Import diagrams (Fig. 4.40).

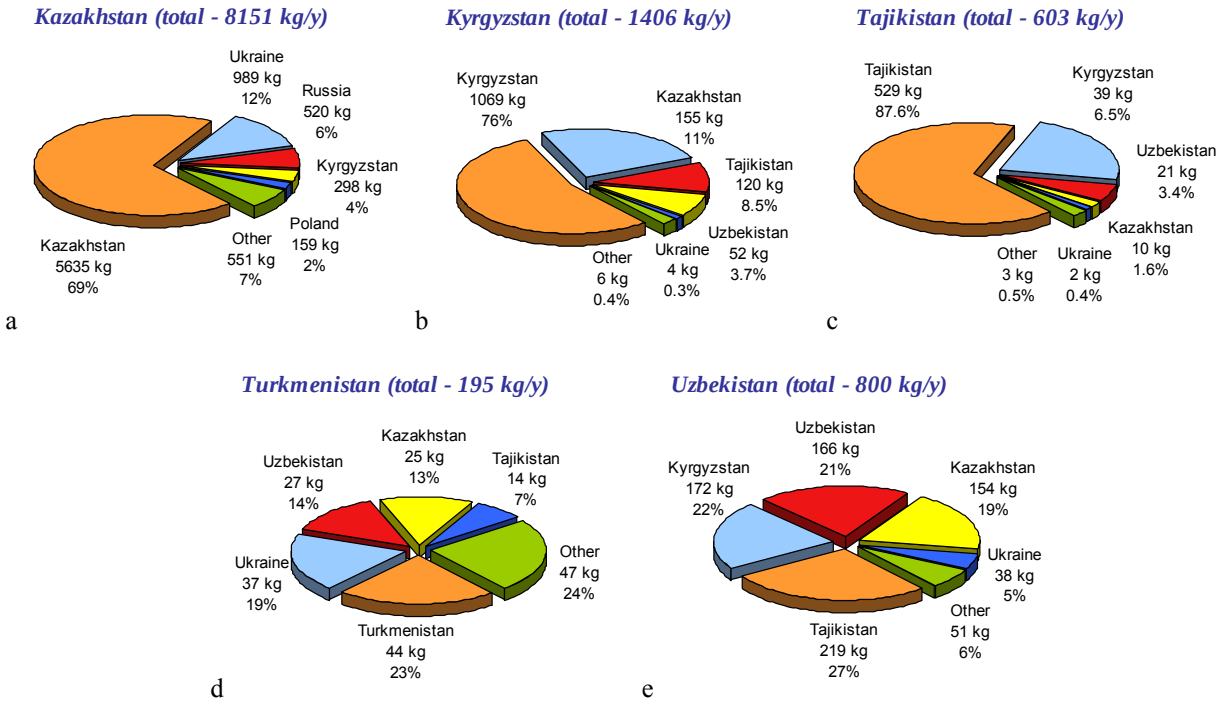

Fig. 4.40. *Transboundary transport to Kazakhstan (a), Kyrgyzstan (b), Tajikistan (c), Turkmenistan (d) and Uzbekistan (e), % of depositions*

f) Spatial distributions of deposition fractions due to transboundary transport.

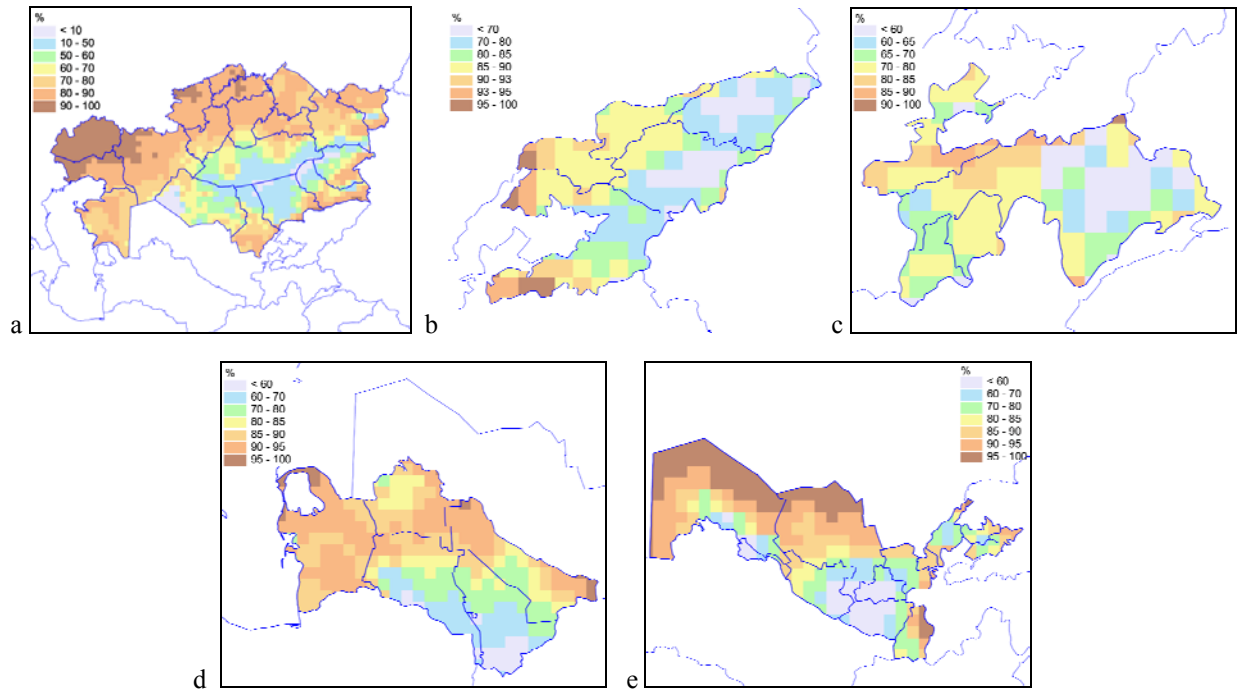

Fig. 4.41. *Spatial distribution of deposition fractions due to transboundary transport for Kazakhstan (a), Kyrgyzstan (b), Tajikistan (c), Turkmenistan (d) and Uzbekistan (e), % of depositions*

Full country-to-country matrices for air concentrations and depositions can be found on MSC-E web-site www.msceast.org Full set of country-specific information will be put on EMEP web-site www.emep.int and on MSC-E web-site www.msceast.org.

The rest indicator PAHs (B[b]F, B[k]F and I_P)

For the rest three indicator PAHs (B[b]F, B[k]F and I_P) evaluation of pollution levels was carried out. The maps of spatial distributions of depositions in comparison with their emissions are shown in Fig. 4.42 a, b and c, respectively.

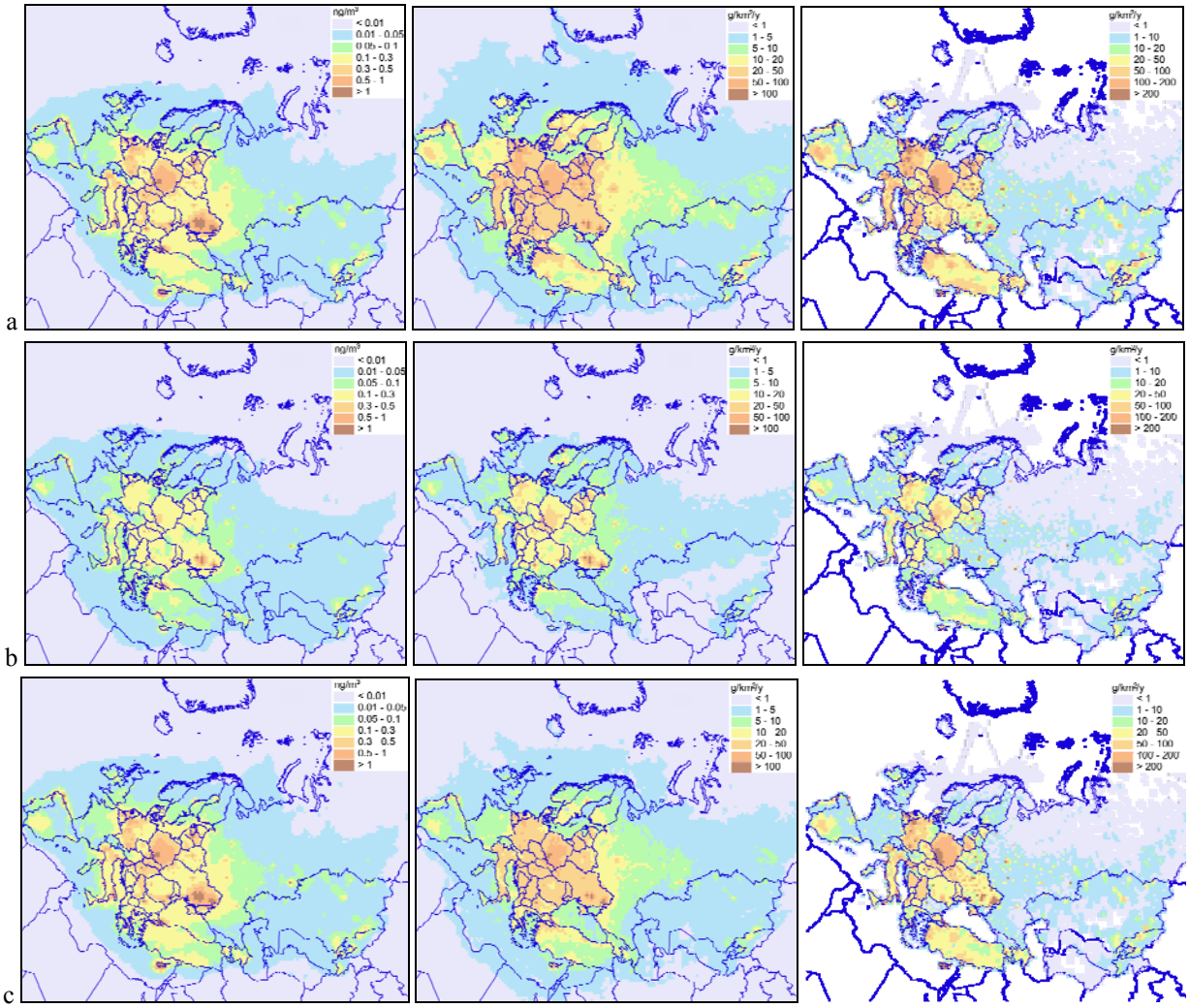

Fig. 4.42. *Calculated air concentrations, ng/m^3 (on the left), deposition fluxes, g/km^2/y (in the middle) and emissions, g/km^2/y (in the middle) of B[b]F (a), B[k]F (b) and I_P (c) in 2006 in comparison with emissions (on the right), g/km^2/y*

Air concentrations of B[b]F and I_P varied from 0.05 ng/m^3 in the Northern part of Europe to more than 1 ng/m^3 in the regions of the Central, Eastern and Southern Europe. Spatial distribution of B[b]F and I_P air concentrations are similar to those for B[a]P. The air concentrations of B[k]F are much smaller

(from 0.01 ng/m^3 to 0.5 ng/m^3). This is conditioned by the relations between emissions of this compound.

The same concerns deposition fluxes. For B[b]F and I_P they vary from low (5 – 10 g/km^2/y) in northern Europe to rather high (50 g/km^2/y and higher) in central Europe. In general, spatial pattern of depositions for these compounds is close to that for B[a]P. Higher emission densities for B[b]F in the northern part of Spain lead to increase of deposition levels in northern Spain and southern France for this pollutant compared with B[a]P.

Deposition fluxes of B[k]F in Europe are lower (from 1 – 5 g/km^2/y in northern Europe and 10 – 20 g/km^2/y in central Europe). Absolute values of deposition fluxes are smaller than for the two above considered pollutants. Again, the reason is that emission levels for B[k]F are considerably lower according to emission data used in modelling. Spatial pattern of air contamination for B[k]F is similar to those for B[a]P, B[b]F and I_P.

4.5.2. Polychlorinated dibenzo(p)dioxins and dibenzofurans (PCDD/Fs)

Calculations of pollution levels of the mixture of 17 toxic PCDD/F congeners were performed with the help of regional model with resolution 50x50 km^2 in the extended EMEP domain for 2006. This domain includes, in particular, Central Asian countries (Kazakhstan, Kyrgyzstan, Tajikistan, Turkmenistan and Uzbekistan). Special attention was paid to the evaluation of contamination in these countries. To take into account the influence of PCDD/F mass accumulated historically in various environmental media (soil, seawater, vegetation) and the influence of intercontinental PCDD/F transport preliminary run of the hemispheric version of MSCE-POP model for the period from 1970 to 2006 were done. The results of this run were used to obtain the initial and boundary conditions for regional calculations. Based on these data regional modelling permitted to evaluate pollution levels and transboundary transport of PCDD/Fs in the EMEP region. The estimates of transboundary transport are presented in the form of country-to-country matrices of depositions.

In calculations, physical-chemical properties of PCDD/F “indicator congener” 2,3,4,7,8-PeCDF were used. Usage of such an approach allows evaluating spatial distributions of the total PCDD/F toxicity in the atmosphere with difference not more than 20% compared with the results of simulations of all 17 toxic congeners. The difference in country-to country matrix is not more than 5% (see EMEP Status Report [*Dutchak et al.,* 2004]). The emission data used in the regional calculations for 2006 are based on official data and include unofficial estimates when official information is not available (Section 4.4.1).

Evaluation of contamination levels

The calculated maps of spatial distributions of PCDD/F concentrations in surface atmospheric layer and depositions in 2006 are shown in Fig. 4.43.

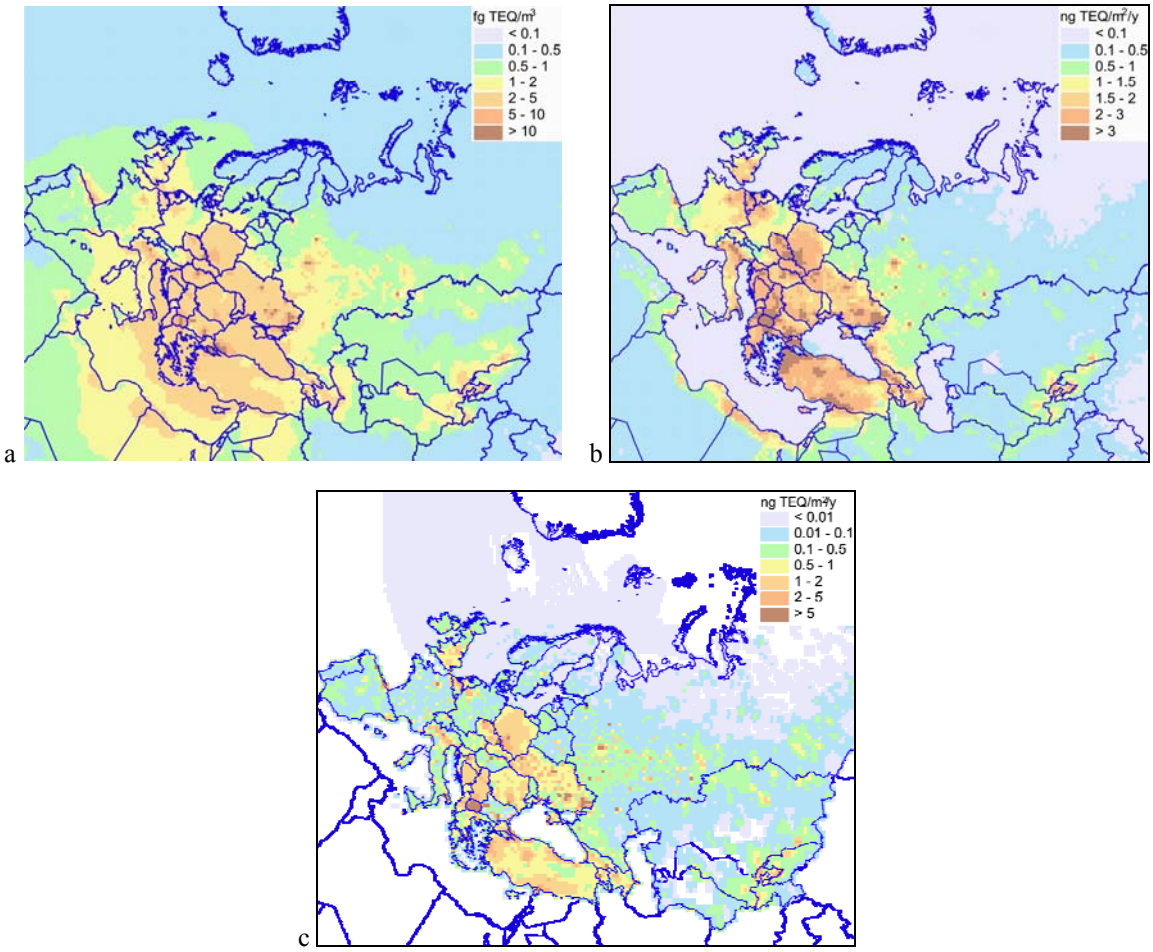

Fig. 4.43. *Calculated air concentrations, fg TEQ/m^3 (a) and deposition fluxes, ng TEQ/m^2/y (b) in comparison with annual emissions, ng TEQ/m^2/y (c) of PCDD/Fs in 2006*

On the basis of these calculations average values of air concentrations and total depositions in the European and the Central Asian countries were evaluated (Table 4.8). Countries in the table are ordered by PCDD/F average air concentrations.

Average value of air concentrations over all countries considered is 1.04 fg TEQ/m^3. Elevated levels of PCDD/F air concentrations (more than three times exceeding EMEP average) are found in Central, Southern and Eastern Europe. The corresponding countries are marked gray in the table. They are: Macedonia, Bulgaria, Hungary, Serbia and Montenegro, the Ukraine, the Czech Republic, Slovakia, Croatia, Albania, Poland, Romania and Greece. The countries with temperate levels of PCDD/F contamination (between 3.12 and 1.04 fg TEQ/m^3) are marked light gray in the table. For the rest countries average PCDD/F concentrations over the country are less than that over the whole EMEP domain.

Table 4.8. *Average air concentrations and total depositions in the European and the Central Asian countries*

Country	Air concentrations, fg TEQ/m^3	Total deposition, g TEQ
Macedonia	8.88	150.8
Bulgaria	4.83	379.0
Hungary	4.16	212.8
Serbia and Montenegro	4.09	284.1
Ukraine	4.01	1375.6
Czech Republic	3.96	228.6
Slovakia	3.89	124.0
Croatia	3.68	137.3
Albania	3.61	78.9
Poland	3.52	703.2
Romania	3.36	480.9
Greece	3.33	285.2
Malta	3.04	0.2
Belgium	3.02	82.9
Turkey	2.90	1933.3
Bosnia and Herzegovina	2.72	115.0
Armenia	2.69	64.3
Slovenia	2.59	40.5
Italy	2.54	528.5
Georgia	2.51	169.9
Republic of Moldova	2.49	46.6
Azerbaijan	2.47	165.6
Cyprus	2.42	16.2
Netherlands	2.31	59.6
Luxembourg	2.20	6.4
Monaco	2.05	0.0
Austria	1.66	112.8
Germany	1.46	498.9
Switzerland	1.30	52.3
Uzbekistan	1.26	249.1
United Kingdom	1.25	308.9
France	1.16	712.5
Belarus	1.15	164.0
Denmark	1.11	35.1
Lithuania	1.02	43.6
Kyrgyzstan	1.01	154.9
Turkmenistan	0.94	177.1
Russian Federation (European part)	0.93	2229.4
Tajikistan	0.86	84.9
Spain	0.86	427.5
Latvia	0.82	39.0
Kazakhstan	0.73	1008.3
Estonia	0.68	25.4
Ireland	0.57	49.0
Portugal	0.51	50.0
Sweden	0.44	163.4
Finland	0.38	99.6
Norway	0.32	129.2
Russian Federation (Asian part)	0.26	821.4
Iceland	0.18	27.0
Annual	1.04	15333

Comparison with calculations of the previous year

In comparison with calculations of previous year contamination levels in most of the European countries do not change essentially. Slight changes may be conditioned by the change in the meteorology. More essential changes are due to changes in emission data. The comparison of depositions to the territories of the EMEP countries calculated in this and previous years together with changes in emission data are shown in Fig. 4.44.

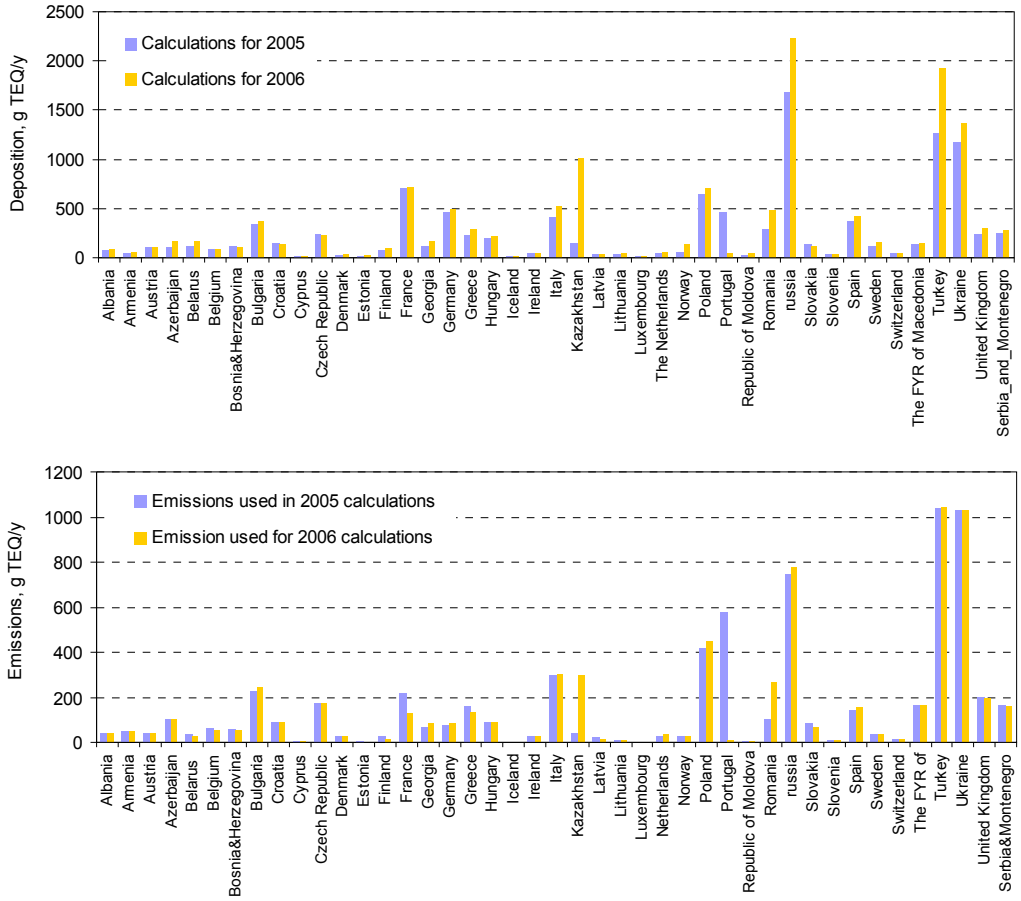

Fig. 4.44. *Comparison of calculated depositions to country's territories for 2005 (calculations of the previous year) and 2006 (calculations of this year) and emission data used in these calculations, g TEQ/y*

The most essential changes in calculated depositions take place in Portugal, Romania, Turkey, the Russian Federation and Kazakhstan. The reduction of depositions in Portugal is clearly connected with strong change of emission data (emissions used in the calculations of this year are about 50 times lower than that used in previous year calculations). For Romania, the increase of PCDD/F depositions in 2006 in comparison with 2005 is conditioned by the increase of national emissions. The increase of depositions in Turkey is mainly due to the change of model description of deposition velocities to the underlying surface. This has lead to the increase of the contribution of re-emissions to depositions to the country. The changes of depositions in the Russian Federation and Kazakhstan can be explained by the extension of EMEP domain to the East. As a result, sources of the Central Asia countries were taken into account.

Transboundary transport of PCDD/Fs

Here the calculated source-receptor relationships in the EMEP region for PCDD/Fs in 2006 are presented. In calculations the above-described emission data were used. Source-receptor matrices for PCDD/Fs in 2006 were calculated both for deposition and for air concentrations. Below we illustrate source-receptor relationships by the example of deposition matrix. In comparison with calculations of the previous year some sources and receptors were added (Kyrgyzstan, Tajikistan, Turkmenistan and Uzbekistan). The territory of Kazakhstan as a whole is considered now as a source/receptor. The part of Asian Russia is also included into the extended EMEP domain.

The following source groups are considered for the evaluation of source-receptor relationship for PCDD/Fs:

- Anthropogenic sources of each European country.
- Anthropogenic sources including emissions outside the EMEP region (emissions of USA and Canada further referred as non-EMEP sources).
- Re-emission due to accumulation of PCDD/Fs in the environmental media from anthropogenic emission sources of the entire Northern Hemisphere during the preceding years.

Each European country is considered as a separate receptor.

To evaluate the transboundary transport of PCDD/Fs, the contributions to air concentrations and depositions from all above emission sources are calculated in the process of simulation of long-range transport. Fig. 4.45 shows spatial distributions of depositions due to emission sources of Switzerland, Denmark and Italy.

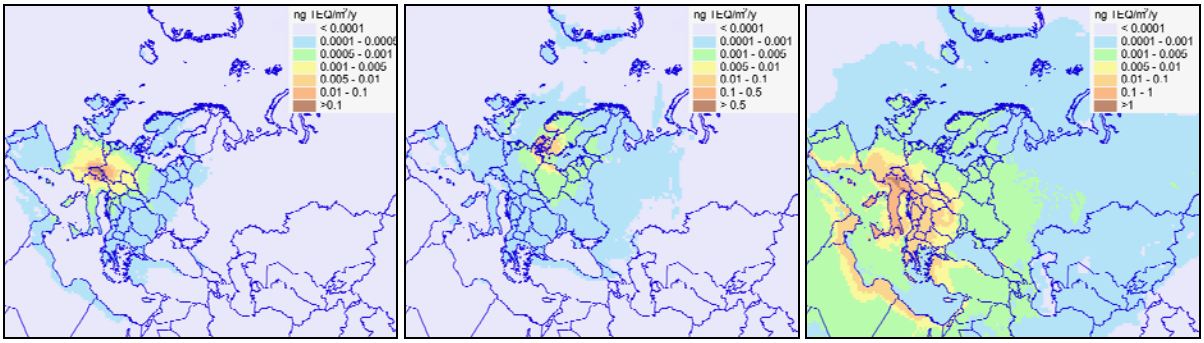

a b c

Fig. 4.45. *Annual total depositions of PCDD/Fs originated from national emissions of Switzerland (a), Denmark (b) and Italy (c), ng TEQ/m^2/y*

On the basis of spatial distribution of depositions caused by each source region, source-receptor relationships (export and import) in the EMEP region were evaluated.

Export. The splitting of total depositions to the EMEP region due to national anthropogenic sources of a country to deposition to the territory of the country itself and deposition to the rest EMEP territory (export) in 2006 is shown in Fig. 4.46.

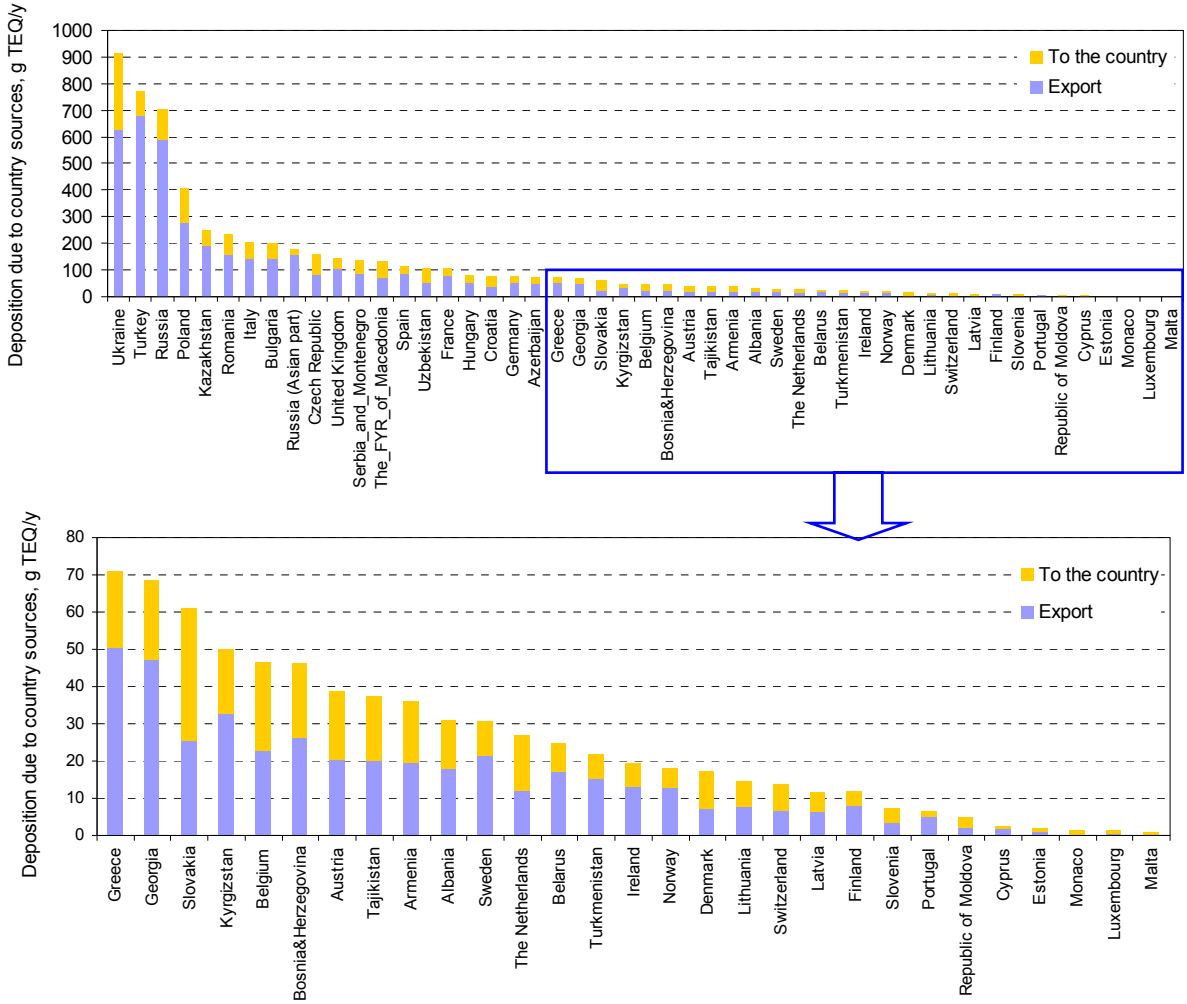

Fig. 4.46. *Depositions of PCDD/Fs to the own territory and depositions to the rest EMEP territory (export) due to national emissions of particular countries, g TEQ/y*

The plot of the fraction of depositions to the entire EMEP domain due to emissions of the given country deposited to the territory of all the rest countries (export fraction) is displayed in Fig. 4.47 Typically, about 20 – 60% of depositions caused by national emission sources of a country are deposited outside this country (such countries are marked by the frame in Fig. 4.47).

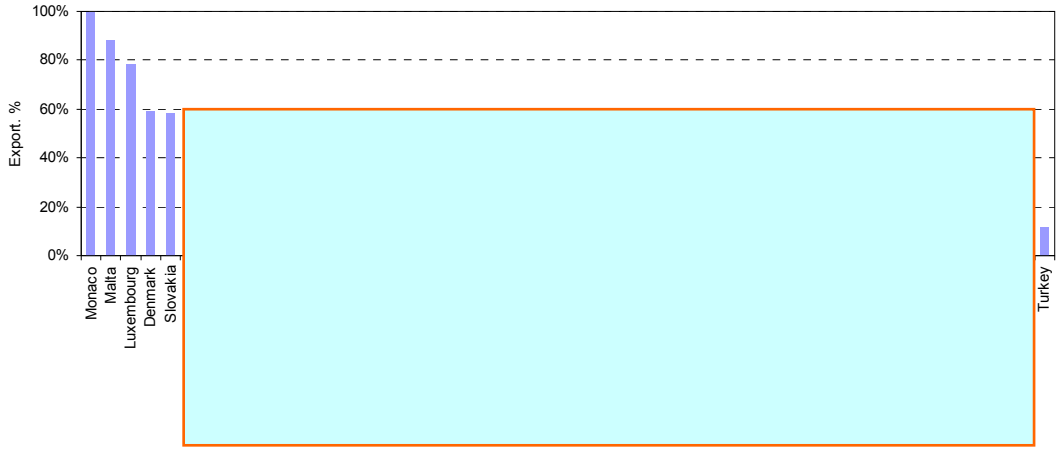

Fig. 4.47. *Export fractions of PCDD/Fs for European countries, %*

The depositions from sources of a particular country can be further specified by calculation fractions of total deposition from sources of a given country to other particular countries. Pie charts showing such specification for the Netherlands (export = 55%), Finland (export = 34%) and Portugal (export = 20%) in Fig. 4.48.

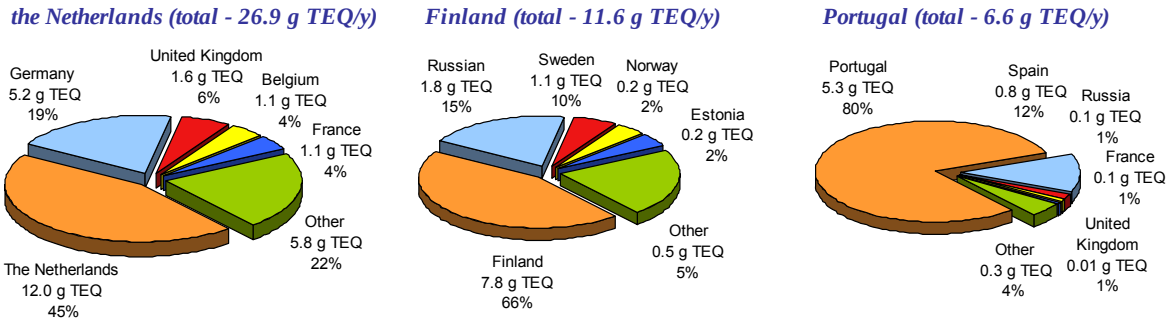

***Fig. 4.48**. Transboundary transport from several countries, % of depositions*

The value of export fraction for a particular country depends on its area, location, and meteorology of the current year. In particular, in Finland export fraction amounts to more than 50%. This means that for this country more than a half of depositions to the EMEP domain caused by their national emissions fall at the territory of the other European countries. On the opposite, export fraction of Portugal amounts to 20% only. This means that the most part of depositions from Portugal sources falls onto the territory of this country, marine regions or is transported outside the EMEP domain.

Import. Total depositions of PCDD/Fs to a country can be split to depositions due to various source categories: sources of the country itself (internal contribution), anthropogenic sources of other European countries (EMEP transboundary), sources of USA and Canada (non-EMEP sources) and pollutant accumulated in the environment during preceding years (re-emission). This splitting is shown by the plot in Fig. 4.49.

The contribution of internal sources to total depositions to the country varies from 4% to 50%, of transboundary transport from other EMEP countries − from 3% to 60%, of transport from non-EMEP sources − from 1% to 33%, and of re-emission − from 30% to 70%.

The contributions of re-emission process to annual total depositions over European countries for 2006 are presented in Fig. 4.50. These contributions are high enough and should be taken into account in the assessment of pollution levels in the European countries.

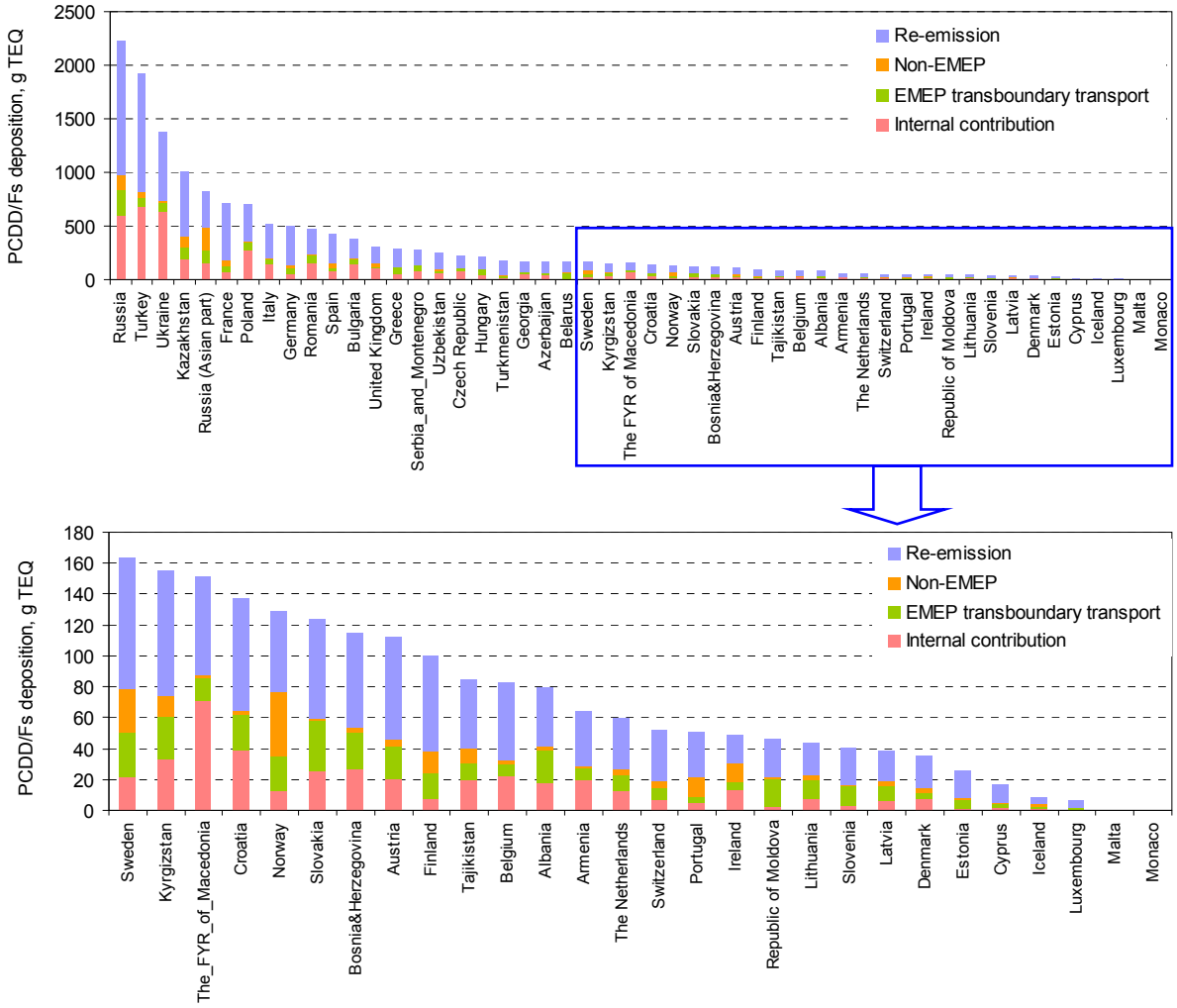

Fig. 4.49. *Structure of total depositions of PCDD/Fs to the territories of European countries in 2006, g TEQ*

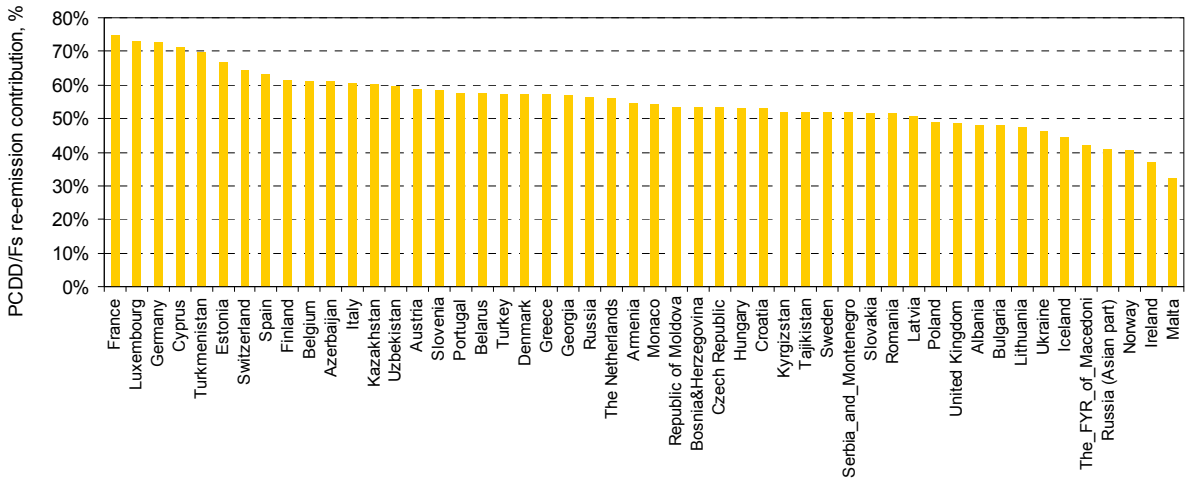

Fig. 4.50. *Contributions of re-emissions of PCDD/Fs to depositions to European countries in 2006, %*

For the analysis of transboundary transport re-emission fraction is excluded from total depositions to European countries, so that from now on only the transport of anthropogenic emissions (from European countries and non-EMEP sources − USA and Canada) is considered. Contributions of transboundary transport (both from EMEP and non-EMEP sources) to each European country are displayed in Fig. 4.51.

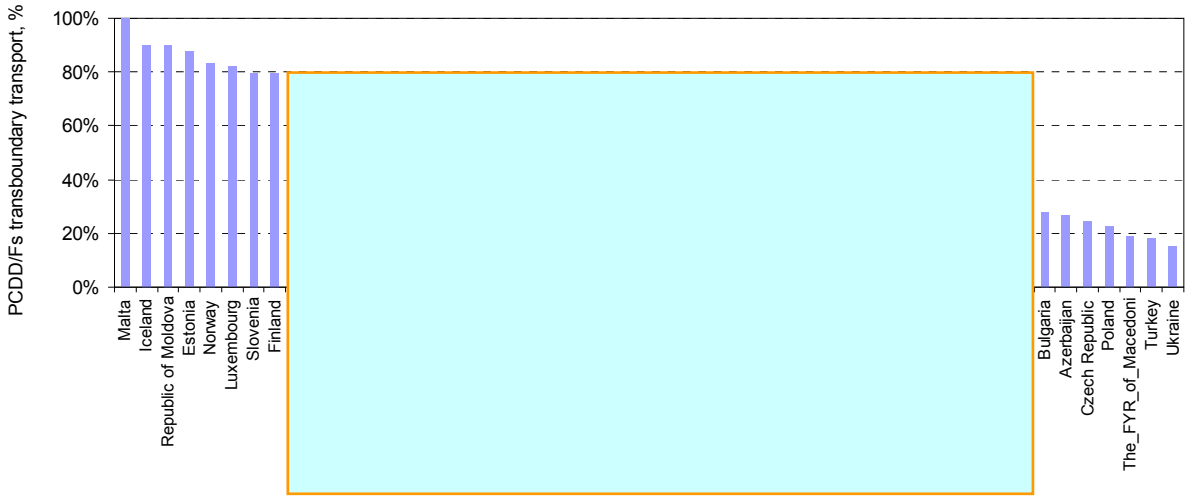

Fig. 4.51. *Contributions of transboundary transport to total annual depositions of PCDD/Fs from anthropogenic emission sources for each European country in 2006, %*

Typically contributions of other countries to the deposition levels of a particular country vary from 30% to 80% (such countries are marked by the frame in Fig. 4.51).

The contributions of non-EMEP sources (USA and Canada) to total depositions to European countries from anthropogenic sources of the current year vary from 2 to 60%. The corresponding fractions are shown by the plot in Fig. 4.52.

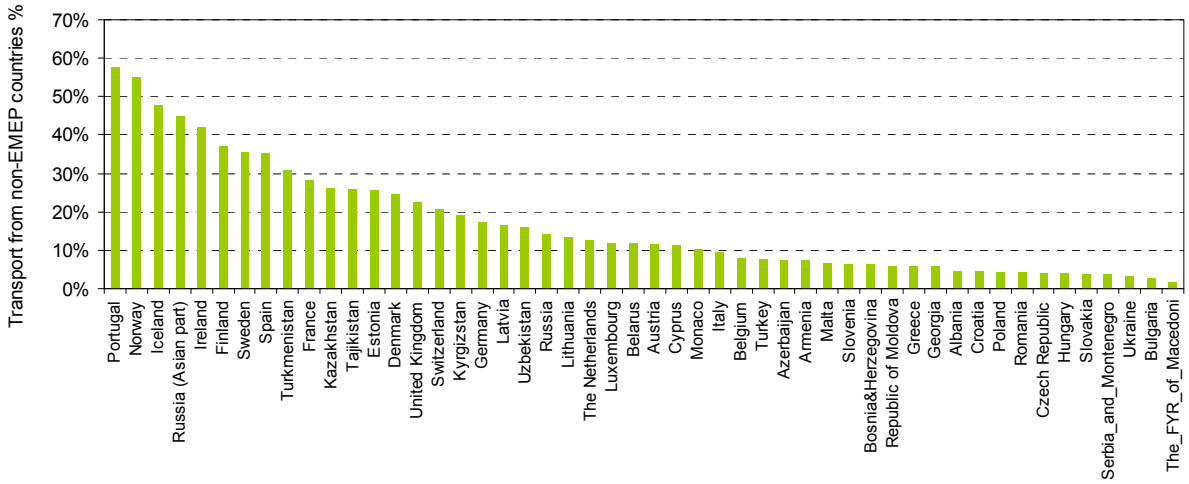

Fig. 4.52. *Contributions of non-EMEP sources of PCDD/Fs to depositions to European countries, %*

Considerable contributions of non-EMEP sources (30% and more) to depositions take place for countries located near the borders of the EMEP domain (Portugal, Norway, Iceland, the Russian Federation, Ireland, Sweden and Spain).

Similarly to the export, the information on import of PCDD/F depositions to European countries due to atmospheric transport can be presented in a more detailed way. Namely, for each country the fractions of total annual deposition determined by emissions of other European countries and non-EMEP sources are calculated. This information is exemplified below by import diagrams for Finland (import fraction 80%), Germany (import fraction 60%) and Hungary (import fraction 47%) (Fig. 4.53).

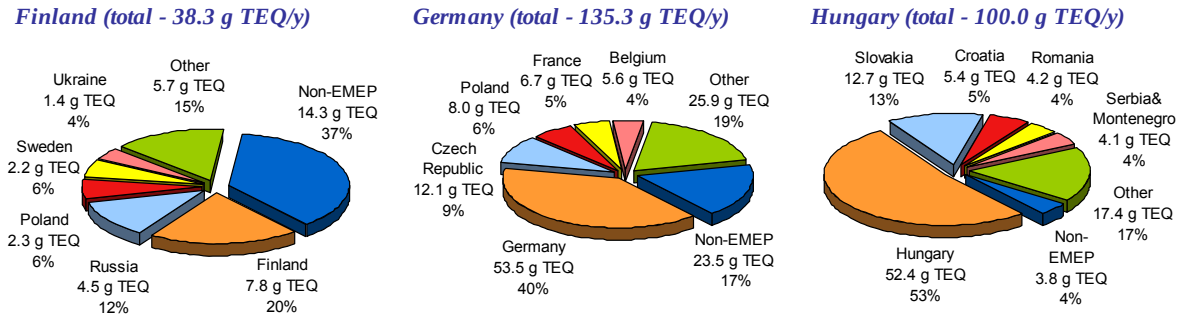

Fig. 4.53. *Fractions of PCDD/F depositions to Finland, Germany and Hungary originated from air transport, %*

It is worth noticing that, in contrast to the case of export, import fraction depends not only on country's area and location, and meteorology of the current year, but also on the fraction of national sources in emission totals. For example, import fraction of Germany is low enough (18% only) due to high fraction of German emissions in the EMEP total (about 8%).

Putting together contributions of the atmospheric transport and re-emissions it is possible to evaluate total depositions for each European country in 2006 and contributions of all above categories of sources (European anthropogenic sources, non-EMEP sources and re-emissions) to these depositions. Examples of import fraction for some European countries for all source categories are presented in Fig. 4.54.

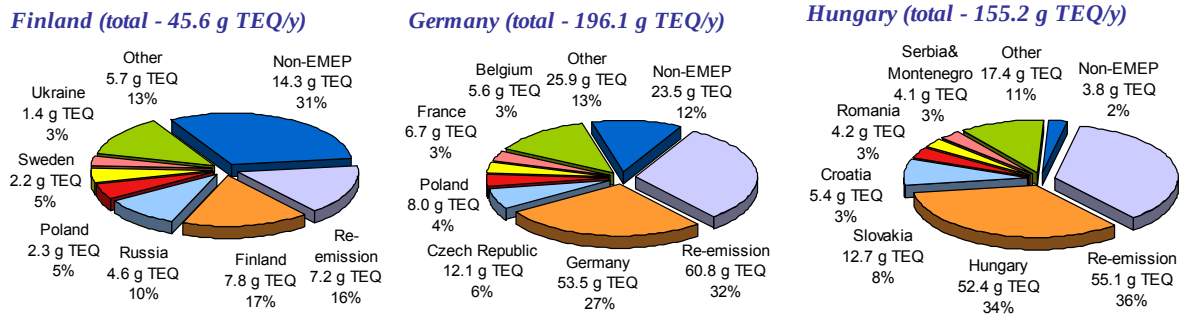

Fig. 4.54. *Contributions of all emission sources to PCDDF depositions over the territories of Finland, Germany and Hungary, %*

The import pie charts present only average figures of the contribution of transboundary transport over the country. However, these contributions are subject to strong spatial variations. Examples of the maps of transboundary transport contributions can be found below in the next subsection devoted to the Central Asian countries.

Contamination of Central Asia countries. Due to the extension of EMEP domain, it became possible to generate the full set of information on contamination levels and transboundary transport of PCDD/Fs for the Central Asian countries (Kazakhstan, Kyrgyzstan, Tajikistan, Turkmenistan and Uzbekistan).

The information includes:

a) Average concentrations of PCDD/Fs in the atmosphere and precipitation and deposition fluxes. This information is contained in Table 4.8 above.

b) Spatial distribution of contamination by national sources, depositions (Fig. 4.55).

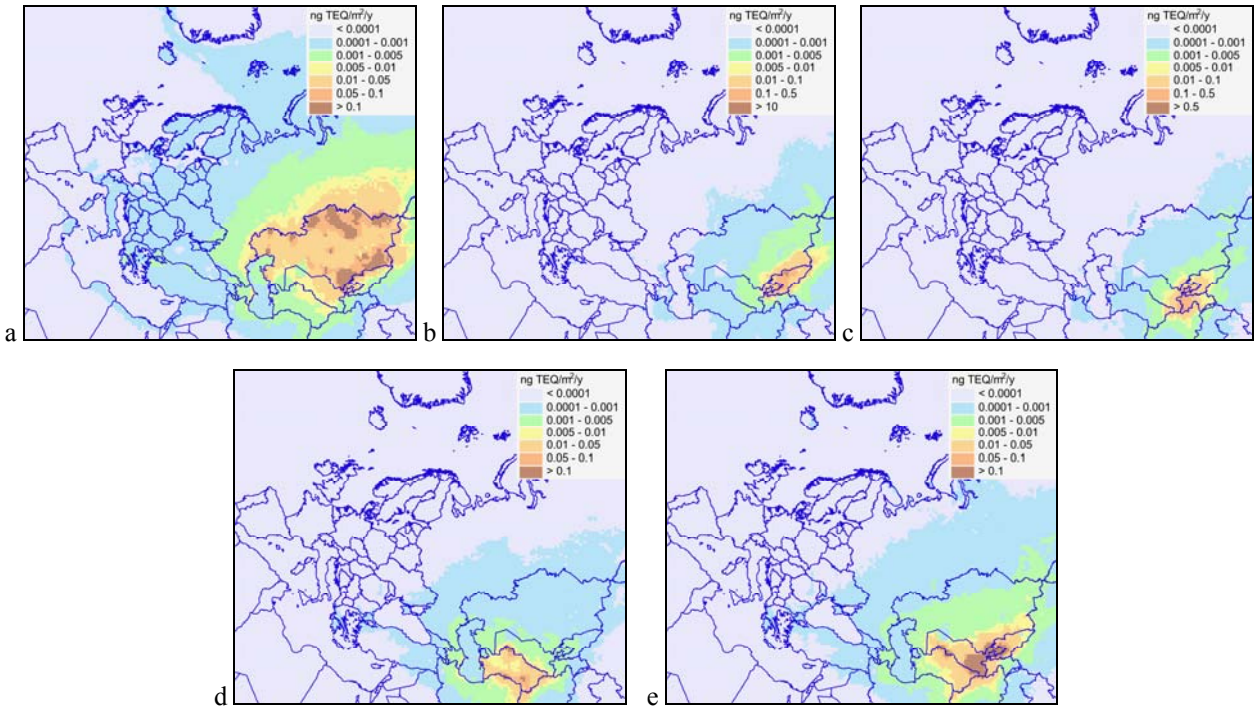

Fig. 4.55. *Spatial distribution of contamination by PCDD/Fs originated by national sources of Kazakhstan (a), Kyrgyzstan (b), Tajikistan (c), Turkmenistan (d) and Uzbekistan (e) in 2006, ng TEQ/m^2/y*

c) Spatial distribution of depositions to the country (Fig. 4.56).

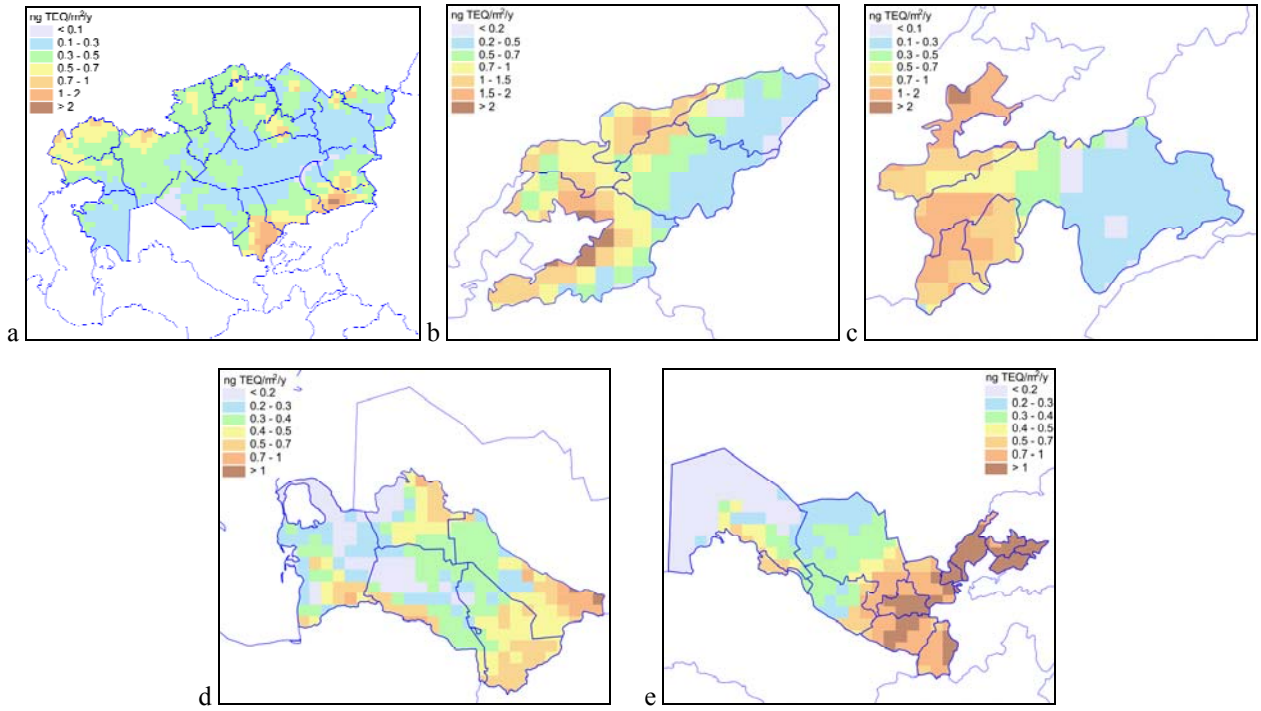

Fig. 4.56. *Spatial distribution of contamination by PCDD/Fs originated in Kazakhstan (a), Kyrgyzstan (b), Tajikistan (c), Turkmenistan (d) and Uzbekistan (e) in 2006, ng TEQ/m²/y*

d) Export diagrams (Fig. 4.57).

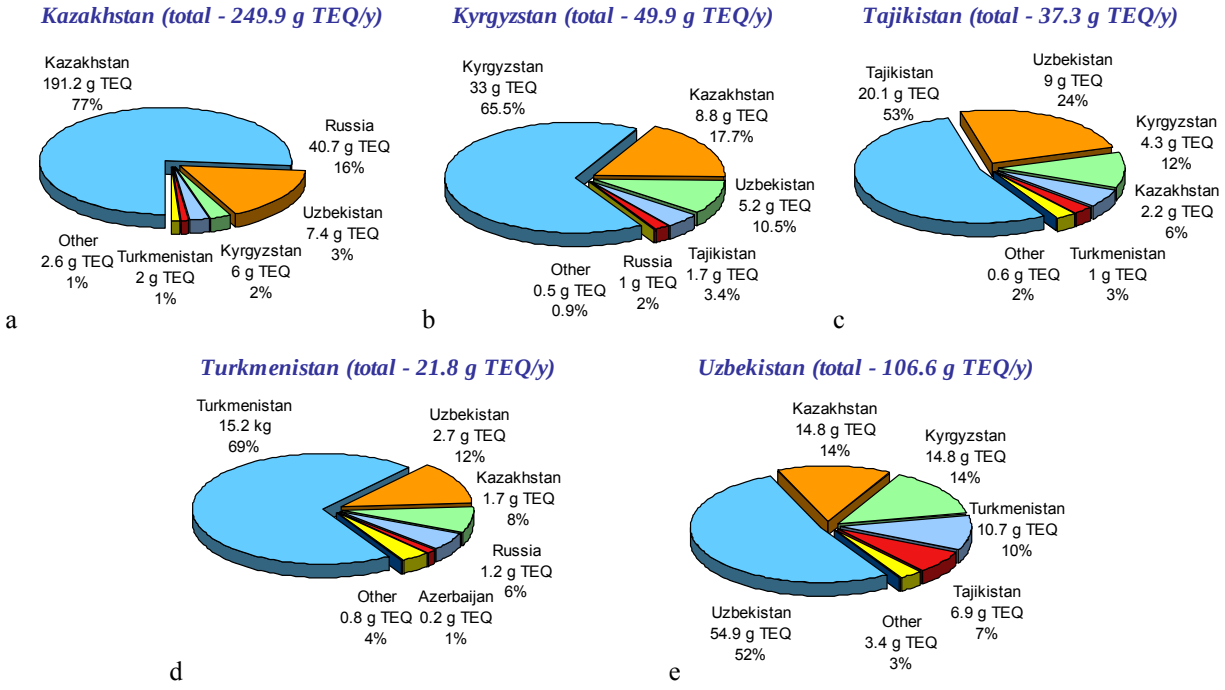

Fig. 4.57*. Transboundary transport of PCDD/Fs from Kazakhstan (a), Kyrgyzstan (b), Tajikistan (c), Turkmenistan (d) and Uzbekistan (e) in 2006, % of depositions*

e) Import diagrams (Fig. 4.58).

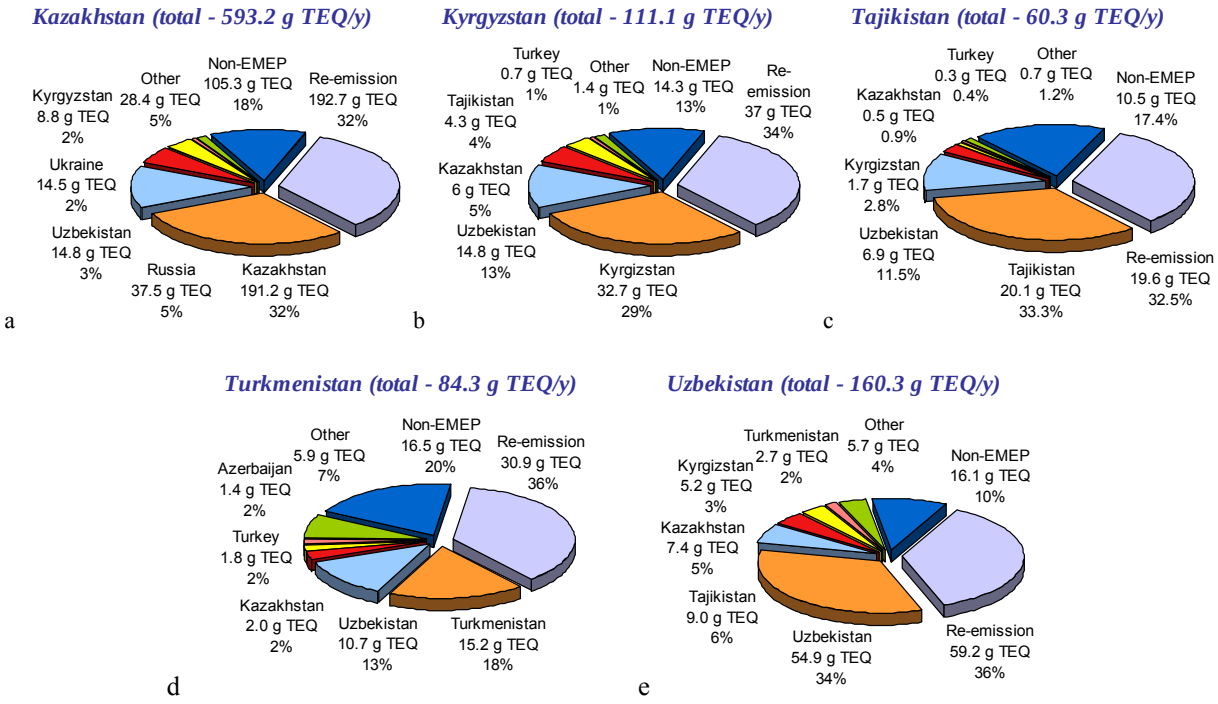

Fig. 4.58. *Transboundary transport of PCDD/Fs to Kazakhstan (a), Kyrgyzstan (b), Tajikistan (c), Turkmenistan (d) and Uzbekistan (e) in 2006, % of depositions*

f) Spatial distributions of deposition fractions due to transboundary transport.

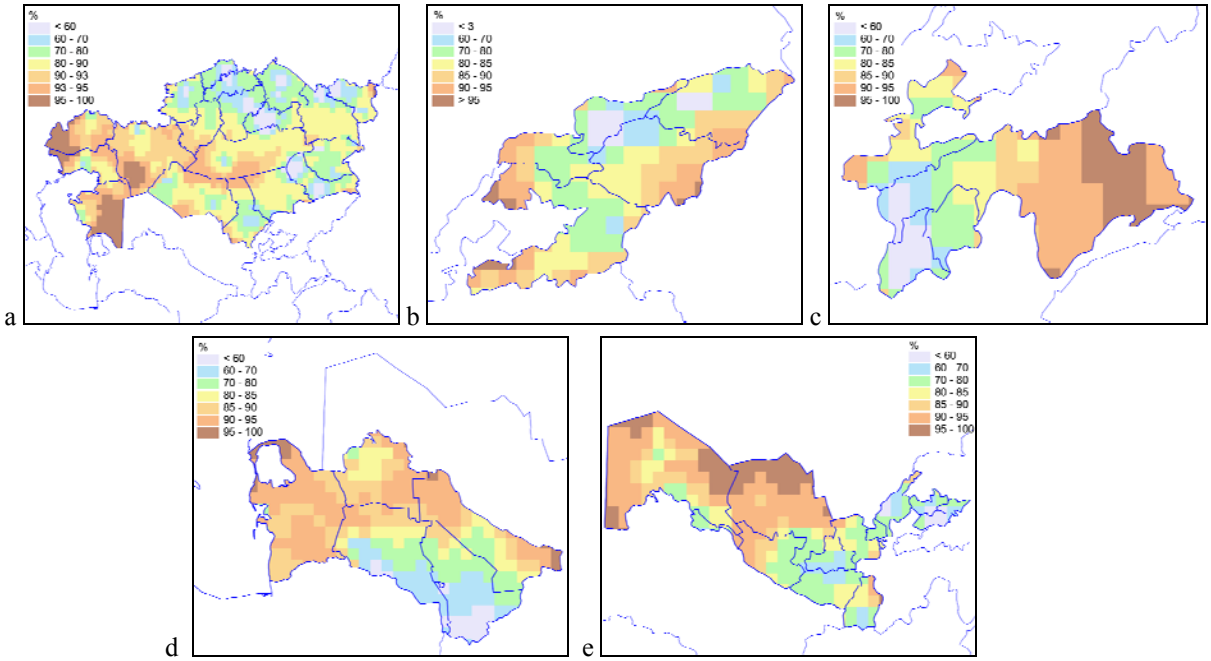

Fig. 4.59. *Spatial distribution of deposition fractions of PCDD/Fs due to transboundary transport for Kazakhstan (a), Kyrgyzstan (b), Tajikistan (c), Turkmenistan (d) and Uzbekistan (e) in 2006, % of depositions*

Full country-to-country matrices for air concentrations and depositions can be found on MSC-E web-site www.msceast.org Full set of country-specific information for 2006 will be put on EMEP web-site www.emep.int and on MSC-E web-site www.msceast.org in autumn 2008.

4.6. Hemispheric transport of POPs for 2006

Investigations of PCB-153, γ-HCH, and HCB intercontinental transport within the Northern Hemisphere and pollution levels over European region for 2006 were continued. Comparing to the previos year the evaluation of pollution levels for these POPs was performed using the nesting of the hemispheric and regional MSCE-POP models.

4.6.1. Polychlorinated biphenyls (PCBs)

Modelling of PCB long-range transport and accumulation in environmental compartments within the Northern Hemisphere was performed with hemispheric MSCE-POP model for the period 1970-2006. Simulations were made for one indicator congener PCB-153 on the basis of the global emission inventory of PCBs prepared by *Breivik et al.* [2007]. Annual emissions of PCB-153 and their spatial distribution for 2006 used for model computations are described in Section 4.4.1 of this chapter. Modelling of PCB distribution in European region for 2006 was carried out using the regional MSCE-POP model over the extended EMEP grid. Simulation results were preliminary compared with PCB measurements of EMEP monitoring sites.

Air concentrations and deposition levels

Spatial distributions of annual mean PCB-153 concentrations in surface air and in upper soil layer are shown in Fig 4.60a and b. It can be seen that most significant levels of air concentrations (3.6 pg/m^3 and above) are characteristic of European region. Moderate annual air concentrations (about 0.9-1.8 pg/m^3) were obtained for North America, Northern Africa, and European part of the Russian Federation. This distribution corresponds with the spatial distribution of PCB-153 annual emission within the Northern Hemisphere (Fig. 4.60a).

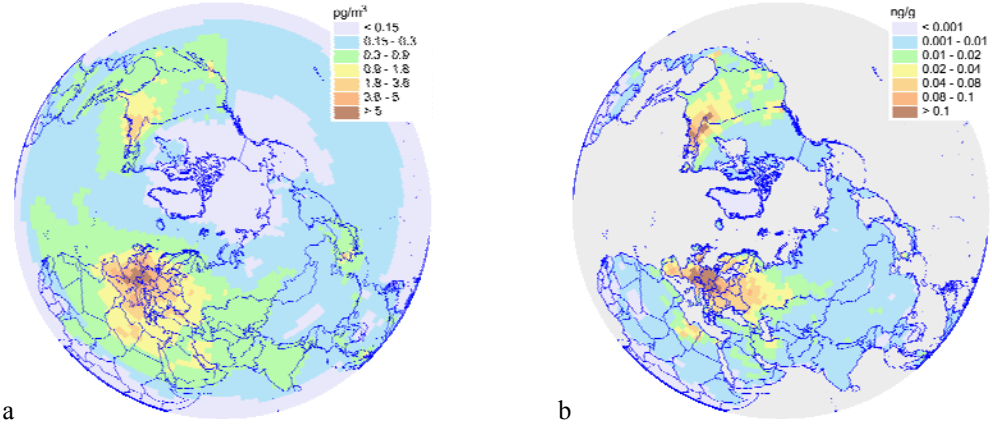

a b

Fig. 4.60. *Spatial distribution of PCB-153 annual mean air concentrations, pg/m^3 (a) and annual mean soil concentrations, ng/g (b) within the Northern Hemisphere for 2006*

Essential air concentrations of PCB-153 can be noticed for the Northern Atlantic, Southwest Asia, and Central Asian countries which can be explained by the long-range transport of the pollutant from the areas with significant PCB emission. Levels of annual mean PCB-153 concentrations in air within the Central Asia region are in the range of 0.3-0.9 pg/m^3.

Spatial distribution of PCB-153 concentrations in upper soil layer represents the accumulation of this pollutant in soil compartment. Accumulation of PCBs in soil is to significant extent determined by a long-term deposition process. Relatively high levels of soil concentrations (0.1 ng/g and above) can be seen in areas of high historical emission of PCBs, in particular, eastern part of North America, Germany, and European part of Russia. The Central Asian countries are characterized by comparatively low PCB-153 concentrations in soil (about 0.001-0.02 ng/g).

Detailed distributions of annual mean PCB-153 air concentrations with resolution 50x50 km^2 is shown in Fig 4.62a. It can be seen that regional MSCE-POP model in general reflects major peculiarities of air concentrations pattern calculated by the hemispheric model.

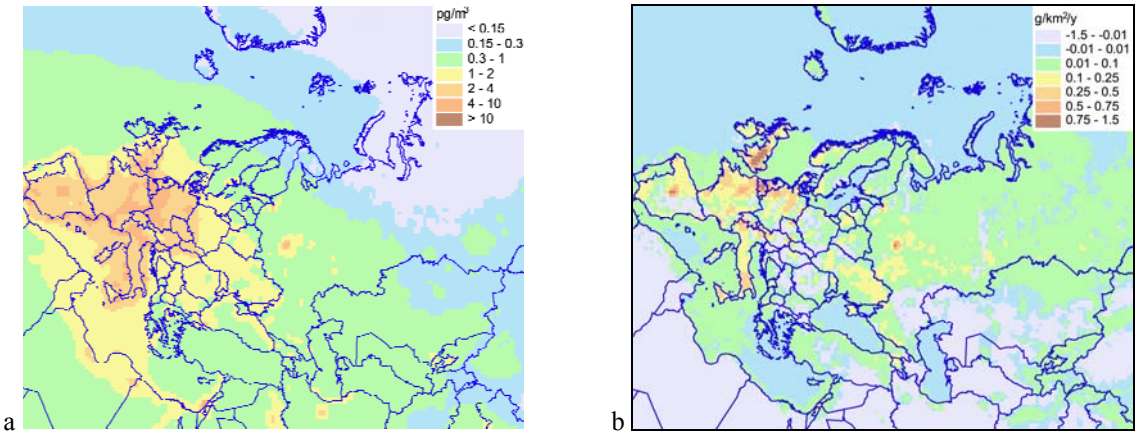

Fig. 4.62. *Spatial distribution of PCB-153 annual mean air concentrations, pg/m^3 (a) and net deposition flux, g/km^2/y (b) within the extended EMEP region for 2006*

Levels of PCB-153 net annual deposition fluxes over the extended EMEP grid are shown in Fig 4.62b. The most significant net deposition fluxes (0.5 g/km^2/y and above) are characteristic of the UK, Belgium, Germany, and France. Essential levels of net deposition fluxes are noted for the countries of southern and eastern Europe, in particular, Spain, Italy, the Ukraine, etc.

It can be seen that the pattern of net deposition fluxes includes the deposition and re-emission fluxes. The re-emission of PCBs resulted from long-term accumulation in environmental compartments can become comparable with primary PCB emissions to the atmosphere especially when these emissions essentially declining. For countries with relatively significant emission the deposition fluxes from the atmosphere to the surface are dominating (the UK, Belgium, France, Germany, etc.). In countries of Southern and Eastern Europe the re-emission fluxes from soil compartment prevail. Net deposition fluxes over the Central Asian countries are in the range -0.1 – 0.1 g/km^2/y.

Comparison of modelling results with measurements

Verification of obtained modelling results for PCB-153 was performed using the measurements of EMEP monitoring network. Calculated PCB-153 concentrations in air and precipitation were confronted with data of 10 monitoring sites.

Results of the comparison of measured and calculated annual mean PCB-153 air concentrations for 2006 are presented in Fig. 4.63a. Computed concentrations reasonably agree with measurements for most of the sites. Significant spatial correlation between observations and model results can be noted. On average, the deviations between computed and measured air concentrations amount to

approximately 60%. It can be seen that for the sites SE14, IS91, NO1, and FI96 model results are in good agreement with measurements (the differences do not exceed 10%). For the sites GB14 and SE12 the model significantly overestimated measured concentrations, in particular, by a factor of 2.8 and 5, respectively. Measurements of the site NO42 were underestimated by a factor of 2.6 by the model.

The overestimation for the sites SE12 and GB14 is most likely connected with the uncertainties of spatial distribution of PCB emission over the 50x50 km^2 grid and representativeness of these sites for the 50x50 km grid cells. In particular, the spatial distribution of PCB emission for this study was obtained by reallocation of gridded emission from the 1°x1° latitude-longitude grid to the grid system of the MSCE-POP regional model which is defined in the stereographic projection. Uncertainties in reallocation process can result in the elevated levels of emissions in grid-cells where the sites are located and smoothing of emissions over nearby grid-cells. Taking this into account further work on refinement of spatial distribution of PCB emissions within the extended EMEP model grid is required.

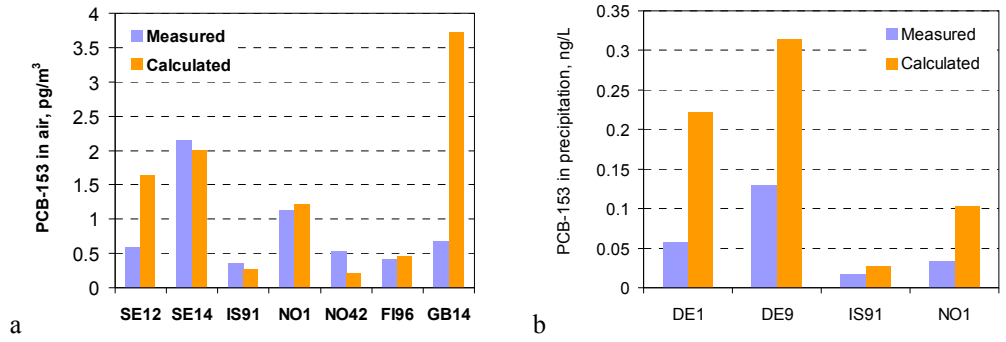

Fig. 4.63. *Comparison of computed annual mean air concentrations (a) and concentrations in precipitation (b) of PCB-153 with measurements of EMEP monitoring sites for 2006*

Comparison of calculated annual mean PCB-153 concentrations in precipitation was carried with the data of four EMEP sites, namely, DE1, DE9, IS91, and NO1. It can be seen that the model reproduced low concentrations for the remote site IS91 and elevated levels for the sites in Western Europe (DE9). At the same time, the model overestimates the observed concentrations in precipitation at DE1, DE9, and NO1 on average by a factor of 2.8 which can be caused by the uncertainties in spatial distribution of PCB emissions and rough spatial resolution of the model. In case of NO1 there is significant difference the observed precipitation amount and used in model calculations (more than a factor of three) which complicates the comparison.

It should be noted that the comparison of calculated and measured concentrations in precipitation is complicated by several factors and should be considered as indicative. In particular, differences can be connected with the description of wet deposition process in the model, where precipitation is equally distributed in model grid cell with resolution 50x50 km^2 while in reality the rainfall can be restricted to rather limited area. Additional discrepancies can be caused by different amount of precipitation used in the model and obtained at the monitoring sites.

4.6.2. Lindane (γ-HCH)

The application of lindane (γ-HCH) for agricultural purposes has been banned or severely restricted in the majority of European countries during two recent decades. Only several countries, namely, the UK, Spain, Belgium, Croatia, and Romania provided information on their emission for recent years

(2000-2006). Most of other European countries reported no use or application of lindane. Annual emissions of γ-HCH for 2006 and their spatial distribution used for model computations are described in Section 4.4.1 of this chapter. Though these data are not complete and are subject of significant uncertainties their application in model simulations can be useful for the description of pollution levels on the hemispheric scale and within the European region.

Similar to PCB-153 evaluation of pollution levels of γ-HCH for European region was carried out on the basis of combined hemispheric/regional modelling approach. The hemispheric MSCE-POP model was applied to estimate intercontinental transport of γ-HCH from three selected groups of emission sources within the Northern Hemisphere (Europe, North America, and Southeast Asia) and to evaluate initial and boundary conditions for the regional MSCE-POP model. Hemispheric scale model simulations were carried out for the period 1985-2006 for Northern Hemisphere with spatial resolution 2.5°x2.5°. Regional scale modelling was performed for 2006 over the extended EMEP domain with spatial resolution 50x50 km^2 on the basis of initial and boundary conditions from hemispheric model.

Air concentrations and deposition levels

Spatial distribution of annual mean γ-HCH concentrations in air and in seawater within the Northern Hemisphere for 2006 is presented in Fig. 4.64. The most significant levels of air concentrations (100 pg/m^3 and above) are characteristic of southern Canada, the UK, and Spain. Moderate annual air concentrations (20-50 pg/m^3) were obtained for the USA, Mexico, eastern part of China, and Western Europe. It can be seen that pollution transport from Chinese emission sources and possibly from other Southeast Asian countries can be essential for Pacific Ocean and under favourable meteorological conditions for the North America. The contribution of γ-HCH emissions of North American and European sources can be important for the pollution of Northern Atlantic and the Arctic region.

Essential γ-HCH concentrations in surface layer of seawater (25-100 pg/L) were obtained for the North, Baltic, and Mediterranean seas, Northern Atlantic, and coastal waters of North America. The levels of γ-HCH in seawater tend to increase toward the northern areas of Pacific and Atlantic oceans.

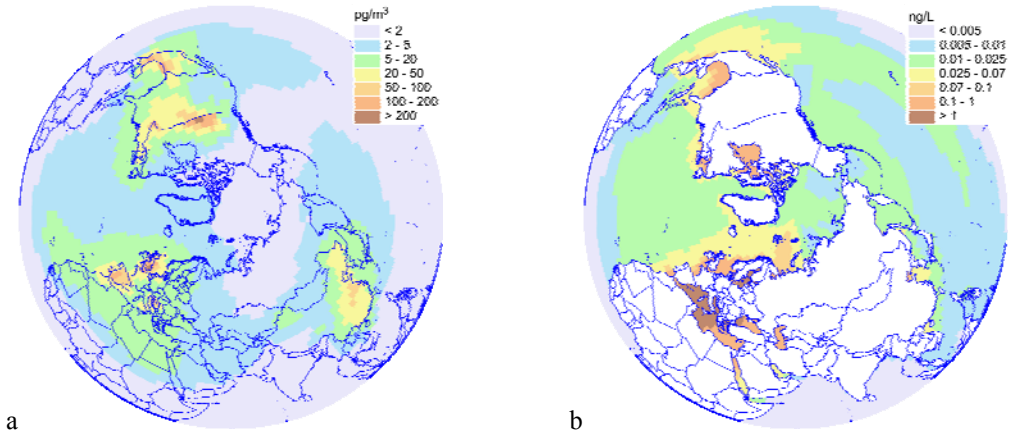

a b

Fig. 4.64. *Spatial distribution of γ-HCH annual mean air concentrations, pg/m^3 (a) and annual mean seawater concentrations, ng/L (b) within the Northern Hemisphere for 2006*

Results of model simulations over the extended EMEP grid with finer spatial resolution 50x50 km^2 are shown in Fig 4.65. It can be seen that similar to the hemispheric model results elevated γ-HCH air concentrations (50 pg/m^3 and above) in 2006 are characteristic of the UK, Spain, and Croatia. Moderate levels of air concentrations were obtained for the countries of Western and Central Europe

(5 – 20 pg/m^3). The countries of Eastern Europe and Central Asia are characterized by particularly low γ-HCH air concentrations (2-5 pg/m^3), which is mainly connected with the absence of information on emissions for these regions.

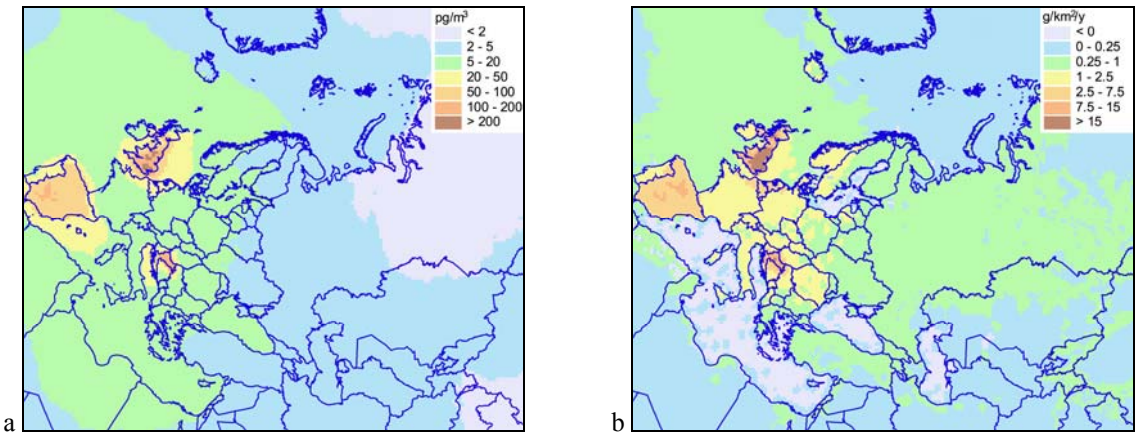

Fig. 4.65. *Spatial distribution of γ-HCH, annual mean air concentrations, pg/m^3 (a) and net deposition flux, g/km^2/y (b) within the extended EMEP region for 2006*

Levels of γ-HCH net annual deposition fluxes over the extended EMEP grid are shown in Fig 4.65b. The most significant net deposition fluxes (2.5 g/km^2/y and above) are characteristic of the UK, Spain, the Netherlands, and Croatia. Essential level of net deposition fluxes are noted for other countries of Western and Central Europe. Low values of deposition fluxes (0 – 0.25 g/km^2/y) can be seen in countries of Eastern Europe and Central Asia and over the North Atlantic. For the Baltic, North, Mediterranean, Black, and Caspian seas the re-emission from seawater can be noted.

Comparison of modelling results with measurements

For the verification of obtained modelling results for γ-HCH preliminary comparison of computed mean annual concentrations in air and in precipitation with measurements of EMEP monitoring sites was carried out. Information of 10 monitoring stations on measured γ-HCH concentrations in air and precipitation was used for the comparison. Results of the comparison of annual mean measured and computed concentrations are given in Fig. 4.66.

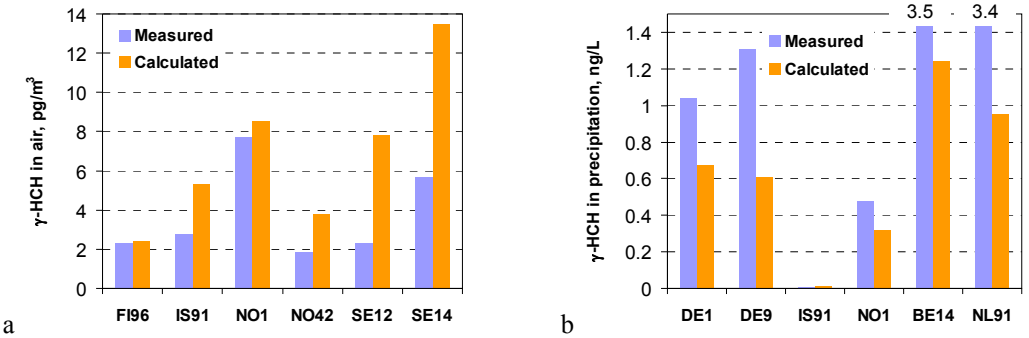

Fig. 4.66. *Comparison of computed annual mean air concentrations of γ-HCH in air (a) and in precipitation (b) with measurements of EMEP monitoring sites for 2006*

On the whole, it can be seen that the regional MSCE-POP model better describes the levels of γ-HCH air concentrations in comparison with the concentrations in precipitation. There is some tendency for overestimation of observed air concentrations by modelling results (on average by 80%). The most significant differences in air concentrations accounting for more than a factor of two are encountered for the sites SE14 and SE12. The reason of the overestimation can be connected with the uncertainties of lindane emissions, its spatial distribution, and seasonal variations especially for countries surrounding Sweden (the UK, France, Germany, etc.). Additional source of differences can be uncertainties in γ-HCH physical-chemical properties and their temperature dependence. For other monitoring sites the differences are lower than a factor of two.

In case of γ-HCH concentrations in precipitation the model tend to underestimate measured levels by a factor of 2.6 on average. The most essential underestimation takes place for the sites BE14 and NL91. There is a need to note that significant part of measured concentrations in precipitation at BE14 and NL91 were below the detection limit. So the actual concentrations could be somewhat lower than the reported estimates. For other sites computed concentrations agree with measurements nearly within a factor of two.

Considering the comparison results it can be seen that parallel measurements of γ-HCH concentrations in air and precipitation in 2006 were performed only at two EMEP sites NO1 and IS91. Other sites carried out only one of these types of measurements. In case of IS91 the model predictions overestimate observed air concentrations by approximately 90% and concentrations in precipitation by 60%. The values of annual mean calculated and measured γ-HCH concentrations in precipitation for IS91 are equal to 15 and 9 pg/L, respectively. So, on average, the model tends to provide higher predictions of concentrations in comparison with measurements of IS91.

In case of NO1 the comparison of γ-HCH concentrations in air demonstrated rather small overestimation of observed values (by 10%). At the same time the comparison of concentrations in precipitation for this site is complicated by the significant difference in measured precipitation amount and used by the model (more than a factor of three). On the whole, taking into account results of this preliminary analysis and significant uncertainties in the emission data used for modelling, the level of agreement between the measurements and model results can be regarded as reasonable.

4.6.3. Hexachlorobenzene (HCB)

Pollution levels of HCB within the Northern Hemisphere were estimated taking into account intercontinental transport from several groups of emission sources. The emission scenario used in model computations is described in Section 4.4.1 of this chapter. Hemispheric modelling was carried out for the period 1970-2006 with spatial resolution 2.5°x2.5°. Regional scale model simulations for 2006 were done over the extended EMEP domain with spatial resolution 50x50 km^2 with the initial and boundary conditions obtained from hemispheric model simulations. The aim of this study was to investigate distribution of HCB over extended EMEP grid with fine spatial resolution and to perform preliminary analysis of agreement of model results with available measurements of EMEP monitoring network. Taking into account significant uncertainties in HCB emissions and its spatial distribution the modelling results on HCB long-range transport and pollution levels are currently of a preliminary character.

Air concentrations and deposition levels

Spatial distribution of annual mean HCB air concentrations in air and in seawater for 2006 is shown in Fig. 4.67. Elevated levels of HCB air concentrations (50 pg/m^3 and above) are obtained for countries of Southeast Asia, European part of Russia, Spain, and Portugal. Significant level of HCB air

concentrations (100 pg/m^3 and above) is characteristic of India. Moderate air concentrations (20 – 50 pg/m^3) of HCB can be noted for eastern part of the USA and countries of Western and Central Europe. Low values of air concentrations (below 15 pg/m^3) were calculated for eastern Russia, Canada, and the Arctic region.

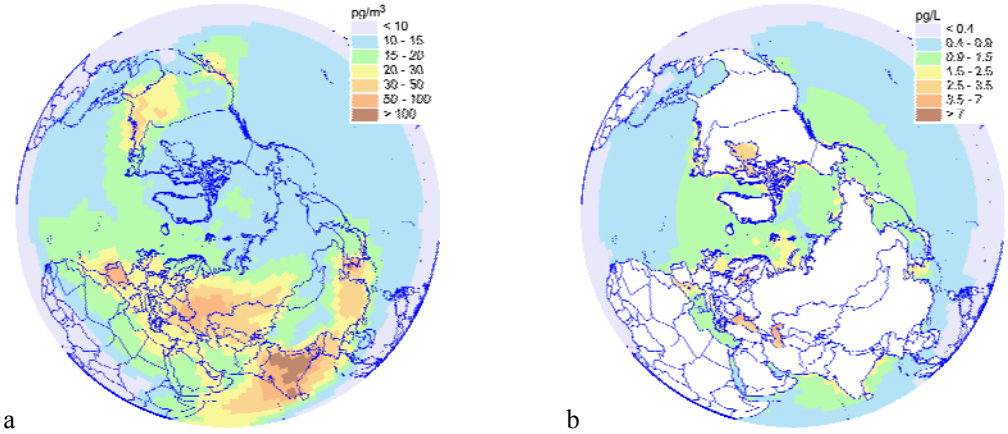

a b

Fig. 4.67. *Spatial distribution of HCB annual mean air concentrations, pg/m^3 (a) and annual mean seawater concentrations, pg/L (b) within the Northern Hemisphere for 2006*

Spatial distribution of HCB seawater concentrations within the Northern Hemisphere for 2006 is shown in Fig. 4.67b. Elevated levels of HCB concentrations in seawater (2.5 pg/L and above) were obtained for the coastal areas of North America and Europe. Similar to γ-HCH there is a north to south gradient in HCB seawater concentrations in the Pacific and Atlantic oceans.

Modelling results over the extended EMEP grid with finer spatial resolution 50x50 km^2 are shown in Fig. 4.68. It can be seen that levels of air concentrations over Spain and the Russian Federation are essentially higher than that over other European countries. These differences can be explained by the uncertainties in currently available information on HCB emissions and, in particular, by significantly different values of HCB emissions used in modelling. In particular, the contribution of annual HCB emissions of Spain and The russian federation to the total European emission for 2006 amounted to 28% and 36%, respectively. It can be seen that the emissions of these countries have substantial influence on the pollution levels of surrounding countries. Thus, countries of Eastern Europe and Central Asia are characterized by elevated HCB air concentrations (20-50 pg/m^3).

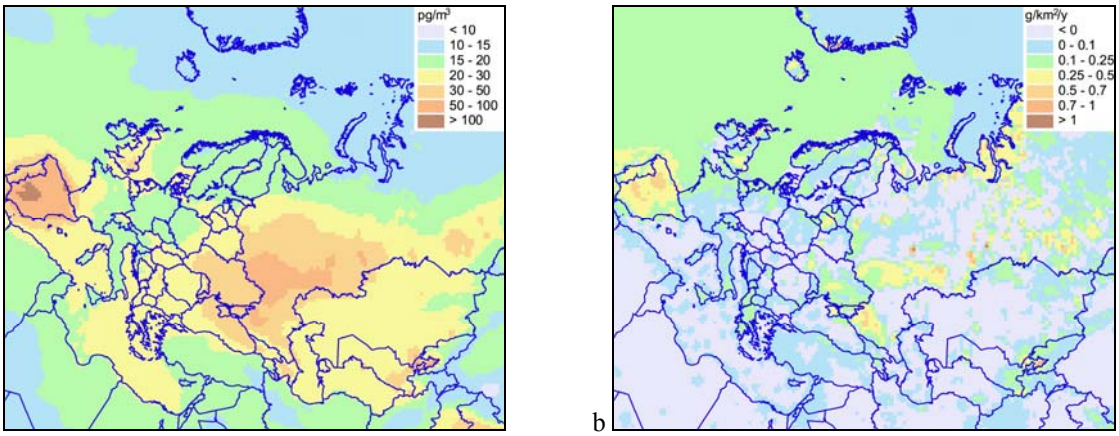

a b

Fig. 4.68. *Spatial distribution of HCB annual mean air concentrations, pg/m^3 (a) and net deposition flux, g/km^2/y (b) within the extended EMEP region for 2006*

Net annual deposition fluxes of HCB over the extended EMEP grid are given in Fig 4.68b. For the significant part of the extended EMEP grid the prevailing of HCB re-emission fluxes over the deposition fluxes can be noticed. This can be explained by essential volatility of this pollutant. The deposition fluxes are higher only in areas with high emission (Spain, The russian federation), over Atlantic, and in areas with comparatively low air temperatures.

Comparison of modelling results with measurements

Preliminary comparison of obtained modelling results with measurements of HCB concentrations in air and in precipitation of 5 EMEP monitoring sites was performed. Summarized results of the comparison of annual mean values of concentrations are presented in Fig. 4.69.

Measurements of HCB concentrations in air were carried out at three EMEP sites NO1, IS91, and NO42. The model underestimates observed levels of HCB in air at sites NO1 and NO42 whereas the observed values at the site IS91 were overestimated by the model. The underestimation of observed concentrations can be connected with the uncertainties of the officially reported HCB emission.

Concentrations in precipitation for HCB were obtained at four sites DE1, DE9, NO1, and IS91. In this case the model also tends to underestimate measured concentrations in precipitation for sites DE1, DE9, and NO1. However, analysis of deviations between model results and observed concentrations for the site NO1 is complicated by the significant difference between precipitation amount measured at the site and used in modelling (more than a factor of three).

Contrary to other sites computed concentrations for IS91 overestimates measured levels both in air and precipitation. The disagreement can be connected with the uncertainties in available information on HCB emissions for European countries and North America. Besides the significant difference between HCB air concentrations measured at IS91 and other two sites (NO42 and NO1) can be noted.

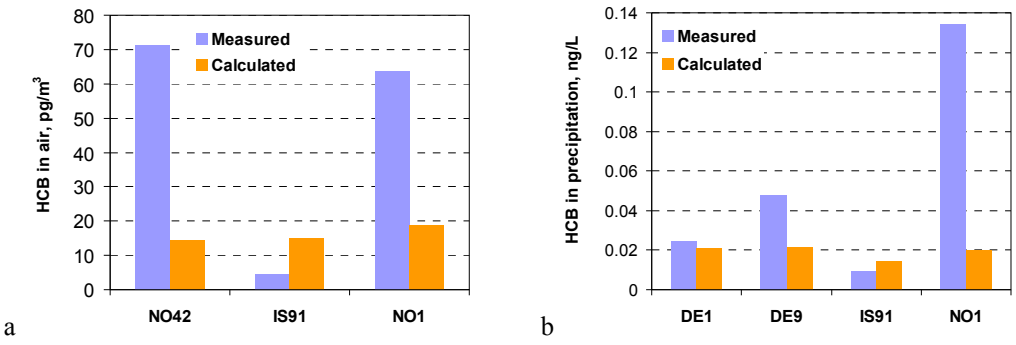

Fig. 4.69. *Comparison of computed annual mean air concentrations of HCB in air (a) and in precipitation (b) with measurements of EMEP monitoring sites for 2005*

Results of this preliminary comparison indicate that the levels of HCB emission in Europe are likely more significant than currently available emission data especially in countries of Western and Northern Europe. Therefore, further work on the refinement of HCB emission data is required.

CONCLUSIONS

This report summarizes the main results of annual activities carried out by MSC-E in the field of development of MSCE-HM and MSCE-POP models and the verification of modelling results. In particular, the transition from NCEP/DOE re-analyses to ECMWF analyses data was completed, the EMEP modelling domain was extended eastward, and the investigation of sensitivity of modelling results on the refining of vertical discretization was initiated. Furthermore, significant experience in use of CMAQ modelling system for generation of input data on atmospheric chemical reactants was gained. The main conclusions are grouped according to the activities and are formulated below.

Transition from NCEP/DOE to ECMWF analyses

1. Over most of the extended EMEP domain air temperatures, wind speeds and precipitation amounts calculated by MM5 on the base of ECMWF analyses are similar to those based on NCEP/DOE re-analyses. This refers to both their annual mean values and temporal variability. Noticeable differences are indicated for specific areas (e.g., coastal zones, mountainous regions etc).

2. Fields of annual mean surface air temperatures simulated by MM5 on the base of ECMWF analyses and NCEP/DOE re-analyses for 2006 are similar. Absolute bias for air temperatures is around ±1 °C. MM5 tends to slightly underestimate surface air temperatures (around 1°C) compared to the observations.

3. Relative bias for annual mean wind speeds, simulated by MM5 on the base of ECMWF and NCEP/DOE is ±5%, and absolute bias - ±0.5 m/s over most of the extended EMEP domain. The use of ECMWF data as input information for MM5 results in overprediction of the observed wind speed on average by 9%, and NCEP/DOE – by 11%. Temporal variability of surface wind speed was reproduced reasonably well by MM5: *Rc* between 6-hour predicted and observed time series is higher than 0.6 over most of stations.

4. Over most of EMEP domain the relative bias between annual precipitation sums simulated by MM5 on the base of ECMWF and NCEP/DOE input data ranges within ±25%. Over dry or arid areas (Sahara, the Mediterranean Sea) as well as over mountainous regions the bias can be higher. Comparison of precipitation sums simulated by MM5 with GPCP data demonstrated relatively good (within ±25%) agreement over the eastern part of Europe, north of Kazakhstan and Scandinavia. Over the central part of Europe and northern Atlantic the bias reaches ±50%.Temporal variability was satisfactorily captured by MM5: *Rc* is more than 0.6 over most of Europe.

5. Over mountainous regions the performance of MM5 lower compared to other regions, regardless whether ECMWF or NCEP/DOE input data were used. Both averaged values and temporal variability of air temperatures, wind speeds and precipitation sums were reproduced with lower accuracy.

6. MM5 tends to overpredict wind speed in the free troposphere, both using ECMWF analyses and NCEP/DOE re-analyses as input data. On average, the overprediction is minor at 925 hPa level and reaches 3.3 m/s at 300 hPa level. Nevertheless, temporal variability is reproduced well by MM5. *Rc* between observed and modelled 12-hour time series of wind speeds is higher than 0.8 at most of stations.

7. MM5 tends to overestimate air temperate in the free atmosphere compared to the observed values. On average, the overprediction reaches 4.5 °C at 300 hPa level. This however, does not seem high compared to mean value of -55°C at this level. Temporal variability of modelled air temperatures was reproduced with significant accuracy: *Rc* between modelled and measured 12-hour time series is higher than 0.8 over most of stations.

Preparation of input data on the base of CMAQ model

- The model underestimates PM10 concentrations in the air by 30% on the average. Air concentrations of PM2.5 are reproduced by the model with a reasonable accuracy. One of the possible reasons for CMAQ underestimation of coarse particles concentrations may be associated with the underestimation of dust emission in Europe.

- Calculations of SO_2 atmospheric transport are in fairly good agreement of measurements. CMAQ reproduces successfully both average levels of SO_2 concentrations in the air and their spatial distribution.

- The model overestimates ozone concentrations in the surface air by 15% on the average. To find the reasons of this overestimation a detailed analysis of the ozone chemical cycle is needed. Such analysis is planned to conduct next year.

- In general results of modelling of OH-radical atmospheric transport are in line with the common view on OH-radical behaviour in the atmosphere and with the available results of global calculations. Currently it is not possible to assess the reliability of the obtained data since regular observations are not performed.

Sensitivity of MSCE-HM model results to input meteorological datasets and to refining of vertical structure

1. Annual mean concentrations of lead, calculated by MSCE-HM on the base of ECMWF are 2.6% higher than those based on NCEP/DOE input data over the European and the Central Asian countries (Kazakhstan, Kyrgyzstan, Uzbekistan, Tajikistan and Turkmenistan). The depositions of lead based on ECMWF data are 0.7% lower, and of mercury 3% higher compared to those based on NCEP/DOE over the same countries. However, over some areas the difference between concentrations computed with the use of the two different meteorological datasets makes up ±25%, and between depositions - up to ±50%.

2. At individual monitoring stations the pollution levels computed on the base of ECMWF data on average exceed those based n NCEP/DOE re-analysis by 7% for annual mean air concentrations, by 10% for concentrations in precipitation and by 2.5% for wet deposition flux.

3. Over most of the extended EMEP domain the difference between TGM annual mean concentrations, calculated on the base of ECMWF and NCEP/DOE input data, is around

±1.5%. The difference in annual total depositions of mercury is within ±25% over most of the EMEP domain, and within ±50% over the Arctic, the Mediterranean Sea and the Central Asian Region.

4. Annual mean concentrations in precipitation averaged over the monitoring stations computed on the base of ECMWF meteorological data are 13% higher and wet deposition fluxes – by 1% lower than those based on NCEP/DOE data. The difference between TGM concentrations is within ±3%.

5. The experiment with reducing thickness of the lowest model layer demonstrated that the reduction leads to some decrease of air concentrations (by 15%) and the depositions (by about 1.5%) over the European and the Central Asian countries on average. The increase of concentrations and depositions is noted for regions with significant emission sources. The comparison of the results based on the two experiments at monitoring stations demonstrated that the reduction of lowest model layer does not lead to evident improvement of the model performance. However, the obtained results are preliminary and need further work on this issue is needed.

Verification of MSCE-HM modelling results.

1. Annual mean air concentrations of lead and cadmium were simulated with significant accuracy. The underestimation of the observed values is around 20%, and spatial correlation coefficient is about 0.7.

2. Calculated concentrations of lead and cadmium in precipitation and their wet deposition fluxes are characterized by higher deviation from the observed quantities. For lead the underestimation of the concentrations and the fluxes is around 30%, and for cadmium – about 50%. Nevertheless, temporal variability of measured concentrations and fluxes was reproduced favourably well: the correlation coefficients are around 0.7.

3. Numerical experiments with different emission data were carried out in order to evaluate sensitivity of modelled concentrations and depositions at measurement stations to selection of emission data and to indicate regions where emissions are possibly underestimated. It was demonstrated that in some cases (e.g., at Finnish stations) the incorrect emission total value and/or its spatial distribution can possible be a reason explaining the underestimation, at least, in some periods of the year. Nevertheless, in some other cases (e.g. at Slovak stations) the possible uncertainties of the emission data alone do not allow to explain the discrepancies between measurements and modelling. In this case possible reason of the discrepancies can be linked with the influence of local emission sources, measurement uncertainties etc.

4. Concentrations of annual mean modelled total gaseous mercury (TGM) agree with the observed ones within ±20%. Modelled concentrations of mercury in precipitation well match the measured ones on average. Wet deposition flux is about 20% lower than the observed one.

5. In addition to annual mean concentrations and depositions of lead, cadmium and mercury, the model is capable of reproducing their short-term variability. Most of the observed peak values were captured by the model both in term of location and magnitude. By means of back trajectory analysis it was shown that the peaks not caught by the model are often associated with air mass transport from regions where emission data used in modelling is low.

Further development of MSCE-POP model

1. Implementation of the recommendations on further development of MSCE-POP model during the current year was focused on the investigation of different approaches to model description of gas-particle partitioning, wet deposition, and wind re-suspension of POPs.

2. Results of model simulations showed that the influence of absorption mechanism in gas-particle partitioning for the four indicator PAHs (B[a]P, B[b]F, B[k]F and I_P) seemed to be negligible. At the same time, for other pollutants (PCBs, PCDD/Fs) absorption mechanism can noticeably change gas/particle partitioning.

3. Data on aerosol particles and OH concentrations in the atmosphere with detailed spatial and temporal resolution were obtained by the CMAQ model and used in experimental MSCE-POP model runs. The possibility to implement the CMAQ model for the preparation of the input data was further elaborated.

4. Modifications of model parameterization of wet deposition of POPs in gaseous phase, taking into account possible influence of organic matter in rain water, were considered and experimental model simulations were made. Results of model simulations suggested that the sorption of POPs on the organic matter within the rain drops can lead to increased wet deposition fluxes. The comparison of these modelling results with measurements showed that the use of modified parameterization of wet deposition led in most cases to better agreement with observed concentrations in precipitation.

5. The analysis of model parameterization of POP re-suspension with aerosol particles was carried out. It was obtained that on average the contribution of POP re-suspension to the total re-emission flux was comparatively small being comparable with re-volatilization flux from soil only in some regions (e.g. in the UK). The comparison of computed B[a]P soil concentrations with measurements revealed that the MSCE-POP model tended to underestimate observed levels of B[a]P soil concentrations which could lead to relatively lower re-suspension fluxes.

6. The regional and hemispheric MSCE-POP models were adapted to the simulations over the extended EMEP modelling domain. These modifications made it possible to provide the Central Asia countries (Kazakhstan, Turkmenistan, Uzbekistan, Kyrgyzstan, and Tajikistan) and the Asian part of Russia with information on pollution levels and transboundary transport of POPs.

Model assessment of POP pollution levels over the extended EMEP domain

1. Assessment pollution levels was performed for the four indicator PAHs (B[a]P, B[b]F, B[k]F and I_P), PCDD/Fs (the mixture of all 17 toxic congeners), PCB-153, γ-HCH and HCB for 2006. Estimates of transboundary transport for PAHs were obtained at the regional scale since these pollutants are mainly particle-bound. For the rest of selected POPs the evaluation of contamination of the EMEP region was carried out on the basis of hemispheric/regional modelling approach.

2. Annual mean B[a]P concentrations in surface atmospheric layer in 2006 within the European region varied from 0.01 to 1 ng/m^3. Average level of B[a]P air concentrations over the European countries was about 0.4 ng/m^3. Elevated B[a]P air concentrations (0.5 ng/m^3 and above) were obtained for the countries in Central and Eastern Europe. Spatial distribution of

pollution levels for the rest three indicator PAHs (B[b]F, B[k]F, and I_P) in 2006 was similar to that of B[a]P. The levels of B[k]F air concentrations were somewhat lower comparing to the air concentrations of the rest three indicator PAHs.

3. Levels of B[a]P deposition fluxes in 2006 within the European region differed from 1 g/km^2/y to about 150 g/km^2/y. High values of deposition fluxes (20 – 150 g/km2/y) were characteristic of the Central, Southern, and Eastern Europe. The contribution of transboundary transport to B[a]P air concentrations and depositions in particular countries was essential and varied typically from 20 to 70%.

4. Average level of PCDD/F annual mean air concentrations over European countries in 2006 was about 1 fg TEQ/m^3. Elevated levels of PCDD/F air concentrations were obtained for the Central, Southern, and Eastern Europe whereas values of air concentrations below 1 fg TEQ/m^3 were characteristic of the Western and Northern Europe.

5. Calculated PCDD/F deposition fluxes ranged from 0.1 – 1 ng TEQ/m^2/y in the Western and Northern Europe to more than 3 ng TEQ/m^2/y in some regions of the Central, Southern and Eastern Europe. In comparison with modelling results for 2005 contamination levels in most of the European countries in 2006 did not change significantly.

6. The transboundary transport of PCDD/Fs was evaluated taking into account national anthropogenic emissions of European countries, non-EMEP anthropogenic sources, and re-emissions. The contribution of transboundary transport to the pollution of the EMEP countries in 2006 ranged from 3% to 60%. Non-EMEP sources contributed to the pollution levels up to 33%, and re-emission − from 30% to 70%. It can be noted that the re-emission of PCDD/Fs is essential and should be taken into account in the assessment of pollution levels in the European countries.

7. Evaluation of PCB-153 intercontinental transport and pollution levels within the European region for 2006 was carried out using unofficial inventory of global PCB emission. Most significant levels of air concentrations (3.6 pg/m^3 and above) are characteristic of European region. Essential air concentrations of PCB-153 can be noticed for the Northern Atlantic, Southwest Asia, and the Central Asia countries which can be explained by the long-range transport of the pollutant from the areas with significant PCB emission.

8. Usage of lindane (γ-HCH) for agricultural purposes has been banned or severely restricted in the majority of European countries during two recent decades. Only several countries, namely, the UK, Spain, Belgium, Croatia, and Romania provided information on their emission for recent years (2000-2006). Essential air concentrations (50-100 pg/m^3 and above) are characteristic of some regions of North America, the Western and Southern Europe. The contribution of γ-HCH emissions of North American and European sources can be important for the pollution of Northern Atlantic and the Arctic region.

9. Evaluation of HCB distribution within the Northern Hemisphere and the extended EMEP grid for 2006 was carried out on the basis of officially reported emissions complemented by unofficial estimates. Elevated levels of HCB air concentrations (50 pg/m^3 and above) are obtained for countries of Southeast Asia, European part of Russia, Spain, and Portugal.

Verification of MSCE-POP modelling results

1. Verification of calculated air concentrations and deposition fluxes of B[a]P in 2006 using the data of EMEP monitoring sites showed reasonable agreement between calculations and measurements. For the majority of calculated annual mean air concentrations and deposition fluxes the level of agreement with measurements is within a factor of two. For some of the stations, namely, SE12, FI96 and CZ3, the difference between the calculated and observed values does not exceed 25%. The model satisfactory reproduced observed seasonal variations of B[a]P concentrations and deposition fluxes.
2. Model results on PCB-153, γ-HCH, and HCB for 2006 were preliminary compared with available measurements. Reasonable agreement between the computed and measured PCB-153 and γ-HCH air concentrations for 2006 along with significant correlation was obtained. For HCB the model underestimated observed levels of concentrations in air and precipitation which was most likely connected with the underestimation of available HCB emission.

REFERENCES

Arp H.P.H, R.P.Schwarzenbach, K-U.Goss [2008] Determination of ambient gas-particle partitioning constants of non-polar and polar organic compounds using inverse gas chromatography. *Atmos. Env*. vol. 42, pp. 303-312.

B.Strukov, Yu.Resnyansky, A.Zelenko, A.Gusev, V.Shatalov [2000] "Modelling of Long-range Transport and Deposition of POPs in the European Region with Emphasis to Sea Currents" MSC-E Technical Note 5/2000.

Bahm K. and Khalil M.A.K. [2004] A new model of tropospheric hydroxyl radical concentrations. *Chemosphere*, vol.54, pp.143-166.

Bailey R. E. [2001] Global hexachlorobenzene emissions. *Chemosphere*, vol. 43, pp.167-182.

Breivik K, A Sweetman, JM Pacyna and KC Jones [2002a] Towards a global historical emission inventory for selected PCB congeners – a mass balance approach. 1. Global production and consumption. *Science of the Total Environment*. vol. 290, pp. 181-198.

Breivik K., Sweetman A., Pacyna J.M. and Jones K.C. [2007] Towards a global historical emission inventory for selected PCB congeners - a mass balance approach. 3. An update. *Science of the Total Environmen*t. vol. 377, No. 2-3, pp. 296-307.

Breivik K., Sweetman A., Pacyna J.M., Jones K.C. [2002b] Towards a global historical emission inventory for selected PCB congeners – a mass balance approach. 2. Emissions. *Science of the Total Environment,* v.290, pp.199-224.

Byun D.W, and K.S. Ching (editors) [1999] Science algorithms of the EPA models-3 community multiscale air quality (CMAQ) modelling system, US EPA, EPA/600/R-99/030, March 1999.

Calvert J.G and Lindberg S.E. [2005] Mechanisms of mercury removal by O_3 and OH in the atmosphere. *Atmospheric Environment*, vol. 39, pp3355 – 3367.

Carter W. P. L. [1996] Condensed atmospheric mechanisms for isoprene. *Atmos. Environ*., vol.30, pp.4275-4290.

Chang J. S., Middleton P. B., Stockwell W. R., Walcek C. J., Pleim J. E., Lansford H. H., Binkowski F. S., Madronich S., Seaman N. L., Stauffer D. R., Byun D., McHenry J. N., Samson P. J., and Hass H. [1990] The regional acid deposition model and engineering model, *Acidic Deposition: State of Science and Technology*, Report 4, National Acid Precipitation Assessment Program.

Chang, J. S., Brost R. A., Isaksen I. S. A., Madronich S., Middleton P., Stockwell W. R., and Walcek C.J. [1987] A Three-Dimensional Acid Deposition Model: Physical Concepts and Formulation. *J. Geophys. Res.,* vol.92, pp.14 681-14 700.

Cohen M., et al. [2002] Modeling the atmospheric transport and deposition of PCDD/F to the great lakes. *Environ. Sci. and Technol.*, vol. 36, pp. 4831-4845.

Denier van der Gon H.A.C., van het Bolscher M., Visschedijk A.J.H. and P.Y.J.Zandveld [2005]. Study to the effectiveness of the UNECE Heavy Metals Protocol and costs of possible additional measures. Phase I: Estimation of emission reduction resulting from the implementation of the HM Protocol. TNO-report B&O-A R 2005/193.

Dennis R. L, McHenry J. N., Barchet W. R., Binkowski F. S. and Byun D. W. [1993] Correcting RADM's sulfate underprediction: Discovery and correction of model errors and testing the corrections through comparisons against field data. *Atmos. Environ.,* vol. 26A, pp.975–997.

Dodge M. C. [1989] A comparison of photochemical oxidant mechanisms. *J. Geophys. Res*., vol. 94, pp.5121-5136.

Dutchak S., V. Shatalov, E. Mantseva, O. Rozovskaya, N. Vulykh, M. Fedyunin [2004] Persistent Organic Pollutants in the Environment. EMEP Status Report 3/2004.

Falconer R.L. [2004] Vapor pressures and predicted particle/gas distributions of polyrinated biphenyl congeners as functions of temperature and ortho-chlorine substitution. *Atmos. Environ.*, vol. 28, pp. 547-554.

Finizio A., D. Mackay, T. Bidleman, T. Harner [1907] Octanol–air partition coefficient as a predictor of partitioning of semi-volatile organic chemicals to aerosols. *Atmos. Environ.* vol. 31, No. 15, pp. 2289-2296.

Fjæraa A. M. and Hjellbrekke A.-G. [2007] Ozone measurements 2005. EMEP/CCC Report 2/2007.

Fraters D., Bouwman A.F. and T.J.M. Thewessen [1993] Soil Organic Matter of Europe. Estimates of soil organic matter content of the topsoil of FAO-Unesco soil units. Report 481505004, National Institute of Public Health and the Environment, Bilthoven. (Dutch text).

Gery M. W., Whitten G. Z., Killus J. P. and Dodge M. C. [1989] A photochemical kinetics mechanism for urban and regional scale computer modeling. *J. Geophys. Res*., vol. 94, pp. 12,925-12,956.

Götz C. W., M. Scheringer, M. Macleod, C. M . Roth, K. Hungerbühler [2007] Alternative Approaches for Modeling Gas-Particle Partitioning of Semivolatile Organic Chemicals: Model Development and Comparison. *Environ. Sci. and Technol.*, vol. 41, No. 4, pp. 1272-1278.

Grell G.A., Dudhia J., Stauffer D.R. [1995] A description of the Fifth-Generation Penn State/NCAR Mesoscale Model (MM5). NCAR Technical note TN-398. National Center for Atmospheric Research, Boulder, Colorado.

Grell, G. A., J. Dudhia, and D. R. Stauffer [1995] A description of the fifth-generation Penn State/NCAR Mesoscale Model (MM5). NCAR/TN-398+STR. NCAR Technical Note. Mesoscale and Microscale Meteorology Division. National Center for Atmospheric Research. Boulder, Colorado. Pp. 122.

Guo, Y.-R., and S. Chen [1994] Terrain and land use for the fifth-generation Penn State/NCAR mesoscale modelling system (MM5): Program TERRAIN. NCAR Tech. Note, NCAR/TN-397+IA, 119 pp. [Available from the National Center for Atmospheric Research, P. O. Box 3000, Boulder, CO 80307.]

Gusev A., E. Mantseva, V. Shatalov, B. Strukov [2005] Regional Multicompartment Model MSCE-POP. EMEP/MSC-E Technical Report 5/2005.

Gusev A., Ilyin I., Travnikov O. and V. Sokovych [2007a] Model assessment of transboundary pollution by lead and PCB-153 of the Central Asian Countries: Kazakhstan, Kyrgyzstan, Tajikistan, Turkmenistan, Uzbekistan. EMEP/MSC-E contribution to the UN ECE CAPACT project. 55p. **+annexes**

Gusev A., O. Rozovskaya, V. Shatalov [2007b] Modelling POP long-range transport and contamination levels by MSCE-POP model. EMEP/MSC-E Technical Report 1/2007.

Harner T., T.F. Bidleman [1998] Octanol–air partition coefficient for describing particle/gas partitioning of aromatic compounds in urban air. *Environ. Sci. & Technol*., vol. 32, No. 10, pp. 1494-1502.

Hillel D. [1982] Introduction to soil physics. Academic, San Diego, California, 364 pp.

Hodjamberdiev I. [2006] Determination of dioxins, furans, PCB sources and anti-POPs campaign in Central Asia. http://www.ecoaccord.org/pop/ipep/hodjamberdiev.htm.

Holoubek I. [2008] Private communications.

Huffman G.J., Adler R.F., Morrissey M.M., Bolvin D.T., Curtis S., Joyce R., McGavock B. and Susskind J. [2001]. Global Precipitation at One-Degree Daily Resolution from Multisatellite Observations. J. of Hydrometeorology, vol 2., pp. 36 – 50.

Ilyin I. and O. Travnikov [2005] Modelling of Heavy Metal Airborne Pollution in Europe: Evaluation of the Model Performance. EMEP/MSC-E Technical Report 8/2005.

Ilyin I., Rozovskaya O., Travnikov O. and Aas W. [2007]. Heavy metals: transboundary pollution of the environment. EMEP Status Report 2/2007. 54p+annexes

Junge C.E. [1977] Basic considerations about trace constituent in the atmosphere is related to the fate of global pollutant. In: Fate of pollutants in the air and water environment. Part I, I.H. Suffet (ed.) (Advanced in *Environ. Sci. Technol.,* v.8), Wiley-Interscience, New York.

Kanamitsu M., Ebisuzaki W., Woolen J., Yang S-K., Hnilo J.J., Fiorino M. and Potter G.L. [2002]. NCEP-DOE AMIP-II reanalysis (R-2). Bulletin of American Meteorological Society, 11, pp. 1631 – 1643

Li Y., G. Jianga, Y. Wanga, Z. Caib, Q. Zhanga [2008] Concentrations, profiles and gas–particle partitioning of polychlorinated dibenzo-p-dioxins and dibenzofurans in the ambient air of Beijing, China. *Atmos. Env*. vol. 42, pp. 2037-2047.

Lin C-J., Pongprueksa P., Lindberg S.E., Pehkonen S.O., Byun D. and Jang C. [2006] Scientific uncertainties in atmospheric mercury models I: Model science evaluation. *Atmospheric Environment*, vol. 40, pp.2911 – 2928.

Lohmann R. and G. Lammel [2004] Adsorptive and Absorptive Contributions to the Gas-Particle Partitioning of Polycyclic Aromatic Hydrocarbons: State of Knowledge and Recommended Parametrization for Modeling. *Environ. Sci. and Technol.*, vol.38, No. 14, pp. 3793-3803.

Lohmann R., R. Gioia, S. J. Eisenreich, K. C. Jones [2007] Assessing the importance of ab- and adsorption to the gas-particle partitioning of PCDD/Fs. *Atmos. Env*., vol.41, pp. 7767-7777.

Meng F., B. Zhang, P. Gbor, D. Wen, F. Yang, C. Shi, J. Aronson, J. Sloan [2007] Models for gas/particle partitioning, transformation and air/water surface exchange of PCBs and PCDD/Fs in CMAQ. *Atmos. Env*. vol. 41, pp. 9111-9127.

Nam J.J., G.O. Thomas, F.M. Jaward, E. Steinnes, O. Gustafsson, K.C. Jones [2008] PAHs in background soils from Western Europe: Influence of atmospheric deposition and soil organic matter. *Chemosphere,* vol. 70, pp. 1596-1602.

Pacyna E. G., Pacyna J. M., Steenhuisen F. and Wilson S. [2006] Global anthropogenic mercury emission inventory for 2000. Atmos. Environ. vol. 40, No. 22, pp.4048-4063.

Pacyna J.M. et al. [1999] Final report for Project POPCYCLING-Baltic. EU DGXII, Environment and Climate Program ENV4-CT96-0214. Available on CD-rom including technical report, the emission and environmental databases as well as the POPCYCLING-Baltic model. NILU, P.O. Box 100, N-2027 Kjeller, Norway.

Pacyna J.M., Scholtz M.T, and Li Y.-F (Arthur). [1995]. Global budget of trace metal sources. Environ. Rev. 3(2): 145–159

Pankow J.F. [1987] Review and comparative analysis of the theories on partitioning between the gas and aerosol particulate phases in the atmosphere. *Atmos. Environ.*, v.21, pp.2275-2283.

Pankow J.F. [1998] Further discussion of the octanol/air partition coefficient Koa as a correlating parameter for gas/particle partitioning coefficients. *Atmos. Environ.*, vol. 32, No. 9, pp. 1493–1497.

Pulles T., Kok H. and U.Quass [2006] Application of the emission inventory model TEAM: uncertainties in dioxin emission estimates for central Europe. *Atmos. Environ.*, vol.40, pp.2321-2332.

Resnyansky Yu.D. and A.A. Zelenko [1999] Effects of synoptic variations of atmospheric impacts in the model of ocean general circulation: direct and indirect manifectation. *Meteorology and Hydrology*, No.9, pp.66-71, (*in* Russian).

Resnyansky Yu.D. and A.A.Zelenko [1991] Parametrization of the upper mixed layer in an ocean general circulation model. - Izvestiya of the USSR Academy of Sciences. *Atmosphere and Ocean Physics*, v.27, No 10, pp.1080-1088.

Resnyansky Yu.D. and A.A.Zelenko [1992] Numerical realization of the ocean general circulation with parametrization of the upper mixed layer. Proceedings of the USSR Hydrometcentre, v.323, pp.3-31.

Riemann C. and P. de Caritat [1998] Chemical elements in the Environment, Factsheets for the Geochemist and Environmental Scientist. Springer, New York, 398 pp.

Rudolf B., Hauschild H., Rueth W. and U. Schneider [1994] Terrestrial precipitation analysis: operational method and required density of point measurements. NATO ASI Series, Vol. I 26, Global Precipitation and Climate Change. Ed. by F. Desalmand. Springer-Verlag Berlin Heidelberg, pp. 173 – 186.

Salminen, R. (Chief-editor), Batista, M. J., Bidovec, M., Demetriades, A., De Vivo, B., De Vos, W., Duris, M., Gilucis, A., Gregorauskiene, V., Halamic, J., Heitzmann, P., Lima, A., Jordan, G., Klaver, G., Klein, P., Lis, J., Locutura, J., Marsina, K., Mazreku, A., O'Connor, P. J., Olsson, S.Å., Ottesen, R.-T., Petersell, V., Plant, J.A., Reeder, S., Salpeteur, I., Sandström, H., Siewers, U., Steenfelt, A., Tarvainen, T. [2005] Geochemical Atlas of Europe. Part 1: Background Information, Methodology and Maps. Espoo, Geological Survey of Finland, 526 pages, 36 figures, 362 maps.

Seigneur C., Vijayaraghavan K and Lohman K. [2006] Atmospheric mercury chemistry: Sensitivity of global model simulations to chemical reactions. *Journal of Geophysical Research*, vol. 111, pp. D22306.

Shatalov V., Gusev A., Dutchak S., Holoubek I., Mantseva E., Rozovskaya O., Sweetman A., Strukov B., Vulykh N. [2005] Modelling of POP Contamination in European Region: Evaluation of the Model Performance. EMEP/MSC-E Technical Report 7/2005.

Spivakovsky C.M., J.A.Logan, S.A.Montzka, Y.J.Balkanski, M.Foreman-Fowler, D.B.A.Jones, L.W.Horowitz, A.C.Fusco, C.A.M.Brenninkmeijer, M.J.Prather, S.C.Wofsy, M.B.McElroy [2000] Three-dimensional climatological distribution of tropospheric OH: Update and evaluation, J. Geophys. Res. 105, 8931-8980.

Tarrason L., Fagerli H., Jonson J.E., Simpson D., Benedictow A., Klein H., Vestreng V., Aas W.and Hjelbrekke A.-G. [2007] Transboundary Acidification, Eutrophication and Ground Level Ozone in Europe in 2005. EMEP Status Report 2007; August 8, 2007.

Toda E. [2005] POPs and heavy metals emission inventory of Japan. http://espreme.ier.uni-stuttgart.de/workshop/papers/Toda%20-%20POPs%20and%20heavy%20metals%20emission%20inventory%20of%20Japan.pdf.

Travnikov O. amd I.Ilyin [2005] Regional Model MSCE-HM of Heavy Metal Transboundary Air Pollution in Europe. EMEP/MSC-E Technical Report 6/2005.

UNEP [1999] Dioxin and Furan Inventories. National and Regional Emissions of PCDD/PCDF. Prepared by UNEP Chemicals. Geneva, Switzerland.

Walcek C. J. and Taylor G. R. [1986] A Theoretical Method for Computing Vertical Distributions of Acidity and Sulfate Production within Cumulus Clouds. *J. Atmos. Sci.,* vol. 43, pp. 339–355.

Wei B., S.Xie M.Yu, L.Wu [2007] QSPR-based prediction of gas/particle partitioning of polychlorinated biphenyls in the atmosphere. *Chemosphere*, vol. 66, pp. 1807-1820.

Xiao H. and F. Wania [2003] Is vapor pressure or the octanol–air partition coefficient a better descriptor of the partitioning between gas phase and organic matter. *Atmos. Env.*, vol.37, pp. 2867-2878.

Yamartino R.J., Scire J.S., Carmichael G.R. and Chang Y.S. [1992] The CALGRID mesoscale photochemical grid model - Part I. Model formulation, *Atmos. Environ.,* vol. 26A, pp. 1493-1512.

Yttri K.-E., Aas W., Tarrason L., Vestreng V., Tsyro S., Simpson D., Putaud J. P., Cavalli F. [2007] Transboundary particulate matter in Europe. EMEP/CCC&MSCW Status Report 4/2007.

Zhang Y. et al. [2004] Development and application of the model of aerosol dynamics, reaction, ionization, and dissolution (MADRID). *J. of Geophysical Research-Atmospheres*, vol. 109, No.13, pp. D01202-1-D01202/31.

Zobler L. [1986] A World Soil File for Global Climate Modelling. NASA Technical Memorandum 87802. NASA Goddard Institute for Space Studies, New York, New York, U.S.A.